3-2023

Small GTPase Regulated Intracellular Protein Trafficking in Endothelium

Caitlin Francis
University of Denver

Small GTPase Regulated Intracellular Protein Trafficking in Endothelium

Abstract

Intracellular protein trafficking is the movement of membrane-bound organelles to and from requisite locations within the cell. Small GTPases are a critical component to the spatiotemporal accuracy of intracellular trafficking pathways as they determine the specificity and direction of organelle transport. There exists over 150 small GTPases categorized into 5 sub-families and are employed across all cell types. Despite their universal expression and relevance to cellular function, small GTPases remain incompletely understood across tissue types. In various instances, the trafficking pathway of a particular Rab in one cell type may belong to a completely disparate pathway in another cell type. Rab27 has been shown to traffic melanosomes in epithelial tissue, however, in endothelium, Rab27 has been linked to the trafficking of an endothelial specific vesicle known as the Weibel-Palade body (WPB). However, information is lacking as to whether Rab27 trafficking is applicable to sprouting angiogenesis. Rab35 is a well-studied Rab involved in a broad spectrum of cellular functions, including cytokinesis, cell migration, and cell polarity across tissue types. Surprisingly, Rab35 lacks investigation in endothelial cells. Like Rab35, Arf6 is also well-studied and implicated in several different cellular functions. It is most associated with cytoskeletal rearrangements, cell migration and endocytosis. Some Arf6 data exists in endothelial cells, but information is lacking on its role in sprouting angiogenesis and lumen formation. Rab8 is reported to traffic cargo exiting the trans-Golgi network bound for the apical membrane. The relevance of Rab8 to apical trafficking in endothelium remains unknown. Our data agrees that Rab27 is linked to the WPB pathway, and it is WPB cargo, Angiopoietin-2, that causes the hyper-sprouting phenotype observed in the absence of Rab27. In our hands, Rab35 does impact a range of endothelial cell processes. The extensive effects Rab35 induces is due to Rab35's regulation of the actin cytoskeleton. We found that Arf6 also regulates the actin cytoskeleton but is critical to the management of transmembrane proteins important for sprouting angiogenesis and lumen formation. Finally, our results show that Rab8 is indeed important to apical trafficking in endothelium, independent of the WPB pathway. Together, these investigations provide insight to the divergent trafficking patterns of small GTPases in endothelium.

Document Type

Dissertation

Degree Name

Ph.D.

Department

Biological Sciences

First Advisor

Erich Kushner

Second Advisor

J. Todd Blankenship

Third Advisor

Martin Margittai

Keywords

Intracellular protein trafficking, GTPase

SMALL GTPASE REGULATED INTRACELLULAR PROTEIN TRAFFICKING IN ENDOTHELIUM

A Dissertation

Presented to

the Faculty of the College of Natural Sciences and Mathematics

University of Denver

In Partial Fulfillment

of the Requirements for the Degree

Doctor of Philosophy

by

Caitlin Francis

March 2023

Advisor: Dr. Erich Kushner

Author: Caitlin Francis
Title: SMALL GTPASE REGULATED INTRACELLULAR TRAFFICKING IN ENDOTHELIUM
Advisor: Dr. Erich Kushner
Degree Date: March 2023

Abstract

Intracellular protein trafficking is the movement of membrane-bound organelles to and from requisite locations within the cell. Small GTPases are a critical component to the spatiotemporal accuracy of intracellular trafficking pathways as they determine the specificity and direction of organelle transport. There exists over 150 small GTPases categorized into 5 sub-families and are employed across all cell types. Despite their universal expression and relevance to cellular function, small GTPases remain incompletely understood across tissue types. In various instances, the trafficking pathway of a particular Rab in one cell type may belong to a completely disparate pathway in another cell type. Rab27 has been shown to traffic melanosomes in epithelial tissue, however, in endothelium, Rab27 has been linked to the trafficking of an endothelial specific vesicle known as the Weibel-Palade body (WPB). However, information is lacking as to whether Rab27 trafficking is applicable to sprouting angiogenesis. Rab35 is a well-studied Rab involved in a broad spectrum of cellular functions, including cytokinesis, cell migration, and cell polarity across tissue types. Surprisingly, Rab35 lacks investigation in endothelial cells. Like Rab35, Arf6 is also well-studied and implicated in several different cellular functions. It is most associated with cytoskeletal rearrangements, cell migration and endocytosis. Some Arf6 data exists in endothelial cells, but information is lacking on its role in sprouting angiogenesis and lumen

formation. Rab8 is reported to traffic cargo exiting the trans-Golgi network bound for the apical membrane. The relevance of Rab8 to apical trafficking in endothelium remains unknown. Our data agrees that Rab27 is linked to the WPB pathway, and it is WPB cargo, Angiopoietin-2, that causes the hyper-sprouting phenotype observed in the absence of Rab27. In our hands, Rab35 does impact a range of endothelial cell processes. The extensive effects Rab35 induces is due to Rab35's regulation of the actin cytoskeleton. We found that Arf6 also regulates the actin cytoskeleton but is critical to the management of transmembrane proteins important for sprouting angiogenesis and lumen formation. Finally, our results show that Rab8 is indeed important to apical trafficking in endothelium, independent of the WPB pathway. Together, these investigations provide insight to the divergent trafficking patterns of small GTPases in endothelium.

Acknowledgements

I am sincerely thankful to my committee members Dr. Todd Blankenship, Dr. Michelle Knowles, and Dr. Joe Angleson; all of whom have offered unique perspectives and guidance throughout the course of this doctorate. Dr. Schuyler Van Engelenburg, my co-mentor, has routinely provided insight through his extensive knowledge of microscopy and the scientific method. His excitement and love for cell biology is infectious and inspiring. My mentor, Dr. Erich Kushner, has been essential to my development as a scientist and his mentorship has enhanced this research tremendously. I am grateful for his steady understanding and support during personally trying times. Each of these individuals have been indispensable to the development and evolution of my scientific investigations.

I appreciate the Department of Biology for the resources to which I performed experiments. I acknowledge the efforts put towards this research by my colleagues and lab members within the department: Dr. Taylor Minckley, Hayle Kincross, Shea Claflin, Makenzie Bell, and Marina Skripnichuk. Lastly, I recognize my father. My father did not live to see the end of my doctorate, only the beginning. I hold the deepest appreciation to my father for teaching me to see no boundary based on gender, that education is freedom, creativity is true intelligence, and to believe that the only bar set for me is one set by myself. The work in this dissertation was supported by the following grants: NIH R01 Research Project Grant (HL155921-02); NIH R15 AREA Grant (HL156106-01A1); NIH R56 High Priority, Short-Term Project Award (1R56HL148450-1); and NIH R00 Pathway to Independence Award (R00HL124311).

Table of Contents

List of Figures

Chapter 1

Chapter 2

Chapter 3

Chapter 4

Chapter 5

Appendix B

Appendix C

Appendix D

Appendix E

List of Tables

Chapter 1

Appendix A

List of Abbreviations

Chapter 1

phorbol 12-myristate 13-acetate ..... PMA
Guanasine Diphosphate ..... GDP
Guanasine Triphosphate ..... GTP
GTPase-activating proteins ..... GAP
Guanine-Exchange Factors ..... GEF
Rab escort protein ..... REP
Rabs to Rab geranyl geranyl transferase ..... RABGGTase
GDI displacement factors ..... GDI
early endosome antigen-1 ..... EEA1
endothelial cell ..... EC
clathrin-mediated endocytosis ..... CME
extracellular matrix ..... ECM
vascular endothelial growth factor ..... VEGF
VEGFR2 receptor VEGFR2
receptor tyrosine kinases ..... RTK
apical membrane initiation site ..... AMIS
trans-Golgi network ..... TGN
Weibel–Palade bodies ..... WPB
synaptotagmin-like protein 2a SLP2a
a disintegrin and metalloprotease ..... ADAM
extracellular domain ..... ECD
intracellular domain ..... ICD
angiopoietin-2 ..... Ang-2
Angiopoietin-1 ..... Ang-1
von Willebrand factor ..... vWF
Delta-like ligand 4 ..... Dll4

Chapter 2

Analysis of Variance ..... ANOVA
synaptotagmin-like protein 4a Slp4a
phosphotidylinositol4,5 bisphosphate PI45P2
wild-type ..... WT
green fluorescent protein ..... GFP
Dimethyl Sulfoxide ..... DMSO
phosphorylated Tie-2 ..... p-TIe2
dorsal longitudinal anastomotic vessels ..... DLAV
intersomitic vessels ..... ISV
not significant ..... NS

Snap Receptor ..... SNARE
VEGF receptor 1 ..... VEGFR1

Chapter 3

Paraformaldehyde ..... PFA
fibrin-bead assay ..... FBA
Podocalyxin ..... Podxl
constitutively active ..... CA
dominant-negative ..... DN
plasma membrane ..... PM
ligand-modulated antibody fragments ..... LAMA
trimethoprim ..... TMP

Chapter 4

Cyan Flourescent Protein ..... CFP
Human umbilical vein cells ..... HUVEC
Knockdown ..... KD
Vascular Endothelial-Cadherin ..... VE-Cad
arbitrary unit ..... AU
lysosomal marker ..... LAMP
Brefeldin A ..... BFA

Chapter One: Introduction to Rab-Mediated Intracellular Protein Trafficking in Endothelium

All eukaryotic cells house membrane-bound compartments and organelles which communicate and react with the cell's environment. Vesicles must quickly shuttle between compartments as part of endocytic (inward transport) and exocytic (outward transport) trafficking pathways. Should any pathway be inherently faulty or become aberrant, organ and tissue function are often impaired. Our evolving understanding of protein trafficking pathways forms the basis for advancements made in the treatment of countless maladies, from cancer to Alzheimer's. Still, the biogenesis and orchestration of intracellular protein pathways remains incompletely understood. To improve disease outcomes, continued exploration of intracellular protein trafficking is of the upmost importance.

1.1 Intracellular Protein Trafficking

Over recent decades, efforts in the field of protein trafficking have targeted the machinery required for vesicular transport, membrane targeting, and exocytic/endocytic processes. Researchers have identified numerous protein-protein interactions as well as lipid-protein interactions which allow for the cell to reversibly translocate vesicles and protein-complexes between subcellular compartments. Stated simply, these macromolecular interactions are governed spatially and temporally in three key ways: (1) small GTPases mediate the association of targeting molecules decorating the surface of

vesicles with their corresponding membrane effectors, (2) reversible, post-translational modifications direct cargo sorting and protein machinery recycling, and (3) cortical actin cytoskeleton remodeling provides the physical force required for trafficking events [5, 292, 293]. Post-translational modifications of proteins as well as the switchable 'on-off' state of small GTPases offers the cell the ability to react quickly to incoming extracellular information, by-passing protein expression changes [4,5].

To further expound on the three fundamental ways in which protein trafficking occurs, first is to address small GTPases. Small GTPases encompass a large family of proteins with several sub-families. Under the small GTPase umbrella falls the Rho, Arf, Ras, Rab and Ran GTPase sub-families [294]. What characteristically identifies a protein as a small GTPase is the capability of binary 'on' or 'off' decisions [294]. This is achieved by the addition ('on' state) or removal ('off' state) of a phosphate [294]. Traditionally, the 'on' state allows for a small GTPase to then bind unique effector proteins and motor proteins, thus creating an interface between a vesicle and its trafficking protein complex (Figure 1) [294]. Should a trafficking pathway necessitate termination, the guanasine triphosphate (GTP) is hydolyzed and the small GTPase enters an inactive, Guanasine Diphosphate (GDP)-bound, state [294]. The considerable size of the small GTPase family is reflective of the many distinct compartments within the cell that require localized small GTPase trafficking.

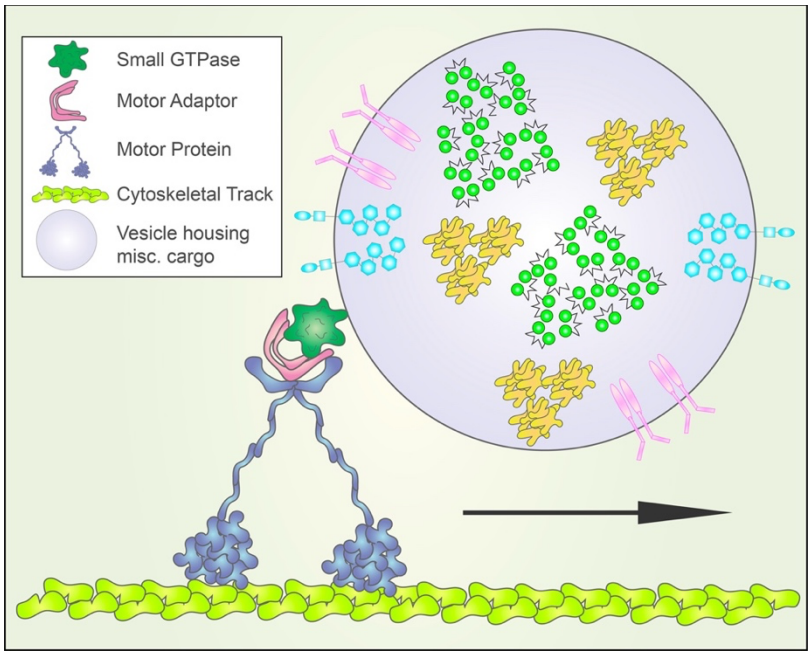

Figure 5: Cartoon Representative of Small GTPase Motor Protein Interface

Next to discuss is post-translational modifications. Protein modification encompasses processing events that change the properties of a protein by adding a modifying group to one or more amino acids or by proteolytic cleavage [295, 296]. Given the breadth of this topic, relevant scenarios will be provided for context. For one example, trans-membrane proteins often communicate extracellular information through a structural modification of its intracellular domain [296]. In some cases, this is a phosphorylation or cleavage of the domain [28, 29, 296]. The change results in downstream trafficking events inducing a reaction of the cell to its environment [28, 29, 296]. In another scenario, a transmembrane protein may become defective or no longer needed. The protein may then be marked with ubiquitination, a signal to be degraded [297]. Finally, it is the post-translational phosphorylation and de-phosphorylation of small GTPases that allow for their role in vesicle transport [294]. While only mentioning a few scenarios here, numerous post-

translational modifications exist for successful protein trafficking programs throughout the cell.

Lastly, cytoskeletal changes are paramount to the budding of vesicles from the Golgi as well as endocytic and exocytic events. The actin cytoskeleton in combination with contractility programs maintain Golgi compartments and facilitate Golgi-associated transport events [298]. During endocytosis, the actin cytoskeleton is required for Clathrin-coated pit formation, constriction and vesicle scission [299]. Cortactin, a protein which binds actin and the motor-protein dynamin, links cytoskeletal changes with dynamin-dependent scission [300]. Unlike endocytosis, during exocytosis filamentous actin is rapidly assembled around the secretory vesicle during membrane fusion [301]. Researchers speculate that the filamentous-actin coat drives closure of fusion pores acting to stabilize the plasma membrane [301]. Disruptions to the actin cytoskeleton can result in impaired endocytosis, exocytosis and Golgi trafficking.

While only discussing three key aspects of intracellular protein trafficking, it is clear how complex and interconnected the proteome is. The explosion of single-cell sequencing data has allowed for expression patterns to be widely identified across tissue types. Yet, investigations into how expressed proteins behave between tissue types, when reacting to extracellular stimuli, as well as in diseased states, are lacking. This information is imperative to our understanding of cell reactivity as well as improved therapeutic measures.

1.2 Rab GTPase Protein Family

There are more than 150 members of the Ras protein superfamily [294]. Rab GTPases, a sub-family to the Ras super-family, comprises roughly 70 of these members

[4-7]. All small GTPases function as monomeric G proteins with slight variations in structure and post-translational modification that specify unique binding partners and subcellular localization [294]. Rab GTPases differ from other Ras family members with a carboxyl terminus which has been implicated in their subcellular targeting [302].

Molecular regulation of Rab GTPases begins with a post-translational modification which allows Rabs to anchor into a membrane. This is achieved through a modification known as prenylation, Rab prenylation is reliant on the Rab escort protein (REP) [303]. REP's will escort nascent Rabs to Rab geranyl geranyl transferase (RabGGTase) where the C-terminus cysteine motifs are then prenylated and subsequently delivered to the membrane [303].

Rab GTPases house a conserved molecular switch mechanism. All Rabs contain a physical fold which includes two switch regions that are responsible for significant conformational changes between activity states [4-7]. The on-state is controlled by Guanine-Exchange Factors (GEFs) [4-7]. GEF's are usually specific to individual Rabs and mediate an exchange of GDP to GTP, inducing a conformation change [4-7]. GTPase-activating proteins (GAPs) switch Rabs to an off-state by hydolyzing GTP to GDP [4-7]. In general, GAPs are less crucial than GEFs as many Rabs intrinsically hydrolyze GTP at a relatively high rate [4-7].

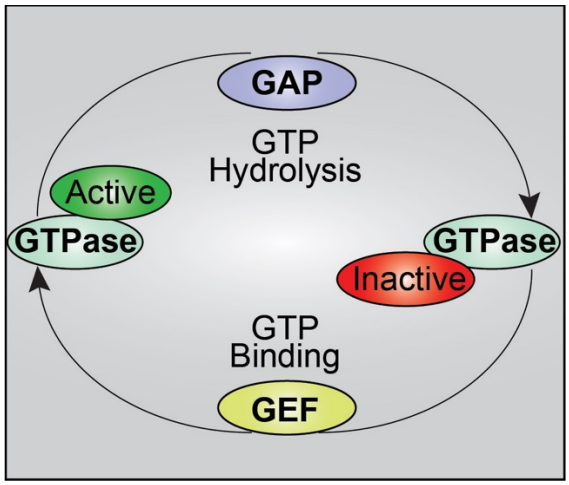

Figure 6: Cartoon Representative of Small GTPase Molecular Regulation

Transferring Rabs between membranes is mediated by Rab GDI's (GDP dissociation inhibitors) [304]. Following GTP hydrolysis a GDI will temporarily sequester a Rab; this is reversed by GDI displacement factors (GDF's) [304]. To summarize, Rab GTPases are governed by proteins belonging to GEF, GAP, REP and GDI families. Clearly, molecular regulation of small GTPases involves a vast network of proteins, all of which must function properly for small GTPase mediated trafficking to occur. These interconnected proteins which allow cells to quickly react to stimuli call for continued examination as there remains a significant void in our understanding of small GTPase regulated intracellular trafficking.

1.3 Protein Trafficking in Endothelium

Blood vessels are the earliest organ system to arise in development owing to their absolute requirement for transport of oxygen and nutrients to growing tissues. Angiogenesis is the proliferation of previously established blood vessels through a variety of highly regulated programs. Understanding how angiogenesis works has had, and continues to have, tremendous medical value. Although, our understanding of these

intricate cell autonomous and tissue-wide programs is still in its infancy on many levels. Recent advances in RNA-Seq and single-cell RNA-Seq have allowed investigators to map complex transcriptional networks with unprecedented resolution; however, we are finding these networks do not entirely reprise the full phenotypic picture.

As taught in entry level biology, mRNA translation is only the start of a protein's journey to becoming functional. Proteins are modified through post-translational modifications and are typically processed through the Golgi apparatus, packaged into vesicles, and then delivered to a precise intracellular location(s). Perturbations of regulatory signaling at any of these steps can have profound consequences on tissue morphogenesis. Moreover, many of these post-Golgi steps can be completely divorced from traditional transcriptional feedback loops; thus, trafficking programs can be self-regulating with little transcriptional input. We contend that both endothelial-specific as well as more ubiquitous trafficking signatures need to be mapped to truly understand angiogenesis during development and in disease. In the following sections, we have broken various components of angiogenesis down by function and discuss the relevant trafficking programs. In many instances there are no endothelial studies to draw upon, in this case we infer function from experiments performed in other systems.

Sprouting Angiogenesis

A primary cellular function during angiogenesis entails endothelial cell(s) sprouting from a parent vessel, typically in response to extrinsic growth factors. For these events, we are referring to a tip cell that would be leading several stalk cells in a canonical tip/stalk cell hierarchy [12]. During this process endothelial cells are sensing growth factor ligands that rearrange cell polarity, promote actin dynamics and integrin-based cell

motility programs, and break-down extracellular matrix, ECM [13-17]. A primary initiator in this event would be an endothelial cell binding a growth factor, namely vascular endothelial growth factor (VEGF) on its cognate VEGFR2 receptor. Receptor endocytosis, particularly VEGFR2 internalization, is an excellent example of how trafficking can mediate endothelial function. This event is likely the most well-studied trafficking-related program in endothelial biology today. As such, there are several reviews that go into detail cited here [2,18-20]; thus, we will cover more recent data related to this phenomenon.

Internalization of VEGFR2 is initiated through clathrin-mediated endocytosis, CME [21,22] in which the receptor is removed from the plasma membrane and internalized in the form of a vesicle. In the inactive, non-ligand bound state, VEGFR2 is plugged into a Rab4a or Rab11a-mediated recycling pathway, continuously being internalized and returned to the plasma membrane [23,24] (Figure 3). There is some data supporting a clathrin-independent pathway, such as caveolin-dependent endocytosis, in receptor internalization [25]; however, recent literature has significantly shifted away from the notion that caveolae participate in endocytic processes, but are primarily membrane reservoirs, buffering changes in membrane tension during cellular dynamics [26,27. Upon ligand binding, newly endocytosed VEGFR2-positive vesicles are marked with Rab5 and early endosome antigen-1 (EEA1). Rab5, is most associated with endocytic events and receptor tyrosine kinase internalization [28,29]. Rab5-positive early endosomes are transitioned to a Rab7 late endosome and targeted to the lysosome for destruction [30,31]. Receptor internalization and degradation will reduce the amount of naïve cell-surface receptors, this in turn, will limit the signaling potential of the ligand.

This pathway is in no way unique to VEGFR2 as many other receptor tyrosine kinases [32] demonstrate a similar mode of endocytic regulation [33,34]. There is some controversy if receptor endocytosis, per se, is required for downstream VEGFR2-related signaling. Several investigations have shown that loss of CME blunts downstream VEGFR2 signaling [35, 36], while others report that loss of CME does not dampen signaling potential [22,37]. In terms of sprouting, any program that alters growth factor signaling duration and amplitude will elicit a profound effect on downstream cellular behaviors.

Table 1 Rab GTPase Regulators, Effectors and Function

Rab GTPase	GEF(s)	GAP(s)	Effector	Function	Citations
Rab 1a/b	TRAPP I, DrrA	TBC1D20	---	ER to golgi trafficking	Lamber, et al., *Current Opinions in Cell Biology*, 2019
Rab2b	---	---	Bicaudal-D, RUND-1, CCCP-1	ER to golgi trafficking	Zhen, et al., *Journal of Cell Science*, 2015; Ailion, et al., *Neuron*, 2014
Rab 4a/b	---	TBC1D11, EVI5-like	Rabip4, Rabaptin-5, RabEP2	Early-endosome trafficking	Stein, et al., *Advanced Drug Delivery Reviews*, 2003; Zografou, et al., *Journal of Cell Science*, 2012
Rab 5a/b/c	Rabex-5 (Vps9), , Rabaptin-5	TBC1D3/RU TBC3/USP6N L	EEA1, RIN2	Early-endosome trafficking, podxl trafficking in epithelium	Stein, et al., *Advanced Drug Delivery Reviews*, 2003; Richards, et al., *Current Biology*, 2015
Rab6	RIC1-RGP1	---	Bicaudal-D	Golgi-localized trafficking	Lamber, et al., *Current Opinions in Cell Biology*, 2019; Zhen, et al., Journal of Cell Science, 2015

Rab7	MON1-CCZ1	TBC1D5	RILP, VPS34, HOPS	Lysosome transport	Lamber, et al., *Current Opinions in Cell Biology*, 2019; Stein, et al., *Advanced Drug Delivery Reviews*, 2003; Zhen, et al., Journal of Cell Science, 2015
Rab 8a	Rabin-8/ GRAB/ Mss450/ C9Orf72	TBC1D1/TBC1D30/TBC1D4	---	TGN trafficking	Müller, et al., *Small GTPases*, 2018
Rab 10	DennD4c	TBC1D1/TBC1D4/ EVI5-L		Basolateral trafficking	Gross, et al., *Angiogenesis*, 2021
Rab 11a/b	SH3BP5 (REI-1)/ SH3BP5 (REI-1)	TBC1D11/TBC1D15/EVI5, TBC1D14	Rip11, RCP, Eferin, Protrudin	Endocytic Uptake and Recycling	Stein, et al., *Advanced Drug Delivery Reviews*, 2003; Zhen, et al., *Journal of Cell Science*, 2015
Rab 13	DennD1C	TBC1D10A, TBC1D25	---	Tubular endosome, TGN trafficking	Müller, et al., *Small GTPases*, 2018; Homma, et al., *The FEBS Journal*, 2021
Rab 14	DennD6	TBC1D1	---	Early endosome trafficking	Müller, et al., *Small GTPases*, 2018;

					Homma, et al., *The FEBS Journal*, 2021
Rab21	---	---	Protein tyrosine phosphatase receptor type f (PTPRF)	Endocytosis of integrins bound to fibronectin	Mana, et al., *Nat Comms*, 2016
Rab25	---	---	---	Podxl trafficking in epithelium	Richards, et al., *Current Biology*, 2015
Rab 27	MADD/DENN/Rab3GEP	TBC1D10A/EPI64/ Rab27-GAPα, TBC1D10B/FLJ13130	Slp2a, MYRIP, Slp4a	WPB negative regulator	Francis, et al., *ATVB*, 2021; Fukuda, et al., *Traffic*, 2013
Rab 35	DENND1a/ DENND1b/ DENND1c	TBC1D10A/ TBC1D10B/ TBC1D10C/ TBC1D13/ TBC1D24	ACAP2, RUSC2, OCRL, MICAL-L1	Plasma Membrane Endocytosis, cytoskeletal re-arrangements	Chaineau, et al., *Traffic*, 2013; Marat, et al., *Molecular Biology of the Cell*, 2012
Rab37	---	---	---	WPB localization	Zografou, et al., *Journal of Cell Science*, 2012
Abbreviations: Podocalyxin (Podxl), Weibel-Palade body (WPB), trans-golgi network (TGN)					

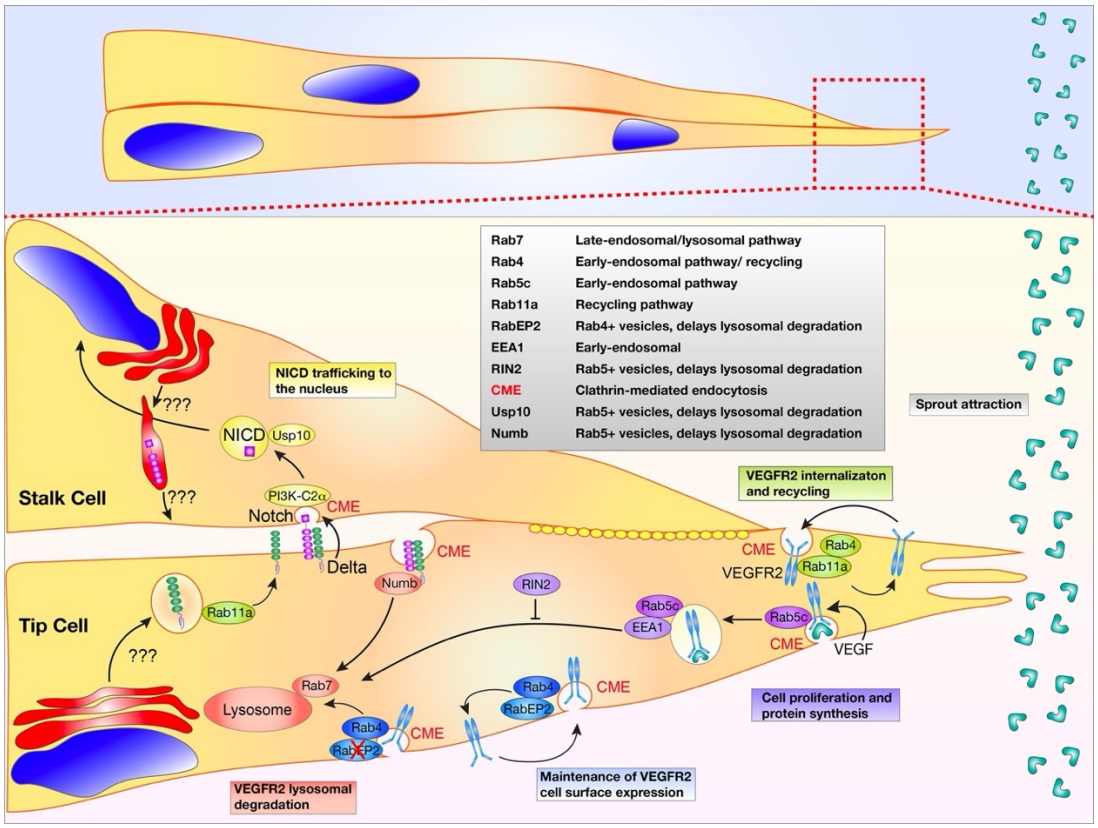

Figure 7: Sprouting Angiogenesis and Notch Trafficking. Sprout migration is dependent on vascular endothelial growth factor receptor 2 (VEGFR2) endocytosis. Upon vascular endothelial growth factor (VEGF) ligand binding, Rab5c and early-endosome antigen 1 (EEA1) decorate the internalizing clathrin-coated pit. RIN2 prevents lysosomal degradation of the Rab5 positive vesicles. VEGFR2 cell surface expression is maintained by both Rab11a and Rab4 recycling. Rab4 aids in maintaining VEGFR2 expression. In the absence of RabEP2, VEGFR2 is transitioned to a Rab7-positive vesicle destined for lysosomal degradation. During Notch and delta-like ligand 4 (Dll4) binding, Dll4 pulls on the Notch receptor using clathrin-mediated endocytosis (CME) allowing for S2 and S3 cleavage events. Thereafter, the released Notch extracellular domain is transcytosed into the Dll4 presenting cell and presumably degraded. The Notch intracellular domain (NICD) is subsequently protected from proteosomal degradation in transit to the nucleus by the deubiquitinase Usp10. Anterograde trafficking of Notch and Dll4 to the plasma membrane is incompletely understood. Table lists proteins depicted in figure with corresponding function

Recently, several groups have identified additional trafficking determinants involved in VEGFR2 endocytosis. VEGFR2's insertion into a recycling pathway on face-value would seem to be more energetically costly than a unidirectional trafficking event where

the receptor is statically plugged into the membrane, primed for ligand binding. However, constitutive recycling of VEGFR2 plays a protective role against receptor shedding. Inhibition of CME will increase shedding of the VEGFR2 ectodomain, indicating that endosomal recycling is important for receptor plasma membrane retention [38]. Using a screen against Rab GAPs, TBC1D10A-C was flagged for its impact on endothelial VEGFR2 signaling, tube formation and cell migration [18]. Here, the authors show the same GAP family members can elicit contrary responses in terms of VEGFR2 signaling, one decreasing downstream ERK activation, while the other enhancing it. This is likely related to each GAPs unique affinity to a particular Rab or group of Rabs. In this case, TBC1D10A has affinity for Rab13, interestingly this has also been shown to be a GAP for Rab27a and Rab35 [39,40]. In another investigation focused on VEGFR2 endocytosis the authors demonstrated that the protein RabEP2 partners with the recycling Rab4 to maintain VEGFR2 cell surface expression. In the absence of RabEP2, Rab4-positive vesicles were diverted to a Rab7 lysosomal pathway, significantly attenuating VEGF signaling [41]. It was also reported that Rab5c partners with RIN2 to delay lysosomal degradation to increase downstream VEGFR2 signaling [3]. In this article, loss of RIN2 or Rab5c-mediated endosomal stabilization blunted VEGFR2 signaling of Akt and ERK leading to defects in sprouting parameters in culture and zebrafish blood vessel development. These reports nicely illustrate how critical endothelial-specific signaling can be fine-tuned by endosomal processes.

An interesting point here is uncoupling Rab-mediated effects on endothelial cell migration from their interactions on the VEGF or other growth factor signaling. For instance, some have purported that knocking out a particular Rab affects endothelial

migration [42-44]; although this is undoubtedly the case, the primary defect is connected to VEGFR2-related viability and chemotaxis, not a direct effect on machinery involved in endothelial cell motility. In this case, there are few studies directly exploring endothelial trafficking factors that influence cell motility, per se. In a candidate screen directed against Rab3a, Rab3b, Rab8a, Rab11a, Rab27a, RalA, RalB and caveolin-1 investigating endothelial tube formation, it was observed that a variety of the Rab GTPases reduced sprouting behaviors [45], suggesting an effect on cell motility programs in some cases; although, the mechanisms for these perturbations were not described. There are many reports that directly test the role of cytoskeletal regulators in endothelial tissues, but few that identify how trafficking regulators interface with these systems. Future research coupling both trafficking and cytoskeletal signaling networks would be important as endothelial cells look and move (collectively and individually) differently from epithelial cells in which the bulk of this type of research has been published.

Integrins are extracellular receptors that engage the ECM and are highly involved with cell migration and general apicobasal polarity [46]. These receptors are part of a large complex called a focal adhesion that links the actin cytoskeleton to the ECM generating the propulsive force to move a cell, or collectively, a sprout [42]. As part of a cyclical process, integrins are continually recycled, placed on the basal cell membrane, anchored to the ECM and endocytosed as the cell propels itself forward [47]. Trafficking factors have been shown to dramatically affect cell migration through regulating the availability of integrin receptors in endothelial cells. For instance, Rab21 with protein tyrosine phosphatase receptor type f has been reported to endocytose $\alpha_5\beta_1$ integrins bound to fibronectin [48]. The cytoskeletal regulator RhoJ has been shown the regulate

endocytic processes including $\alpha_5\beta_1$ integrin trafficking [49]. Similarly, Arf6 has been shown to be a potent activator of integrin recycling across many cell types, controlling both fast and slow integrin treadmilling [50-52]. Arf6 influences CME as well as recycling, interfacing with Rab11a [53]. Loss of Arf6 and downstream perturbations in integrin activation can have a profound effect on sprouting angiogenesis [54].

Cell to Cell Junction Regulation

Junctional regulation is paramount to physiological blood vessel development. Individual endothelial cell junctions must work in concert to stabilize or loosen cell–cell connections by differentially recruiting or removing junctional proteins. In endothelial cells, a major junction protein of interest is VE-cadherin. VE-cadherin is an endothelial-specific adherens junction and several excellent reviews on its regulation, interactions with the actin cytoskeleton and crosstalk with growth factor signaling are cited here [55-57]. In terms of trafficking two questions are essential: (1) how does VE-cadherin arrive at basolateral junctions (?); and (2) how is it destabilized during sprouting morphogenesis? Once at the plasma membrane VE-cadherin is likely plugged into a Rab11a recycling pathway as knockout of the Rab11a has been shown to decrease endothelial barrier function [58]. Similarly, it has been reported that Rab11a directly binds VE-cadherin [59]. This data would suggest that VE-cadherin is plugged into a recycling loop similar to RTK receptors. This finding is congruent with Rab11a-based E-cadherin trafficking in epithelial cells [60]. However, caution should be taken when ascribing direct function to Rab11a recycling as so many peripheral trafficking programs leverage this network.

With regard to the initial anterograde trafficking, how newly translated VE-cadherin is first transported from the Golgi apparatus to junctional complexes is largely uncharacterized. Rab11a is typically a terminal trafficking destination, such that, the early post-Golgi Rab-based mediators that are responsible for delivery of VE-cadherin to Rab11a have not been charted to our knowledge. To this point, Malinova, et al., more recently reported a complex involving PACSIN2, EHD4, and MICAL-L1 which influenced VE-cadherin asymmetric localization during sprouting [61] (Figure 4). In this investigation, PACSIN2 recruited the trafficking regulators EHD4 and MICAL-L1 to the rear of asymmetric adherens junctions. Given this complex has been associated with tubular transport in other tissue types, it could be posited that VE-cadherin is shuttled by Rab6a, Rab8, or Rab10 which have all been shown to interface with MICAL-L1 on tubulated vesicles [62].

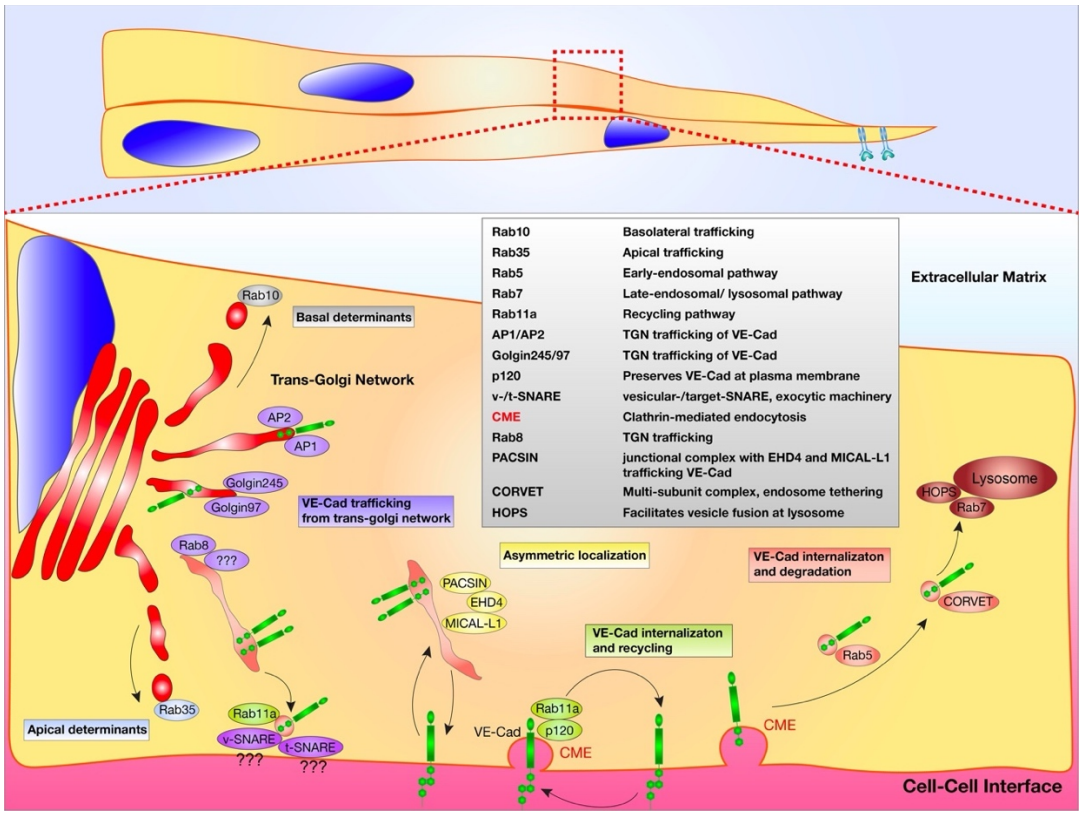

Figure 8: VE-Cadherin Trafficking Regulation.VE-Cadherin (VE-Cad) trafficking from the Golgi apparatus to the plasma membrane is potentially aided by AP1, AP2, golgin97 and golgin245. Post-Golgi transporter Rab8 is positioned at the trans-Golgi network, where it may be involved in trafficking to the plasma membrane. At the plasma membrane exocytic machinery, such as vesicular (v)-SNARE's and tethering (t)-SNARE's play a role in vesicle capture and docking. Once plugged into the plasma membrane, VE-Cad is maintained in a recycling loop via Rab11a and p120. Asymmetric localization of VE-Cad is thought to involve a PACSIN/EHD4/MICAL-L1 complex. VE-Cad endocytosis may be regulated by Rab5-mediated shuttling to the CORVET and HOPS complex prior to lysosomal degradation. Rab35 and Rab10 act as either apical or basolateral determinants, respectively. Table lists proteins depicted in figure with corresponding function.

Lumen Formation

An endothelial cell's ability to polarize and create a hollow cavity is one of the most notable anatomic characteristics of blood vessels as a tubular fluid transport system. The intrinsic signaling programs that allow endothelial cells to create de novo luminal

surfaces are vital to both blood vessel morphogenesis and general function. Trafficking programs play a substantial role in the formation of a new apical membrane (also termed luminal membrane) that will be the plasma membrane surface adjacent to the lumen cavity and later will be in contact with circulating blood constituents. For this review, we will focus on trafficking factors that influence the establishment of the apical membrane during lumen biogenesis. Cytoskeletal factors, principally actin regulating proteins, also play a fundamental role in this process and the following reviews cover this topic in detail [77-80].

During lumen initiation a clustering of vesicular deliveries are focused to internal sites of cell–cell contact, this area is termed the apical membrane initiation site, AMIS [81] (Figure 5). The AMIS location is dependent on both internal cell–cell contacts and basal membrane integrin engagement to provide the cell with a rudimentary polarity cue. This dependency on a polarity axis informed by junctions and ECM engagement is well established as loss of junctional stability and/or integrin signaling in nearly any system significantly precludes lumen formation [82]. Once an AMIS is present, it can be presumed that the cell generally has three distinct membrane surfaces, apical, basal and junctional (or basolateral) that exhibit disparate, local signaling and trafficking programs. In endothelial biology, trafficking mediators that participate in AMIS formation are nowhere near as characterized as their epithelial counterparts. This is in large part due to their rectangular shape and spatially segregated apical and basal domains, while ECs are exceedingly flat exhibiting a mesenchymal morphology [83]. In some instances, the distance between the apical and basal domains in ECs are diffraction limited (≤ 500 nm), hindering imaging of either membrane surface. Adding to the complexity, several

investigations, including our work, demonstrate that epithelial apical trafficking programs are largely divergent in endothelial cells [84]; thus, this literature should not be viewed as completely interchangeable.

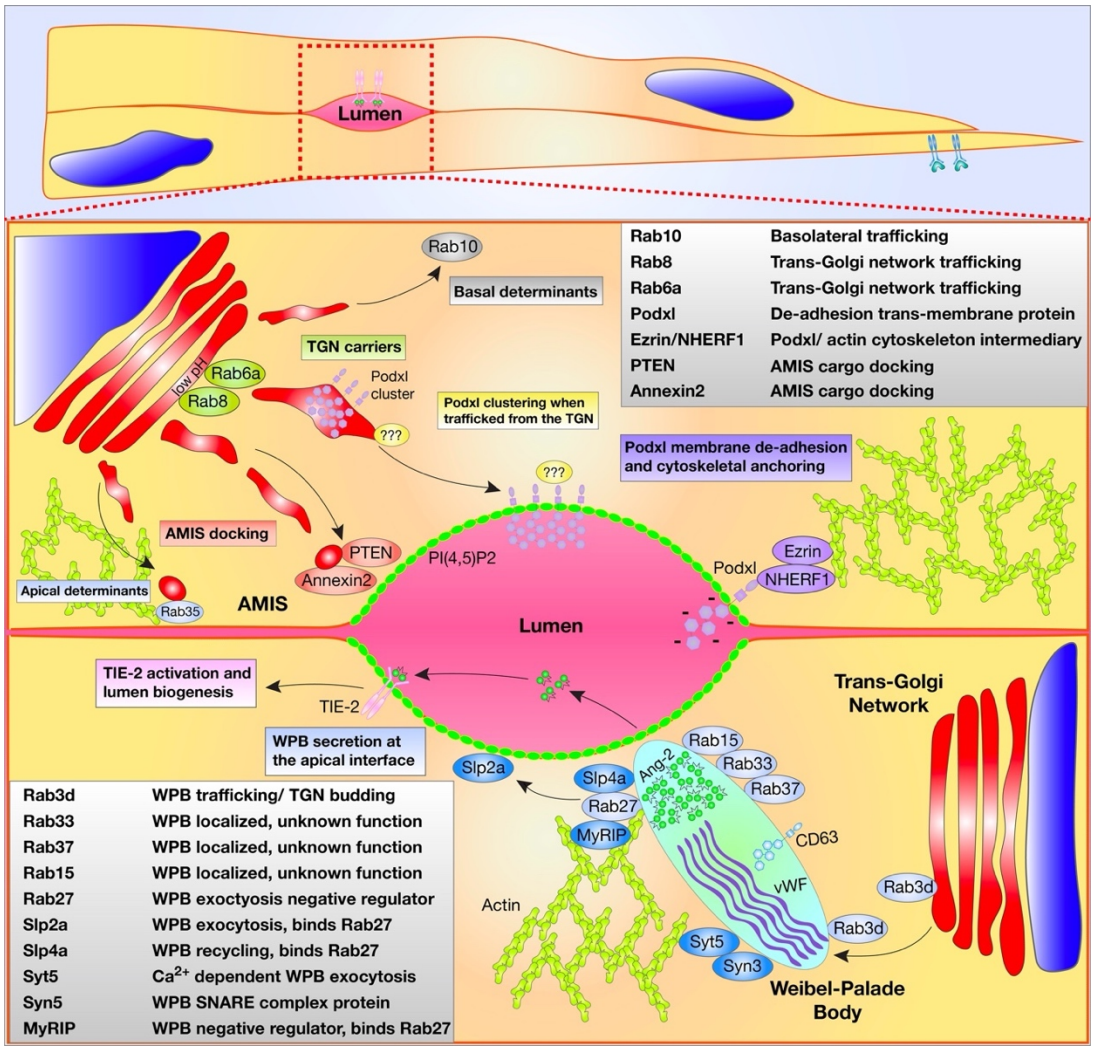

Figure 9: Endothelial Lumen Formation and Secretion. Top cell depicts trafficking of proteins related to lumen formation. From the Golgi complex, apically destined cargo may be transported within Rab6 and Rab8 vesicles or tubular networks. Podocalyxin (Podxl), a required luminal transmembrane protein, may be first recognized at the acidic trans-Golgi network (TGN) via protein clustering aided by addition of carbohydrate moieties. Lipid modification such as PI(4,5)P2 decorate the apical membrane initiation site (AMIS). Once Podxl is deposited into the apical membrane, NHERF1 and Ezrin complex with Podxl and the actin cytoskeleton. Other apical determinants involved in lumenogenesis localize to the AMIS such as Rab35, Annexin2 and PTEN. Bottom cell Weibel–Palade body (WPB) trafficking. Many Rab GTPases have been connected to the

trafficking of WPB's, shown are Rab3d, Rab37, Rab33, Rab15, and Rab27a. Furthermore, exocytic machinery is shown including Syn3, Syt5, Slp4a and Slp2a. MyRIP and Rab27a are negative regulators of WPB secretion sequestering WPBs within the actin cytoskeleton. Secretion of angiopoietin-2 (Ang2) from WPBs causes activation of the TIE-2 receptor and signaling related to lumen formation. Each table lists proteins depicted in figure with corresponding function.

Trafficking directed to the AMIS is first instructed by the presence of various lipid species. For instance, PIP_2 is one of the earliest apical membrane lipid types being highly enriched at the forming AMIS. PIP_2 promotes the recruitment of many proteins such as those in the synaptotagmin-like protein family [85]. This protein family also contains a Rab-binding domain to tether Rabs proximal to the apical membrane allowing for fusion of their contents. Our work recently demonstrated that synaptotagmin-like protein 2a (Slp2a) robustly recruits to the apical membrane where it binds to Rab27a tethered to exocytic Weibel–Palade bodies (WPBs) [84]. PIP_2 also recruits other apical carriers such as Annexin 2 and PTEN that can locally modify the AMIS to provide a molecular landing pad to tether and dock incoming vesicular traffic [86, 87].

What vesicular cargo is destined to be delivered to the apical membrane during vascular lumen formation(?), and what are the carriers? Definitive studies focusing on post-Golgi carrier's involvement in AMIS formation and downstream lumen biogenesis are almost completely absent in ECs; however, there is abundant literature detailing proteins that generally affect lumen formation. Podocalyxin is a well-characterized glycoprotein that is one of the first proteins to be transcytosed from the basal surface to the AMIS where it complexes with NHERF1/Ezrin [88]. Podocalyxin is required to initiate cell–cell deadhesion during lumen biogenesis and maintain proper barrier function in ECs [89-92]. As such, podocalyxin is not only regarded as one of the first

proteins to be trafficked to the apical membrane, but also a proxy for other required glycoproteins that are delivered at the same time. Although, podocalyxin has been shown to be trafficked by Slp2a, Slp4a, Rab27a, Rab35, Rab8a, Rab11a and others in epithelial cells [45,93], it is still an outstanding question in endothelial biology. Our data, and others, have demonstrated that Slp2a, Slp4a, and Rab27a have been allocated to WPB trafficking in ECs [83,84,94]. Additionally, our unpublished data investigating Rab35, demonstrates that Rab35 is an actin regulator, further signifying disparities between epithelial and endothelial trafficking of podocalyxin. In 2D culture ECs, it has been shown that podocalyxin colocalized with the early endosome marker Rab5 and Rab25 [95]; potentially suggesting a non-Rab11a endocytic or recycling route. As this was a peripheral finding by this group, this association has yet to be confirmed with further experimentation. To our knowledge, there is no singular publication that has comprehensively detailed post-Golgi carriers for podocalyxin in endothelial tissue, and by extension, other important apically targeted glycoproteins. Juxtaposing this finding with epithelial cells highlights the disparity in trafficking-related literature as podocalyxin has been comprehensively investigated in epithelial cyst development.

In the absence of directed ECs studies, we can only speculate as to how apical targeting occurs, leveraging the existing epithelial literature. Many apically targeted proteins such as receptors and sialomucins are heavily glycosylated. This commonality of apical cargo with an inherent heterogeneity of protein domain structures and trafficking-related binding motifs has moved the field away from the idea that every apically targeted protein contains a unique motif that is then recognized by a singular Rab or related effector that would be solely responsible for the delivery of the cargo. Rather, what has

come to light more recently is that addition of carbohydrate groups in the acidic TGN can promote oligomerization of apical cargo allowing for a more non-targeted, bulk recognition of this class of proteins by apical carriers [96]. The center piece of this argument is that neutralization of the TGN pH greatly diminishes the delivery of apical cargo, notably glycoproteins such as podocalyxin and p75 [97, 98]. Consequently, the question of what specific Rab may transport podocalyxin is less relevant, but then becomes, what Rab may be responsible for transporting a group of glycoproteins to the AMIS that includes podocalyxin? Rab8, Rab6, and Rab10 have all been implicated as TGN carriers [99,100], most of which have not been investigated for a role in vascular lumen development. Equally intriguing is the hypothesis that the TGN could play a more regulatory part in staging a bolus release of glycoproteins during lumen formation by differentially regulating its acidity. To this end, the GEF GBF1 has been shown to selectively modulate Golgi transport of anterograde trafficking WPB components in ECs; although its effect on the TGN, per se, has not been tested [101]. This type of signaling could be a developmental control lever for apical membrane-related trafficking; further studies on networks that regulate the aperture of flow through the Golgi are needed. Generally, there are many more questions than answers in the vascular lumen development field. Overtime, it will be interesting to know which programs will display unique organotypic signatures or will be shared between various tissue systems as these trafficking networks are mapped.

Blood Vessel Stabilization

Central to blood vessel stabilization is the Notch signaling pathway [102]. Although each Notch receptor (1–4) is present in the vasculature, Notch1 is the predominant

receptor involved in angiogenesis [102]. ECs with elevated Notch activation adopt a stalk cell phenotype, whereas ECs deficient in Notch signaling will assume a tip cell identity. Notch1 itself, is a transmembrane protein composed of an extracellular domain (NECD) and an intracellular domain (NICD). Importantly, the NECD is composed of 36 epidermal growth factor (EGF) repeats and a negative regulatory region (NRR). The NRR contains three Lin-12-Notch (LNR) repeats that interact with a heterodimerization domain (HD) [103,104]. Obscured within the interaction between LNR and HD at a resting state is a cleavage site (termed S2). When exposed, the S2 cleavage site is cut by a disintegrin and metalloprotease (ADAM) complex [105]. This cutting event on the S2 extracellular domain precedes cleavage by γ-secretase at the S3 cleavage site to release the NICD. Once freed, the NICD translocates to the nucleus, binding the transcription factor RBPJ/CSL to upregulate downstream genes that promote lateral inhibition [106]. This mechanism necessitates the need for a mechanical force generated by the Notch ligand, Delta-like ligand 4 (Dll4). In this case, Dll4 is presented by the tip cell which pulls on the Notch1 receptor exposing the S2 and downstream S3 domains for cleavage and activation.

How this pulling force is generated is hypothesized to be derived from several scenarios. First, natural cell movement from a leader or tip cell could account for tension needed to separate the LNR and HD domains. Second, and the most reported mechanism, is that upon ligand binding is that Delta undergoes CME (Figure 3). Two investigations focusing on Dll1 and Notch pulling reported that any perturbation to the CME pathway significantly dampened Notch activation. Using optical tweezers, both groups independently demonstrated that blockade of CME machinery such as epsin, AP-2 or

dynamin significantly reduced the pulling force on bead-tethered NECD bound to Dll1 [107,108]. In endothelial cells, our group demonstrated that CME does not seem to affect Dll4 transcytosis, and presumably pulling forces [109]; thus, it is possible that Dll4 endocytosis is intrinsically different than Dll1, or simply divergent in endothelial tissue. In general, there are currently few studies that have directly looked at Dll4 endosomal pulling forces and Notch activation in endothelial tissue.

With regard to Dll1, it has been shown that Dll1 endocytosis does not require ubiquitination, but ubiquitination is necessary for its recycling back to the plasma membrane and efficient interaction with Notch1 [110]. There is some controversy as others have shown that Dll1 requires ubiquitination to be endocytosed when employing epsin [110]. Regardless, Dll1 has been purported to be contained by a Rab11a recycling loop prior to binding with NECD [111]. Very little has been published directly mapping endothelial-specific Dll4 endocytic mechanisms. Adams, et al., demonstrated that synaptojanin-2 binding protein can interact with Dll4 via PDZ binding [112]. In this study, it was hypothesized that synaptojanin-2 binding protein protected Dll4 from lysosomal degradation. Plasma membrane recycling of the other Notch ligand Jagged has been shown to be regulated, in part, by the intermediate filament vimentin [113]. In a more recent investigation, it was reported that Numb acts as a Notch antagonist by controlling the intracellular destination and stability of Dll4 through a post-endocytic-sorting process [114]. Furthermore, Numb negatively controlled the Dll4 plasma membrane recycling through AP1. Given Dll4 is plugged into a Rab11a recycling pathway, it is likely there are other uncharacterized trafficking factors that usher the post-Golgi transport of Dll4 from the TGN to the plasma membrane.

Several reviews on Notch trafficking exist that cover the exocytic and endocytic pathways employed in non-vertebrate organisms [111,115]; however, in endothelial tissue very little has been published on how Notch is sorted to the plasma membrane or degraded following ligand binding. In other systems, it has long been known that the Notch receptor is ubiquitinated prior to its removal from the plasma membrane [116,117]. A proteomic approach identified a de-ubiquitinase called USP10 that functions as an NICD1 de-ubiquitinase, capable of fine-tuning endothelial Notch responses during angiogenic sprouting [118]. Depletion of USP10 reduced NICD1 abundance and stability and diminished Notch-induced target gene expression in ECs in vitro and in vivo. In a separate investigation, it was shown that RHOQ is essential for the NICD nuclear translocation. The authors report that in the absence of RHOQ, Notch1 becomes targeted for degradation in the autophagy-lysosomal pathway [119]. Testing the interplay between Dll1 and Notch in *Drosophila* neurogenesis, it was found that Dll1 expression induces a quick degradation of Notch in late endosomes. Thus, intracellular trafficking of Notch orchestrates the temporal dynamics of Notch activity [120]. Indeed, it would be interesting to speculate that mechanisms like USP10 are conserved across other Notch pathways. Lastly, it was recently demonstrated how lipid components can interact with Notch trafficking. Shimizu, et al., reported that PI3K-C2α is required for the CME of the γ-secretase complex, which allows for the cleavage of endocytosed Notch1 to generate NICD1 in ECs [121]. Overall, there are many unexplored opportunities to further characterize how both Dll4 and Notch are endosomally and exosomally sorted in endothelial tissue, thereby controlling blood vessel stability and homeostasis.

Secretion in Angiogenic Development

Due to the endothelium's role as the primary barrier between the blood constituents and the neighboring tissue, ECs secrete wide swathes of molecules both during development and in adult homeostasis. For the purposes of this review, we will focus on recent reports detailing apical secretion events related to angiogenic blood vessel development. A well-known endothelial-specific secretion mechanism is those that employ WPBs. WPBs are cigar-shaped secretory granules that are primarily found within the endothelium. The most predominant protein housed in this structure is pro-thrombotic von Willebrand factor (VWF), a large multimeric protein capable of initiating the clotting cascade [122]. WPBs are formed at the acidic trans-Golgi and produce their unmistakable shape through folding VWF into a cylindrical structure [123] (Figure 5). Several reviews go into great depth regarding WPB biogenesis, general trafficking patterns and role in hemostasis referenced here [124-126]. The interesting biology pertaining to WPBs is that their generalized function is entirely contingent on intracellular trafficking.

WPBs have been shown to play other non-clotting related roles required for blood vessel formation. In addition to VWF, more than 183 other proteins have been shown to be associated with WPBs ranging from interleukins to cell surface lectins [127]. The tremendous plasticity of cargo constituents is related to WPBs being a lysosome-related organelle; thus WPBs can be functionally grouped with other structures such as multi-vesicular bodies, melanosomes and secretory lysosomes that regularly intermingle with many other trafficking compartments [128]. Transmission electron microscopy of WPBs shows intraluminal vesicles that contain factors such as CD63, suggesting post-Golgi fusion events can also change the cadre of WPB-house proteins [129]. This finding is

exciting as this data suggests the WPB secretory payload could be tailored to match a developmental or homeostatic condition [130].

In angiogenesis, a protein called angiopoietin-2 (Ang2) is secreted via WPB exocytosis. Ang2 can work in both an autocrine and paracrine fashion binding to the Tie-2 receptor. Angiopoietin-1 (Ang1) is outcompeted by Ang2, thus Ang2 was purely considered an Ang1 antagonist [131]. However, more recent evidence has demonstrated that Ang2 can play dual roles in both promoting and repressing blood vessel development [84,132,133]. Our lab recently discovered that WPB-mediated exocytosis requires a protein called Slp2a [84]. In the absence of Slp2a, WPBs are still capable of trafficking to the apical membrane, but are not able to fuse, blocking release of WPB cargo. Blockade of WPB-mediated release of Ang2 reduced lumen biogenesis as mentioned above. It is possible the proangiogenic factors galectin-1 or galectin-3 [134,135] which are also housed in WPBs were mis-trafficked in the absence of Slp2a; however, this was not tested. Other investigations have reported similar findings in which Rab27a, MyRIP, syntaxin-3, synaptotagmin-5, synaptotagmin-like protein-4a, VAMP8, Rab15, Rab33, Rab37, and Rab3d also significantly altered WPB secretion dynamics [94,136-139]. Of note, the vast majority of the WPB-related trafficking regulators have yet to be tied back to perturbations in angiogenesis, as all studies were primarily conducted in endothelial cells on a 2-dimensional culture dish. Our groups more recent work looking at WPB trafficking in 3-dimensional models both highlight the trafficking and downstream angiogenic ramifications when WPB pathways are perturbed [83].

Future Directions and Challenges

In a bulk comparison between epithelial and endothelial studies related to characterizing general trafficking signatures, it is easy to see how little we really understand about how endothelial trafficking events are orchestrated and con- tribute to physiological and pathological blood vessel development. As mentioned above, a potential reason for this is that epithelial cells exhibit a stereotyped rectangular shape and spatially segregated apical and basal domains allowing for relatively easy imaging of processes at either membrane. Additionally, epithelial cells readily set up apicobasal polarity in 2D culture, thus do not require much in the way of physical or chemical cues to elicit a defined polarity axis [14]. In 2D culture, removed from a sprouting structure, endothelial cells on a dish do not show a commitment to an apical or basal membrane identity. Moving forward, testing 3D sprouting models that provide the necessary cellular cues to reproduce angiogenic morphodynamics with ample sub-cellular imaging will be imperative. Likewise, engineering novel transgenic animals to both visualized vesicular sorting in endothelial cells as well as classic loss and gain of function platforms would significantly aid in our efforts towards identifying novel blood vessel trafficking signatures. Overall, the arena of trafficking-based regulation in endothelial tissues is vast with relatively few full-time occupants. This provides a fantastic research opportunity for truly novel discoveries pertaining to blood vessel biology as well as potential disease therapeutics. We hope to spark many more conversations in the realm of endothelial trafficking as it's clear that endosomal sorting plays a critically important role in all aspects of blood vessel biology.

Chapter Two: Rab27 Regulates Weibel-Palade Body Cargo, Ang-2, Trafficking Through Synaptotagmin-like Protein 2a

3.1 Introduction

During development, new blood vessels emerge from preexisting vasculature, a process termed angiogenesis [140-142]. During this time, endothelial cells (ECs) form a hollow opening or central lumen. Vascular lumen formation can be roughly broken into 3 phases: (1) formation of a common cell-cell interface; (2) establishment of an apical membrane initiation site at the specific cell-cell interface promoting membrane deadhesion; and (3) lumen expansion. First, cadherin and integrin-binding provide the initial cues for apical-basal polarity signaling in ECs [143,144]. Thereafter, cell-cell adhesions localize laterally to allow for separation between neighboring cells [145,146]. Concurrently, the apical membrane initiation site located on the luminal membrane serves as a hub for asymmetrical intracellular protein delivery to the maturing apical membrane. These apical membrane initiation site trafficking events are responsible for delivering factors that cause deadhesion of opposing cell membranes as well as substantial cell shape changes leading to lumen cavity enlargement during angiogenesis [147-149]. For example, trafficking of sialomucin-laden glycoproteins, such as podocalyxin and CD34, to the apical membrane are required for lumen formation across multiple developmental models [147,148,150]. Precise trafficking of proteins to the maturing apical membrane

are paramount to its biogenesis; however, what factors are involved in regulating trafficking during this critical period of vascular lumen formation are incompletely understood. Slp2a (synaptotagmin-like protein 2a), also called exophilin-4, is a phospholipid-binding protein with high affinity for the apically enriched phospholipid, phosphotidylinositol4,5 bisphosphate (PIP2) [151]. Characteristic of synaptotagmin family members, Slp2a interacts with phospholipids via its tandem C2 domains, C2A and C2B. Additionally, Slp2a's Rab-binding domain provides interactions with Rab GTPases towing specific vesicle populations [152]. Existing evidence, based largely on studies in epithelia and melanocytes, indicates Slp2a principally binds Rab27a [153-156]. In ECs, Rab27a has been reported to decorate Weibel-Palade Bodies (WPBs), a prothrombotic secretory granule, and negatively regulate its exocytic activity [157]. Rab27a has also been shown to influence recycling of vascular-endothelial growth factor receptor 1 [158]. In epithelium, Slp2a has been reported to tether podocalyxin-rich vesicles via Rab27a binding in cooperation with its family member Slp4a (synaptotagmin-like protein 4a) to promote lumen formation [154]. Slp2a has yet to be investigated in any aspect of blood vessel development.

In this report, our aim was to characterize Slp2a's function during sprouting angiogenesis, with emphasis on its putative role in lumen formation. Our results demonstrate that Slp2a is required for vascular lumen formation in developing endothelial sprouts. We determine that in ECs, Slp2a is resident at the apical membrane during lumen initiation and expansion downstream of PIP2 lipid binding. Interestingly, deletion of the PIP2 interacting domains localized Slp2a exclusively to WPBs. We show that Slp2a is one of the most upstream components required for WPB secretion.

Mechanistically, we determine that loss of Slp2a impedes Ang-2 (angiopoietin-2) secretion resulting in inhibited Tie-2 autocrine signaling, preventing lumen formation. Overall, our results demonstrate a novel role of Slp2a in regulating exocytic trafficking at the apical membrane and, in doing so, controlling Ang-2 release during blood vessel lumen formation.

3.2 Materials and Methods

Cell Culture

See Annex A.

Sprouting Angiogenesis Assay

See Annex A.

Plasmid Constructs

See Annex A and Table 6.

Lentivirus Generation and Transduction

See Annex A.

Immunoblotting and Protein Pull-Down

See Appendix A.

Immunoflourescence and Microscopy

See Appendix A.

Zebrafish Transgenics

The transgenic lines used in this study include Tg(kdrl:GFP) and Tg(kdrl:mCherry). Tol2- mediated transgenesis was used to generate mosaic intersomitic blood vessels as previously described [140-143]. Briefly, Tol2 transposase mRNA were synthesized

(pT3TS-Tol2 was a gift from Stephen Ekker, Addgene plasmid # 31831) using an SP6 RNA polymerase (mMessage mMachine, ThermoFisher). A total of 400ng of transposase and 200ng of plasmid vector were combined and brought up to 10μL with phenol red in ddH2O. The mixture was injected into embryos at the 1-2 cell stage. Injected zebrafish were screened for mosaic expression at 48 hpf and imaged. CRISPR/cas9-mediated knockouts were performed as previously described [145]. Briefly, equal volumes of chemically synthesized AltR® crRNA (100 μM) and tracrRNAr RNA (100 μM) were annealed by heating and gradual cooling to room temperature. Thereafter the 50:50 crRNA:tracrRNA duplex stock solution was further diluted to 25 μM using supplied duplex buffer. Prior to injection 25 μM crRNA:tracrRNA duplex stock solution was mixed with 25 μM Cas9 protein (Alt-R® S.p. Cas9 nuclease, v.3, IDT) stock solution in 20mM HEPES-NaOH (pH 7.5), 350mM KCl, 20% glycerol) and diluted to 5μM by diluting with water. Prior to microinjection, the RNP complex solution was incubated at 37oC, 5 min and then placed on ice. The injection mixture was micro-injected into 1-2 cell stage embryos. Confirmation of CRISPR-mediated gene knockout was validated by RT-PCR. Approximately 20 embryos at 48 hpf were homogenized and dissolved in TRIZOL reagent (Sigma Aldrich) according to the manufacturer's instructions. Reverse transcription was achieved by using the Biosystems High-Capacity cDNA Reverse Transcription Kit (ThermoFisher) and then PCR was used with relevant controls (See table 1.1 for DNA oligos and sgRNA sequences used) to determine transcript levels. Crispant DNA was retrieved via PCR and subjected to sanger sequencing to visualize indel formation.

Zebrafish Microangiography

See Appendix A.

Zebrafish Live Imaging and Quantification

See Appendix A.

Statistical Analysis

Experiments were repeated a minimum of 3×. Statistical analysis and graphing was performed using GraphPad Prism. Statistical significance was assessed with a Student unpaired *t* test for a 2-group comparison. Multiple group comparisons were performed using a 1-way ANOVA followed by a Dunnett multiple comparisons test. Data was scrutinized for normality using Kolmogorov-Smirnov test. Zebrafish sex distribution was not adjusted as sex determination did not occur at the stage of development in which the specimens were assayed. Statistical significance set a priori at $P<0.05$.

3.3 Results

Slp2a Is Apically Localized and Required for Lumen Formation In Vitro

We first sought to determine Slp2a's localization and function in vitro given its spatial organization in vascular sprouting was not previously characterized. To do so, we transduced an mCherry-tagged Slp2a virus into primary ECs in a 3-dimensional (3D)-sprouting assay that closely mimics in vivo sprouting angiogenesis (Figure 6A) [159,160]. Here, ECs are coated onto microcarrier beads, embedded in a fibrin matrix, and allowed to sprout for 4 to 5 days. Transduced ECs were stained for the junctional marker vascular-endothelial cadherin to identify cell-cell interfaces as well as moesin and podocalyxin to delineate the apical membrane (Figure 6B). Before lumen formation, Slp2a heavily colocalized with all three proteins at cell-cell junctions (Supplemental

Figure 1A). However, in sprouts with an established lumen opening, Slp2a was only located on the apical membrane, strongly colocalizing with apical markers moesin and podocalyxin but distinct from vascular-endothelial cadherin at cell-cell interfaces (Figure 6B). These results indicate that Slp2a is preferentially localized to the apical membrane before and throughout lumen formation, consistent with reports in epithelial tissues [154]. Slp2a's C2AB domains are purported to bind PIP_2, a well-known apical lipid species [152,154,161]. We confirmed this interaction in ECs using a PIP_2 biosensor (PH-GFP) in which Slp2a and PH-GFP dynamically colocalized at junctions in 2D culture (Supplemental Figure 1B, C) [162]. Overall, these results demonstrate that Slp2a is resident at the apical membrane downstream of binding to PIP_2.

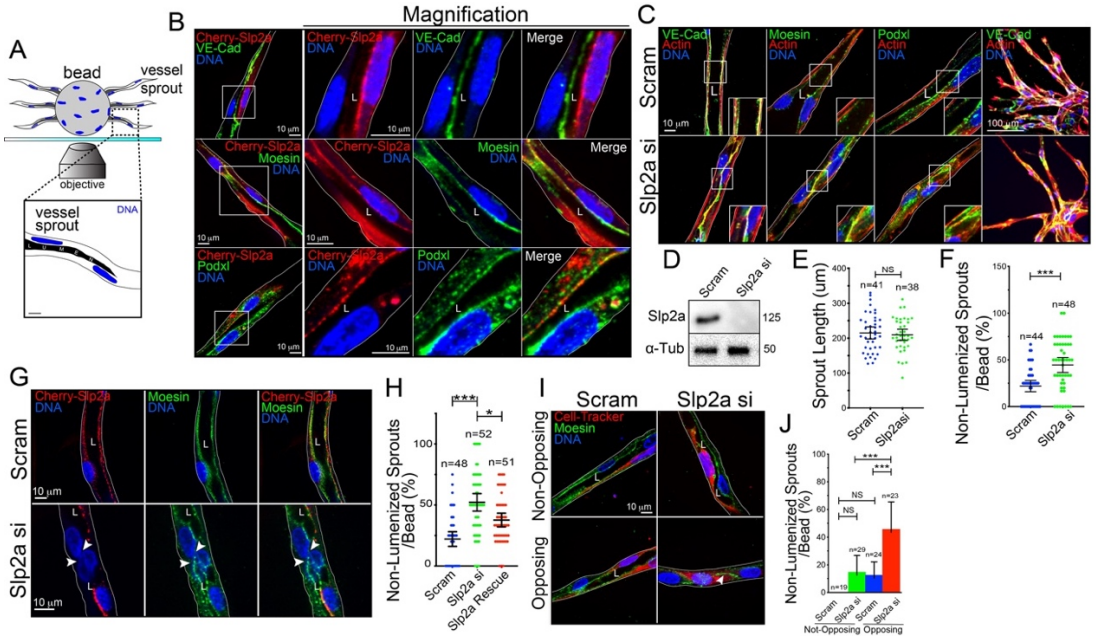

Figure 6: Slp2a (synaptotagmin-like protein-2a) is an apically localized protein required for sprout formation. A. Cartoon model of 3-dimensional sprouting assay denoting imaging setup. B. Localization of transduced mCherry (Cherry)-Slp2a during lumen formation in sprouts stained for VE-Cadherin (VE-Cad), moesin, and podocalyxin (Podxl). C. Images of Slp2a siRNA (si) knockdown and scramble (scram) control sprouts stained for indicated proteins. D. Representative confirmation of Slp2a siRNA-mediated knockdown by Western blot probed for Slp2a and α-Tub (α-tubulin). n=3 individual

Western blot experiments. E. Quantification of sprout length for indicated groups. F. Quantification of nonlumenized sprouts between indicated groups. G. Mosaic rescue experiment in which cells were treated with indicated siRNAs and transduced with Cherry-Slp2a (red). Arrows indicate a lack of lumen in addition to a lack of Cherry-Slp2a expression. H. Quantification of percent nonlumenized sprouts between indicated groups. I. Mosaic knockdown experiment in which cells were treated with Slp2a siRNA (red) and then mixed with scramble-treated cells (nonfluorescent) and then challenged to sprout. Top row depicts nonopposing siRNA-treated cells. Bottom row depicts opposing siRNA-treated cells. Arrow denotes a lack of lumen. J. Quantification of mosaic KD sprouts with percent nonlumenized sprouts. All experiments used human umbilical vein endothelial cells. In all parts, L denotes lumen; white box denotes magnification; white lines denote exterior of sprout; values are means±SEM; n=individual sprouts across 3 experimental repeats; NS indicates not significant; significance: *P<0.05 and ***P<0.0005. Statistical significance was assessed with an unpaired t test or a 1-way ANOVA followed by a Dunnett multiple comparisons test.

We next asked if Slp2a played a role in angiogenic sprouting and lumen formation via loss of function using siRNA knockdown. Morphologically, Slp2a knockdown did not alter migration programs as sprout lengths were unaffected (Figure 6E); however, the sprouts were visibly thinner in appearance compared with controls (Figure 6C, D and Supplemental Figure ID). To investigate this phenotype, we quantified the percentage of non-lumenized sprouts (sprouts with no discernable, or contiguous, lumen cavity). We determined that loss of Slp2a significantly increased the percentage of non-lumenized sprouts compared with controls (Figure 6F). We next performed a rescue experiment by mosaically overexpressing mCherry-Slp2a on a Slp2a knockdown background to further examine if Slp2a deficiency was underlying the lack of lumen formation. ECs expressing mCherry-Slp2a exhibited a significant increase in lumen formation compared with non-transduced controls (Figure 6G, H). In a similar approach, we tested if loss of Slp2a was cell autonomous in terms of its impact on lumenogenesis. To do so, we knocked down Slp2a in a population of ECs that were then labeled with red CellTracker. This population was mixed with scramble siRNA-treated ECs and challenged to sprout. We observed that

in Slp2a knockdown ECs opposite wild-type (WT) a lumen opening was maintained, albeit small; while 2 opposing knockdown ECs failed to create a luminal cavity (Figure6I, J). These results suggest that Slp2a is cell autonomous and required for lumen formation in vitro.

Slp2a Interacts with WPBs

To better understand the mechanism(s) by which a Slp2a deficiency results in lumen defects, we employed two Slp2a domain mutants: (1) a deletion of the PIP_2 binding C2AB domains (Slp2a-ΔC2AB) and (2) expression of only the C2AB domains (Slp2a-C2AB; Figure 7A). In a mosaic rescue assay, both mCherry-Slp2a-ΔC2AB and mCherry-Slp2a-C2AB mutants were transduced into sprouts on a Slp2a siRNA knockdown background. Neither mutant proved capable of rescuing lumen abnormalities (Figure 7B-D), suggesting both domains are required for Slp2a to function properly during vascular lumen formation. Upon further inspection, the Slp2a-C2AB mutant localized largely to the apical membrane similar to WT Slp2a in lumenized sprouts. Conversely, the mCherry-Slp2a-ΔC2AB mutant no longer localized to the apical membrane, but decorated rod-like puncta that strongly colocalized with VWF, a well-established WPB marker (Figure 7E and Supplemental Figure 2A) [157]. We next determined if the Slp2a-ΔC2AB-decorated WPBs showed any localization preference during the lumenization process. The Slp2a-ΔC2AB–decorated WPBs exhibited a heightened cytoplasmic distribution in non-lumenized sprouts. However, in sprouts with a defined lumen, the Slp2a-ΔC2AB–decorated WPBs, preferentially localized to the apical membrane (Figure 7F, G and Supplemental Figure 2B,C). Taken together, in the absence of membrane

binding, Slp2a's default localization is on WPBs that are being actively transported to the apical membrane during lumenogenesis.

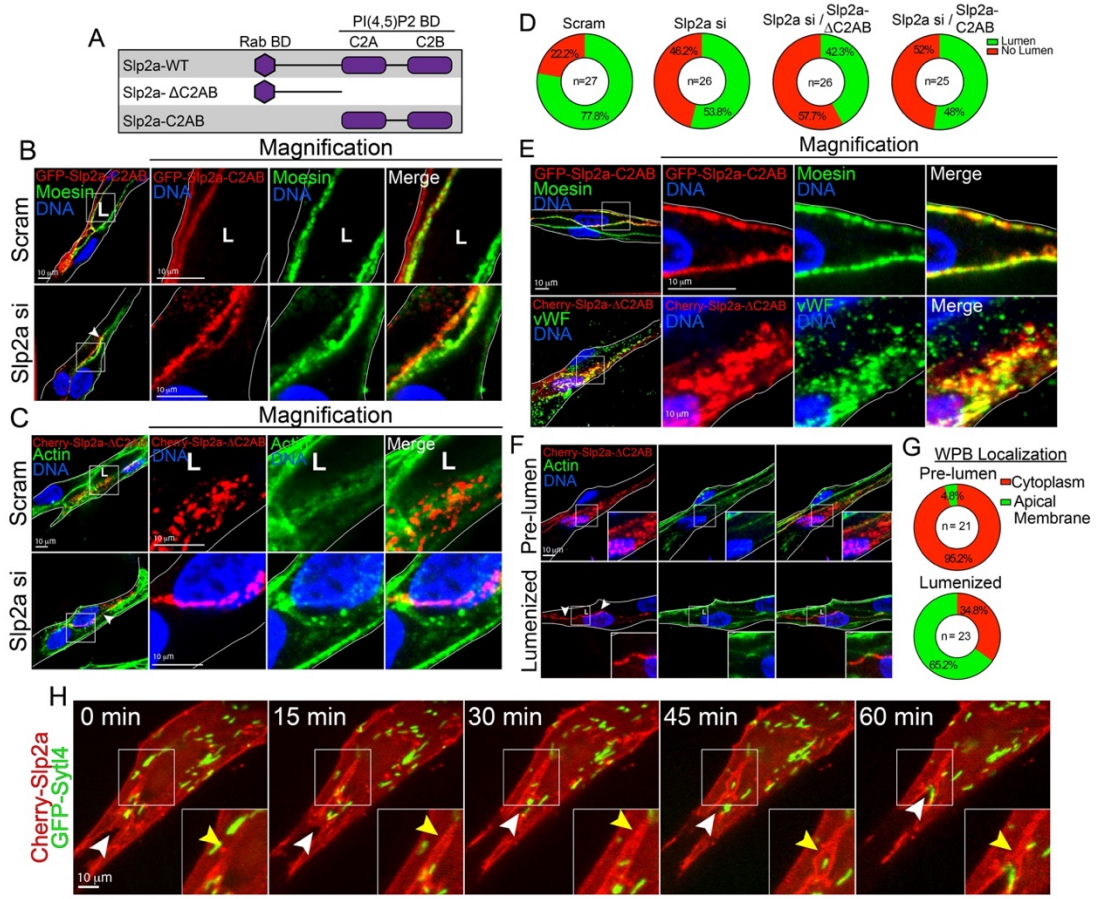

Figure 7: Slp2a (synaptotagmin-like protein-2a) lacking C2 domains localizes to Weibel-Palade bodies. A. Cartoon model of Slp2a domains and mutants used for experimentation. Slp2a-ΔC2AB lacks 2 phospholipid-binding C2 domains. Slp2a-C2AB mutant lacks the Rab-binding domain as well as residues linking it to the C2AB domains. B. GFP (green fluorescent protein)-Slp2a-C2AB expressing in both scramble (scram) and Slp2a siRNA(si) knockdown groups and stained for indicated proteins. Arrow indicates lack of lumen. C. MCherry(Cherry)-Slp2a-ΔC2AB expressing in both scramble and Slp2a siRNA knockdown groups and stained for indicated proteins. Arrow indicates lack of lumen. D. Quantification of lumen formation of individual sprouts. Cells were treated with scramble or Slp2a siRNA and then infected with indicated constructs. Green represents lumen formation, and red represents non-lumenized sprouts. N value represents individual sprouts across 3 experimental repeats. E. GFP-Slp2a-C2AB and Cherry-Slp2a-ΔC2AB expressing in sprouts stained for moesin and with Weibel-Palade body (WPB) marker, VWF (von Willebrand factor). F. Localization of Cherry-Slp2a-ΔC2AB before lumen opening (pre-lumen, top) and after lumen opening (lumenized,

bottom). Arrows indicate heavy localization at the apical membrane. G. Quantification of Cherry-Slp2a-ΔC2AB localization pre-lumen and during lumenogenesis (lumenized). N value represents individual sprouts across three experimental repeats. H. Live imaging of mCherry-Slp2a-wild-type (WT) and GFP-Slp4a-WT. Yellow arrow identifies future lumen expansion and white arrow indicates open lumen. All experiments use human umbilical vein endothelial cells. In all parts, L denotes lumen; white box denotes magnification.

Slp4a has previously been reported to interact with Slp2a in epithelial cells [154]. In endothelium, Slp4a is reported to decorate WPBs but has not yet been functionally linked to Slp2a [163]. To determine if Slp4a interacted with Slp2a, we expressed both family members at the same time. Slp2a and Slp4a exhibited disparate localization patterns; Slp2a maintained its localization at the apical membrane, while Slp4a resided on WPBs (Supplemental Figure 3A, B). Similarly, live imaging of Slp2a and Slp4a in 3D sprouts revealed that areas of lumen formation were decorated by Slp2a, while Slp4a-positive WPBs trafficked to the apical membrane, presumably for exocytosis of WPB secretory granules into the luminal space (Figure 7H). Given Slp2a and Slp4a's previous association, we wanted to determine if Slp4a played a role in lumen formation. Knockdown of Slp4a did not affect sprouting or lumen formation parameters (Supplemental Figure 3C, D). These data suggest that Slp2a is distinct from Slp4a in its localization and role in lumen formation.

Slp2a Binds Rab27a Resident on WPBs

Rab27a has been shown to directly bind Slp2a in other systems as well as in ECs [152,154,157]. To test if this was true in our model, we overexpressed a GFP-tagged Rab27a construct. Overexpression of WT Rab27a in 2D culture produced colocalization with WT Slp2a at discrete puncta, while Slp2a was also located at the membrane (Figure 8A). Slp2a-ΔC2AB mutant overexpression in 2D strongly colocalized with Rab27a

puncta only (Figure 8A). In 3D sprouts, Rab27a and Slp2a did not show similar localization patterns. Slp2a localized solely to the apical membrane while Rab27a was on WPB puncta and, to some extent, on the apical membrane (Figure 8B). However, expression of Slp2a-ΔC2AB mutant exhibited strong colocalization with Rab27a puncta that were localized to WPBs in sprouts (Figure 8B and Supplemental Figure 4A). We confirmed this direct interaction via immunoprecipitation using a GST (glutathione S-transferase)-tagged Slp2a as bait and detected Rab27a binding (Figure 8C). Next, we performed a mitochondrial mis-targeting assay. Here, a mitochondrial-targeting sequence (Tom20) was added to the N-terminal GFP-tag to unnaturally anchor Rab27a to the outer mitochondrial membrane (Figure 8D) [164]. This allowed us to visualize what proteins or complexes were pulled along with Rab27a to the mitochondria as an intracellular readout for binding interactions. WT Slp2a moderately and the Slp2a-ΔC2AB mutant strongly localized to the mitochondria in ECs expressing Tom20-GFP-Rab27a, suggesting that Slp2a is binding Rab27a (Figure 8E). To determine if this binding was dependent on Rab27a's activation state, either an inactive form (GDP [guanosine diphosphate]) or an active form (GTP [guanosine triphosphate]), we performed the same experiment using a constitutively active (CA, Q78L) and a dominant-negative (L130P) Rab27a mutant [165]. Co-expression of Slp2a-ΔC2AB with Rab27a constitutively active exhibited robust colocalization at the mitochondria, while expression of the Rab27a dominant-negative mutant abolished mitochondrial localization of Slp2a-ΔC2AB (Figure 8E). Overall scoring of Slp2a localization between all above conditions clearly indicated that Slp2a binds Rab27a in a GTP-dependent fashion (Figure 8F). Given Rab27a was located on WPBs, we also probed for VWF to determine if mis-localizing Rab27a also distorted the

spatial distribution of WPB cargo. Mitochondrial-targeted Rab27a demonstrated a mixed phenotype: in some instances, WPBs were mislocalized to the mitochondria; however, in others, WPBs were not mistargeted (Supplemental Figure 4B, C). Overall, this data suggests the Rab27a and Slp2a are robust binding partners.

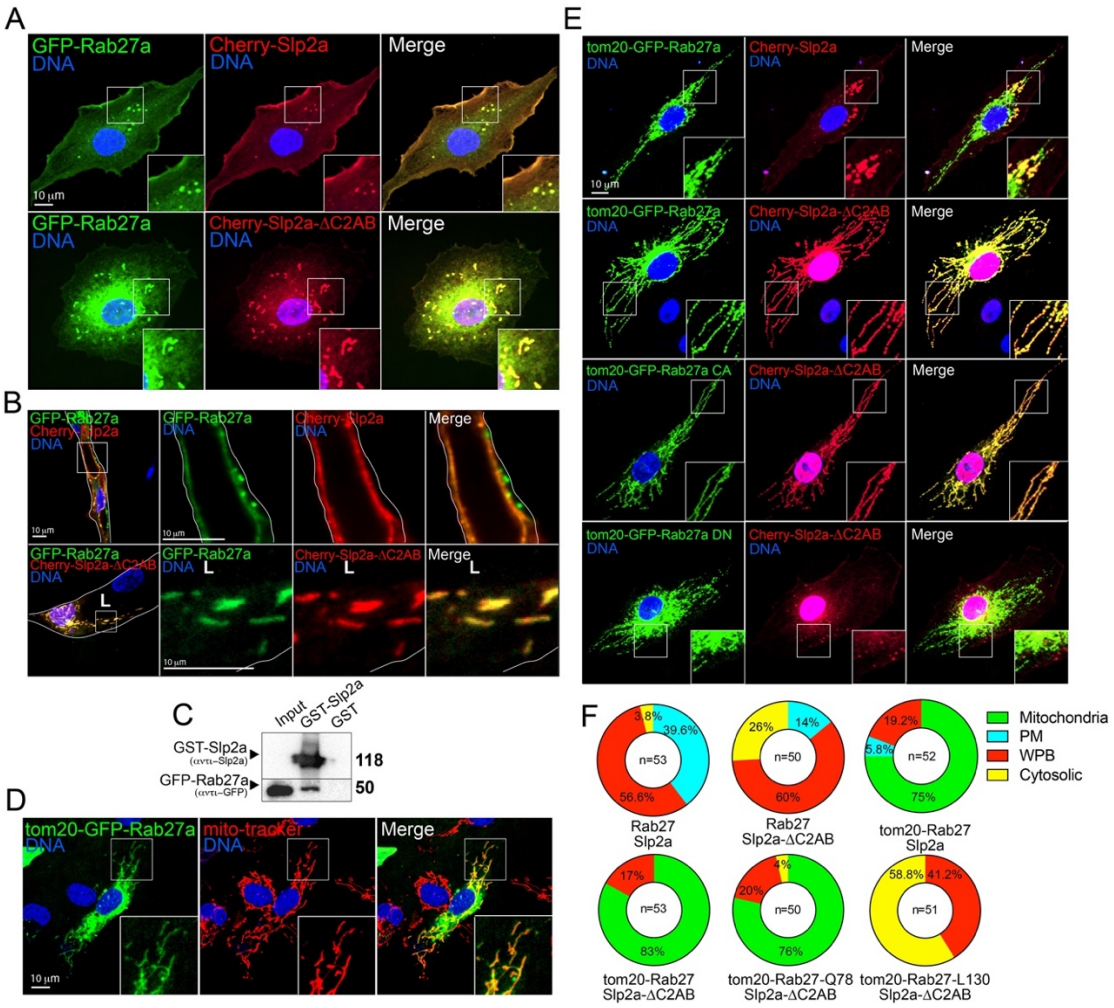

Figure 8: Slp2a (synaptotagmin-like protein-2a) binds Rab27a. A. Two-dimensional (2D) localization of mCherry (Cherry)-Slp2a and GFP (green fluorescent protein)-Rab27a in top. Bottom, localization of Cherry-Slp2a-ΔC2AB and GFP-Rab27a. B. Localization of Cherry-Slp2a and GFP-Rab27a in sprouts (top) and Cherry-Slp2a-ΔC2AB and GFP-Rab27a (bottom). C. Representative image of immunoprecipitation of GST (glutathione S-transferase)-tagged Slp2a and GST (control) proteins used to probe for Rab27a binding. Image is one of 3 experimental repeats. D. Tom20-tagged GFP-Rab27a expressing cells also stained for mitochondria (Mito-tracker). E. Tom20-GFP-Rab27a mis-localization experiments in 2D to test for binding interactions. Rab27a constitutively

active (CA, Q78L) and dominant-negative (DN, L130P) mutants were co-expressed with Cherry-Slp2a-ΔC2AB and Cherry-Slp2a. F. Quantification of localization of Cherry-Slp2a-ΔC2AB and mCherry-Slp2a in each of the 2D experiments presented in E. n=number of individual cells over 3 experimental repeats. All experiments use human umbilical vein endothelial cells. In all parts, L denotes lumen; white box denotes magnification; and white lines denote exterior of sprout. WPB indicates Weibel-Palade body.

Previous studies in nonendothelial tissues have reported that Rab27a transports podocalyxin, a negatively charged glycoprotein shown to be required for lumen formation [147,148,150,166]. Thus, Slp2a may be mediating podocalyxin transport by way of Rab27a. This association could potentially explain why loss of Slp2a results in lumen formation defects. To explore this, we determined the localization of both Rab27a and podocalyxin in lumenizing sprouts. Neither Rab27a or VWF colocalized with podocalyxin, suggesting Rab27a is not interfacing with this protein during vascular lumenogenesis (Supplemental Figure 4D). Additionally, Rab27a knockdown did not affect podocalyxin localization; also suggesting that Rab27a does not transport podocalyxin in ECs (Supplemental Figure 4E).

Slp2a Regulates WPB Exocytosis

Since Slp2a and Rab27a demonstrated direct binding, we next tested whether Rab27a was involved in lumen formation during angiogenic sprouting. In the 3D sprouting assay, siRNA knockdown of Rab27a did not affect lumen formation compared with a Slp2a knockdown (Figure 9A, B). Interestingly, lumen diameter was significantly larger in the absence of Rab27a, whereas ablation of Slp2a in any condition abolished lumen formation resulting in significantly thinner sprouts (Figure 9C). This data suggests that although Slp2a and Rab27a are bona fide binding partners Rab27a does not negatively impact lumen biogenesis during angiogenic sprouting but enhances lumen width.

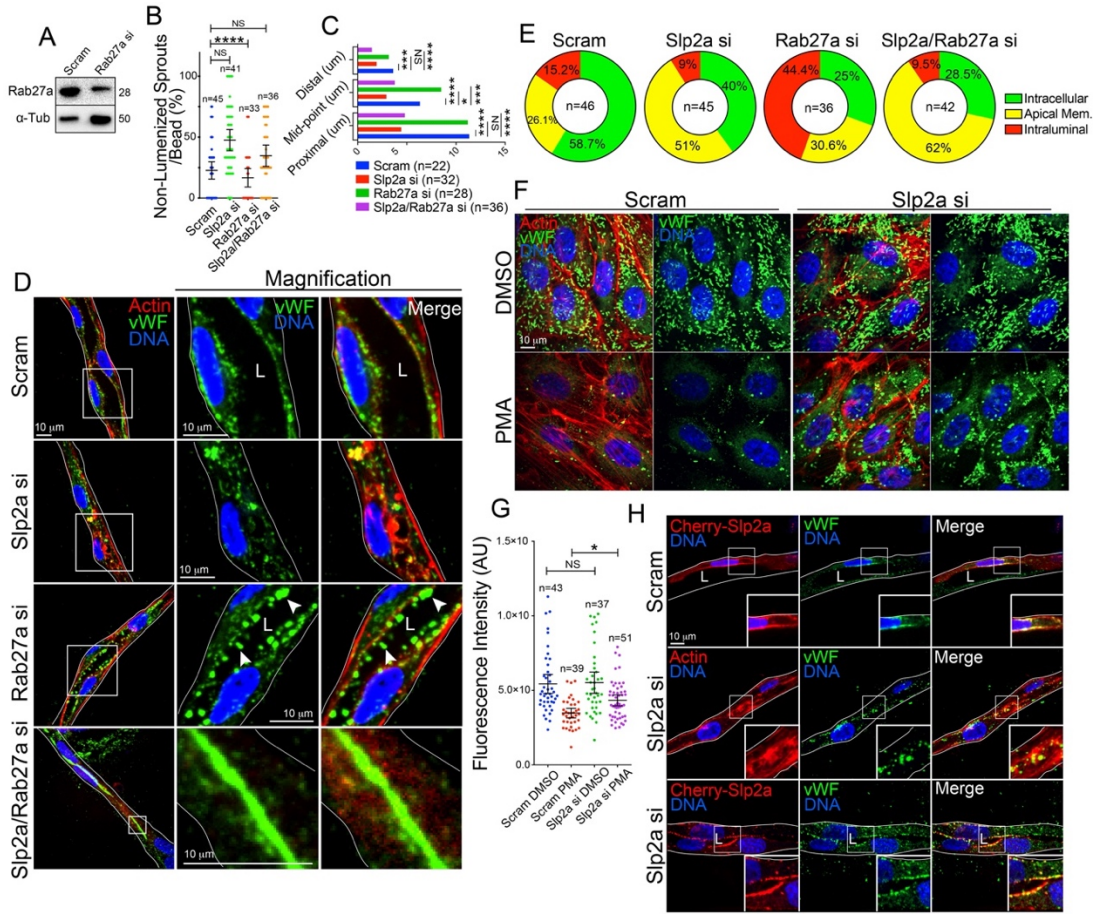

Figure 9: Slp2a (synaptotagmin-like protein-2a) is required for WPB exocytosis. A. Representative Western blot confirmation of Rab27a siRNA (si) knockdown. n=3 individual Western blots. B. Quantification of non-lumenized sprouts in indicated groups. n=individual sprouts over 3 experimental repeats. C. Quantification of lumen diameter at multiple locations within sprouts. Distances were measured proximally, at the midpoint, and distally from the bead. n=individual sprouts over 3 experimental repeats. D. Localization of Weibel-Palade body cargo VWF (von Willebrand Factor), during lumen formation between siRNA-treated groups. Arrows indicate accumulation of VWF within the lumen. E. Quantification of VWF localization in indicated siRNA-treated groups. n=individual cells located in sprouts across 3 experimental repeats. F. Images of phorbol 12-myristate 13-acetate (PMA)- and vehicle (DMSO)-treated cells between indicated groups. G. Quantification of VWF fluorescent intensity between indicated conditions. n=individual cells across three experimental repeats. H. Mosaic rescue effect on VWF localization in sprouts between indicated groups. Cells were transduced with mCherry (Cherry)-Slp2a and treated with indicated siRNA. All experiments use human umbilical vein endothelial cells. AU indicates arbitrary unit; NS, not significant; and α-Tub, α-tubulin. In all parts, L denotes lumen; white box denotes magnification; white lines denote exterior of sprout; values are means±SEM; significance: *P<0.05, ***P<0.001,

****P<0.0001. Statistical significance was assessed with a 1-way ANOVA followed by a Dunnett multiple comparisons test.

Given both Slp2a and Rab27a interact with WPBs, we next tested their respective roles in WPB-mediated exocytosis of VWF in 3D sprouts. As previously shown (Figure 6C-F), loss of Slp2a resulted in a lack of lumen formation, thus there was little-to-no apical space for VWF to be secreted. As such, in Slp2a knockdown sprouts, we observed VWF contained within the cytoplasm adjacent to sites of vacuolation (Figure 9D). In this condition, VWF puncta did not accumulate at interior junctions, the presumptive sites of lumen expansion. By contrast, knockdown of Rab27a resulted in a robust secretion of VWF into the luminal cavity compared with controls (Figure 9D). This finding is in line with previous literature designating Rab27a as a negative regulator of WPB exocytosis, although, this has not been demonstrated in 3D sprouts [163]. Double knockdown of Slp2a and Rab27a resulted in a dramatic accumulation of VWF at cell-cell junctions (Figure 9D, E). As the loss of Slp2a abolished lumen formation, we could not ascertain if the VWF was able to be secreted into the lumen or was trapped in the subapical space. To address this, we performed the same experiment in 2D culture to track VWF secretion. First, we compared phorbol myristate acetate–induced VWF secretion with and without Slp2a knockdown. Loss of Slp2a significantly reduced the ability of VWF to be secreted into the media compared with controls (Figure 9F, G). Histamine-mediated release of VWF was also blunted in the absence of Slp2a compared with controls (Supplemental Figure 5A-C). To further test Slp2a's involvement in VWF secretion, we performed a rescue experiment by overexpressing mCherry-Slp2a on a knockdown background. We observed that ECs overexpressing mCherry-Slp2a were capable of trafficking VWF to

the apical membrane to a greater extent than non-transduced controls (Figure 9H). Overall, these results indicate that Slp2a is likely an upstream regulator of WPB exocytosis.

We next aimed to understand if Slp2a or Rab27a affected each other's localization in 3D sprouts. In other words, is there a dependency between Slp2a and Rab27a for localization to the apical membrane or on WPBs? Loss of Slp2a did not affect Rab27a or Slp4a's localization to WPBs (Supplemental Figure 6A, B). Similarly, knockdown of Rab27a did not affect Slp2a localization to the apical membrane during lumen formation or Slp4a's localization to WPBs (Supplemental Figure 6C, D). To also explore if knocking down either Slp2a or Slp4a altered each other's expression levels, we probed for protein levels. Knockdown of Slp2a did not affect expression of Slp4a and vice versa (Supplemental Figure 6E). Similarly, overexpression of Slp2a-ΔC2AB did not affect levels of Slp4a on WPBs (Supplemental Figure 6F, G). These data indicate that Slp2a does not affect Rab27a and Slp4a's ability to localize to WPBs. In addition, Slp2a localization to the apical membrane is not dependent on Rab27a.

Secretion of Ang-2 is Required for Lumen Formation

Given loss of Slp2a results in elevated non-lumenized sprouts and ablated WPB exocytosis, we postulated that vascular lumenization required the secretion of a WPB-housed factor(s) whose secretion was being controlled by Slp2a. Of the many proteins reported to be contained within WPBs, Ang-2 has been shown to have a proangiogenic effect in certain circumstances by differentially regulating Tie-2 signaling [167,168]. To determine if Ang-2 was resident in the same WPB population that Slp2a decorated, we constructed an RFP (red fluorescence protein) and GFP-tagged version of Ang-2.

Expression of Ang-2 demonstrated strong colocalization with VWF, Rab27a, and Slp2a-ΔC2AB positive WPBs in 2D culture (Figure 10A). Here, we did observe some Slp2a-ΔC2AB puncta that did not colocalize with Ang-2, Ang-2 potentially being in non-WPB cytoplasmic granules (Figure 10B). Interestingly, we also observed that in ECs containing WPBs, Ang-2 was packaged into dense WPB puncta; however, in ECs lacking WPBs Ang-2 was largely scattered throughout the cytoplasm in granular puncta (Figure 10D). This phenotype was not observed in 3D sprouts (Figure 10C, D), suggesting the 3D environment promotes Ang-2 trafficking via the WPB pathway to a greater extent than 2D culture. Next, we investigated when Ang-2 was being released during lumen formation. In sprouts actively forming a luminal surface, there was elevated levels of Ang-2 localized to the apical membrane as compared with sprouts that already established a stable lumen cavity (Figure 10E, F). In total, these data suggest that Ang-2

is housed in Slp2a-decorated WPBs and is targeted to the apical membrane during lumen formation.

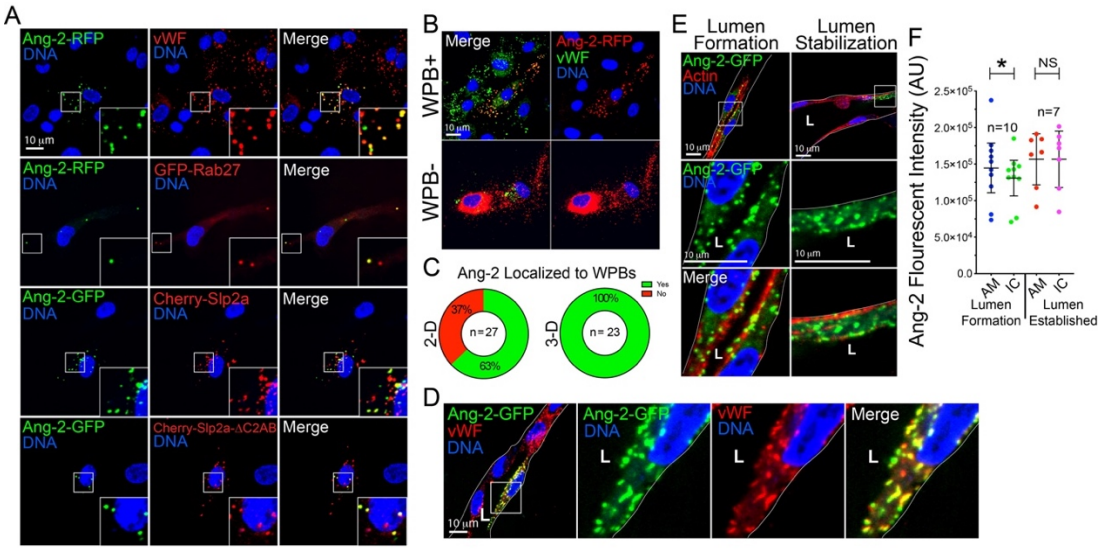

Figure 10: Ang-2 (angiopoietin-2) is housed within Slp2a (synaptotagmin-like protein-2a)-ΔC2AB positive WPBs. A. Ang-2 colocalization experiments in 2-dimensional (2D) culture. Images show localization of Ang-2-RFP (red fluorescence protein), GFP (green fluorescent protein)-Rab27a, VWF (von Willebrand Factor), mCherry (Cherry)-Slp2a, and Cherry-Slp2a-ΔC2AB. B. Ang-2 in cells with and without Weibel-Palade bodies (WPBs) denoted by VWF-positive staining. C. Quantification of Ang-2-GFP localization to WPBs between 2D culture and 3D sprouts. n=localization measurement in individual cells across 3 experimental repeats. D. Ang-2-GFP and VWF localization in 3D sprouts. E. Ang-2-GFP localization at different time points during sprout development. The left are localization during the early stage of lumen formation, and the right are after lumens are established. F. Quantification of Ang-2-GFP localization at different developmental time points. n=intensity measurement in individual cells located in sprouts across 3 experimental repeats. AM indicates apical membrane; AU, arbitrary unit; IC, intracellular; and NS, not significant. n=individual sprouts over 3 experimental repeats. All experiments use human umbilical vein endothelial cells. In all parts, L denotes lumen; white box denotes magnification; white lines denote exterior of sprout; values are means±SEM; significance: *P<0.05. Statistical significance was assessed with an unpaired t test.

To determine if Ang-2 was required for lumen formation, we knocked down Ang-2 in 3D sprouts. Loss of Ang-2 phenocopied Slp2a knockdown in significantly elevating the percentage of non-lumenized sprouts (Figure 11B,C and Supplemental Figure 7A). This

finding also fits our previous result demonstrating Rab27a knockdown did not affect lumen biogenesis, but significantly increased lumen diameter presumably from increased Ang-2 release (Figure 9C, D). Depending on the context, Ang-2 has been shown to both activate Tie-2 signaling or act as an antagonist to Ang-1 limiting Tie-2 activation [168-176]. Staining pTie-2 (phosphorylated Tie-2) revealed strong localization at the apical membrane and at cell-cell junctions in sprouts undergoing active lumen formation (Figure 11A). Loss of Slp2a or Ang-2 significantly reduced pTie-2 activation at the apical membrane (Figure 11D), indicating that Ang-2 is enforcing Tie-2 activation during lumen formation. To investigate if Tie-2 activation was necessary for lumen development, we added the Tie-2 inhibitor Bay-826 on different days during lumen development (Figure 11E, F and Supplemental Figure 7B). Tie-2 inhibition significantly increased the percentage of non-lumenized sprouts on day 1 and day 2 which coincide with the key stages of lumen formation (Figure 11G). However, inhibiting Tie-2 activation on day 3 did not significantly impact lumen development, indicating Tie-2 activation is required for lumen formation, not maintenance. To ensure, Slp2a was controlling Ang-2 release, we assayed for secreted Ang-2 in the culture media. Knockdown of Slp2a reduced the amount of Ang-2 present in the media, suggesting blunted secretion (Figure 11H). Likewise, we assayed the intracellular Ang-2 pool, reasoning that if Slp2a is diminishing secretion there would be increased intracellular retention. Indeed, loss of Slp2a resulted in higher intracellular Ang-2 compared with control (Figure 11I). Overall, our results suggest that Slp2a regulates the release of Ang-2 which is necessary for lumen formation via activation of Tie-2 signaling.

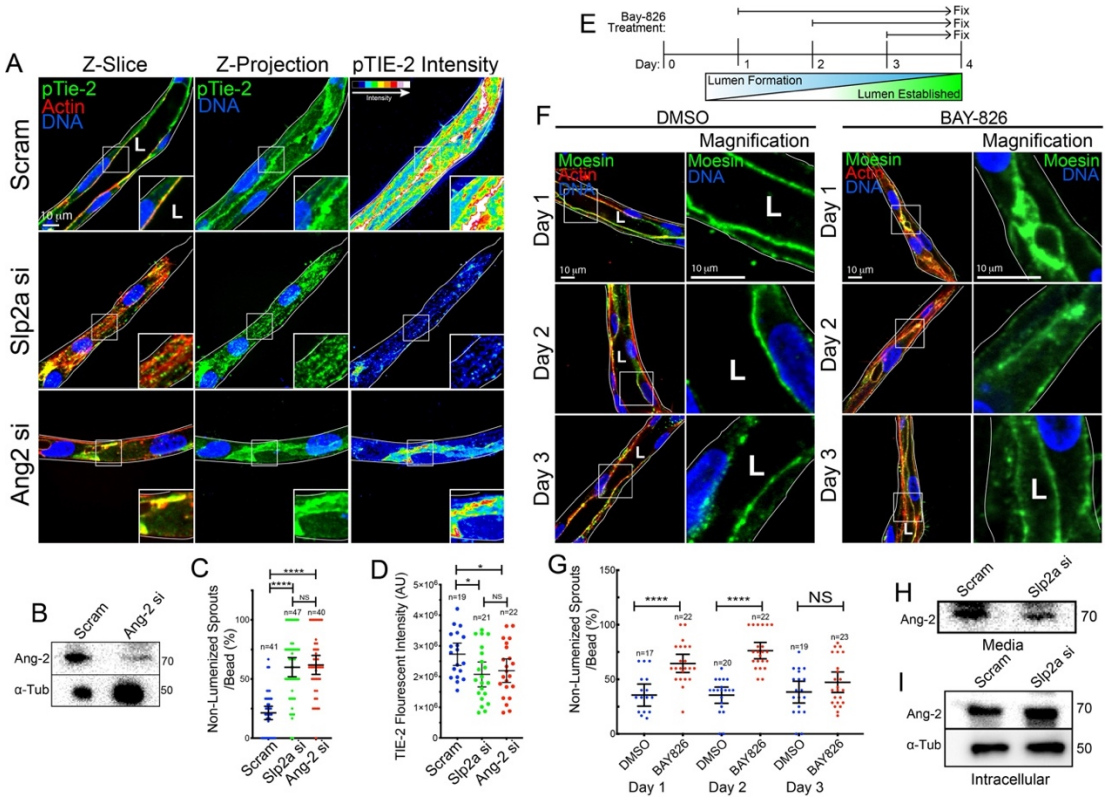

Figure 11: Slp2a (synaptotagmin-like protein-2a) mediates Ang-2 (angiopoietin-2) secretion and downstream Tie-2 signaling during lumen formation. A. Images of scramble (scram), Slp2a, and Ang-2 siRNA (si) knockdown sprouts stained with actin and phosphorylated Tie-2 (pTie-2). Last column pseudo-colored to visualize antibody staining intensity. B. Representative confirmation of Ang-2 knockdown via Western blot probed for Ang-2 and α-Tub (α-tubulin). n=4 Western blots. C. Quantification of percent nonlumenized sprouts between indicated groups. n=individual sprouts across 3 experimental repeats. D. Quantification of pTie-2 fluorescent intensity between indicated groups. n=individual cell intensities across 3 experimental repeats. E. Schematic of experimental setup with Tie-2 inhibitor Bay-826 to determine effect of Tie-2 signaling on lumen formation. F. Representative images of sprouts treated with Bay-826 or DMSO (control) on indicated day and stained for luminal marker moesin and actin. G. Quantification of percent nonlumenized sprouts between indicated groups. n=individual sprouts across 3 experimental repeats. H. Representative Western blotting for Ang-2 secretion into culture media between indicated conditions. n=3 individual Western blots. I. Representative Western blot probing for intracellular Ang-2 by indicated groups. n=3 individual Western blots. All experiments use human umbilical vein endothelial cells. AU indicates arbitrary unit; and NS, not significant. In all parts, L denotes lumen; white box denotes magnification; white lines denotes exterior of sprout; values are means±SEM; n=individual sprouts across 3 experimental repeats; significance: *P<0.05 and ****P<0.00005. Statistical significance was assessed with a 1-way ANOVA followed by a Dunnett multiple comparisons test.

Slp2a/b and Tie-2 Signaling Are Required for Lumen Formation in Developing Zebrafish Blood Vessels

To confirm our results in vivo, we turned to the zebrafish model of vascular development. Zebrafish blood vessel development is an established model of vascular lumen formation demonstrating stereotyped blood vessel morphology with an easily identifiable lumen cavity [177]. Furthermore, zebrafish are exceptionally well-suited for gene knockout studies using CRISPR/Cas9 editing [189-181]. Using CRISPR/Cas9 targeting as previously described, we knocked out both paralogs of Slp2 (A and B) [178]. Our sequence analysis showed an 75% indel formation with a ≈50% reduction in both Slp2a and Slp2b transcripts (Figure 12A). Knockouts, singly or in combination, did not alter larvae body plan or growth kinetics (Supplemental Figure 8A). Inspection of the intersomitic vessels (ISVs) showed an increase in non-lumenzed ISVs particularly in the Slp2a/b crispants compared with scrambled sgRNA (single-guide RNA) injected controls (Supplemental Figure 8B). Interestingly, ISVs were fully formed, connecting to the dorsal longitudinal anastomotic vessels (DLAV) at 36 hours post fertilization (Supplemental Figure 8B), suggesting migratory processes were unaffected. Also, we did not observe any major differences in survival, ectopic, or incomplete ISVs at 36 or 48 hours post fertilization (Supplemental Figure 8C-H). Next, we used microangiography to demarcate blood vessels with an open, contiguous luminal cavity. This method allowed us to conclusively assess whether vascular lumens were open, narrowed, or nonexistent (Figure 12B). Compared with controls, knockout of both Slp2 paralogs significantly increased the percentage of nonperfused ISVs (Figure 12C, D). This result tracked with significantly elevated number of nonlumenized ISVs in the double Slp2a/b knockout

compared with individual paralogs knockouts or controls (Figure 12E). This increase in nonlumenized vessels was independent of defects in ISVs as there was no difference in the number of formed ISVs between groups (Figure 12F). Using a different approach, we marked the apical membrane of the forming ISVs by expressing PHluorin-podocalyxin. PHluorin is a GFP variant that is nonfluorescent in acidified vesicles, but fluorescence is rescued at neutral pH following membrane fusion [182]. This method allowed us to visualize podocalyxin that was inserted into the plasma membrane, clearing defining the apical surface (Supplemental Figure 9A). Using this marker, knockout of Slp2a/b also demonstrated a defined collapse of the apical membrane marked by a loss of PHluorin-podocalyxin signal (Supplemental Figure 9B). Overall, this data suggests that Slp2a/b is necessary for lumen formation in vivo.

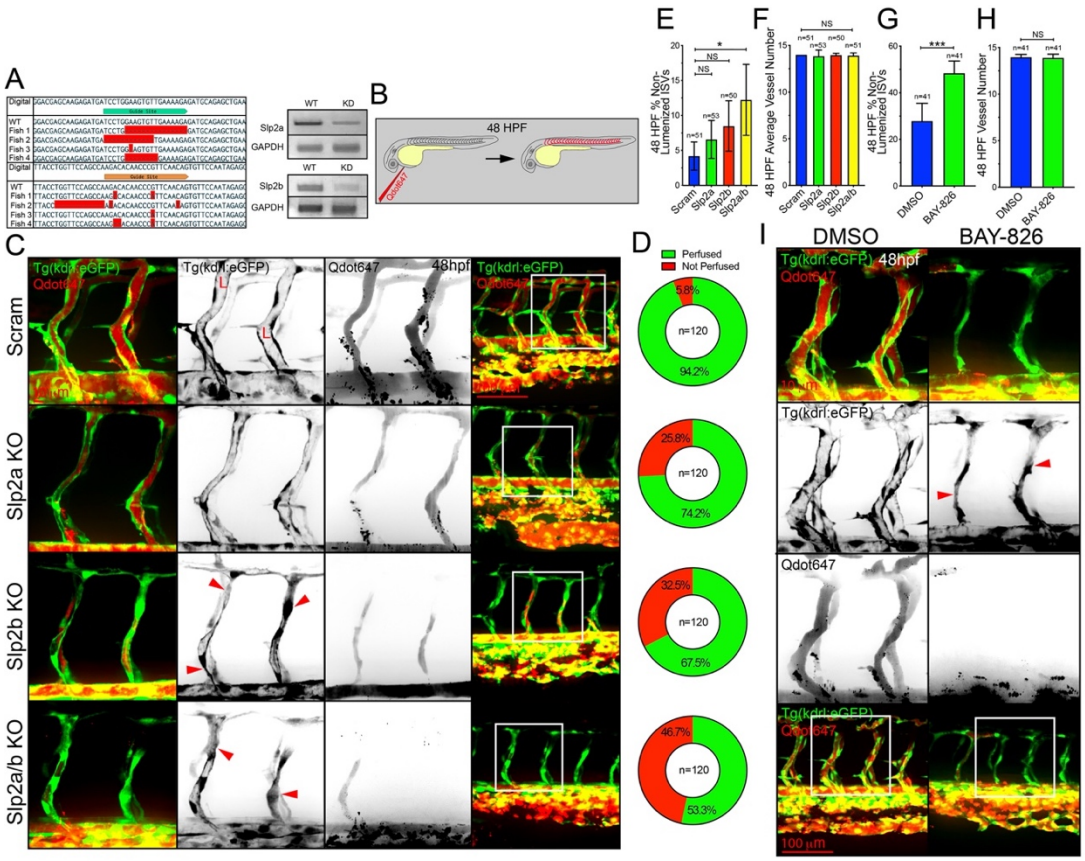

Figure 12: Genetic knockdown of Slp2a (synaptotagmin-like protein-2a)/b in zebrafish blunts lumen formation. A. Sequence of fish targeting sites after CRISPR/Cas9 gene-editing aligned to wild-type (WT) sequence. Bands are RT-PCR analysis of mRNA transcript levels in zebrafish injected with indicated sgRNA (single-guide RNA) normalized to a GAPDH expression control. Four fish per guide were analyzed for targeting analysis, and 20 fish per condition were homogenized for RT-PCR over 3 experimental repeats. In a pooled sample expression of Slp2a/b KD is ≈50% reduced relative to WT. B. Cartoon schematic of microangiography. Zebrafish were perfused with Quantum dot 647 (Qdot647) to highlight the vascular lumen cavity. C. Forty-eight hours post fertilization (hpf) zebrafish tg(kdrl:GFP [green fluorescent protein]) perfused with Qdot 647 between indicated conditions. Arrowheads indicate sites of lumen collapse. D. Quantification of percentage of perfused intersomitic vessels (ISVs) between indicated crispant groups. n=numbers of ISVs over 3 experimental repeats. E. Quantification of percentage of nonlumenized ISVs at 48 hpf. n=individual fish over 3 experimental repeats. F. Quantification of number of ISVs between indicated crispant groups. N value represents individual fish over 3 experimental repeats. G. Quantification of nonlumenized ISVs between DMSO (control) and Bay-826 (small molecule Tie-2 inhibitor). N values represent individual fish over 3 experimental repeats. H. Quantification of ISV number between indicated groups. N values represent individual fish over 3 experimental repeats. I. Representative images of 48 hpf zebrafish ISVs perfused with Qdot 647 between

indicated conditions. In all panels, L denotes lumen; arrowheads denote lumen failure; values are means±SEM; NS indicates not significant; significance: *P<0.05 and ***P<0.001. Statistical significance was assessed with an unpaired students t test or 1-way ANOVA followed by a Dunnett multiple comparisons test.

To test if Slp2a or Rab27a maintained their cellular localization patterns in forming zebrafish blood vessels, we mosaically overexpressed tagged-version of Rab27a, pro-VWF, and Slp2a. Similar to our in vitro results, we observed both VWF and Rab27a were located in intracellular puncta in zebrafish ISVs (Supplemental Figure 9C) [163]. Interestingly, overexpression of pro-VWF also accumulated in the luminal space, suggestive of clot formation. Overexpression of tagged-Slp2a also demonstrated similar localization patterns as compared with our in vitro sprouting model. Both Slp2a WT and Slp2a-C2AB were membranous, while the Slp2a-ΔC2AB mutant was cytoplasmic (Supplemental Figure 9D).

To further substantiate our in vitro results, we applied the Tie-2 inhibitor Bay-826 used previously to larvae at 24 hours post fertilization and then quantified for lumen defects at 48 hours post fertilization. During this time, ISVs sprout dorsally from the dorsal aorta and lumenize before forming the DLAV. In line with our in vitro results, we observed a significant increase in the number of non-lumenized ISVs compared with a vehicle control (Figure 12G, I). Again, these results were independent of alterations in ISV number or body plan (Figure 12H, Supplemental Figure 8I). Cumulatively, our data indicates that Tie-2 signaling is required for blood vessel lumenogenesis in vivo (Figure 13).

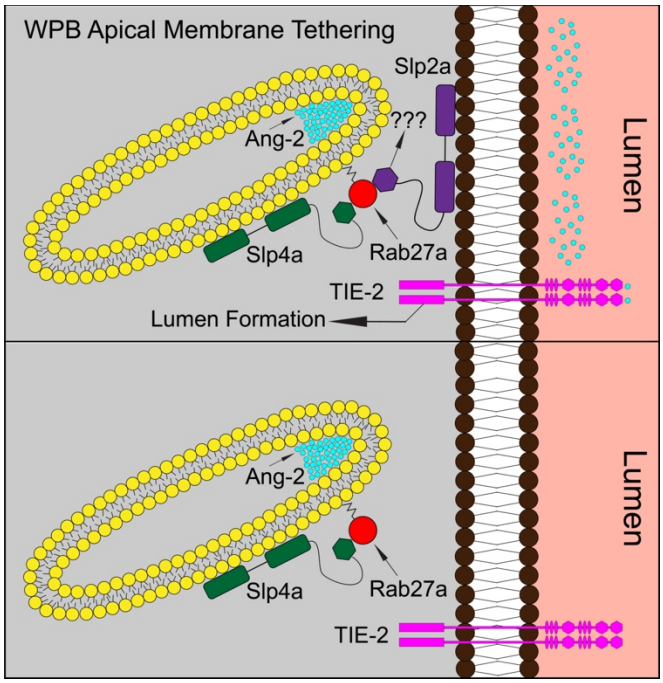

Figure 13: Proposed model of Slp2a (synaptotagmin-like protein-2a) function in vascular lumen formation. Top cartoon representation of Slp2a acting as a tether at the apical membrane for WPBs (Weibel-Palade bodies) binding. Ang-2 housed within the WPBs are then successfully targeted to the apical membrane and secreted. Once secreted, Ang-2 (angiopoietin-2) binds the activates Tie-2 leading to downstream signaling promoting lumen formation and sprout stabilization. The bottom cartoon is lacking Slp2a. Loss of Slp2a prevents WPBs from properly exocytosing their cargo, reducing Ang-2 secretion and autocrine activation of Tie-2 signaling cascade.

3.4 Discussion

In the present investigation, we demonstrate that Slp2a is required for vascular lumen formation. Our results establish that Slp2a resides at the apical membrane where it can tether Rab27a positive vesicles. Unique to endothelial tissue, Slp2a controls the fusion of WPBs for secretion of their contents into the luminal space during angiogenesis. Ang-2 is a Tie-2 receptor ligand that is selectively exocytosed from WPB secretory granules and is necessary for proper blood vessel development in specific contexts [175]. In the absence of Slp2a, WPB contents cannot fuse with the apical membrane precluding the release of Ang-2, diminishing Tie-2 signaling necessary for proper lumen formation (Figure 13).

Overall, our results demonstrate that Slp2a is required for targeting secretory vesicles to the apical membrane during vascular lumen development and a core component of the WPB secretory pathway.

A fundamental morphogenic program during blood vessel development is the creation of a continuous lumen as a conduit for blood flow [145, 146, 174]. This feat requires the establishment of apicobasal membrane polarities via the recruitment of lipids and proteins to differential plasma membrane domains. In the present investigation, we demonstrate that Slp2a is necessary for lumen formation in vascular development by regulating the secretion of WPB vesicles at the apical membrane. We believe as all blood vessels form a lumen during their development, Slp2a could be a major contributor to lumenogenesis in all vessel beds ranging from small capillaries to large arteries. Interestingly, and unlike epithelial tissue, Slp2a's trafficking partner Rab27a does not deliver podocalyxin in ECs but is intimately involved in WPB granule secretion. This novel association highlights an endothelial-specific function as ECs are the predominant harbor of WPBs due to their central role in hemostasis. This finding brings into question if Rab27a is not transporting podocalyxin, what other(s) trafficking pathway has been evoked in its place?

Rab27a is one of the best characterized exocytic Rab GTPase family members [153, 175, 176]. Rab27a function in vascular tissue has been shown to regulate VEGFR1 (VEGF receptor 1) trafficking by directing palmitoylation, con- trolling receptor recycling or through receptor degradation.19 In the current investigation, Rab27a localized only to WPBs—we did not detect any obvious receptor labeling. Our findings were congruent with Nightingale, et al., in which Rab27a was a negative regulator of

WPB exocytosis. Our results show that when Rab27a is ablated, WPB cargo is readily released, while lumen formation was not reduced, but increased. However, in the absence of Slp2a, Rab27a-evoked WPB exocytosis is halted at the apical membrane precluding cargo release. If Rab27a binding to Slp2a was a requisite for WPB cargo secretion, then knockdown of Rab27a would have also blunted VWF and Ang-2 release, we did not observe this. Thus, the exact mechanism by which Slp2a is tethering WPBs at the apical membrane remains unknown, we can only conclude that it is required for this process. To this effect, Slp2a could be also required for membrane fusion, such as in SNARE (SNAP receptor), Unc13 (protein UNC 13) (protein UNC 13), VAMP (vesicle-associated membrane protein) mediated events and not simply involved in tethering WPBs adjacent to the apical membrane [177, 184, 185]. To this end, Zhou, et al., reported that loss of CCM3 (cerebral cavernous malformations 3), a causative gene in cerebral cavernous malformations, suppressed UNC13B/VAMP3-dependent exocytosis in brain ECs leading to elevated Ang-2 secretion [186]. It is tempting to speculate that Slp2a may also be involved in the CCM or UNC13B/VAMP3-dependent exocytosis pathway given our results suggests that Slp2a tethering is required for secretion of Ang-2. Additionally, other Ca2+-dependent synaptotagmins could be aiding in exocytic events at the luminal membrane [187]. Indeed, further experiments are required to fully understand Slp2a's role in WPB docking and fusion at the apical membrane as well as its other potential functions as an exocytic regulator during angiogenic development.

The spatiotemporal regulation of WPB trafficking is complex demonstrating both constitutive and induced exocytic behaviors in ECs. In addition to this complexity, the contents of WPBs are vast, with as many as 40 proteins cited as WPB cargo [188]. It has

been reported that sub-populations of WPB granules exhibit preferential housing of certain proteins, to the exclusion of others [157, 172]. For example, P-selectin and Ang-2 occupy mutually exclusive WPB populations [183]. Our results support this notion as we observed some selectivity in Ang-2 localization compared with VWF-positive WPBs. These observations necessitate the notion of unique trafficking programs that WPBs execute to complement their growing role as a dynamic exocytic depot. We also observed that the nonmembrane binding Slp2a-ΔC2AB mutant decorated virtually all VWF and Ang-2 positive vesicles, indicating that regardless of the WPB sub-population, Slp2a is likely a requirement for apical membrane tethering and secretion.

Due to the continuously growing body of new data, Ang-2's exact contribution to angiogenesis has yet to be resolved and is at present considered context dependent. Both Ang-1 and Ang-2 can bind the Tie-2 receptor. Initial Ang-2 investigations provided evidence for Ang-2 solely functioning as an antagonist of Ang-1, in which Ang-1 binding promoted Akt signaling, fortifying vascular barrier function [169, 190, 191]. In this context, Zhou, et al., reported that super-physiological levels of Ang-2 antagonize Ang-1's Tie-2 activation leading to loss of blood vessel stabilization programs [186]. Contrary to these results, other studies reported Ang-2 expression can promote Tie-2 activation as well as interacting with integrins [171, 191]. Like our results, an investigation by Mochizuki, et al., demonstrated that Ang-2 promoted tube-like structure formation down-stream of c-Fes and c-Fyn [171]. This phenomenon has been observed during tumor-induced angiogenesis as well as in inflamed endothelium [172, 192]. Further complicating this interplay is the unique expression patterns between ECs and pericytes. Ang-1 is primarily secreted by pericytes whereas Ang-2 is released from the endothelium

[193, 194]. In the absence of pericyte-derived Ang-1, we observed that knockdown of Ang-2 drastically affected vascular lumen formation. Furthermore, reduction of Ang-2 resulted in lower phosphorylated Tie-2 levels at the apical membrane in vascular sprouts, signifying an activating role in our model. Given these results, it is tempting to speculate that our fibrin-bead sprouting model may be more akin to tumor angiogenesis in which Ang-2 is converted to a Tie-2 activating ligand in the absence of pericyte-derived Ang-1. Our experiments also demonstrate elevated Ang-2 exocytosis into the luminal space during the beginning phases of lumen development and a reduction of luminal Ang-2 after sprouts were lumenized. To our knowledge, this is the first direct evidence of a graded secretion of Ang-2 into the lumen space, supportive of a requirement for Ang-2-mediated Tie-2 activation during lumen formation. Additionally, we provide new evidence for Slp2a acting as a gatekeeper for exocytic events involving WPB fusion at the apical membrane.

In summary, the present study provides a novel characterization of Slp2a and its role as an upstream apical membrane tether required for vascular lumen formation. Our evidence highlights a direct association between Slp2a, Rab27a, and WPBs in which Slp2a functions to facilitate WPB secretion. Our results also show that WPB-housed Ang-2 is a critical secreted factor for physiological progression of vascular lumen formation. Cumulatively, Slp2a is a major upstream apical mem- brane protein controlling regulated secretion programs during angiogenic development, which may have other uncharacterized roles in both angiogenesis and adult blood vessel homeostasis controlling trafficking at the apical membrane.

Chapter Three: Rab35 Regulates Actin Dynamics at the Plasma Membrane

4.1 Introduction

Angiogenesis is the process of sprouting and growth of new blood vessels from preexisting ones and is the primary driver of network expansion [195-198]. Many extrinsic and intrinsic biological systems have been shown to affect endothelial biology and, by extension, blood vessel formation. Membrane trafficking is one such system that is less well-characterized in endothelial tissue but has recently become more appreciated as additional organotypic trafficking signatures are aligned with important endothelial behaviors [199-202]. Membrane trafficking refers to vesicular transport of protein(s) to, or in vicinity of, the plasma membrane [203-205]. Here, trafficking regulators, such as Rab GTPases, interface with a host of effectors involved in receptor recycling, cytoskeletal regulation, shunting to degradative organelles, lumen formation, basement membrane secretion, and many other signaling events [203, 206, 207]. Indeed, critical to the understanding of how endothelial cells build dynamic and resilient vascular structures is the regulation of membrane trafficking during angiogenic development [208].

The GTPase Rab35 has been shown to be a multi-faceted regulator of membrane trafficking and continues to be an intensely researched Rab family member [209]. The promiscuity of Rab35 touching multiple pathways has created a cognitive bottleneck in attempting to assign function in any system, due to its seemingly endless diversity of roles. For instance, Rab35 has been shown to be involved in cytokinesis as well as transcytosis of the apical protein podocalyxin during lumen biogenesis in epithelial cysts

[210, 211]. In other investigations, Rab35 has been reported to be a negative regulator of the integrin recycling protein Arf6 via its effector ACAP2 [212-214]. Additionally, MICAL-1 has been shown to also facilitate Rab35's association with Arf6 and play a role in actin turnover [214-216]. In Drosophila, Rab35 regulates apical constriction during germband extension as well as actin bundling via recruitment of Fascin [217, 218]. To date, there is no unified study on Rab35 taking into account its many disparate functions in any tissue. Regarding blood vessel function, no endothelial studies exist detailing how, or if, Rab35 functions in sprouting angiogenesis.

In the current study, our goal was to comprehensively characterize Rab35's role in sprouting angiogenesis. To do so, we took a holistic approach in investigating established partners of Rab35 and characterized their effect on sprouting behaviors and downstream cellular morphodynamics in vitro and in vivo. Primarily using a three-dimensional sprouting assay, our results reveal that Rab35 is required for sprouting as its loss significantly disrupts apicobasal polarity. Focusing on Rab35 effectors, we demonstrate that of the many reported effectors only ACAP2 is capable of directly binding Rab35 in endothelial cells. However, upon investigating ACAP2 and its target Arf6, we determine this established Rab35 trafficking cascade is largely insignificant with regard to sprouting angiogenesis. Excluding all other pathways, we focused on the Rab35 guanine exchange factor (GEF), DENNd1c, and its role in localizing Rab35 to actin structures. Our results demonstrate that DENNd1c facilitates Rab35 tethering to the actin cytoskeleton. Once on actin, Rab35 acts as a negative regulator of actin polymerization and is critical for the formation of proper actin architecture. In vivo, we show the requirement of Rab35 in zebrafish blood vessel development using a gene editing approach. Overall, our results

provide evidence of a focused role for Rab35 as a regulator of actin assembly during sprouting angiogenesis.

4.2 Materials and Methods

Cell Culture

See Annex A.

Sprouting Angiogenesis Assay

See Appendix A.

Lentivirus and Adenovirus Generation and Transduction

See Appendix A.

Antibody Feeding Assay

Antibody feeding assay was carried out as previously described [265]. Briefly, cells were moved to 4 °C for 30 min, and then β1-integrin antibody was added to the culture for an additional 30 min. Following incubation, cells were washed and moved back into the 37 °C incubator for 20 min and then fixed with 4% Paraformaldehyde. β1-integrin antibody was added once more for 45 min to label extracellular integrins, washed, and then incubated with the secondary antibody. The secondary was washed, and cells were permeabilized with 0.5% Triton-X for 10 min to gain access to the endocytosed β1-integrin pool. Then a complementary secondary antibody was added for 20 min to label the endocytosed integrins.

Migration Assay

Treated cells were moved to Ibidi culture insert plates with a two well silicone insert allowing for a defined cell-free gap. At 3 days post siRNA treatment the silicone insert

was removed, and cells were allowed to migrate for 6 h. Thereafter, cells were fixed, and immunohistochemistry was performed. The distance traveled into the cell free space was measured between groups.

Immunoblotting and Protein Pull-Down

See Appendix A.

Detection of Globular and Filamentous Actin

Globular and filamentous actin ratios were determined by western blot as described by commercially available G-actin/ F-actin In Vivo Assay Kit (Appendix A, Table 2). Globular and filamentous immunocytochemistry was performed as previously described [243]. Briefly, cells were fixed with 4% PFA for 10 min and permeabilized in ice cold acetone for 5 min and washed. Cells were then incubated for 15 min in 2% BSA with globular actin-binding protein GC globulin (Sigma). Following incubation, cells were washed three times in PBS. After washes cells incubated with an anti-GC antibody in BSA for 15 min, washed three times, and incubated in anti-rabbit-555 secondary prior to imaging.

Tracking of Cell Dynamics

Cell tracking was performed in Image J (Fiji) using the ADAPT plug-in, as previously described [240].

Immunoflourescence and Microscopy

See Appendix A.

Zebrafish Transplantation, Microangiography, and Gene Editing

All animal studies were approved by the University of Denver IACUC in accordance with AAALAC recommendations. Zebrafish (Danio rerio, AB strain) larvae between 24

and 72 h post fertilization were used for all animal experiments, no adults were used. Zebrafish transplantations were performed as previously described [244]. Briefly, cells were harvested at the blastula stage from a tg(kdrl:mCherry) line and treated with CRISPR (described below) line using an Eppendorf CellTram and deposited into recipients harboring a tg(kdrl:eGFP) transgene allowing us to distinguish between host and recipient blood vessels.

For microangiography, see Appendix A.

Tol2-mediated transgenesis was used to generate mosaic intersomitic blood vessels as previously described [196, 197]. Briefly, Tol2 transposase mRNA were synthesized (pT3TS-Tol2 was a gift from Stephen Ekker, Addgene plasmid # 31831) using an SP6 RNA polymerase (mMessage Machine, ThermoFisher) [198]. A total of 400 ng of transposase and 200 ng of plasmid vector were combined and brought up to 10 μL with phenol red in ddH2O. The mixture was injected into embryos at the 1–2 cell stage. Injected zebrafish were screened for mosaic expression at 48 hpf and imaged.

CRISPR/cas9-mediated knockouts were performed as previously described [199]. Briefly, equal volumes of chemically synthesized AltR® crRNA (100 μM) and tracrRNAr RNA (100 μM) were annealed by heating and gradual cooling to room temperature. Thereafter the 50:50 crRNA:tracrRNA duplex stock solution was further diluted to 25 μM using supplied duplex buffer. Prior to injection 25 μM crRNA:tracrRNA duplex stock solution was mixed with 25 μM Cas9 protein (Alt-R® S.p. Cas9 nuclease, v.3, IDT) stock solution in 20 mM HEPES-NaOH (pH 7.5), 350 mM KCl, 20% glycerol) and diluted to 5 μM by diluting with water. Prior to microinjection, the RNP complex solution was incubated at 37 °C, 5 min and then placed on ice. The injection mixture was

micro-injected into 1–2 cell stage embryos. Crispant DNA was retrieved via PCR and subjected to sanger sequencing to visualize indel formation (Supplementary Table 5).

Zebrafish Live Imaging and Quantification

See Appendix A.

Scanning Electron Microscopy

Cells fixed for SEM were followed the procedure outlined by Watanabe, et al. [267]. Scanning electron microscopy was performed at the University of Colorado Anschutz Medical Campus by Dr. Eric Wortchow.

Statistical Analysis

Experiments were repeated a minimum of three times. Statistical analysis and graphing were performed using GraphPad Prism. Statistical significance was assessed with a student's unpaired t-test for a two-group comparison. Multiple group comparisons were carried out using a one-way analysis of variance (ANOVA) followed by a Dunnett multiple comparisons test. Data was scrutinized for normality using Kolmogorov–Smirnov test. Zebrafish sex distribution was not adjusted as sex determination did not occur at the stage of development in which the specimens were assayed. Statistical significance set a priori at $p < 0.05$.

4.3 Results

Rab35 is Required for Sprouting Angiogenesis

To characterize the role of Rab35 in sprouting angiogenesis, we first cloned a fluorescently tagged version of Rab35 into a lentivirus expression system [219]. Thereafter, we transduced ECs and then challenged the cells to sprout in a fibrin-bead assay (Figure 14A) [220, 221]. Rab35 in 3-dimensional (3D) sprouts demonstrated strong

membrane localization, co localizing with apical marker podocalyxin and luminal actin, opposite basally located β1-integrin (Figure 14B). To test whether Rab35 was necessary for endothelial sprouting, we knocked down Rab35 using siRNA (Figure 14C). Loss of Rab35 reduced sprout length and sprouts per bead by ~50%, with a significant increase in the percentage of non-lumenized sprouts (Figure 14D-G). Morphologically, the sprouts appeared stubby, non-lumenized, and generally dysmorphic compared with controls (Figure 14D). These results indicate that Rab35 is required for proper sprout development.

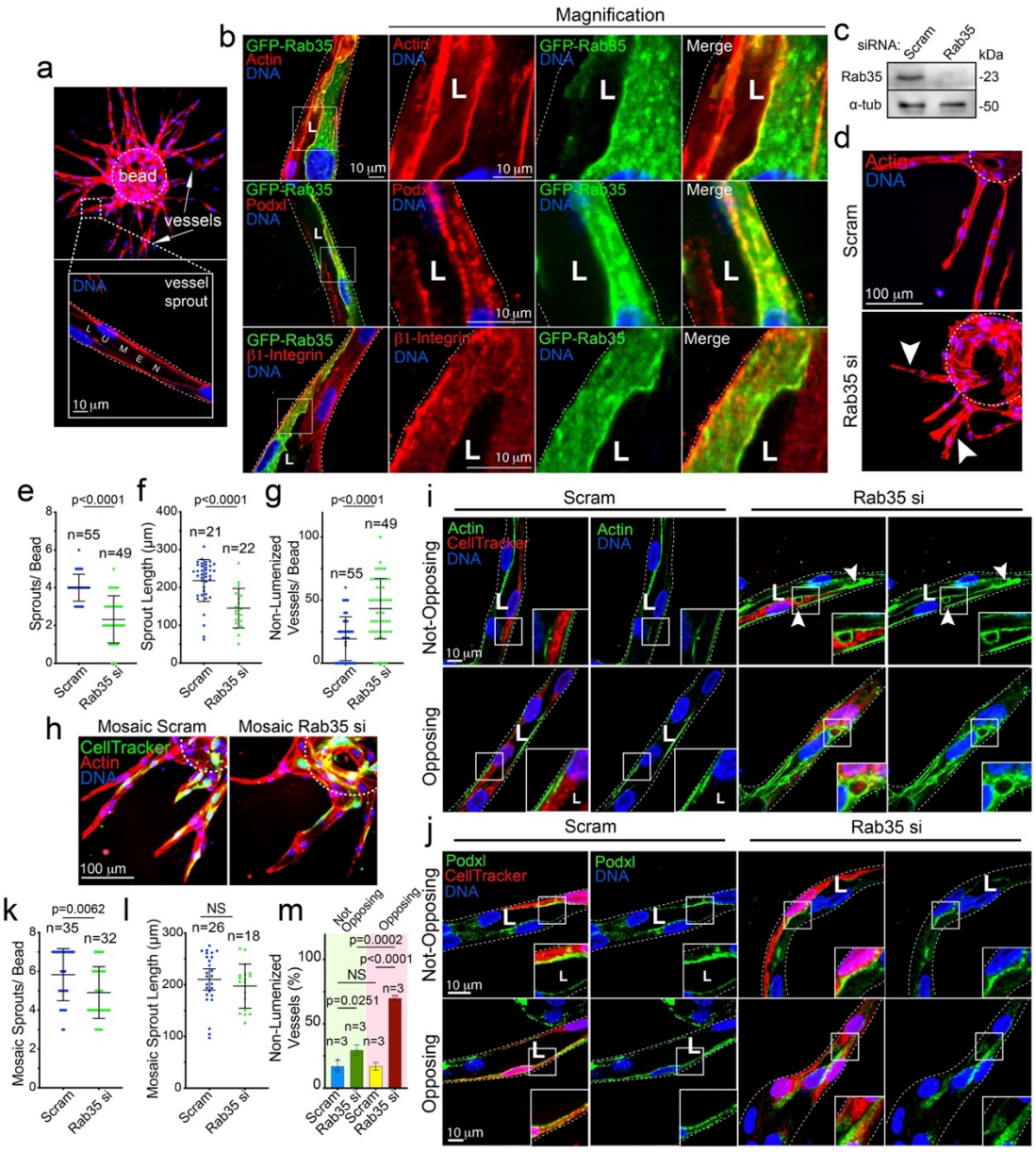

Figure 14: Rab35 is an apical membrane protein required for sprout formation. A. Representative images of the fibrin-bead assay (FBA) at low and high magnification. Arrows mark sprout structures. Inset depicts lumenized sprout. b GFP-Rab35 localization in endothelial sprouts with actin (top panels), podocalyxin (Podxl, middle panels), and β1-integrin (bottom panels). c Western blot confirmation of siRNA (si) knockdown (KD) of Rab35 (average 72.5% KD relative to control, n = 3). d Representative image of scramble (Scram) control and Rab35 siRNA KD sprouts. Arrowheads denote short and non-lumenized sprouts. Dashed lines outline the microbead. e–g Graphs of indicated sprouting parameters between groups. n = number of sprouts. Error bars represent standard deviation, middle bars are the mean. h Representative images of sprout morphology of mosaic Scram and Rab35 KD cells, green indicates cell tracker of siRNA

treated cells. i, j Representative images of non-opposing (top panels, an isolated siRNA treated cell) and opposing (bottom panels, two adjacent siRNA treated cells) cells stained as indicated. Arrowheads denote aberrant actin accumulations. k, l Quantification of indicated parameters across groups. n = number of sprouts. Error bars represent standard deviation, middle bars are the mean. m Quantification of non-lumenized sprout area across indicated groups. n = mean percentage of each experimental repeat (each group contains >20 cells). Error bars represent standard deviation, middle bars are the mean. In all images L denotes lumen. NS = non-significant. Statistical significance was assessed with an unpaired t-test or a 1-way ANOVA followed by a Dunnett multiple comparisons test. Insets are areas of higher magnification. White dotted lines mark sprout exterior. All experiments were done using Human umbilical vein endothelial cells in triplicate.

Given Rab35 depletion exhibited such a profound impact on sprouting parameters, we stained for various cytoskeletal, apical, and basal markers to determine if Rab35 was affecting specific polarity pathways or producing a more global cellular defect. Imaging for VE-cadherin (cell-cell junctions), podocalyxin, β1-integrin (basal membrane), moesin (cytoskeletal, apical membrane), synaptotagmin-like protein-2 (apical membrane), and phosphorylated-Tie2 (apical membrane) revealed that Rab35 knockdown affected all protein localization (Supplementary Figure 10A), suggesting that loss of Rab35 globally disturbs cell polarity programs. Emblematic of this was the significant lack of lumen formation and the increase in discontinuous vacuoles in the Rab35 depleted condition (Supplementary Figure 10B), as lumenogenesis requires proper apicobasal signaling to form [208, 221]. We also observed that Rab35 knockdown reduced the number of nuclei per sprout, indicating the presence of cell division defects in line with other reports (Supplementary Figure 10C) [211, 222-224]. We tested for Rab35 knockdown efficiency in prolonged 2D culture to ensure our siRNA knockdown was not diminished at day 4 of sprouting. At day-4 and day-5, Rab35 expression was dramatically lower than controls (Supplementary Figure 10D). Overall, this data suggests that Rab35 plays a significant role in establishing cell polarity during angiogenic sprouting.

Using a mosaic approach, we determined the cell autonomous nature of Rab35 depletion in a sprout collective. To do so, we treated ECs with either Rab35 siRNA or a scramble control and then mixed 50:50 with wild-type ECs. The resulting mosaic sprouts contained a mixture of siRNA-treated and untreated ECs (Figure 14H). Cells contained within sprouts were then binned into two categories: (1) not-opposing, an isolated siRNA-treated cell; or (2) opposing, two adjacent siRNA-treated ECs (Figure 14I, J). Rab35 knockdown in not-opposing ECs contained actin-labeled vacuolations and polarity defects as indicated by a reduction in lumen formation compared with scramble-treated controls (Figure 14K-M). For Rab35 depleted ECs in the opposing orientation, defects were more pronounced with complete lumen failures at these sites, while also exhibiting multiple vacuolations and polarity defects (Figure 14M). Overall, these results indicate that Rab35 is cell autonomous and is required for EC polarity.

Rab35 Resides at the Apical Membrane During Sprouting

Next, we sought to better understand Rab35's cellular localization to gain insight into its potential function. In sprouts, quantification of Rab35 enrichment between different cellular compartments showed a preference for the apical membrane for wild-type (WT) and constitutively active (CA) Rab35 variants, while the dominant-negative (DN) Rab35 mutant resided in the cytoplasm (Figure 15A). Subcellular imaging of WT and CA Rab35 showed a strong colocalization with apical podocalyxin (Figure 15B). Similar to loss of Rab35, expression of the DN Rab35 also produced polarity defects, such as mis-localization of podocalyxin and large actin accumulations (Figure 15B). To more conclusively assign Rab35 phenotypes, we performed several rescue assays by knocking down the endogenous Rab35 protein and then over-expressing Rab35 variants in sprouts.

Expression of WT or CA Rab35 decreased the number of non-lumenized sites in sprouts compared to Rab35 knockdown alone expressing a GFP control, but not to levels in the scramble treated group (Figure 15C-D and Supplementary Figure 11A, B). Rab35 knockdown and expression of the DN Rab35 mutant showed the highest increase in dysmorphic sprouts, exhibiting numerous accumulations of actin puncta and lumen defects, again suggesting Rab35 is associated with sprout function.

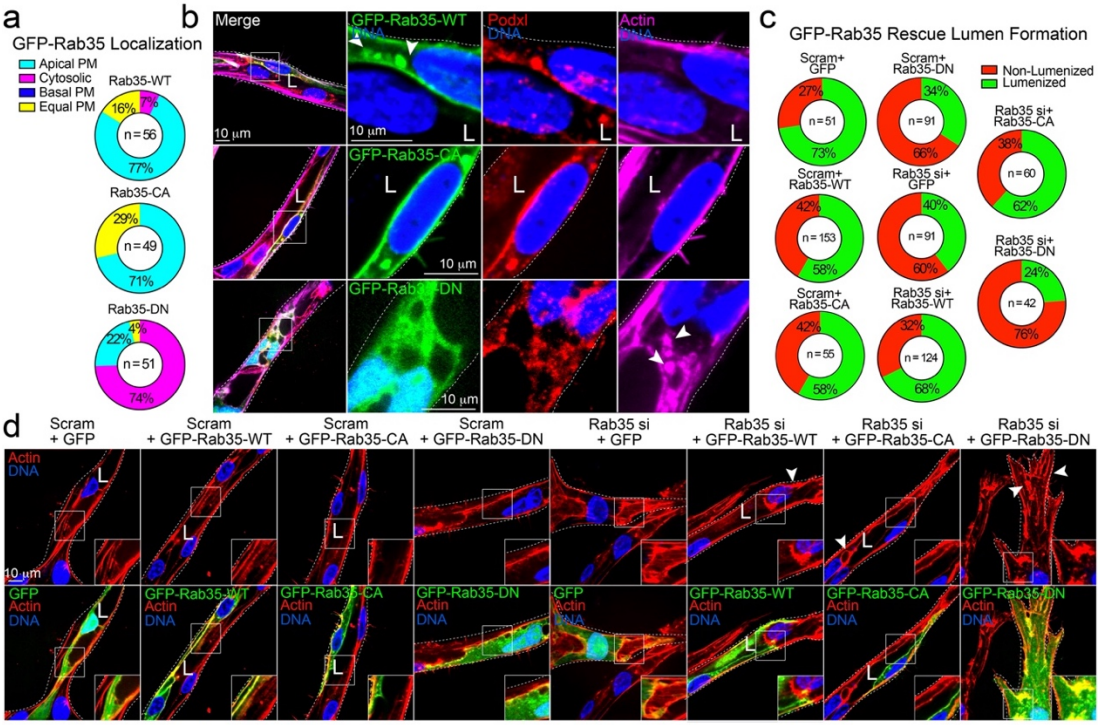

Figure 15: Rab35 mutant localization and rescue in endothelial sprouts. A. Quantification of GFP-Rab35 wild-type (WT), constitutively-active (CA), and dominant-negative (DN) localization in endothelial sprouts. Apical plasma membrane (PM, uniformly localized to apical membrane), basal PM (Rab35 uniformly located at the basal membrane), cytosolic (localized in the cytoplasm), equal PM (Rab35 equally distributed between the apical and basal membranes). n = number of cells. B. GFP-Rab35 WT (top panels), CA (middle panels), and DN (bottom panels) localization in endothelial sprouts. Co-staining with podocalyxin (Podxl) and actin. Arrowheads in top panels denote Rab35 apical localization and puncta. Arrowheads in bottom panels denote abnormal accumulations of actin. C. Rescue experiment using scrambled (Scram) or Rab35 siRNA (si)-mediated knockdown (KD) with overexpression of indicated constructs. Percentages represent quantification of lumen formation in described conditions. n = number of sprouts. D.

Representative images of Scram and Rab35 KD sprouts expressing either GFP (control), or GFP-Rab35-WT/CA/DN. Arrowheads denote actin accumulations. White dotted lines mark sprout exterior. L denotes lumen in all images. Insets are areas of higher magnification. All experiments were done using human umbilical vein endothelial cells in triplicate.

Within the sprout body, Rab35 also localized to actin at cytokinetic bridges as previously described but had no preference for filopodia extensions or tip-cell positioning (Supplementary Figure 12A, B and Supplementary Figure 13A-C) [211, 222, 224]. We also observed that Rab35 modestly colocalized with filamentous actin in a monolayer; however, this association was reduced in migratory cells (Supplementary Figure 12C, D). Previous reports have implicated Rab35 in Wiebel Palade Body (WPB) granule release; although, in our hands, Rab35 did not colocalize with these structures in 2D or 3D culture systems (Supplementary Figure 12E, F) [225]. These results indicate that Rab35 is largely localized to the apical membrane in its active form as well as areas of high actin density.

Reports in epithelial tissue suggest that Rab35 participates in trafficking of podocalyxin to the apical membrane [210, 211]. In the sprouting model, we indeed observed a strong colocalization of Rab35 and podocalyxin at the apical membrane as well as mislocalization of podocalyxin in the absence of Rab35. This data could be interpreted as a loss of, or defective, podocalyxin trafficking given Rab35's previous association with this pathway. As colocalization of podocalyxin and Rab35 at the apical membrane could be circumstantial as numerous proteins localize to the apical membrane during lumenogenesis, we overexpressed TagRFP-Rab35 and stained for endogenous podocalyxin in 2D culture and did not detect any significant signal overlap (Supplementary Figure 14A). Previous literature showed that Rab35 directly binds to the

cytoplasmic tail of podocalyxin [211]. Overexpression of the human podocalyxin cytoplasmic domain (residues 476–551) and TagRFP-Rab35 also did not show any obvious association (Supplementary Figure 14A). To further probe for binding between Rab35 and podocalyxin, we engineered a mitochondrial-targeted (Tom20) Rab35 to test what proteins or complexes bind Rab35 and are then 'pulled' along to mitochondria. Expression of WT or CA Tom20-Rab35 did not show any association with endogenous podocalyxin or overexpression of its cytoplasmic tail domain (Supplementary Figure14B, C). We next reasoned if mistrafficking of podocalyxin by way of Rab35 depletion was the predominant mechanism underpinning the sprouting defects, then knocking down podocalyxin would produce a similar phenotype as compared with loss of Rab35. Knockdown of podocalyxin did not phenocopy Rab35-mediated sprouting defects (Supplementary Figure 14D-I). The only exception was that podocalyxin knockdown increased the percentage of non-lumenized sprouts compared with controls. Overall, our data suggests that Rab35 does not directly participate in podocalyxin trafficking in ECs.

Rab35 Interacts with ACAP2 in Endothelial Cells

To take a more holistic approach in determining how Rab35 functions in endothelial tissue, we performed a functional screen by knocking down the most highly cited Rab35 effectors (ACAP2, Rusc2, OCRL, MICAL-L1, MICAL-1, and Fascin) singly and in combination, to determine if any effector phenocopied Rab35 sprouting defects (Figure 16A, B) [210, 212-215, 223, 225-228]. First, we found that Rab35 itself did not produce a significant effect on 2D cell motility, suggesting the primary defect in sprouting may be due to altered apicobasal polarity only detectable in a 3D sprout environment (Supplementary Figure 15A, B). As Rab35 and ACAP2 have been shown to affect the

integrin recycling pathway via their association with Arf6, we also assayed for integrin recycling as defective integrin signaling could also affect cell polarity. As compared with the scramble controls, knockdown of Rab35, ACAP2, and MICAL-L1 significantly increased integrin recycling, while OCRL, MICAL-1, and Fascin (treated with inhibitor NP-G2-044) had no effect or were directionally dissimilar (Supplementary Figure 15C, D).

Next, we determined that Rusc2 protein levels were not detectable in ECs, thus was excluded from our screen (Supplementary Figure 15E). Focusing on single knockdowns, ACAP2, OCRL, MICAL-L1, MICAL-1, and Fascin demonstrated phenotypic similarity to Rab35 knockdown with regard to sprouting parameters (Figure 16C-F). Upon closer inspection, all proteins, excluding MICAL-L1, were associated with elevated frequencies of non-lumenized sprouts with varying degrees of disorganized actin; albeit, to a much a lesser extent than compared with Rab35 (Figure 16G). Unlike loss of Rab35, individual knockdowns of all other proteins did not significantly reduce sprout length, suggesting a potential difference in phenotypes. For double knockdowns, we primarily focused on associations with ACAP2 as this is a more established Rab35 effector. Similar to individual knockdowns, loss of any combination of effectors significantly promoted lumen defects; although, no combination phenocopied Rab35 knockdown sprouting length defects (Supplementary Figure 15F-I).

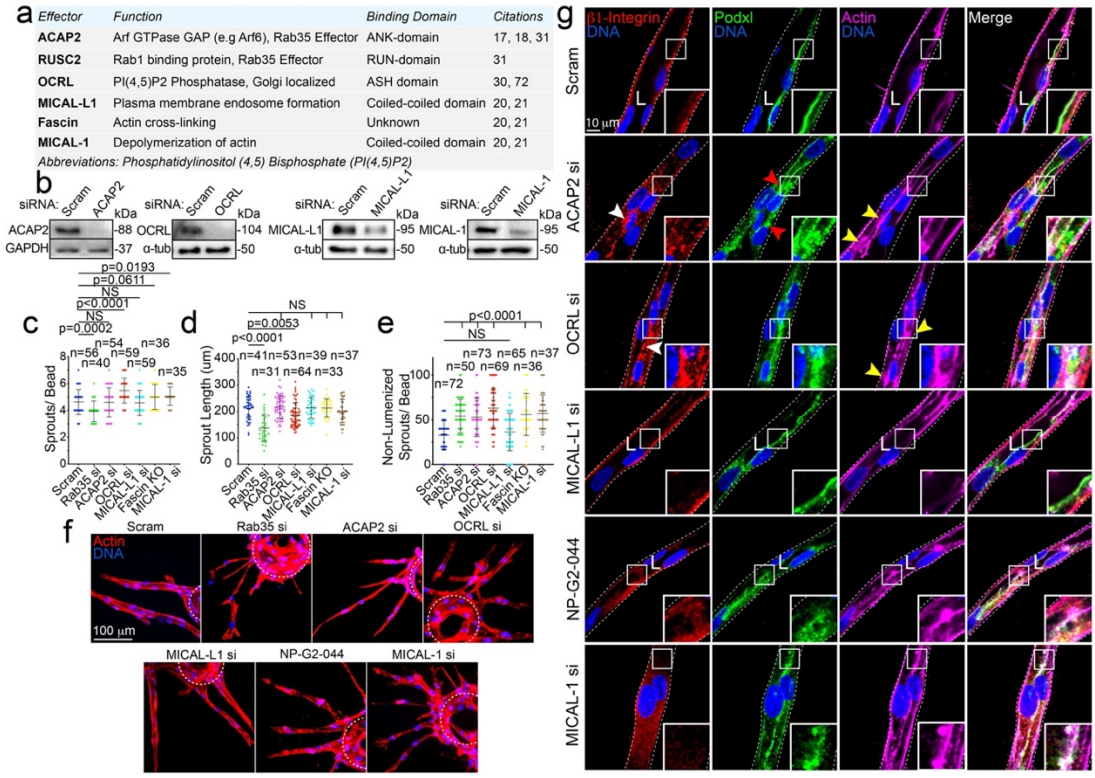

Figure 16: Rab35 effector localization and requirement for sprouting. A. Table listing each effector, respective function, and citations. B. ACAP2, OCRL, MICAL-L1 and MICAL-1 knockdown (KD) validation by western blotting (ACAP2 average 70.5% KD relative to control, n = 3; OCRL average 72.9% KD relative to control, n = 3; MICAL-L1 average 61.5% KD relative to control, n = 3; MICAL-1 average 69.3% KD relative to control, n = 4). C-E. Graphs of indicated sprout parameters between groups. n=number of sprouts. Error bars represent standard deviation, middle bars are the mean. F. Representative images of sprout morphology between indicated siRNA (si) KD groups. Dashed lines outline microbeads. G. Representative images of siRNA-mediated KD of each effector. White arrowhead denotes abnormal localization of β1-integrin. Red arrowheads denote abnormal podocalyxin (Podxl) localization. Yellow arrowheads denote abnormal actin accumulations. White dotted lines mark sprout exterior. In all images L denotes lumen. NS = non-significant. Statistical significance was assessed with an unpaired t-test or a 1-way ANOVA followed by a Dunnett multiple comparisons test. n = number of sprouts. Insets are areas of higher magnification. All experiments were done using human umbilical vein endothelial cells in triplicate.

Both ACAP2 and OCRL have been reported to directly bind Rab35; however, this interaction has not been validated in ECs [212-214, 223, 225, 228]. First, we overexpressed tagged versions of ACAP2, OCRL, MICAL-L1, MICAL-1, and Fascin to

visualize their localization patterns with Rab35 in ECs. Only ACAP2 and Fascin showed strong colocalization with Rab35 at the plasma membrane along with peripheral actin (Figure 17A, B). We again used the mitochondrial-targeted Tom20-Rab35 to visualize any physical association between Rab35 and these previously published effectors. Co-expression of WT and CA Tom20-Rab35 with ACAP2 demonstrated strong colocalization at the mitochondria, while the DN Rab35 showed no significant binding of ACAP2 (Figure 17C, D and Supplementary Figure 16A, B). We performed this same experiment using ACAP2 with the ankyrin repeat domain deleted and observed no binding, indicating Rab35 directly interacts with this domain (Supplementary Figure 16B). As a control, we also co-expressed a tom20-Rab27a and ACAP2 and observed no mislocalization of ACAP2 (Supplementary Figure 16C). Co-expression of WT, CA or DN Tom20-Rab35 with OCRL, MICAL-L1, MICAL-1 or Fascin did not show any colocalization at the mitochondria, signifying a lack of binding (Figure 17C, D and Supplementary Figure 16d-H). These results demonstrate that only ACAP2 directly interacts with Rab35 in endothelial tissue.

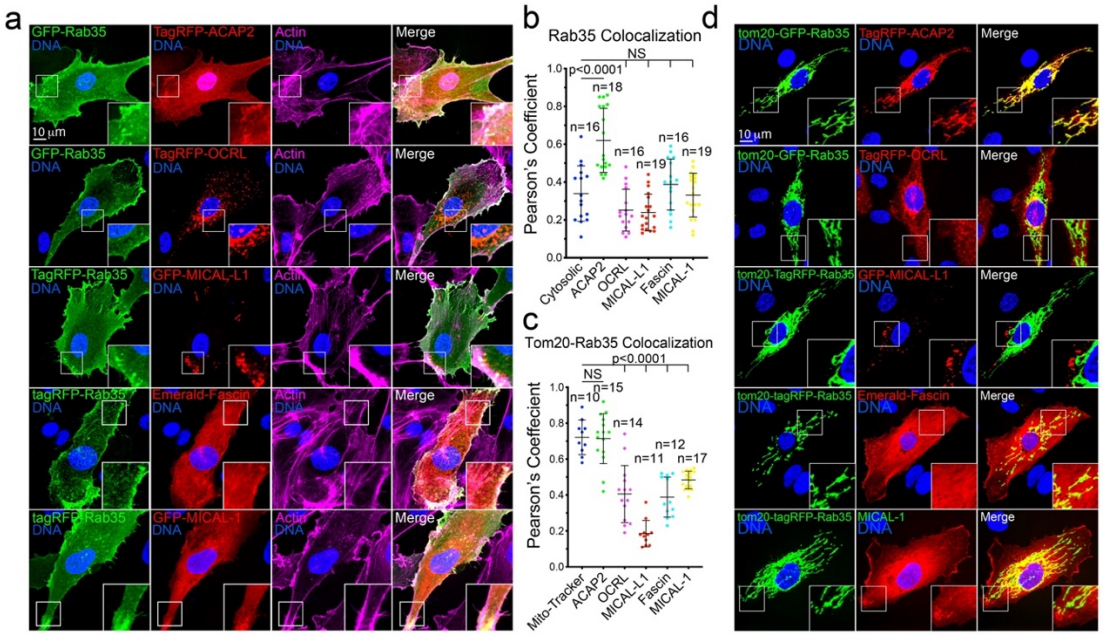

Figure 17: ACAP2 binds with Rab35. A. Two-dimensional localization of GFP-Rab35 or TagRFP-Rab35 with indicated effectors and stained for actin. B. Pearson's Coefficient between Rab35 and indicated effectors. n = number of cells. Error bars represent standard deviation, middle bars are the mean. C. Pearson's Coefficient between Tom20-Rab35 and indicated effectors. n= number of cells. Error bars represent standard deviation, middle bars are the mean. D. Representative images of mitochondrial mis-localization experiment. Rab35 was tethered to the mitochondria with a tom20 N-terminal tag to test if indicated effectors were also mislocalized. NS = non-significant. Statistical significance was assessed with an unpaired t-test or a 1-way ANOVA followed by a Dunnett multiple comparisons test. Insets are areas of higher magnification. All experiments were done using Human umbilical vein endothelial cells in triplicate.

Rab35 Activates Arf6 Activity in Endothelial Cells

ACAP2 has been implicated as a GTPase activating protein (GAP) with Rab35 to inactivate the GTPase Arf6 [212, 213, 226]. To test if this association exists in ECs, we first determined the localization of Arf6 relative to Rab35 and ACAP2 in culture. Cells expressing Rab35 and Arf6, or ACAP2 and Arf6 demonstrated modest colocalization primarily at the cell cortex (Supplementary Figure 17A, B). Using WT, CA, and DN versions of Arf6, we probed for actin to determine if Arf6, like Rab35, associated with these filaments. Wild-type and CA Arf6 demonstrated moderate colocalization with

actin; however, this association did not persist on filamentous actin located towards the cell interior (Supplementary Figure 17C). In sprouts, Arf6 showed modest localization to the apical membrane as compared to Rab35 (Supplementary Figure 17D). Mitochondrial-targeted Rab35 or ACAP2 did not pull Arf6, indicating a lack of binding interaction (Supplementary Figure 17E). We reasoned that the lack of binding between Arf6 and ACAP2 could be due to an insufficiency of Rab35; however, simultaneous expression of Tom20-GFP-Rab35 and TagRFP-ACAP2 did not localize HA-Arf6 to mitochondria, suggesting ACAP2 does not directly act upon Arf6, or that this signaling does not require a robust binding interaction in ECs (Supplementary Figure 17F).

Due to the wealth of literature demonstrating loss of Rab35 increases Arf6 activity in non-endothelial tissues, we sought to confirm this signaling biochemically. First, we expressed WT, CA, and DN versions of Arf6 in ECs and used recombinant GGA3 to pulldown the active form of Arf6 (Supplementary Figure 18A) [229]. Knockdown of Rab35 increased Arf6 activity as others have described (Supplementary Figure 18B, C) [212, 213,222]. Given our mitochondrial-mistargeting results, this may be due to a more transient protein-protein interaction between the Rab35/ACAP2 complex and Arf6, or potentially mediated through other unidentified Rab35 effectors. These results suggest that loss of Rab35 increases Arf6 activation; thus, we next tested if overactivation of Arf6 would phenocopy the Rab35 loss of function sprouting phenotype. We observed that overexpression of Arf6 marginally affected sprouting parameters with the WT and CA Arf6 increasing the frequency of lumen failures (Supplementary Figure 18D). Inconsistent with Rab35 knockdown-associated actin aggregates and non-apical podocalyxin, ECs expressing CA Arf6 demonstrated normal actin architecture as well as

typical polarity markers (Supplementary Figure 17D). These results suggest that overactivation of Arf6 due to loss of Rab35 is likely not the causative pathway underlying sprouting defects.

Exploring the Arf6 axis further, we knocked down Arf6 to determine how this would affect sprouting parameters. Loss of Arf6 significantly increased the proportion of non-lumenized sprouts to a greater extent than Rab35 (Supplementary Figure 18E-I). Interestingly, double knockdown of Rab35 and Arf6 did not further exacerbate this phenotype, suggesting that Arf6's effect on sprouting is independent from, or upstream of Rab35. Lastly, we tested if there was a dependency of Rab35 on Arf6, or vice versa, for proper localization in 3D sprouts. Knockdown of either protein did not prevent normal localization to apical actin (Supplementary Figure 18J), suggesting Rab35's and Arf6's localization behaviors are likely not functionally linked during angiogenesis.

DENNd1c is Required for Rab35 Function

We were intrigued by the idea that other roles of Rab35 were being unaccounted for as Arf6 overactivation could not fully reprise the Rab35 knockdown phenotype. To this end, Rab35 has three GEFs, DENNd1a-c [230-233]. DENNd1c has been shown to be not involved with GTP hydrolysis but has the lone ability to bind to both globular and filamentous actin, potentially mediating Rab35 localization [230]. Exploring this association, we knocked down DENNd1a-c individually and in combination. Loss of DENNd1a and DENNd1b did not produce any significant impact on sprouting morphology; however, knockdown of DENNd1c alone resulted in growth of dysmorphic sprouts mirroring Rab35 loss of function (Figure 18A-G). Knockdown of all DENNd1s produced the greatest effect on sprouting behaviors, presumably because the GEF activity

provided by DENNd1a/b was also lost (Figure 18D-F). Knocking down any given DENNd1 did not result in a compensatory increase in expression of the remaining DENNd1s (Supplementary Figure 19A). We next cloned and tagged DENNd1c and confirmed colocalization with Rab35 on actin in 2D cell culture (Supplementary Figure 19B, C). We also expressed Rab35 with the integral actin protein Arp2 known to mediate actin branching [234]. Rab35, Arp2, and filamentous (F)-actin strongly colocalized in the cell cortex (Supplementary Figure 19B). To explore if DENNd1c, per se, was responsible for tethering Rab35 to actin, we individually knocked down all three DENNd1s and quantified the relative amount of Rab35 uniformly localized at the plasma membrane, accumulated at the plasma membrane or in the cytoplasm. DENNd1c knockdown exhibited the greatest increase in apical plasma membrane accumulations compared with DENNd1a or DENNd1b (Figure 18H). These data indicate that loss of DENNd1c phenocopies the Rab35 knockdown effect on sprouting parameters and the actin cytoskeleton.

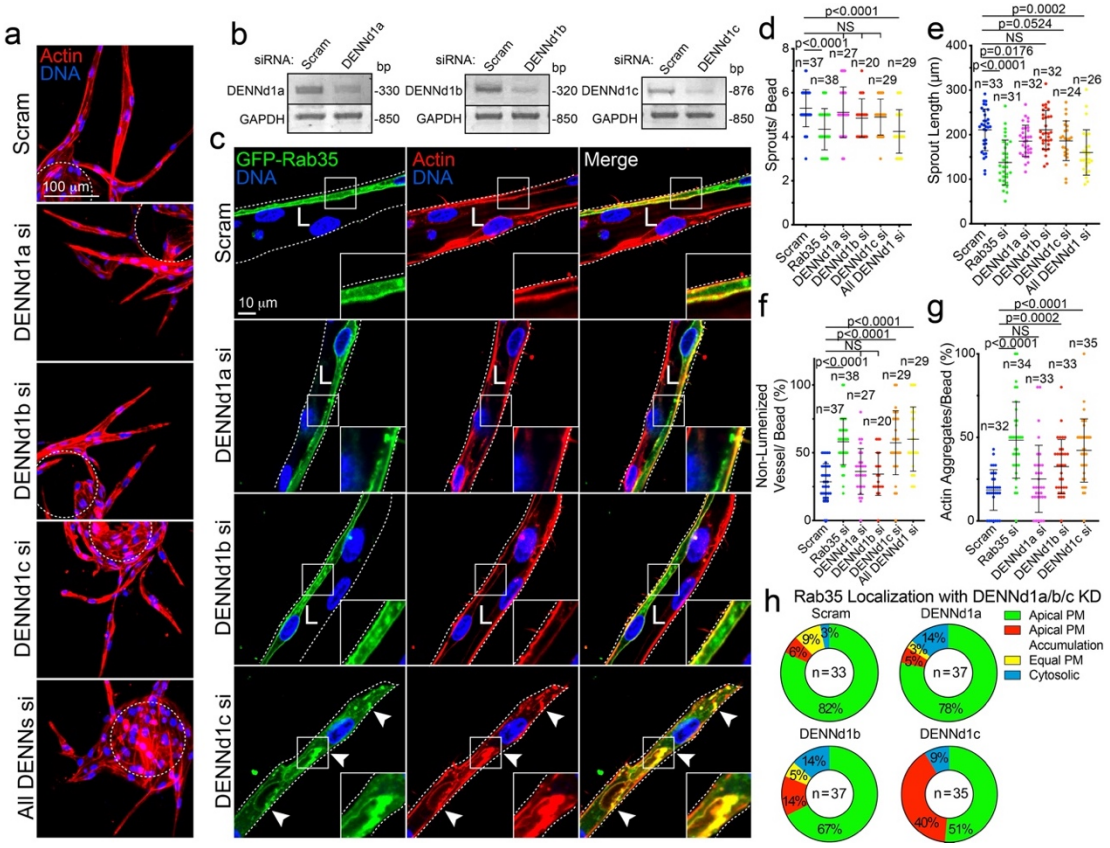

Figure 18: DENNd1c is required for sprouting and Rab35 function. A. Sprout morphology of scramble (Scram), DENNd1a-c, and combined siRNA (si)-treated sprouts, stained with actin to denote the general morphology. Dashed line denotes microbead. B. Knockdown confirmations for DENNd1a-c by RT-PCR. Base-pair (BP). C. Representative images of siRNA knockdowns described in panel A with GFP-Rab35 localization. L denotes lumen and arrowheads denote abnormal actin accumulations. White dotted lines mark sprout exterior. D-G. Graphs of indicated sprout parameters across groups. n = number of sprouts. Error bars represent standard deviation, middle bars are the mean. h GFP-Rab35 localization in DENNd1a-c siRNA-treated sprouts. Localizations were binned to apical plasma membrane (PM, Rab35 > 80% at apical membrane), apical PM accumulations (non-continuous, visible puncta), equal PM (equally enriched at apical and basal membranes), and cytosolic. n = number of sprouts. NS = non-significant. Statistical significance was assessed with an unpaired t-test or a 1-way ANOVA followed by a Dunnett multiple comparisons test. Insets are areas of higher magnification. All experiments were done using human umbilical vein endothelial cells in triplicate.

Rab35 and DENNd1c Localize to Sites of Actin Polymerization

We next characterized the association between Rab35, DENNd1c, and branched actin. Both Rab35 and DENNd1c demonstrated strong colocalization to Arp2 and the underlying actin (Figure 19A). To perturb the branched actin network, we next treated cells with the Arp2/3 inhibitor CK-666 and then determined the effect on Rab35 and DENNd1c localization [235]. In 3D sprouts, inhibition of branching actin resulted in normal sprouting with elevated indices of actin puncta similar to the Rab35 knockdowns (Figure 19B and Supplementary Figure 19D). In 2D culture, CK-666 treatment rapidly depleted actin at the cell cortex (Figure 19C). Rab35 prior to CK-666 administration exhibited a uniform distribution in the plasma membrane with enrichment at sites of actin. Following CK-666, Rab35 collapsed into discrete puncta scattered throughout the cytoplasm (Figure 19C). As a control, we performed the same experiment with Rab11a and did not observe any alteration in Rab11a localization with CK-666 treatment (Supplementary Figure 19E). Using the same approach, we observed that DENNd1c was highly enriched at cortical actin and CK-666 effectively depleted DENNd1c from this actin population (Figure 19D). Unlike Rab35, CK-666 treatment did not cause the formation of puncta, but the redistribution of DENNd1c to unaffected actin, such as F-actin towards the cell interior (Figure 19E). As a control, we treated cells with CK-666 expressing both Rab35 and Arp2. As expected, Arp2 was no longer located at the cell cortex, collapsing into puncta, while remaining adjacent to Rab35 (Figure 19E). These data suggest that Rab35 and DENNd1c are recruited to actin filaments.

To visualize Rab35's temporospatial recruitment to cortical actin, we employed a chemically switchable GFP-binding nanobody, termed ligand-modulated antibody

fragments (LAMAs) [236]. This method sequesters GFP-tagged Rab35 at the mitochondria and then rapidly releases the protein upon drug treatment, enabling dynamic imaging of localization patterns (Supplementary Figure 19F). Using GFP-Rab35, LAMA and TagRFP647-LifeAct expressing cells, we released GFP-Rab35 from mitochondria and live-imaged its subsequent localization [237]. Rab35 quickly localized to the cell periphery following trimethoprim (TMP) treatment, avoiding longer-lived F-actin (Figure 19F). When repeated with Arp2 and DENNd1c, Rab35 quickly (~2 min) localized to both proteins on the cell cortex (Figure 19G, H). Next, we released Rab35, and then treated with CK-666 to determine how this association would be affected. Administration of CK-666 rapidly dissociated Rab35 and Arp2 at the cortex (Figure 19I). Lastly, to test if DENNd1c was responsible for recruiting Rab35 to branched actin, we knocked down DENNd1c and observed a significant reduction in Rab35's ability to localize to cortical Arp2 (Figure 19J, K). Overall, these data suggest that Rab35 is rapidly recruited to the actin cortex and is anchored by DENNd1c.

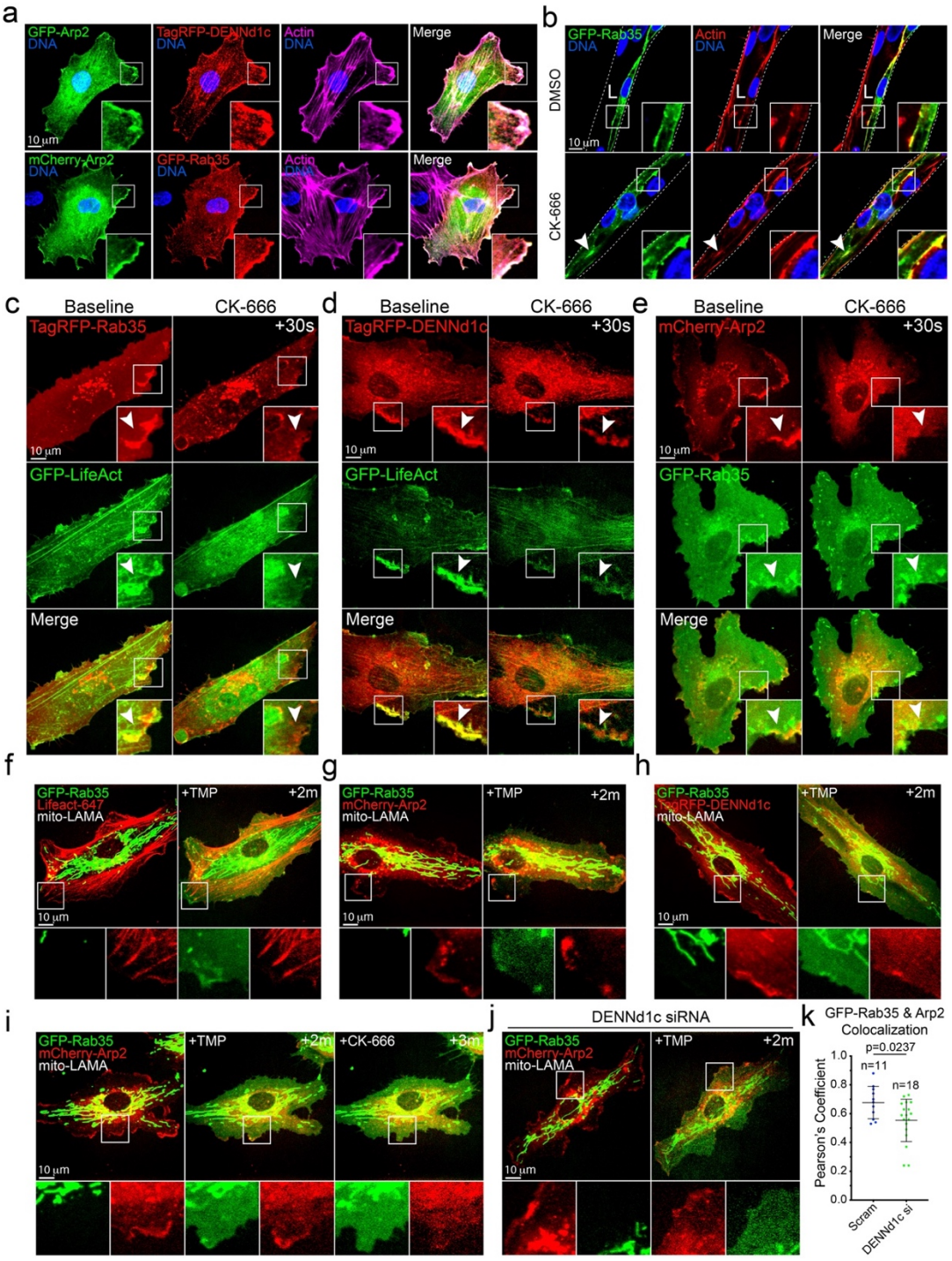

Figure 19: Rab35 localizes to cortical actin. A. Two-dimensional localization of GFP-Arp2 with DENNd1c (top panels) and GFP-Rab35 (bottom panels). B. Representative images of DMSO and CK-666 (Arp Inhibitor) treated sprouts expressing GFP-Rab35. L denotes lumen. C, D. Live imaging of GFP-Rab35 or TagRFP-DENNd1c with TagRFP647-LifeAct at baseline and after treatment with CK-666. White arrowheads

denote the disappearance of Rab35 puncta over time. E. Representative live-images of a cell expressing mCherry-Arp2 and GFP-Rab35 before and after CK-666 treatment. White arrowheads denote the disappearance of Rab35 puncta over time. F. Live-image of a cell expressing GFP-Rab35, TagRFP647 (647)-LifeAct and ligand-modulated antibody fragments targeted to the mitochondria (mito-LAMA) before and after TMP administration. G. Live-image of a cell expressing GFP-Rab35, mCherry-Arp2, and mito-LAMA before and after TMP administration. H. Live-image of a cell expressing GFP-Rab35, TagRFP-DENNd1c, and mito-LAMA before and after TMP administration. I. Live-image of a cell expressing GFP-Rab35, mCherry-Arp2, and mito-LAMA before and after TMP administration and then treated with CK-666. J. Live-image of a cell expressing GFP-Rab35, mCherry-Arp2, and mito-LAMA treated with DENNd1c siRNA (si) before and after TMP administration. K. Pearson's Coefficient of Rab35 and Arp between Scram and DENNd1c siRNA treated cells 2 min following TMP treatment. n = number of cells. Error bars represent standard deviation, middle bars are the mean. Statistical significance was assessed with an unpaired t-test. Insets are areas of higher magnification. All experiments were done using human umbilical vein endothelial cells in triplicate.

Rab35 Regulates Actin Assembly

Our next aim was to test whether Rab35 affected actin polymerization, per se. Prior literature indicates that Rab35 would increase actin polymerization via its purported trafficking interactions with Cdc42 and Rac1; however, others have claimed Rab35 may act as a brake for actin polymerization through its association with MICAL-1 [216, 230, 231, 233].To explore how Rab35 impacts actin in ECs, we transfected Rab35 variants WT, CA, and DN into freely migrating ECs. It is well-established that lamellipodia protrusions and retractions are primarily mediated by local actin assembly and disassembly [238, 239]. To monitor lamellipodia dynamics, we employed the open-source software ADAPT [240]. Our analysis determined that only the Rab35-CA mutant significantly increased both the cells protrusive and retractive capabilities, a finding in line with enhanced migration (Figure 20A, B) [241]. Interestingly, knockdown of Rab35 did not shift 2D-membrane dynamics significantly, potentially suggesting Rab35-based actin regulation may play a more central role in 3D sprouting.

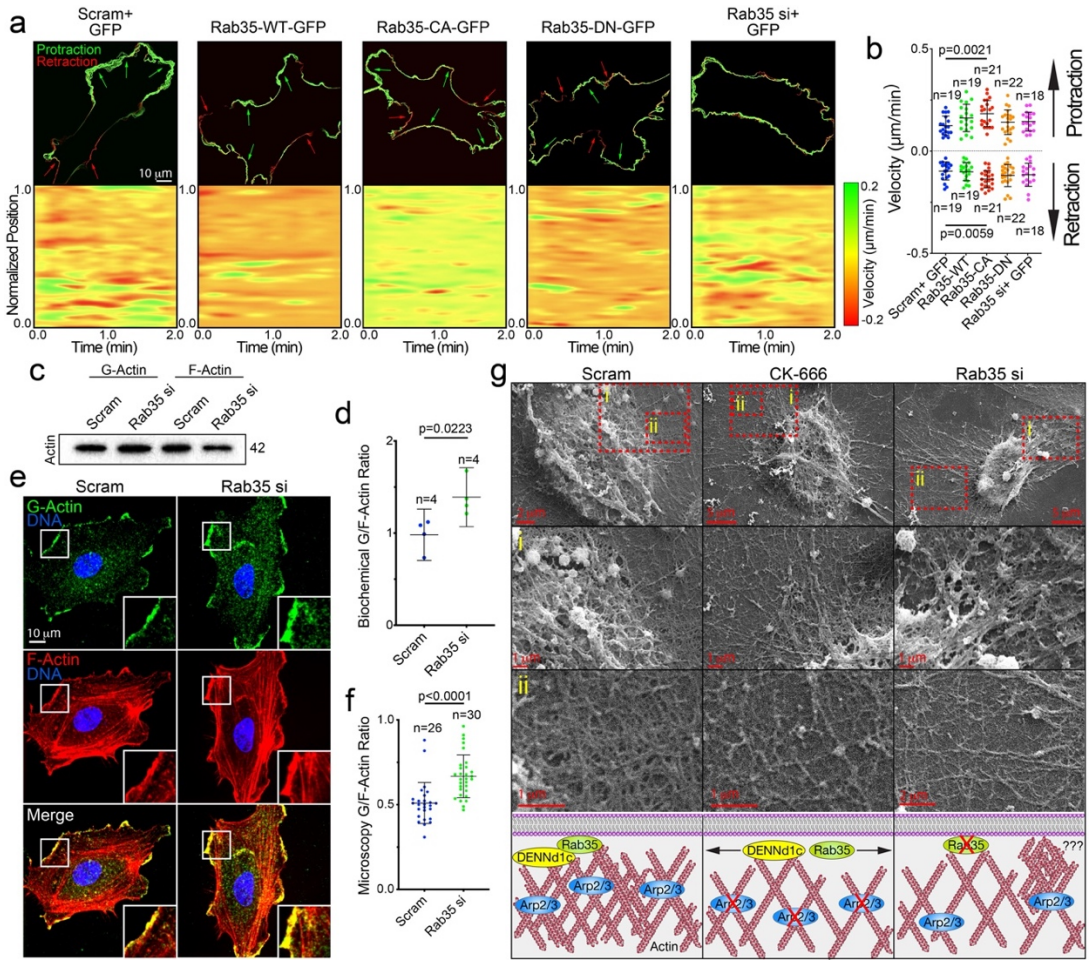

Figure 20: Rab35 Regulates Actin Dynamics. A. Top panels depict change in membrane velocities over time in described conditions. Green represents protraction and red represents retraction of cell membrane. Arrows indicate directionality. The bottom panels are heat maps in which the Red is indicative of retractive movement and green is protractive movement over time. Yellow indicates no change in velocity. B. Quantification of cell membrane velocities between indicated groups. Above the dashed line is the protractive velocities and below the dashed line is retractive velocities. n = number of cells. Error bars represent standard deviation, middle bars are the mean. C. Western blot of globular (G) and filamentous (F) actin in siRNA (si)-treated groups. D. Quantification of the ratio of globular to filamentous actin from blots represented in panel (c). n = number of cells. Error bars represent standard deviation, middle bars are the mean. E. Representative images of cells stained for globular and filamentous actin between indicated conditions. F. Quantification of the ratio of globular to filamentous actin fluorescent intensities. n = number of cells. Error bars represent standard deviation, middle bars are the mean. G. Scanning electron microscopy of filament network between groups. Top panel is the lowest magnification with higher magnifications in panels (i) and (ii). Bottom- cartoon representation of SEM filament network and hypothesized role of Rab35. NS = non-significant. Statistical significance was assessed with an unpaired t-

test or a 1-way ANOVA followed by a Dunnett multiple comparisons test. Insets are areas of higher magnification. All experiments were done using human umbilical vein endothelial cells in triplicate.

We reasoned that if Rab35 was involved with actin polymerization, then knockdown of Rab35 would shift the balance between globular (G) and F-actin to skew more globular, assuming less filaments are being assembled. We isolated the G- and F-actin pools and found that Rab35 knockdown significantly increased the G-actin ratio compared with control (Figure 20C, D) [242]. In staining for G-actin using GC-globulin and phalloidin to detect F-actin, we observed a significant increase in the G/F-actin ratio in the absence of Rab35 as compared with controls (Figure 20E, F) [243]. Co-staining for G/F actin while expressing Rab35, we validated Rab35 colocalized with both actin populations (Supplementary Figure 19G). This data suggests that loss of Rab35 is associated with elevated cellular G-actin.

Using scanning electron microscopy, we visualized the filament network in ECs depleted of Rab35 or treated with CK-666. Qualitatively, there was reduced filament density in the lamellipodia regions of the Rab35 depleted and CK-666 treated conditions as compared with control (Figure 20G). In Rab35 depleted ECs, we also observed elevated instances of disorganized actin bundles (Figure 20G), potentially representing nodes of atypical actin polymerization. Overall, these results suggest that Rab35 is associated with regulating local sites of actin assembly.

Loss of Rab35 Promotes Chronic Cytoskeletal Rearrangements

Cumulatively, our data suggests that Rab35 has a potent ability to perturb actin dynamics; however, we were still uncertain to how this was being achieved mechanistically. In other words, does the loss of Rab35 decrease actin polymerization

programs or enhance it? Given Rab35 naturally localizes to the actin cortex in 2D, we investigated how loss of Rab35 impacted two actin networks interfacing through Rac1 or RhoA. Rac1 is a highly characterized GTPase that mediates branched actin polymerization, while RhoA mediates assembly of actin stress fibers [244]. To our surprise, we observed that both Rac1 and RhoA activity were elevated in the absence of Rab35 (Figure 21A-D) This finding is in line with DENNd1c's ability to bind both actin populations; although, it is contrary to our previous assumption that loss of Rab35 reduced actin polymerization. To our knowledge, this is the first indication that loss of Rab35 promotes chronic actin rearrangements.

We next sought to reconcile our previous results showing elevated G-actin in Rab35 knockdown cells. Curious as to why stimulating two of the most prominent *pro*-actin polymerization pathways resulted in more G-actin, we treated cells with combinations of Rac1 and RhoA inhibitors (NSC23766 and Y27632) as well as activating compounds (CN02 and CN03). Over-activation of RhoA significantly skewed cells towards elevated G-actin, while over-activation of Rac1 did not affect G-/F-actin ratio (Figure 21E-H). This result agrees with our finding that Rab35 loss of function biases the actin pool towards more globular state likely due to increased RhoA activity.

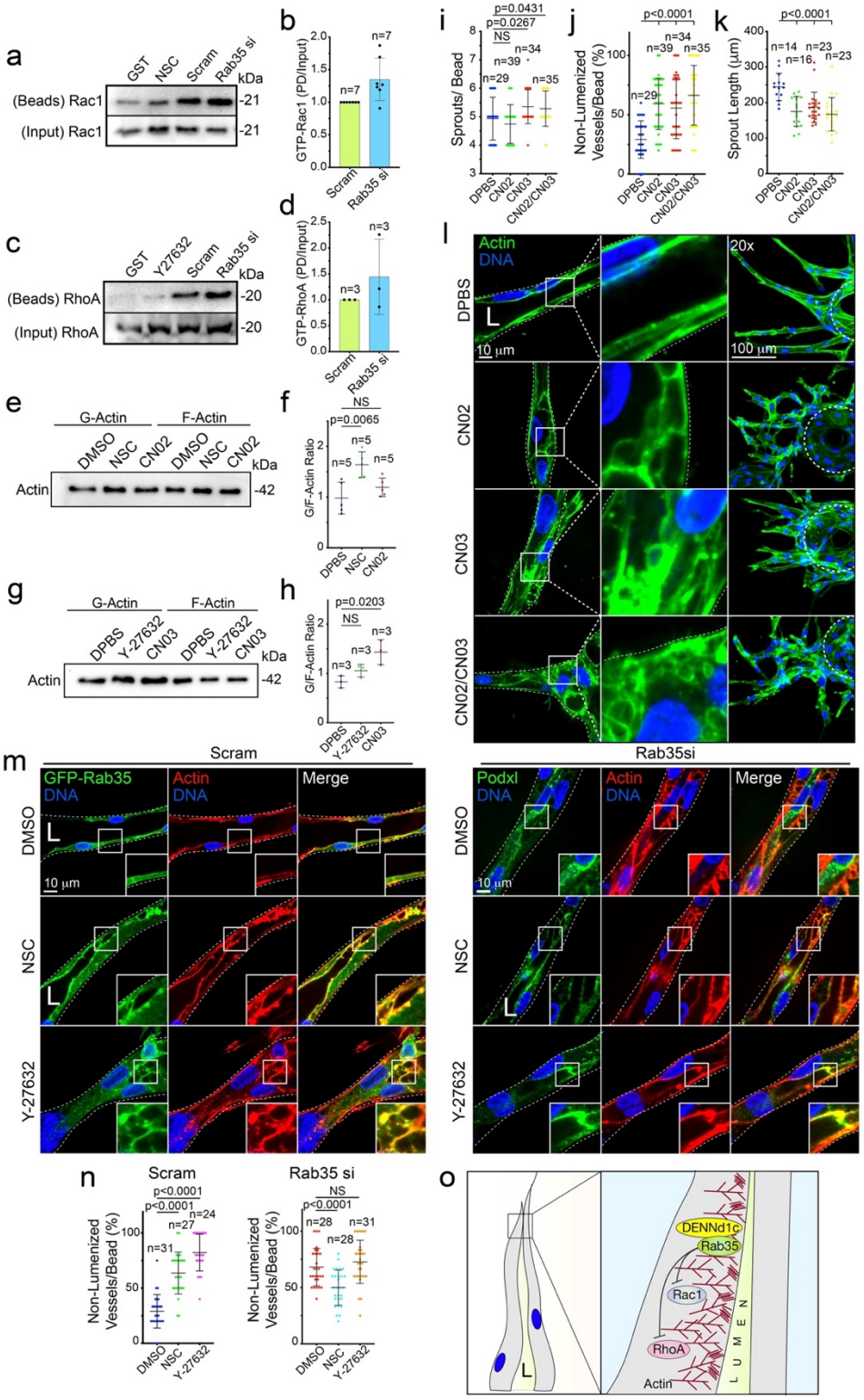

Figure 21: Loss of Rab35 promotes chronic actin remodeling. A. Representative western blot pulldown for activated Rac1. Cells were treated with scramble (Scram) and Rab35

siRNA (si) or treated with Rac Inhibitor NSC23766 (NSC) then probed for active (GTP) Rac1. B. Quantification of Rac1 activity between indicated groups normalized to control. n = number of pull-downs. Error bars represent standard deviation, middle bars are the mean. C. Representative western blot pulldown for activated RhoA. Cells were treated with scramble and Rab35 siRNA or ROCK inhibitor (Y27632). D. Quantification of RhoA activity between indicated groups normalized to control. n = number of pull-downs. Error bars represent standard deviation, middle bars are the mean. E. Western blot of globular (G) and filamentous (F) actin populations treated with DPBS (vehicle), NSC, or Rac1 activator (CN02). F. Quantification of the ratio of globular to filamentous actin from blots represented in panel (e). n = number of blots. Error bars represent standard deviation, middle bars are the mean. G. Western blot of globular and filamentous actin population treated with DPBS, Y27632, and RhoA activator (CN03). H. Quantification of the ratio of globular to filamentous actin from blots represented in panel (g). n = number of blots. Error bars represent standard deviation, middle bars are the mean. I-K. Graphs of indicated sprout parameters across groups. n = number of sprouts. Error bars represent standard deviation, middle bars are the mean. L. Representative images of sprouts treated with indicated compounds. M. Representative images of Scram (left figure) and Rab35 si (right figure) treated sprouts with indicated drug treatments. N. Quantification of non-lumenized vessels/bead from experiments in panel (m). n = number of sprouts. Error bars represent standard deviation, middle bars are the mean. O. Model of Rab35 mechanism. In all panels, L denotes lumen. NS = non-significant. Statistical significance was assessed with an unpaired t-test or a 1-way ANOVA followed by a Dunnett multiple comparisons test. Insets are areas of higher magnification. All experiments were done using human umbilical vein endothelial cells in triplicate.

To understand how aberrant Rac1 and RhoA activation affected sprouting, we over-activated both Rac1 and RhoA in sprouts. Over-activation of either protein caused significantly increased lumen failures as well as generalized sprouting defects (Figure 21I-L). To further confirm over-activation of RhoA downstream of Rab35 knockdown, we transduced sprouts with a RhoA localization sensor (C-terminus of Anillin) [245]. In control sprouts, ECs showed limited localization of the Biosensor on actin after lumenogenesis; however, in the Rab35 knockdown sprouts the biosensor was primarily distributed on F-actin (Supplementary Figure 20A). Lastly, we used Rac1 and RhoA inhibitors to reduce chronic activation of these pathways on a Rab35 loss of function background. Indeed, dampening of Rac1, not RhoA, significantly improved the

percentage of lumenized sprouts on a Rab35 knockdown background (Figure 21M-O). Overall, this data suggests that loss of Rab35 promotes chronic over-activation of both Rac1 and RhoA; however, aberrant Rac1 activity is likely the underlying mechanism driving chronic actin remodeling and generalized sprout dysmorphogenesis.

Rab35 is Required for Blood Vessel Development in Zebrafish

We next generated a Rab35 knockout in zebrafish using CRISPR/Cas9 gene editing to test if Rab35 was also required for in vivo angiogenic processes [246]. In zebrafish, we targeted both Rab35 paralogs, Rab35A and Rab35B (Figure 22A and Supplementary Figure 20B). Double Rab35A/B knockout was embryonic lethal marked by a lack of normal development as compared with scramble guide injected controls, suggesting Rab35 is critical for normal embryonic development (Figure 22B). However, we did produce a spectrum of developmental defects when the single-guide RNA amount was diluted. In a vascular Lifeact-GFP expressing line injected with a sublethal dosage of Rab35A/B single-guide RNA, we focused on actin defects. Here, we did not quantify vascular defects due to the generalized tissue dysmorphogenesis of these embryos; alternatively, our goal was to determine if similar actin accumulations occurred in vivo as observed in vitro. In line with our in vitro data, we observed a significant increase in actin aggregations in the Rab35A/B knockout group compared with controls (Figure 22C, D). Vascular overexpression of the DN Rab35 mutant or treatment with CK-666 also promoted an increase in aberrant Rab35 accumulations, presumably bound to actin (Figure 22E, F). To subvert the lethality of global Rab35A/B deletion, we generated chimeric embryos using blastomere transplants [247]. Transfer of Rab35A/B CRISPR injected cells into a WT host generated mosaic intersomitic blood vessels (ISVs) allowing

for comparison of both WT and Rab35A/B null blood vessels side-by-side. Similar to our in vitro results, Rab35A/B null ISVs were dysmorphic, marked by a thin appearance and the absence of a lumen as assessed by microangiography (Figure 22G, H). Overall, these results indicate Rab35 is necessary for organismal viability and actin homeostasis in vivo.

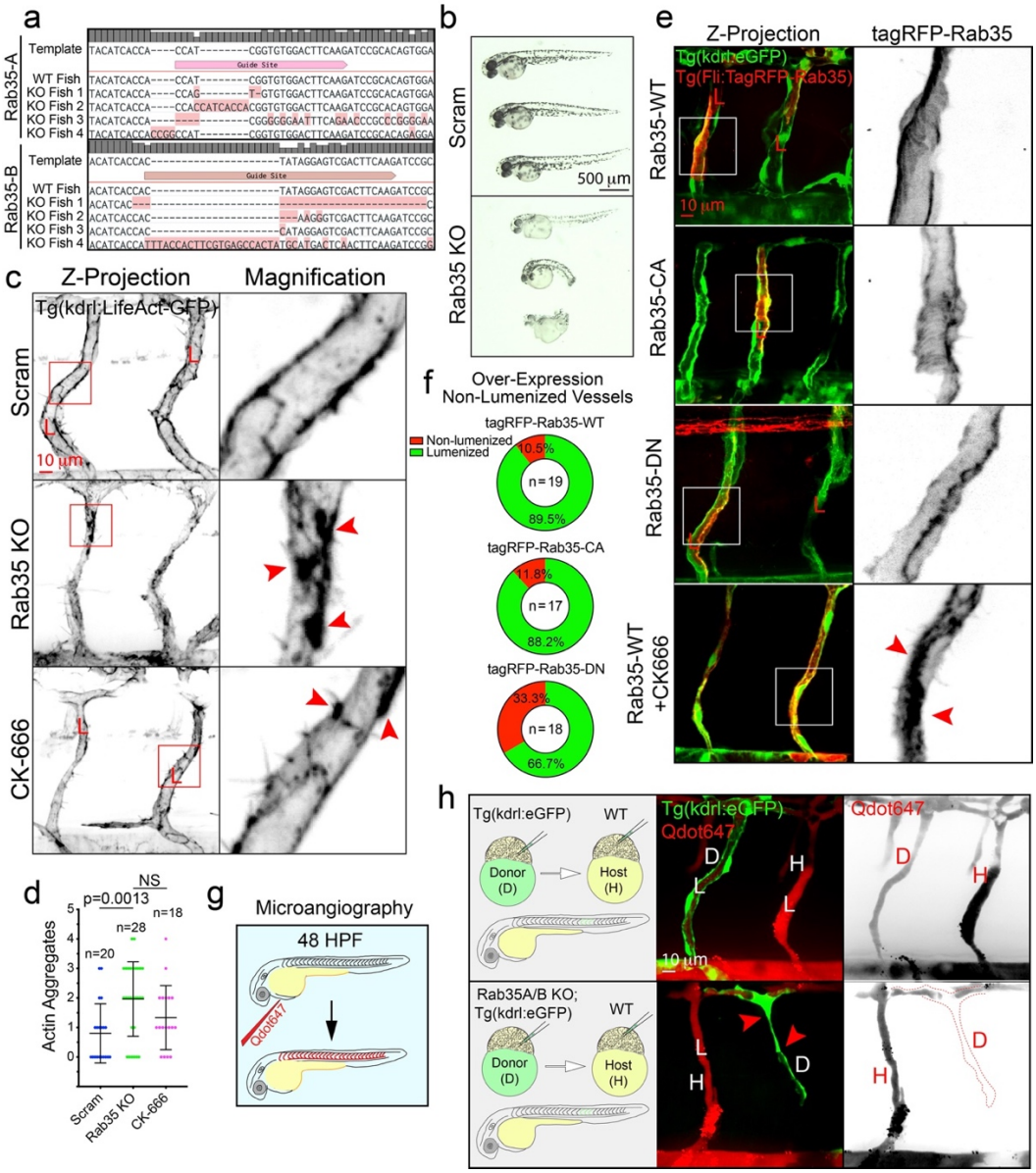

Figure 22: Rab35 is required for blood vessel development in zebrafish. A. CRISPR-mediated knockout of Rab35A/B confirmation by sequencing. Four random fish were sequenced following CRISPR/guide injections. B. Zebrafish morphology at 48 h post fertilization (hpf) post injection of scramble (Scram) and Rab35A/B CRISPR guides. C.

Representative images of intersomitic blood vessels (ISVs) of Scram and Rab35A/B knockout, as well as CK-666 (Arp Inhibitor), treated zebrafish at 48 hpf expressing endothelial specific LifeAct-GFP. Red arrowheads indicate abnormal aggregates of actin. D. Quantification of actin aggregates between groups. n = number of ISVs. A minimum of 5 fish were used per group. Error bars represent standard deviation, middle bars are the mean. E. Representative images of mosaic expression of Tag-RFP-Rab35 WT (top row), CA (second row), DN (third row), and WT with CK-666 treatment in zebrafish at 48 hpf. Red arrowheads depict excess of Rab35 at the plasma membrane. F. Percentage of non-lumenized vessels at 48 hpf between groups mentioned in panel (e). n = number of ISVs. G. Cartoon representation of microangiography in zebrafish larvae using quantum dots 647 (Qdot647) at 48 hpf. H. Representative images of ISVs after transplantation of Tg(kdrl:GFP) donor (D) into Tg(kdrl:mCherry) host (H) (top panels). Bottom panels-representative images of ISVs after transplantation of Rab35A/B knockout donor cells from Tg(kdrl:GFP) line into Tg(kdrl:mCherry) host. Red arrowheads indicate lumen failure. NS = non-significant. Error bars represent standard deviation. Statistical significance was assessed with an unpaired t-test or a 1-way ANOVA followed by a Dunnett multiple comparisons test. Insets are areas of higher magnification. All experiments were done in triplicate.

4.4 Discussion

The primary goal of this work was to interpret what of the many reported functions of Rab35 matters most during blood vessel morphogenesis by systematically characterizing Rab35 itself and the downstream effector pathways. Using a combination of 3D sprouting, biochemistry and in vivo gene editing, we demonstrate that Rab35's most prominent function is to regulate actin dynamics during angiogenesis. More specifically, we show that the GEF DENNd1c tethers active Rab35 to the actin cytoskeleton. Once localized to actin, Rab35 limits actin polymerization and remodeling required for sprout formation (Figure 21O). To our knowledge, this is the only investigation demonstrating the requirement of Rab35 for blood vessel function and the only investigation in any tissue dissecting Rab35's most dominant biological role accounting for the most prominent effector pathways.

The current project was originally aimed to characterize how podocalyxin was trafficking in ECs, as this is still an outstanding question in the field. Our past work

demonstrated Rab27a, that was largely implicated in podocalyxin trafficking in epithelial cells, was not related to this pathway, thus our very next candidate was Rab35 [201]. Others have comprehensively established a direct association between Rab35 and podocalyxin as well as the downstream impact on lumen biogenesis [210, 211]. Our data in the current investigation once again shows that endothelial trafficking signatures greatly differ from epithelial programs. We expansively tested for both localization and direct binding interaction between Rab35 and podocalyxin of which we found none. Although, this negative result prompted us to further investigate Rab35 function during angiogenic sprouting.

Rab35 has been shown to have many roles that vary by tissue type, organism, and developmental stage. In distilling the literature, it can be argued that Rab35 has six major effectors that mediate its function in vertebrates: Rusc2, MICAL-L1, MICAL1, ACAP2, OCRL, and Fascin. We began by first establishing that Rab35 was required for sprouting, and then determined how each effector contributed to the loss of Rab35 phenotype. Surprisingly, most effectors failed to directly bind Rab35. ACAP2 exhibited the best phenotype for recapitulating the Rab35 loss of function effect. The predominant hypothesis is that GTP Rab35 binds ACAP2 sequestering its ability to inactivate Arf6, resulting in a gain of function for Arf6. In ECs, we confirmed direct binding between ACAP2, and also observed that Rab35 knockdown increased Arf6 activity as previously reported [212-214, 222, 225, 226, 248, 249]. However, overexpression of CA Arf6 did not phenocopy the Rab35 loss of function effect on sprouting, suggesting that aberrantly high Arf6 activity was likely not causing sprout dysmorphogenesis in the absence of Rab35.

A major finding was that the GEF DENNd1c played a key role in Rab35 function. Canonically, GEFs primarily convert proteins from a GDP to GTP-bound state; however, DENNd1c is evolutionarily divergent from both DENNd1a/b that solely control Rab35 GTPase activity [231]. In our hands, DENNd1c localized Rab35 to actin fibrils. Knockdown of DENNd1c strongly phenocopied loss of Rab35 suggesting that localization to actin is a primary function of Rab35 during sprouting angiogenesis.

Actin plays a pivotal role in angiogenesis both from a cell migration and vessel stabilization aspect [250-254]. Loss of normal actin architecture has been shown to drastically affect virtually all facets of blood vessel formation [255- 259]. In this sense, our results are not surprising in that actin mis-regulation promoted such a profound negative effect on sprouting parameters. However, given Rab35's broad scope of function as well as never being characterized in angiogenic processes, it would be exceedingly hard to predict. Our results paint a scenario that trafficking-based regulators can control vital crosstalk with the actin cytoskeleton. Our results strongly indicate that Rab35 limits the activation of Rac1 and RhoA-mediated cytoskeletal rearrangement. Whereby loss of Rab35 creates a scenario in which the actin cytoskeleton is never fully stabilized promoting gross polarity defects in sprouts. It is still an outstanding question as to how this activation is achieved or what is the Rab35 interactome. Importantly, our results may provide an additional mechanism of why loss of Rab35 causes elevated cancer invasiveness through loss of tissue architecture [260-262].

Overall, our investigation is the first to systematically rule out other known Rab35 pathways, highlighting Rab35's function in mediating actin dynamics during blood vessel formation in vitro and in vivo. In general, we contend that mapping endothelial

trafficking patterns will shed important light on how ECs orchestrate blood vessel formation by integrating both cell-autonomous and collective-cell signaling.

Chapter Four: Arf6 Regulates Endocytosis by Promoting Filamentous Actin Assembly in Endothelium

2.1 Introduction

Small GTPases are most recognized for their contribution to vesicular and organellar transport. This large family of proteins tightly regulate intracellular traffic by characteristically switching between an active (GTP-bound) or an inactive (GDP-bound) state [4]. ADP-ribosylation factor (Arf) GTPases are a sub-family of small GTPases with six isoforms identified [289]. Within this subfamily, Arf6 is reported to operate at the plasma membrane with a well-defined role in cytoskeleton rearrangement [268, 289]. This localization is highly distant from the other Arf family members which are associated with Golgi trafficking [268]. Arf6 remodels plasma membrane actin by promoting the assembly of filamentous actin; however, the mechanism by which it achieves this remains uncertain [283].

In addition to its role in modifying plasma membrane actin architecture, Arf6 is well known to facilitate membrane protein internalization [269, 270]. Moravec, et al., show that Arf6 co-localizes with Clathrin-coated pits and is required for β-integrin endocytosis in epithelium [269]. In endothelium, Hongu and colleagues' data suggests that Arf6 is required for hepatocyte growth factor (HGF)-induced tumor neo-angiogenesis and growth [279]. In this study, Arf6 knockout abolished HGF-stimulated β-integrin

recycling and slowed tumor vascularization [279]. Beyond the mentioning of these two studies, Arf6 has been linked to many endocytic pathways across tissue types.

Several proteins have been linked to the molecular regulation of Arf6. Like other small GTPases, Arf6 is activated by guanine nucleotide exchange factors (GEFs) and inactivated by GTPase-activating proteins (GAPs) [4]. Out of fifteen Arf-family GEFs identified, eight have been clarified to promote GDP/GTP exchange specific to Arf6 [290]. From the Arf GAP family of thirty-one proteins, nine are identified that inactivate Arf6 [291]. ARNO, a GEF to Arf6, is reported to cycle Arf6 activation at the plasma membrane and induce cytoskeletal rearrangements and endocytic events in epithelium and neurons [271-273, 282, 284]. ACAP2, a proposed GAP of Arf6, is equally important to the cycling of activity states to regulate actin and endocytosis [212, 213, 226, 228, 281]. However, limited information is available regarding these effectors roles in sprouting angiogenesis and lumen formation.

Research on Arf6 in endothelium has focused on cancer metastasis and vascular permeability [275-280]. Several studies echo the importance of Arf6 in stabilizing cell-cell junctions [276, 278]. Arf6 is the focus of therapeutic targeting as it positively regulates internalization of growth factor and integrins, both pathways are conducive to cancer cell migration [279, 280]. Consistent with other reports of growth factor internalization, an investigation by Ikeda, et al., reported Arf6 co-localized with VEGFR2 and is necessary for autophosphorylation of VEGFR2 [275]. Their data suggests an important role for Arf6 in VEGF signaling linked to sprouting angiogenesis.

We investigated Arf6 using the 3-dimensional fibrin bead assay (FBA). This assay allowed for live imaging of Arf6 trafficking as well as in depth imaging analysis of Arf6

with a range of endothelial specific transmembrane proteins. Our findings indicate that Arf6 is imperative to filamentous actin assembly in addition to membrane protein internalization. VEGFR2, VE-Cadherin and podocalyxin internalization are all disrupted in the absence of Arf6. Our data suggests that the regulation of cortical actin by Arf6 is the key mechanism of action. While Arf6 localizes to sites of Clathrin-mediated endocytosis, it will only dissociate from the plasma membrane when Arp is inhibited, however, not when Clathrin-mediated endocytosis is inhibited. This data provides insight into the broad role of Arf6 in sprouting angiogenesis. Our findings also agree with previous reports of Arf6 regulating filamentous actin turnover as well as ligand internalization. This contextualizes the role of Arf6 at the plasma membrane with its regulation of actin and endocytic events in endothelium.

2.2 Materials and Methods

Cell Culture

See Annex A.

Sprouting Angiogenesis Assay

See Annex A.

Plasmid Constructs

See Annex A Table 6.

Lentivirus and Adenovirus Generation and Transduction

See Annex A.

Membrane Fraction Assay

Membrane fractions were performed according to the guidelines provided using the Thermo-Scientific Mem-PER Plus Membrane Protein Extraction Kit (Appendix A, Table 2). Total concentration of protein in membrane fraction lysate was quantified using the Pierce™ BCA Protein Assay Kit measured at 562 nm and compared to a standard curve. Samples were then prepared for immunoblotting as described in Appendix A: Immunoblotting and protein pull-down.

Immunoblotting and Protein Pull-Down

See Appendix A.

Immunofluorescence and Microscopy

See Appendix A.

Quantification of Fluorescent Intensity

Fluorescent intensity was determined by first projecting the entire sprout to a single image, setting the scale of the image and designating a region of interest around a sprout. The resulting intensity was then divided by the area of the sprout. For quantifying western blot band intensity between groups, the area was set constant from band to band and fluorescent intensity was compared with equal areas.

Statistical Analysis

See Appendix A.

2.3 Results

Arf6 Localizes to the Plasma Membrane and is Required for Sprouting Angiogenesis and Lumenogenesis

Arf6 is widely reported to localize to the plasma membrane across tissue types. To validate this in endothelium, we employed the 3-dimensional (3D) fibrin bead assay (FBA) to validate this [159]. In this assay, human umbilical vein cells (HUVECs) were adhered to microbeads and challenged to sprout into surrounding fibrin matrix [159, 160]. As HUVECs are highly sensitive primary cells, lentiviral transduction has served as the best delivery for plasmid over-expression. Thus, Arf6-CFP (Cyan Fluorescent Protein) was transduced to HUVECs and live-imaged in sprouts and fixed for immunohistochemistry. Live Arf6-CFP showed enrichment at sites of lumen formation as well as decorating vesicles at the membrane. In fixed sprouts, Arf6-CFP co-localized with podocalyxin (podxl), a transmembrane protein implicated in endothelial lumen formation (Figure 23A). Overall, Arf6-CFP was enriched in the apical plasma membrane but often equally enriched basally and apically (Figure 23B).

Next, we aimed to determine the requirement of Ar6 expression during sprouting angiogenesis. Sprouts were treated with scram control and Arf6 siRNA and sprouting parameters were compared following four days of growth. Arf6 knockdown (KD) sprouts produced shorter, thinner sprouts with no discernable lumen (Figure 23C-F). There were also more vacuolations present in knockdown sprouts, a possible compensatory effort by the sprout to form a lumen cavity (Supplemental Figure 21B). Interestingly, in two-dimensions (2D) we did not observe a significant difference in migration of scram and Arf6 siRNA treated sprouts (Supplemental Figure 21C, D). It appears that Arf6 is more

important to cell migration as part of collective cellular movement in a 3D environment. Our siRNA-mediated knockdown was confirmed using western blotting (Figure 23G).

Given the severity of the Arf6 knockdown, we shifted our 3D assays to a mosaic Arf6 KD. To accomplish this, a population of siRNA treated cells were applied with cell tracker, then combined with untreated cells. The mosaic sprouts presented two sprout scenarios, sprouts with not-opposing knockdown cells and sprouts with knockdown cells opposing. The mosaicism rescued sprout length and sprouts per bead (Figure 23I-K). However, in both scenario, sprouts were significantly less lumenized in the presence of knockdown cells, with the phenotype more severe when knockdown cells were opposing (Figure 23L). Notably, knockdown cells have diminished filamentous actin (f-actin) as well as instances where actin appears to accumulate abnormally (Figure 23I). In the same assay, β-integrin localization appears abnormal in KD cells, with it localized apically rather than basally (Supplemental Figure 21A).

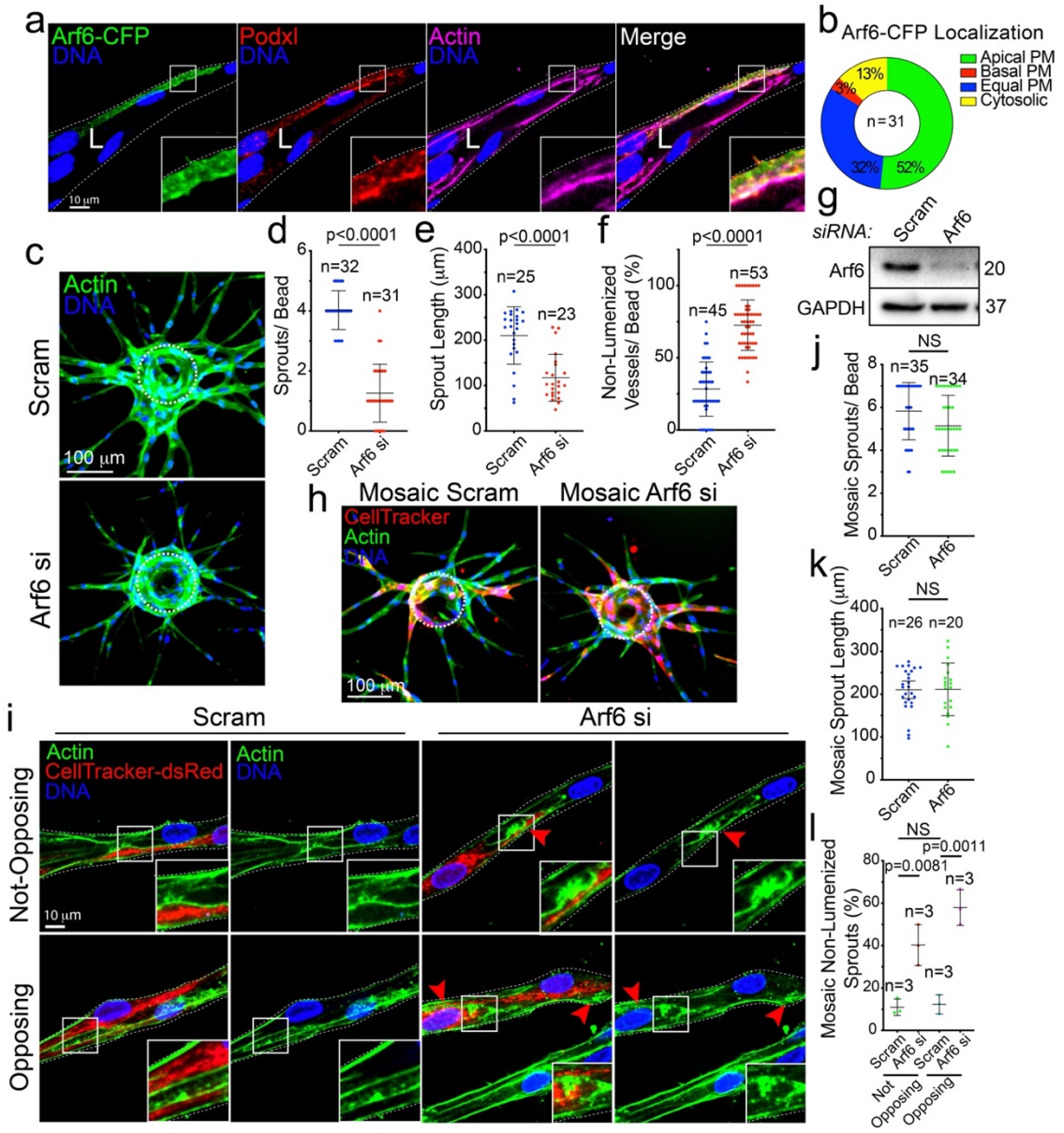

Figure 23: Arf6 Localizes Apically and is Required for Vessel Formation. A. Representative image of Arf6-CFP expression in the fibrin-bead assay (FBA) with podocalyxin (red) and actin (magenta). B. Quantification of Arf6-CFP localization in the FBA. C. Representative sprout morphology images of scramble (Scram) control and Arf6 siRNA knockdown (KD) sprouts. Dashed lines outline the microbead. D-F. Graphs of indicated sprouting parameters between groups. n = number of sprouts. Error bars represent standard deviation, middle bars are the mean. G. Western blot confirmation of siRNA (si) knockdown (KD) of Arf6 (average 60.8% KD relative to control, n = 3). H. Representative images of sprout morphology of mosaic Scram and Arf6 siRNA KD cells. Dashed lines outline the microbead. I. Representative images of non-opposing (top panels, an isolated siRNA treated cell) and opposing (bottom panels, two adjacent siRNA

treated cells) cells stained as indicated. Arrowheads denote aberrant actin accumulations. K-L. Quantification of indicated parameters across groups. n = number of sprouts. Error bars represent standard deviation, middle bars are the mean. m Quantification of non-lumenized sprout area across indicated groups. n = mean percentage of each experimental repeat (each group contains >20 cells). Error bars represent standard deviation, middle bars are the mean. In all images L denotes lumen. NS = non-significant. Statistical significance was assessed with an unpaired t-test or a 1-way ANOVA followed by a Dunnett multiple comparisons test. Insets are areas of higher magnification. White dashed lines mark sprout exterior. All experiments were done using Human umbilical vein endothelial cells in triplicate.

In agreement with previous reports, our data confirmed that Arf6 localizes to the plasma membrane and cells deficient in Arf6 present abnormalities in f-actin and β-integrin. Unique to our model, we show Arf6 is required for sprout migration and lumen formation. Considering the severity of the phenotype we observed, this led us to question whether endothelial specific transmembrane proteins are also disrupted in the absence of Arf6.

Arf6 is Required for Transmembrane Protein Internalization

Potentially, the mechanism behind the necessity of Arf6 for angiogenesis is the failure of transmembrane proteins to be internalized. Thus, we again siRNA treated sprouts with scram control and Arf6 siRNA and stained for endogenous transmembrane proteins of relevant to sprouting angiogenesis. Podocalyxin (podxl) is involved in lumenogenesis, Vascular Endothelial-Cadherin (VE-Cad) maintains cell-cell junctions, β-integrin binds the extracellular matrix, and Vascular Endothelial Growth Factor Receptor 2 (VEGFR2) is a receptor-tyrosine kinase which receives and transmits growth factor signal [317-319]. Finally, Tyrosine-protein kinase receptor 2 (TIE-2) acts as a cell-surface receptor for Angiopoietin-1, -2, and -4 (Ang-1,-2,-4) and regulates angiogenesis, endothelial cell survival, proliferation, migration, adhesion, and reorganization of the

actin cytoskeleton [307,320-321]. All the proteins presented abnormally in Arf6 siRNA treated sprouts when compared with scram control sprouts (Figure 24A). Quantification of fluorescent intensity resulted in higher signal detected for all probed proteins, however, only podxl and β-integrin were significantly higher (Figure 24B). In addition to the KD assays, we observed co-localization of each of these proteins with Arf6-CFP transduced in sprouts. Sites of enrichment of Arf6-CFP co-localized particularly with podxl, VEGFR2, and TIE-2 but less so with β-integrin and VE-Cad (Supplemental Figure 22A). This is potentially context dependent, as sprouts were fixed during lumen formation.

To attempt a closer examination of these results, membrane fractions were isolated from scram and Arf6 siRNA populations of cells and probed for the same proteins assessed in sprouts. VE-Cad and podxl resulted in significantly higher detection relative to scram cells, where TIE-2, VEGFR2, and β-integrin did not (Figure 24C-D). We also employed a seeding assay to examine more carefully the requirement of Arf6 for internalization. Our results show that β-integrin is internalized significantly less in Arf6 KD cells compared with control cells (Supplemental Figure 22B-C). The discrepancies in our 2D results could be attributed to differences in protein expression and trafficking behaviors between 2Dand 3D environments [83].

It is clear from our results that Arf6 is required for the endocytosis of a range of transmembrane proteins, highlighting the ubiquitous nature of Arf6. While Arf6-mediated internalization is likely under strict regulation by its effectors, the polar

specificity of the membrane proteins that Arf6 internalizes is unclear. In our hands, basal, junctional and apical transmembrane proteins were impacted by Arf6.

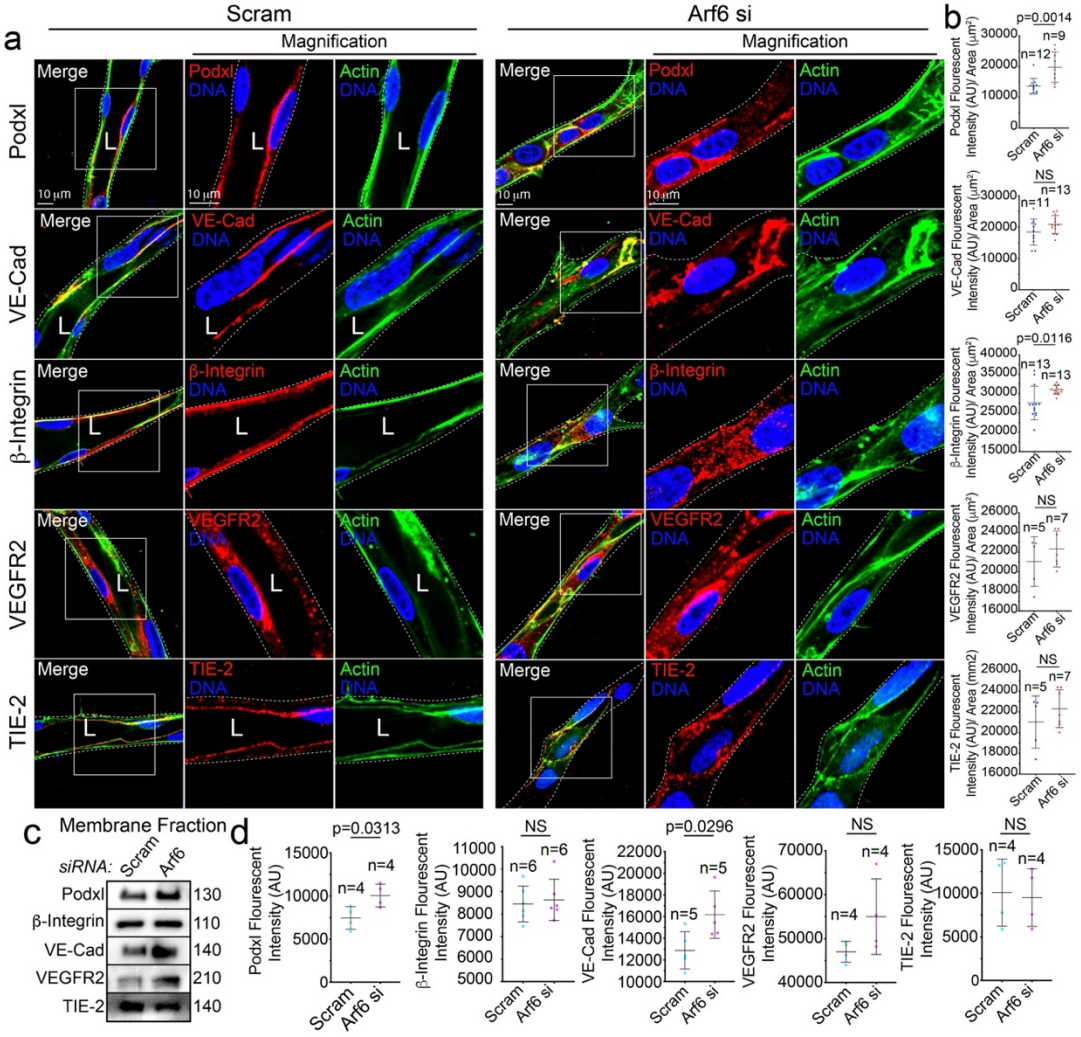

Figure 24: Loss of Arf6 Results in Accumulation of Transmembrane Proteins. A. Representative images of scramble (Scram) control and Arf6 siRNA knockdown (KD) sprouts in the fibrin bead assay (FBA) with endogenous podocalyxin (podxl, top panels), VE-Cadherin (VE-Cad, second panels), β-integrin (third panels), Vascular Endothelial Growth Factor Receptor 2 (VEGFR2, fourth panels), and TIE-2 (bottom panels). Actin (green) is shown in all sprouts. In all panels, L denotes lumen. White box is area of magnification. Insets are areas of higher magnification. Dashed lines mark sprout exterior. B. Quantification of fluorescent intensity for proteins in A. n = number of sprouts. AU is arbitrary unit. Error bars represent standard deviation, middle bars are the mean. C. Western blotting of membrane fractions isolated from Scram and Arf6 siRNA KD cells. D. Quantification of band fluorescent intensity from membrane fractions in G. n = individual membrane fraction experiments. Error bars represent standard deviation,

middle bars are the mean. NS = non-significant. Statistical significance was assessed with an unpaired t-test or a 1-way ANOVA followed by a Dunnett multiple comparisons test. All experiments were done in Human umbilical vein endothelial cells in triplicate

Arf6 Promotes the Assembly of Filamentous Actin

Having further characterized endocytic defects, we re-visited the initial actin defects reported in Figure 23. First, we were curious about the dynamics of actin in 3D between scram and Arf6 siRNA mediated KD sprouts. We observed a thinner network of filaments in addition to overall disorganized actin architecture in the Arf6 KD sprout compared with a control sprout (Figure 25A). In fixed sprouts, quantification of f-actin intensity was significantly lower in Arf6 KD sprouts compared with control sprouts (Figure 25B).

Next, we wanted to compare the population of globular actin (g-actin) to filamentous actin (f-actin). Again, we observed a thinner network of f-actin where the population of g-actin is comparable to that of scram cells (Figure 25C). When quantified, the proportion of f-actin to g-actin was lower in Arf6 KD cells (Figure 25D). Finally, we observed Arf6-CFP localization upon treatment with an Arp inhibitor (CK-666). We established baseline Arf6-CFP localization, then promptly recorded changes in localization upon treatment with the Arp inhibitor. Following treatment, Arf6-CFP abruptly abandoned its localization in the plasma membrane and appeared to aggregate internally (Figure 25E). Co-localization with mCherry-Arp2 was significantly diminished (Figure 25F).

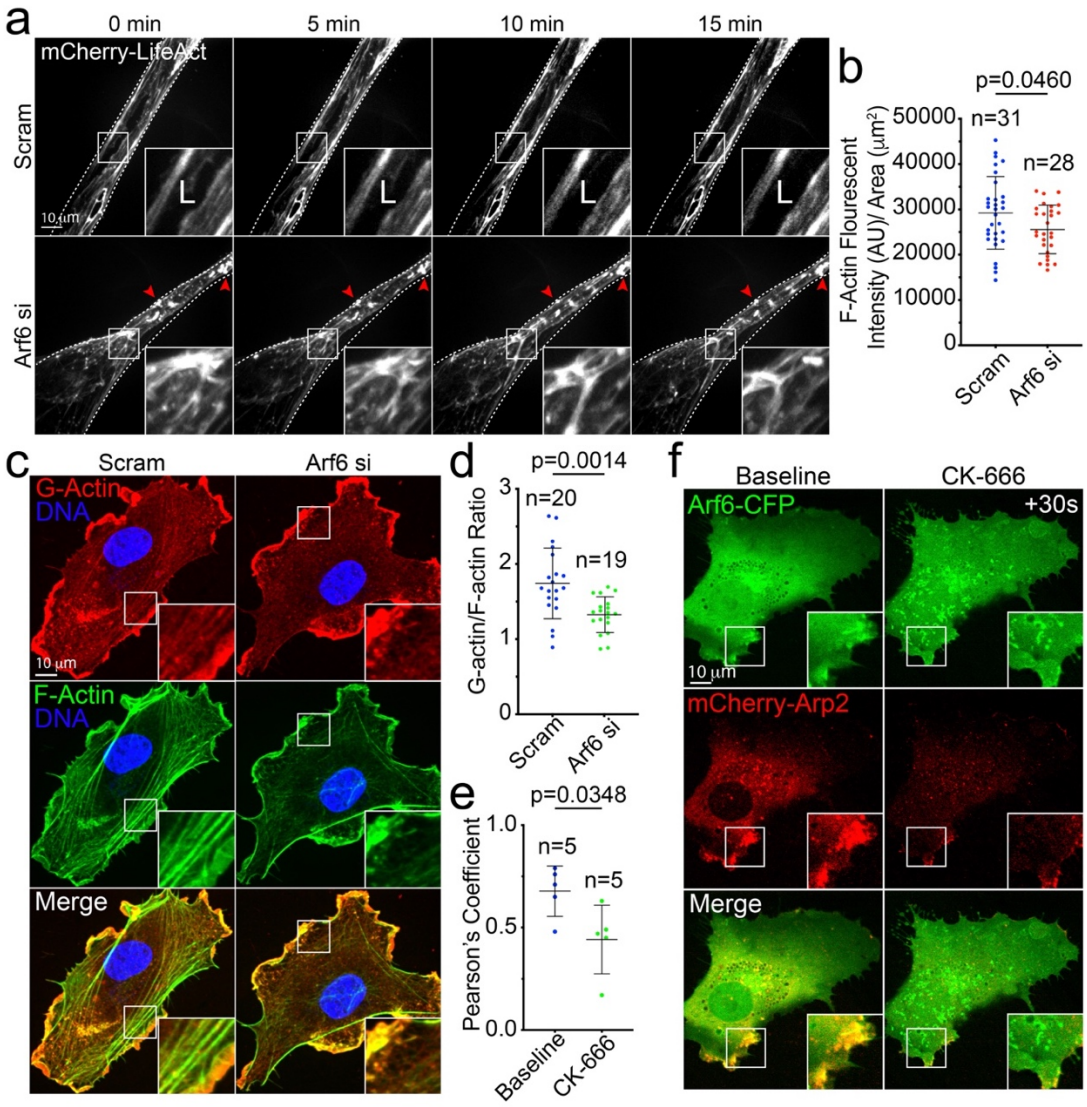

Figure 25: Arf6 Promotes Filamentous Actin Assembly. A. Live imaging of scramble (Scram) control and Arf6 siRNA knockdown (KD) sprouts expressing mCherry-LifeAct lentivirus at indicated timepoints. Red arrowheads denote actin aggregates. Dashed line denotes sprout exterior. B. Quantification of filamentous-actin (F-Actin) fluorescent intensity in Scram and Arf6 siRNA knockdown sprouts. n = number of sprouts. AU is arbitrary unit. C. Image representatives of cells stained for globular (G-Actin) and F-Actin between indicated conditions. D. Quantification of the ratio of globular to filamentous actin fluorescent intensities. n = number of cells. E. Pearson's Coefficient of Arf6-CFP and mCherry-Arp2 between Scram and Arf6 siRNA treated cells following CK-666 treatment. n = number of cells. F. Live imaging of Arf6-CFP with mCherry-Arp2 at baseline and after treatment with CK-666. In all images L denotes lumen. White box denotes area of magnification. Error bars represent standard deviation, middle bars are the mean. NS = non-significant. Statistical significance was assessed with an unpaired t-

test or a 1-way ANOVA followed by a Dunnett multiple comparisons test. All experiments were done in Human umbilical vein endothelial cells in triplicate.

Once more, our findings agreed with previous reports of Arf6 promoting filamentous-actin assembly. However, it remained unclear whether Arf6's primary role was to promote the assembly of actin filaments or to act as a member of the protein complex required for protein internalization.

Arf6 and Cortical Actin Localize to Sites of Clathrin-Mediated Endocytosis

Thus far, our data indicated that Arf6 was required for endocytosis at the plasma membrane and that it impacted the assembly of f-actin. What remained unclear was whether Arf6 was a component of Clathrin-coated pits or if it simply promoted actin assembly required for endocytic events. To begin to address this, we first looked at whether Arf6-CFP co-localized with tagRFP-Clathrin. We observed significant overlap between these proteins (Figure 26A-B). Next, we sought to determine whether depletion of Arf6 would alter the localization, or amount, of Clathrin detectable at the plasma membrane. We were surprised by the significant difference in detectable Clathrin in 3D sprouts (Figure 26C, D). These results indicated that Arf6 had preference for sites of Clathrin in addition to cortical actin. The accumulation of Clathrin in the membrane may be indicative of endocytic failures occurring.

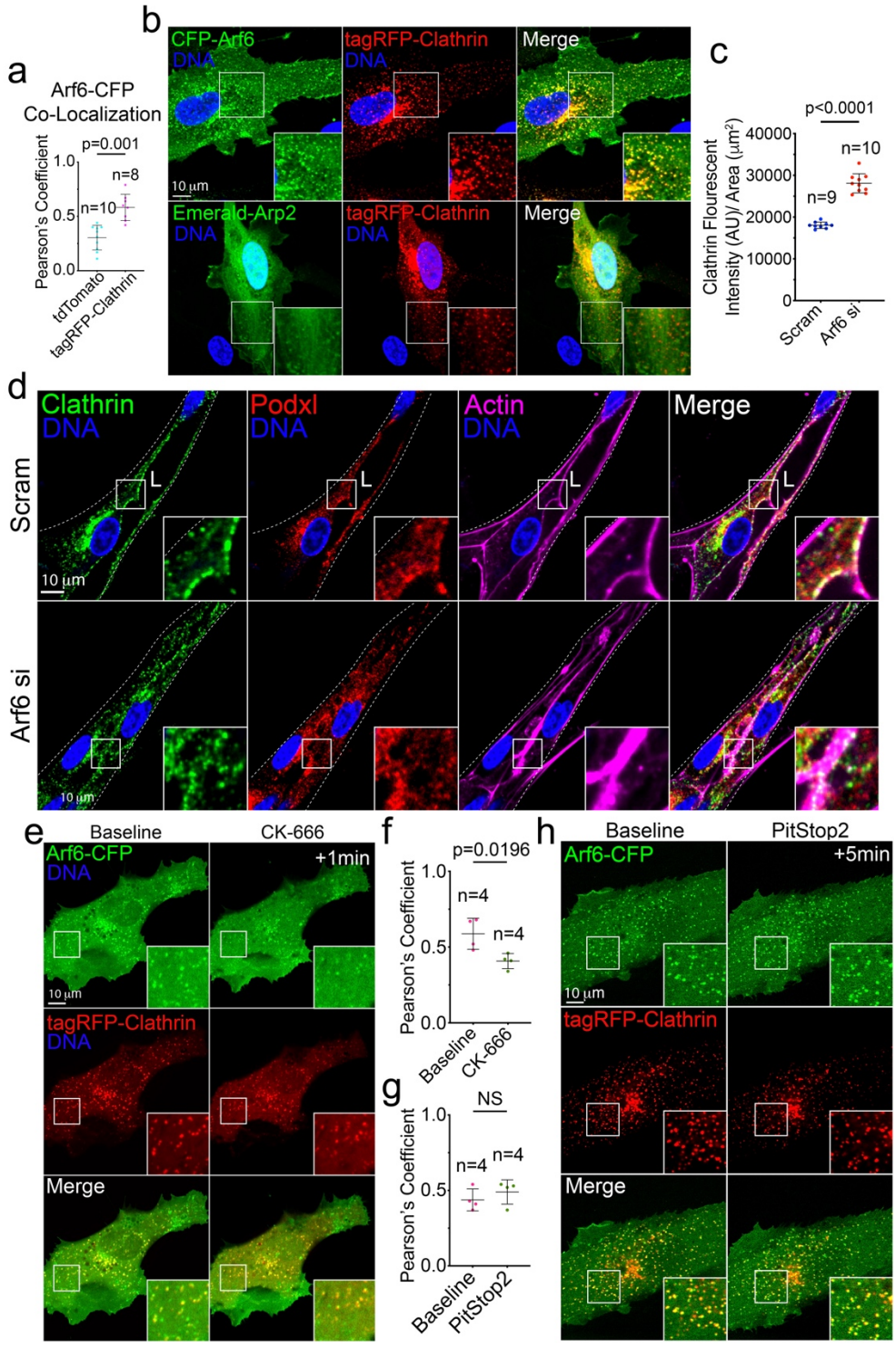

Figure 26: Arf6 Promotes Actin Assembly at Sites of Clathrin-Mediated Endocytosis. A. Pearson's Correlation of cytosolic tdTomato control and tagRFP-Clathrin with Arf6-CFP, and Pearson's Correlation of cytosolic tdTomato control and tagRFP-Clathrin with Emerald-Arp2. B. Image representatives of 2-dimensional localization of Arf6-CFP (top

panels) and Emerald-Arp2 (bottom panels) with tagRFP-Clathrin. C. Quantification of Clathrin fluorescent intensity for indicated conditions. AU is arbitrary unit. D. Image representatives of scramble (Scram) and Arf6 siRNA knockdown (KD) sprouts with Clathrin (green), podocalyxin (podxl, red) and actin (magenta). L denotes lumen. Dashed white lines mark sprout exterior. E. Live imaging of Arf6-CFP with tagRFP-Clathrin at baseline and after treatment with CK-666. F. Pearson's Coefficient of Arf6-CFP and tagRFP-Clathrin between Scram and Arf6 siRNA treated cells following CK-666 treatment. n = number of cells. G. Pearson's Coefficient of Arf6-CFP and tagRFP-Clathrin between Scram and Arf6 siRNA treated cells following PitStop2 treatment. n = number of cells. H. Live imaging of Arf6-CFP with tagRFP-Clathrin at baseline and after treatment with PitStop2. In all images white box denotes area of magnification. Error bars represent standard deviation, middle bars are the mean. NS = non-significant. Statistical significance was assessed with an unpaired t-test or a 1-way ANOVA followed by a Dunnett multiple comparisons test. All experiments were done in Human umbilical vein endothelial cells in triplicate.

To provide insight to whether Arf6 KD induced accumulations at Clathrin were due to, or independent of, the accumulation of cortical actin, we co-expressed Arf6-CFP with tagRFP-Clathrin and collected live baseline activity. We then treated the cells with an Arp inhibitor to observe whether Arf6-CFP disassociated from tagRFP-Clathrin. With Arp inhibited, Arf6-CFP and Clathrin co-localization was reduced (Figure 26E,F). We repeated the same experiment with PitStop2, a potent inhibitor of Clathrin-mediated endocytosis. In this case we did see some shifting of Arf6-CFP localization but not to the same degree as the Arp inhibitor (Figure 26G,H). These experiments suggested that Arf6 primarily localized to cortical actin, and the accumulations observed with Clathrin were simply due to accumulations of cortical actin.

Arf6 Localizes to Cortical Actin and Clathrin Via ARNO

The molecular regulation of Arf's are linked to eight GEFs and nine GAPs [217, 291]. Compartment and substrate specificity narrowed Arf6s regulation to GEFs and GAPs which operate at the cell periphery [217]. We investigated the GEF, ACAP2, as it both compartment restricted and was reported to regulate cytoskeletal changes through

modulation of Arf6 activity [217, 271]. We also investigated the GAP, ARNO, given similar reports [272-274]. First, we over-expressed Arf6-CFP with ACAP2 and ARNO to confirm co-localization of the proteins. As predicted, Arf6-CFP co-localized well with both tagRFP-ACAP2 and GFP-ARNO (Figure 27A,B).

The next step in our characterization was to determine whether ACAP2 or ARNO impacted the activity state of Arf6. We incubated cell lysate treated scam, ACAP2, or ARNO siRNA with GGA3-PBD beads which recognize and bind the active (GTP-bound) form of Arf6 [275]. There was a slight increase in detectable active-Arf6 in lysate deficient in ACAP2, whereas the opposite was the case in lysate deficient in ARNO (Figure 27C, D). Knockdowns were validated by western blotting (Figure 27E).

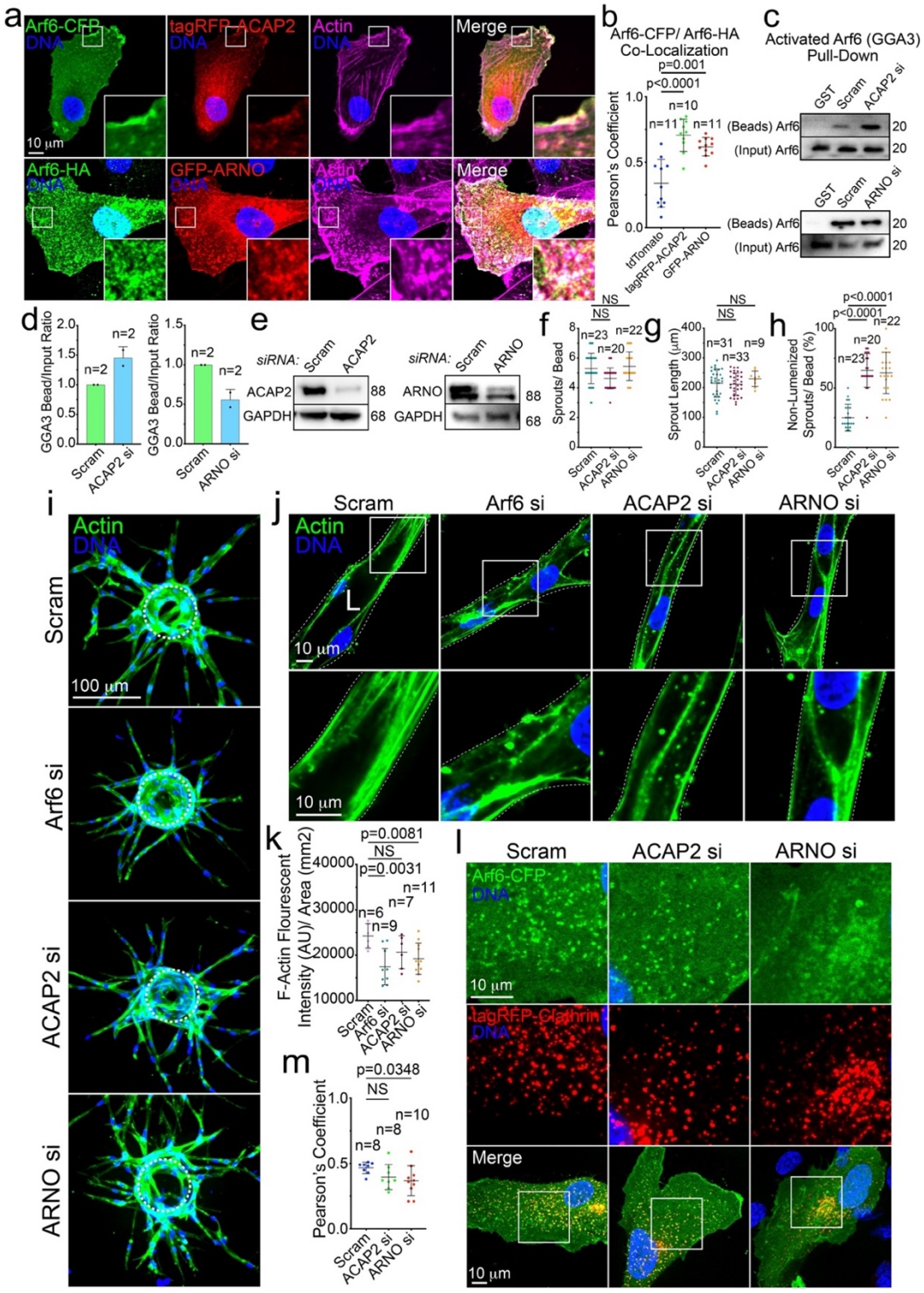

Figure 27: ARNO Coordinates Arf6 Activity at Sites of Clathrin-Mediated Endocytosis. A. Image representatives of 2-Dimensional localization of Arf6-CFP with tagRFP-ACAP2 (top panels) and Arf6-HA with GFP-ARNO (bottom panels). B.

Pearson's Correlation between Arf6-CFP (or Arf6-HA) and cytosolic tdTomato control, tagRFP-ACAP2, and GFP-ARNO. n = number of cells. C. Pulldown assay using GGA3 to probe for activated Arf6. Cells were treated with scramble (Scram) control, ACAP2 siRNA (si) or ARNO si [285]. D. Quantification of Arf6 activity. n=number of pull-downs. E. Western blot confirmation of siRNA knockdown (KD) of ACAP2 (average 70.5% KD relative to control, n = 3) and ARNO (average 41.7% KD relative to control). F-H. Graphs of indicated sprouting parameters between groups. n = number of sprouts. I. Representative sprout morphology images of Scram, Arf6, ACAP2 and ARNO siRNA KD sprouts. Dashed lines outline the microbead. J. Image representatives of actin in Scram, Arf6, ACAP2 and ARNO siRNA KD sprouts. K. Quantification of actin fluorescent intensity for indicated conditions. AU is arbitrary unit L. Image representatives of Arf6-CFP and tagRFP-Clathrin in cells treated with scram, ACAP2 and ARNO siRNA. M. Pearson's Correlation of Arf6-CFP with tagRFP-Clathrin for indicated KD conditions. In all images L denotes lumen. White box denotes area of magnification. Error bars represent standard deviation, middle bars are the mean. NS = non-significant. Statistical significance was assessed with an unpaired t-test or a 1-way ANOVA followed by a Dunnett multiple comparisons test. All experiments were done in Human umbilical vein endothelial cells in triplicate.

Thus far, our data validated reports of ACAP2 in-activating Arf6 and ARNO activating Arf6. We wanted to target the regulator that was key to Arf6's mechanism of cytoskeletal regulation. Our first approach was to compare sprouting parameters of scram, ACAP2 and ARNO siRNA KD sprouts. Unlike Arf6 KDs, ACAP2 and ARNO sprouts showed no significant difference in sprouts per bead or sprout length (Figure 27F, G). However, non-lumenized sprouts were significantly higher in both ACAP2 and ARNO KD sprouts (Figure 27H). The sprout morphology of ACAP2 and ARNO KDs were like Arf6 in their thinner presentation, yet they migrated further (Figure 27I). This data suggested that Arf6's molecular regulation was clearly more complex than the effects of the single GEF and GAP we investigate here.

We wanted to focus our investigation on the cytoskeletal effects of both ACAP2 and ARNO KD, so we analyzed actin defects when sprouts were depleted of either protein. Frustratingly, both ACAP2 and ARNO KD sprouts produced defects in the actin

cytoskeleton (Figure 27J, K). This finding was consistent with previous reports but did not help our aim of identifying a key effector. We gathered that the effectors could disrupt localization of Arf6 with cortical actin or with Clathrin. We again performed KDs of scram, ACAP2 and ARNO and transduced cells with Arf6-CFP in 3D to assess differences in Arf6-CFP localization. ARNO KD sprouts resulted in little change, however, ACAP2 KD sprouts reduced the apical membrane localization of Arf6-CFP (Supplemental Figure 24A, B). In 2D, ARNO KD reduced the co-localization of Arf6-CFP with tagRFP-Clathrin (Figure 27L, M). These results indicate that ARNO's molecular regulation of Arf6 is important for its function at sites of cortical actin and clatrhin-mediated endocytosis. ACAP2-mediated activity state turnover of Arf6 could be relevant to its localization.

2.4 Discussion

Arf6 is a widely studied small GTPase with hundreds of investigations associated with its cellular function [305, 306]. Our primary contribution to the existing body of Arf6 literature is the relevance of Arf6 to sprouting angiogenesis and lumen formation. Sprouting parameters were significantly diminished in sprouts depleted of Arf6 and they harbored pronounced cytoskeletal defects. In addition to this, we sought to clarify whether Arf6 functioned more as a generic cytoskeleton regulator or specifically at sites of Clathrin-coated invaginations. We concluded that Arf6 localized preferentially to Clathrin, however this can be disturbed by inhibiting Arp-mediated actin branching.

To our knowledge, Arf6 has not yet been linked to podxl or TIE-2 internalization. We speculate that Arf6 could be required for internalization of many membrane proteins. This seems logical since Arf6's mechanism is linked to such diverse cellular processes. If

endocytosis is universally hindered, the downstream effects of this could be broad. Remodeling cell surface protein composition is imperative, evidenced by diseases, such as Alzheimer's, directly linked to impaired clearance [325-327]. A key regulator of membrane protein turnover and trafficking is ubiquitination [325, 326]. In the future, it would be interesting to assess ubiquitination of membrane proteins in Arf6 KD cells.

We examined ACAP2 and ARNO in association with Arf6 and concluded that other Arf GAPs and GEFs modulate Arf6's mechanism. GIT1, an Arf6 GAP, when over-expressed has been shown to inhibit Clathrin-dependent endocytosis [286]. This other method of Arf6 downregulation could be site, or context, specific. Additionally, Hongu, et al., report an Arf6 specific GEF, Grp1, mediated growth factor stimulated β-integrin internalization in endothelium [280]. Thus, another possible activator of Arf6. For a more complete picture of Arf6's molecular regulation, a comprehensive screening of Arf6 specific GAPs and GEFs is warranted. Which GAPs and GEFs function together to coordinate the complex cellular activities of Arf6 remains an outstanding question.

Overall, our combination of 3D assays and biochemistry provides another piece to the Arf6 mechanism puzzle. We contend that investigations, such as this, investigating proteins across tissue types is relevant to our understanding of cell biology and the improvement of more targeted therapeutic measures.

Chapter Five: Rab8 Traffics Apically Bound Cargo at the Trans Golgi Network Independent of the WPB Pathway

2.1 Introduction

The Golgi Apparatus is a dynamic organelle which balances the continuous arrival and departure of membrane-bound vesicles, tubules, and compartments. At steady state, there is a predictable makeup of Golgi cisternae. Cisternae at the entrance of the Golgi (cis-Golgi), receive vesicles from the endoplasmic reticulum (ER) [308-311]. Proteins traffic through the intermediate compartment of the Golgi, undergoing post-translational modifications and sorting, until reaching the Golgi exit site known as the trans-Golgi network (TGN) [308-311]. This constant shuttling of membrane requires tightly regulated trafficking in order to maintain distinct Golgi cisternae.

Rab GTPases are master regulators of membrane and vesicular transport. They achieve this by interfacing with a broad spectrum of tethering complexes, motor proteins, and lipids. Of the roughly 70 identified human Rabs, approximately one third of them interact with either ER or Golgi membranes [308, 309]. In several studies, when Golgi Rabs, or Golgi Rab effectors, are altered there is a significant disruption of Golgi architecture as well as impaired trafficking of cargo [308, 309]. Together, this data suggests that Rabs play a significant role in the maintenance and morphology of the Golgi network.

The role of each Golgi Rab is generally consistent across tissue types. However, trafficking pattern discrepancies do occur, and it is important to identify these inconsistencies. Endothelial cells must traffic apically destined proteins in a timely manner in order to initiate lumen formation. Additionally, endothelial cells generate a unique secretory vesicle known as a Weibel-Palade Body (WPB) [125]. This is a relatively large, cigar-shaped vesicle which buds from the Golgi and is housed in the actin cytoskeleton in a primed state [125]. It remains unclear which Golgi Rabs contribute to the formation and budding of WPBs from the Golgi and whether there is overlap with apical trafficking pathways.

Rab8 is identified as a TGN specific Rab important for trafficking cargo from the TGN to the apical membrane in a polarized cell [312-314, 335]. In one investigation, Rab8 was critical to trafficking of podocalyxin (podxl), an apical transmembrane protein important for lumen formation [315]. However, this study, and nearly every other study, of Rab8 was not in endothelium, nor in a 3-dimensional (3D) environment. Therefore, we investigated Rab8 in 3D endothelium to determine whether it was required for podxl trafficking from the TGN.

In our hands, Rab8 was involved in the trafficking of podxl. Surprisingly, Rab8 deficient sprouts resulted in higher levels of detectable podxl in the plasma membrane. The absence of Rab8 did not disrupt basolateral trafficking, Weibel-Palade body (WPB) formation, or endothelial specific receptors TIE-2 and VEGFR2. Of note, apically destined proteins were still delivered in the absence of Rab8, however vessel defects persisted. This suggested apical trafficking was still disrupted. Interestingly, despite the apical targeting of WPB's, their biogenesis was independent from Rab8 trafficking. Our

data distinguishes the WPB biogenesis pathway was separate prior to reaching Rab8 decorated TGN cisternae.

2.2 Materials and Methods

Cell Culture

See Annex A.

Sprouting Angiogenesis Assay

See Annex A.

Plasmid Constructs

See Annex A Table 6.

Lentivirus and Adenovirus Generation and Transduction

See Annex A.

Membrane Fraction Assay

Membrane fractions were performed according to the guidelines provided using the Thermo-Scientific Mem-PER Plus Membrane Protein Extraction Kit [Appendix Table 2]. Total concentration of protein in membrane fraction lysate was quantified using the Pierce™ BCA Protein Assay Kit measured at 562 nm and compared to a standard curve. Samples were then prepared for immunoblotting as described in Appendix A.

Immunoblotting

See Appendix A.

Immunofluorescence and Microscopy

See Appendix A.

Zebrafish Transgenics

The transgenic lines used in this study include Tg(kdrl:GFP) and Tg(UAS:GFP; kdrl:GAL4FF). Tol2- mediated transgenesis was used to generate mosaic intersomitic blood vessels as previously described [140-143]. Briefly, Tol2 transposase mRNA were synthesized (pT3TS-Tol2 was a gift from Stephen Ekker, Addgene plasmid # 31831) using an SP6 RNA polymerase (mMessage mMachine, ThermoFisher). Tol2 injection mixture consisted of 500ng of DNA, 500ng of Transposase (1uL), and 1 uL 0.1% Phenol Red with total volume brought up to 5uL.

Zebrafish Live Imaging and Quantification

See Appendix A.

Quantification of Fluorescent Intensity

Fluorescent intensity was determined by first projecting the entire sprout to a single image, setting the scale of the image and designating a region of interest around a sprout. The resulting intensity was then divided by the area of the sprout. For quantifying western blot band intensity between groups, the area was set constant from band to band and fluorescent intensity was compared with equal areas.

Statistical Analysis

See Appendix A.

2.3 Results

Rab8 is Golgi Localized and Required for Lumen Formation In Vitro

Rab8 is a well-established resident to the trans-Golgi network (TGN), we first aimed to validate this in endothelium in 3-dimensions (3D). We transduced a tagRFP-Rab8 virus into primary endothelial cells and challenged them to sprout in the fibrin-bead assay

(FBA) [159]. We fixed and stained sprouts for podocalyxin (podxl) and actin. TagRFP-Rab8 appeared Golgi localized with some overlap of podxl (Figure 28A). We stained for Golgi matrix protein 130 (GM130) with tagRFP-Rab8-wildtype (WT), constitutively active (CA, Q67L), and dominant negative (DN, T22N) [328]. TagRFP-Rab8-WT and CA strongly co-localized with GM130, but this association is diminished with the DN mutant (Supplemental Figure 25A).

We next sought to determine the requirement of Rab8 for sprouting angiogenesis. We grew scramble (scram) control and Rab8 siRNA-mediated knockdown (KD) sprouts for four days and observed podxl (apical membrane), β-integrin (basal membrane) and actin localization. Each protein localized correctly, however vessels lacked a lumen (Figure 28B, F). Unexpectedly, we observed hyper-sprouting in Rab8 KD sprouts (Figure 28C). Quantification of sprouts per bead indicate significantly more sprouts on Rab8 KD beads compared with control beads (Figure 28E). Sprout length was no different between groups (Figure 28G). KDs were confirmed by western blotting (Figure 28D). Taken together, these results indicate that sprouts maintain migration and polarity programs in the absence of Rab8.

To better establish our Rab8 KD phenotype, we performed a rescue assay. Cells were siRNA-treated and transduced with either GFP (control) or tagRFP-Rab8 virus to allow for mosaic rescue. Our results validate that the lumen failures are rescued in cells expressing tagRFP-Rab8 (Figure 28H-I). Our results indicate that Rab8 is necessary for lumen formation as well as the regulation of sprouting in endothelium.

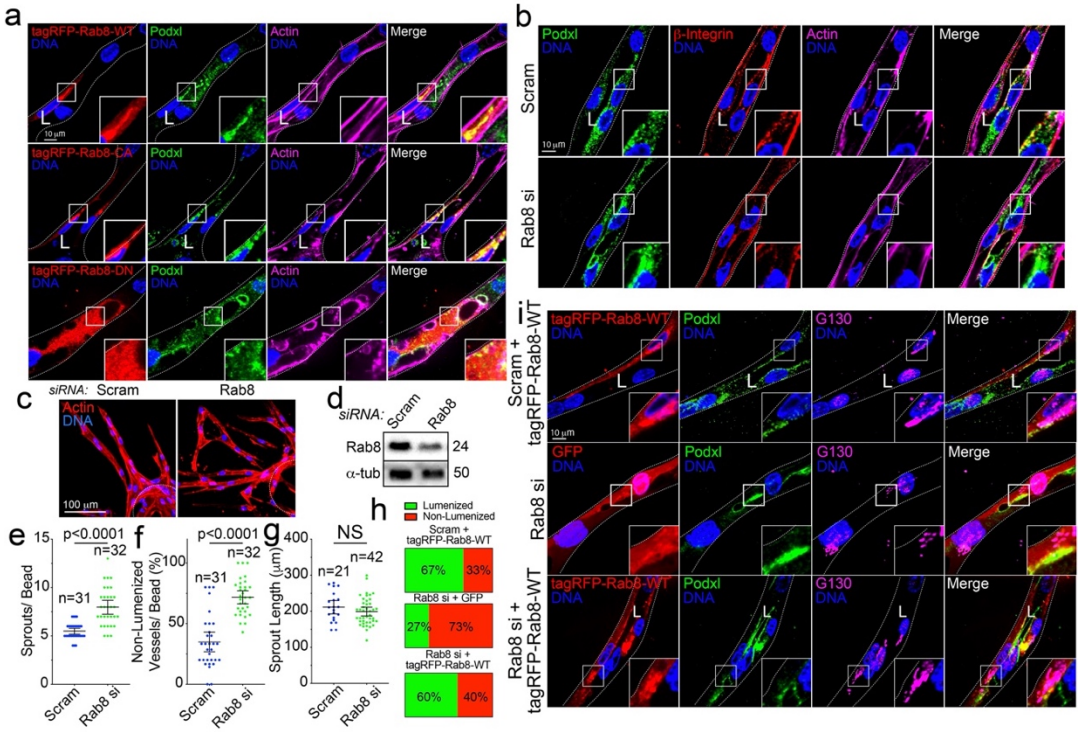

Figure 28: Rab8 is Golgi Localized and Required for Endothelial Lumen Formation. A. TagRFP-Rab8-wildtype (WT), -constitutively active (CA), and -dominant negative (DN) in endothelial sprouts with podocalyxin (Podxl, green), and actin (magenta). B. Representative image of scramble (Scram) control and Rab8 siRNA KD sprouts. Dashed lines outline the microbead. C. Representative images of sprout morphology of Scram and Rab8 KD cells. Dashed line outlines microbead. D. Western blot confirmation of siRNA (si) knockdown (KD) of Rab8. E-G. Graphs of indicated sprouting parameters between groups. n = number of sprouts. Error bars represent standard deviation, middle bars are the mean. H. Rescue experiment using scram or Rab8 siRNA (si)-mediated KD with overexpression of indicated constructs. Percentages represent quantification of lumen formation in described conditions. n = number of sprouts. I. Representative images of Scram and Rab8 KD sprouts expressing either GFP (control), or tagRFP-Rab8-WT. White dashed lines mark sprout exterior. L denotes lumen in all images. Insets are areas of higher magnification. NS = non-significant. Statistical significance was assessed with an unpaired t-test or a 1-way ANOVA followed by a Dunnett multiple comparisons test. Insets are areas of higher magnification. All experiments were done using human umbilical vein endothelial cells in triplicate.

Rab8 Does Not Directly Target Podocalyxin in Endothelium

We next investigated whether Rab8 directly targeted podxl. In 2D, tagRFP-Rab8-WT, -CA, and -DN localization was compared with the localization of endogenous podxl as well as podxl-cytosolic-tail (Supplemental Figure 25B). While there was co-localization

between podxl and tagRFP-Rab8, podxl could simply be localized to the Golgi and not necessarily specific to Rab8. Therefore, we mis-localized Rab8 to the mitochondria using a tom20-tag and assessed whether podxl mis-localized to the Golgi with it (Supplemental Figure 25C). Tom20-tagRFP-Rab8-WT did not co-localize with podxl or podxl-tail (Supplemental Figure 25D). Additionally, the tom20-taRFP-Rab8-CA and -DN did not co-localize with podxl (Supplemental Figure 25E). These findings suggest that Rab8 does not bind directly to podxl. This does not rule out the possibility that podxl is cargo that Rab8 traffics indirectly.

Rab8 Traffics Apical Cargo in 3D Sprouts

Many reports suggest Rab8 traffics apically bound cargo from the TGN. However, much of this data is sourced from 2D assays. There could exist discrepancies in Rab8-mediated trafficking in a 3D environment. Thus, we investigated transmembrane proteins specific to different membrane domains. We probed the junctional VE-Cadherin (VE-Cad), the basal β-integrin, apical podxl, apical and junctional TIE-2, and finally Vascular Endothelial Growth Factor Receptor 2 (VEGFR2) which is ubiquitously localized [317-321]. First, we visualized localization of tagRFP-Rab8 positive vesicles and tubules with the aforementioned proteins. Of note, we did not focus on localization at the Golgi, this would be redundant as all of the proteins stated localize at the Golgi at one point. We observed Rab8 decorated tubules and vesicles primarily targeting the apical membrane (Figure 29A, B). TagRFP-Rab8-WT co-localized with podxl, phosphorylated-TIE-2 (p-TIE2), and, variably, with VE-Cad (Figure 29A). We did not observe co-localization between VEGFR2 or β-integrin and tagRFP-Rab8-WT sprouts.

In addition to fixed imaging, we employed live imaging of tagRFP-Rab8 to visualize vesicles and tubules actively target the apical membrane. Indeed, we captured these events occurring over 20 minutes in vessel sprouts (Figure 29B). However, we recognized that over-expressing protein could result in atypical localization. To ensure that Rab8 does traffic beyond the TGN we also transduced another Golgi resident, GFP-Rab6, in sprouts to control for this. We did not observe GFP-Rab6 outside of the Golgi, suggesting that Rab8 traffics cargo beyond the Golgi (Supplemental Figure 26). Our results specify Rab8 trafficking targeting the apical and junctional membrane in 3D sprouts.

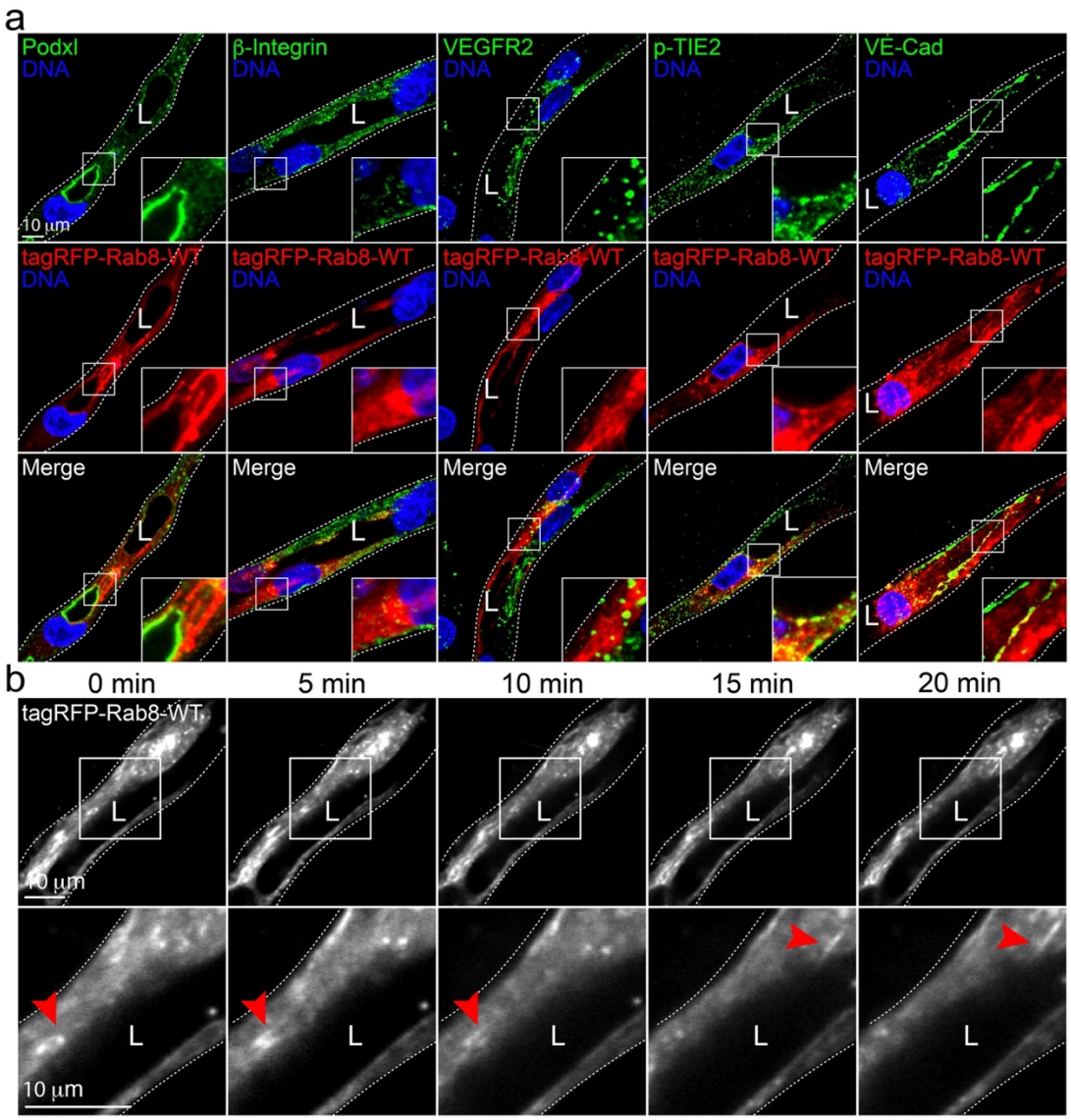

Figure 29: Rab8 Co-Localizes with Apical Transmembrane Proteins but is not Required for Their Delivery to the Membrane in 2D. A. Representative images of tagRFP-Rab8-wildtype (WT, middle panels) localization in the fibrin bead assay (FBA) with endogenous podocalyxin (podxl, first column), β-Integrin (seond column), VE-Cadherin (VE-Cad, third column), phosphorylated-TIE-2 (p-TIE2, fourth column), and Vascular Endothelial Growth Factor Receptor 2 (VEGFR2, last column). B. Live imaging of tagRFP-Rab8-WT in sprouts over 20 minutes. Red arrowheads indicate apically targeted vesicles and tubules. In all panels, L denotes lumen. White box is area of magnification. Insets are areas of higher magnification. Dashed lines mark sprout exterior. All experiments were done in Human umbilical vein endothelial cells.

Rab8 Knockdown Results in Greater Detectable Podxl in 3D but not in 2D Cells

Thus far, we determined Rab8 was required for lumen formation and trafficked to apical and junctional plasma membrane domains. However, we lacked a mechanism for our Rab8 KD phenotypes. Therefore, we repeated our KDs in sprouts and tested whether there was more, or less, endogenous protein in the plasma membrane. We compared the fluorescent intensity of podxl, VE-Cad, and β-integrin. β-integrin and VE-Cad resulted in no significant difference, however, podxl had significantly higher endogenous protein detected in Rab8 KD sprouts (Figure 30A-E).

The Weibel-Palade body (WPB) pathway is unique to endothelium and has yet to be investigated with respect to Rab8. WPBs generally traffic apically and could require Rab8 for their biogenesis, albeit indirectly. Thus, we quantified the number of WPBs in scram and Rab8 KD sprouts (Figure 30G-H). We found no significant difference in the number of WPBs between conditions, suggesting the pathways are independent of each other.

To address the Rab8 hyper-sprouting phenotype, we assessed VEGFR2 in Rab8 KD sprouts. VEGFR2 signaling leads to new vessel sprouting and formation [329]. Since podxl detection was greater in Rab8 KD sprouts, we gathered that if VEGFR2 were more prevalent this could account for excessive sprouting. Nevertheless, VEGFR2 clusters were not significantly different between scram and rab8 KD sprouts (Figure 30G, I). In the same vein, if too much protein were exiting the TGN, perhaps more lysosomes would be present in order to degrade the excess. Therefore, we quantified lysosomes in sprouts by staining for lysosomal marker, LAMP. Again, there were no difference in the number of LAMP-positive puncta between scram and Rab8 KD sprouts (Figure 30D, F).

Next, we sought to supplement our imaging analysis of membrane proteins with biochemistry. We isolated membrane fractions from scram and Rab8 KO cells and probed for podxl, β-integrin, VEGFR2, p-TIE2, and VE-Cad. There were no significant differences between conditions (Figure 30J, K). Taken together, our results indicated that plasma membrane protein composition is almost no different between scram and Rab8 KD cells. The greater detection of podxl in 3D was unexpected but could provide insight to Rab8's mechanistic role at the TGN. The discrepancy between podxl detection in membrane fractions could be attributed to variations in expression of podxl between 2D and 3D miceoenvironments [330, 331].

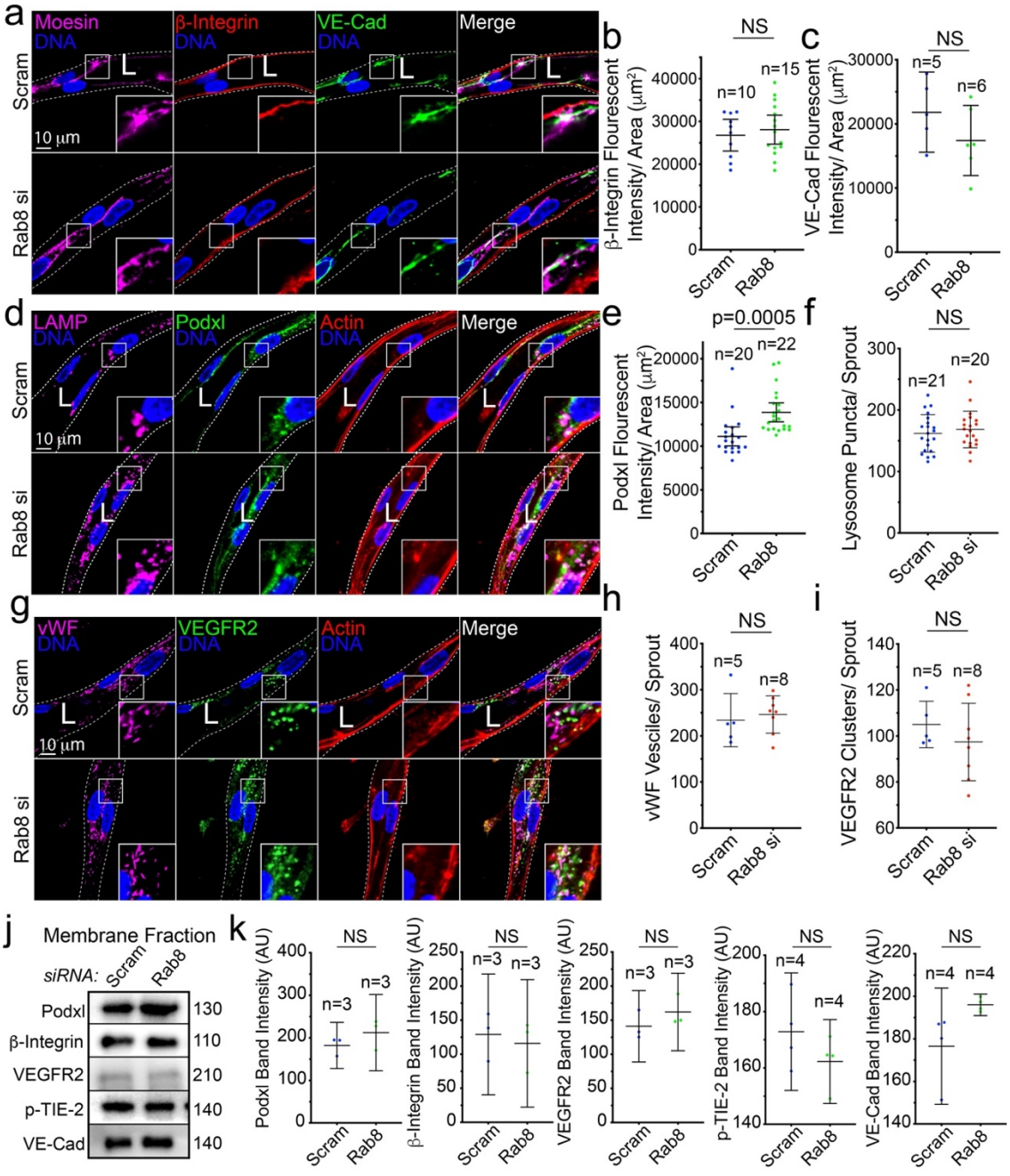

Figure 30: Rab8 Knockdown Results in Greater Detectable Podxl in 3D but not in 2D. A. Image representatives of scramble (Scram) control and Rab8 siRNA knockdown (KD) sprouts in the fibrin bead assay (FBA) with endogenous moesin (magenta), β-integrin (red), and VE-Cadherin (VE-Cad, green). B-C. Quantification of fluorescent intensity for indicated proteins. n = number of sprouts. D. Image representatives of scram and Rab8 siRNA KD sprouts in the fibrin bead assay (FBA) with endogenous LAMP (magenta), actin (red), and podocalyxin (Podxl, green). E-F. Quantification of fluorescent intensity for indicated proteins. . n = number of sprouts. G. Image representatives of

scram and Rab8 siRNA KD sprouts in the fibrin bead assay (FBA) with endogenous von Willebrand factor (vWF, magenta), actin (red), and Vascular Endothelial Growth Factor Receptor 2 (VEGFR2, green). H-I. Quantification of fluorescent intensity for indicated proteins. n = number of sprouts. J. Western blotting of membrane fractions isolated from Scram and Arf6 siRNA KD cells with indicated probes. K. Quantification of band fluorescent intensity from membrane fractions in J. n = individual membrane fraction experiments. Error bars represent standard deviation, middle bars are the mean. In all panels, L denotes lumen. Dashed line outlines sprout exterior. White box denotes area of inset. Error bars represent standard deviation, middle bars are the mean. NS = non-significant. AU is arbitrary unit. Statistical significance was assessed with an unpaired t-test or a 1-way ANOVA followed by a Dunnett multiple comparisons test. All experiments were done in Human umbilical vein endothelial cells in triplicate.

Rab8 Trafficking is Independent to WPB Trafficking in Endothelium

There was no difference in the number of WPBs in 3D. To ensure no overlap between the Rab8 and WPB trafficking pathways, we investigated WPB-positive Rab3d and Rab27 with Rab8. Both Rab3d and Rab27 localize to WPBs with little overlap to Rab8 at the Golgi (Figure 31A). To ensure the Golgi is required for WPB formation at all, we treated cells with Brefeldin A to ablate the Golgi and stained for WPB marker von Willebrand Factor (vWF). Brefeldin-A ablated both the Golgi and WPB formation, indicating the organelle is indeed required for WPB formation (Figure 31B, C).

Next, we next compared Rab27-positive and Rab3d-positive WPBs in scram and Rab8 KD cells. There were no observable differences in Rab27-positive or Rab3d-positive WPBs (Figure 31D, E). We quantified the total fluorescent intensity of vWF in scram and Rab8 KD cells and found no significant difference in detectable vWF (Figure 31F-G). Together these results suggest that while the Golgi is required for WPB formation, Rab8 trafficking from the TGN is independent from this pathway.

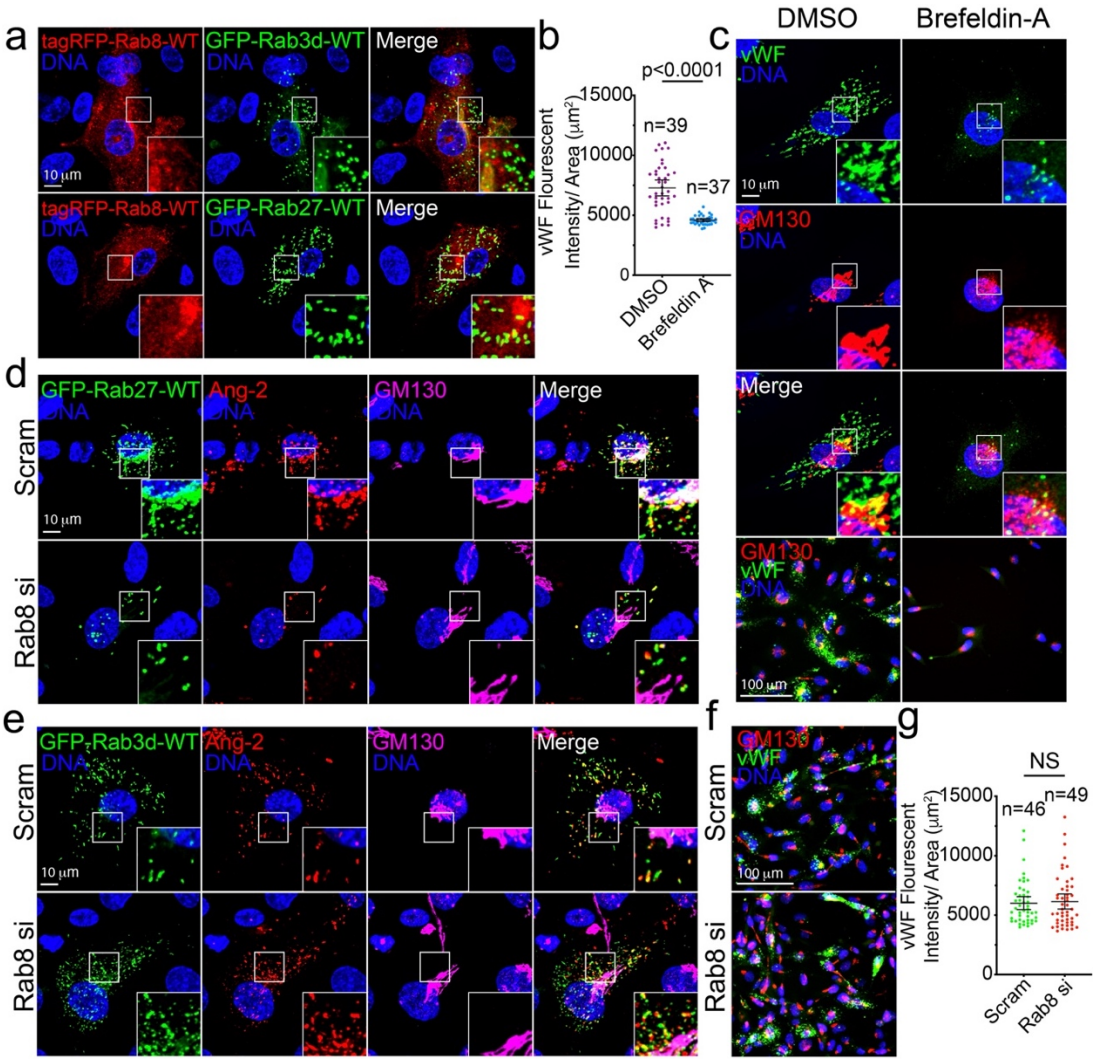

Figure 31: Rab8 is Not Required for the Biogenesis of WPB's. A. Image representatives of tagRFP-Rab8 with GFP-Rab3d (top panels) and GFP-Rab27 (bottom panels) in 2-dimensions. B. Quantification of von Willebrand factor (vWF) fluorescent intensity in DMSO and Brefeldin A treated cells. n = number of cells. C. Image representatives of DMSO and Brefeldin A (BFA) treated cells with vWF (green) and Golgi matrix protein 130 GM130 (red). Bottom row are image representatives at 20x magnification. D. Image representatives of scramble (Scram) and Rab8 siRNA knockdown (KD) cells with Weibel-Palade body cargo angiopoietin-2 (Ang-2, red), GM130 (magenta), GFP-Rab27, and E. GFP-Rab3d. F. Scram and Rab8 KD knockdown cells with vWF (green) and GM130 (red) at 20x magnification. G. Quantification of vWF fluorescent intensity in scram and Rab8si KD cells. In all panels, white box denotes area of inset. n = number of cells. AU is arbitrary unit. Error bars represent standard deviation, middle bars are the mean. NS = non-significant. Statistical significance was assessed with an unpaired t-test or a 1-way ANOVA followed by a Dunnett multiple comparisons test. All experiments were done in Human umbilical vein endothelial cells in triplicate.

Rab8 is Golgi Localized but is Not Required for Lumen Formation In Vivo

To substantiate our results in vivo, we used Zebrafish given the excellent resolution of vessel development. Using CRISPR/Cas9 gene editing, we targeted both paralogs of Rab8 (Rab8A and Rab8B) [145]. Knockout (KO) of Rab8 resulted in a modest phenotype with slightly smaller embryos and delayed intersomitic vessel (ISVs) development (Figure 32A-B). When quantified, the vessel number was no different between scram and Rab8 KO embryos, however the number of abnormal ISVs were significantly higher in Rab8 KO embryos (Figure 32C-D).

We also aimed to visualize Rab8 live in embryo vessels. To accomplish this, we used the Gal4/UAS transgenic tool to express tagRFP-Rab8-WT, -CA, and -DN exclusively in endothelial cells [332]. Each mutant localized similarly as in vitro, although we do not mark the Golgi (Figure 32E). Overall, over-expression of Rab8 and its mutants did not produce an abnormal phenotype in vivo (Figure 32F). Altogether, these results are consistent with our observations in vitro.

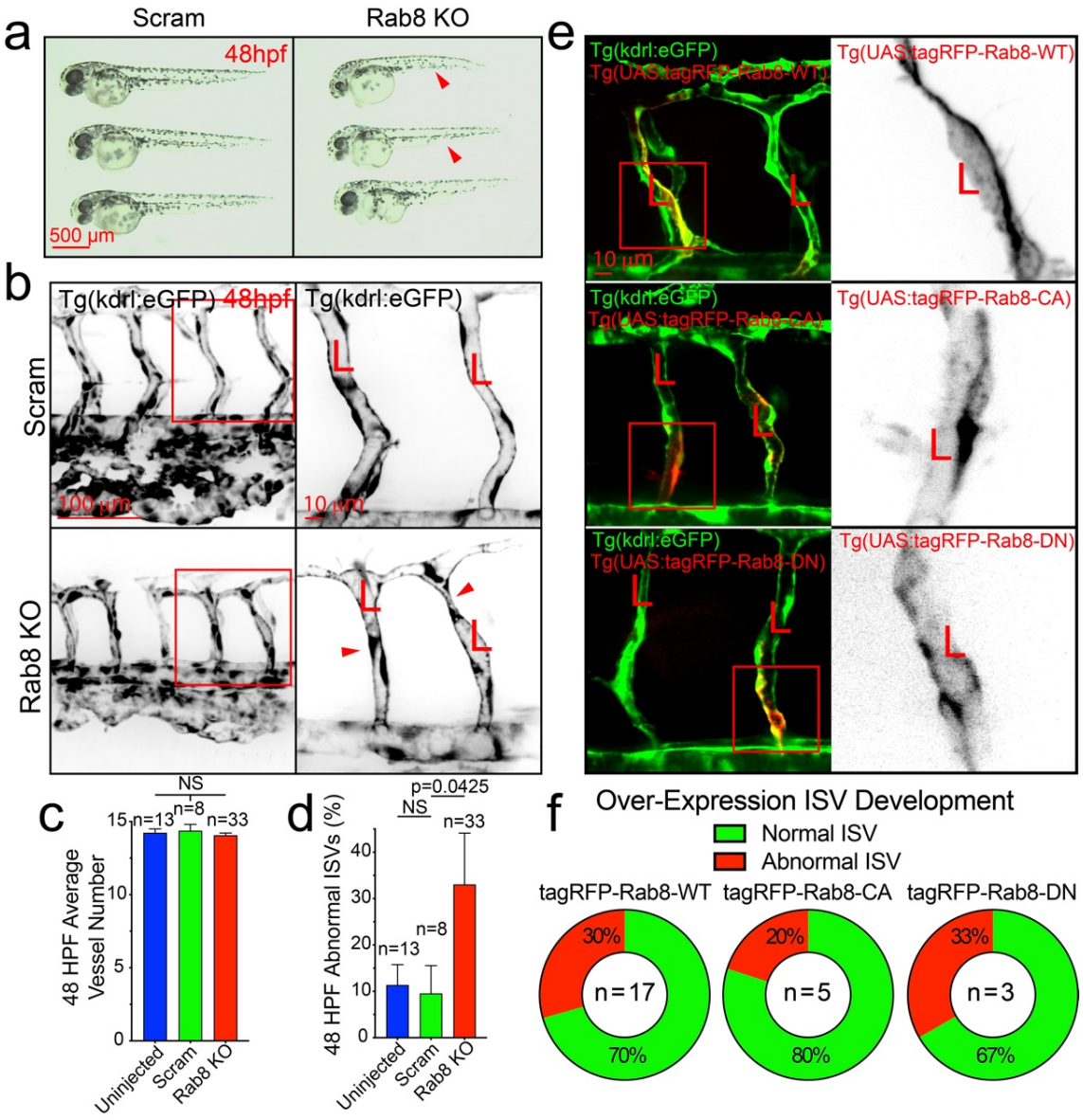

Figure 32: Rab8 is Required for Proper Intersomitic Vessel Development in Zebrafish. A. CRISPR-mediated knockout (KO) of scramble (Scram) control and Rab8 in Zebrafish embryos at 48 hours post fertilization (hpf). Red arrowhead indicates smaller bodyplan. B. Scram and Rab8 KO Zebrafish intersomitic vessels (ISVs) at 20x magnification (left column) and 40x magnification (right column). Arrowheads denote vessel narrowing and lack of chevron shape. Red box indicates area of magnification. C. Quantification of ISV number, and D. percent of abnormal vessels at 48hpf. E. Localization of tagRFP-Rab8-wild-type (WT), constitutively-active (CA), and dominant-negative (DN) in Zebrafish. F. Quantification of ISV abnormalities in indicated over-expression plasmids. In all panels, L denotes lumen. n = number of cells. Error bars represent standard deviation, middle bars are the mean. NS = non-significant. Statistical

significance was assessed with an unpaired t-test or a 1-way ANOVA followed by a Dunnett multiple comparisons test. All experiments were done in Zebrafish in triplicate.

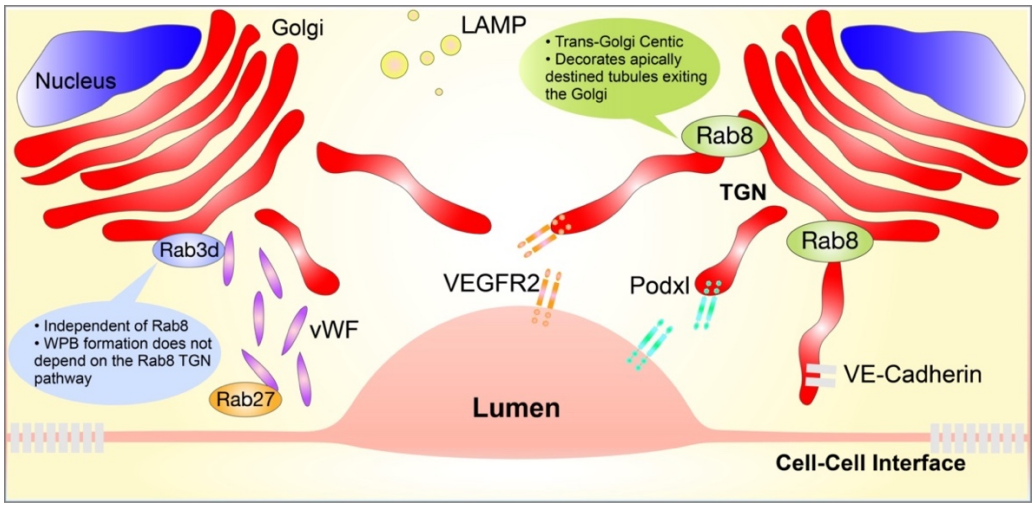

Figure 33: Model of Rab8 Function in Endothelium.

2.4 Discussion

The objective of this work was to assess the role of Rab8 in endothelial cell trafficking and its relevance to sprouting angiogenesis and lumenogenesis. Using 3D sprouting assays, biochemistry, and in vivo gene editing we illustrate that Rab8 is required for lumen formation, the downregulation of vessel sprouting, and trafficking of podxl (Figure 33). Moreover, we show Rab8 mediated trafficking is independent of the endothelial specific WPB pathway. To our knowledge, this is the first characterization of Rab8 with membrane proteins in 3D vessel sprouting.

What initially inspired the current investigation was to characterize podxl trafficking in endothelium. Previously, we investigated Rab27 as it was implicated in podxl trafficking in epithelial cells, however Rab27 was not related in endothelium [84]. We next characterized Rab35 as it was also reported to traffic podxl in epithelium. In fact, others have comprehensively established a direct association between podxl and Rab35 [210, 211]. Once more, this was not the case in endothelium [322]. Thus, we turned to

Rab8, which has again been reported to traffic podxl in epithelium [166, 315]. In sprouts deficient of Rab8, we observed an accumulation of podxl at the membrane. While we were excited to discover a potential candidate for podxl trafficking, this was an unexpected result. It also did not explain hyper-sprouting or lumen failures caused by Rab8 KD.

Rab8 trafficking is relatively broad. With so many proteins trafficked by Rab8, it is extremely difficult to test for the root cause of our phenotypes. We chose to investigate proteins belonging to specific membrane domains to provide insight to the directionality of proteins exported through the Rab8 pathway. All proteins investigated were ultimately delivered to their destination in the plasma membrane, despite the absence of Rab8. While disappointing, this does not rule out trafficking defects. Even with Golgi cisternae ablated with Brefeldin A, proteins can still reach their destination [323]. Moving forward, experiments focusing on the temporal aspect of protein delivery in the absence of Rab8 should follow this report.

WPBs are unique to endothelium and involve many trafficking proteins. The proteins which directly target WPBs are well documented, and Rab8 has not been directly linked to their biogenesis [324]. However, there was the possibility Rab8 was upstream of their biogenesis and thus still required for WPBs to form. Our data shows that this is not the case, and that Rab8 is independent of the WPB pathway. Once proteins reach the TGN there appears to be clear distinction between proteins trafficked out via the WPB pathway or via the Rab8 pathway.

Overall, our data supports previous evidence of Rab8 localized to the trans-Golgi network and involved in the trafficking of apically bound cargo. Limitations of the

present study include, and are not limited to, the inability to address hyper-sprouting, lacked a mechanism for excess detectable protein in the plasma membrane, and no in vivo data. It is unclear if the excessive protein detected is a result of a direct trafficking defect from Rab8 KD or an indirect effect, such as changes in expression resulting from Rab8 KD.

Chapter Six: Conclusions

Small GTPase regulated intracellular protein trafficking encompasses a highly complex and interesting sect of cell biology. The 30,000 to 40,000 gene products produced by the cell are largely transported by this family of proteins. Even a singular defect in any cellular trafficking programs can cause devastating, if not fatal, consequences for an organism. Therefore, the work presented in this dissertation advances our collective understanding of small GTPase trafficking and organellar transport and advances our understanding of this critically important protein family. What's more, each project utilized a 3-dimensional (3D) assay in endothelium to analyze polarized trafficking. All the investigations showed variability between 2-dimensional (2D) and 3D work as well as dissimilarity of cargo trafficked in endothelium. The results of the Rab27 investigation demonstrated both points very well.

Rab27 trafficking in endothelium is unique to an endothelial specific organelle, the Weibel-Palade body (WPB). It housed WPBs in the actin cytoskeleton primed for secretion. The excessive secretion resulting from loss of Rab27 in 3D was far more pronounced compared with 2D knockdowns (KD). Moreover, the hyper-growth observed in 3D would not have been evident in 2D. In future investigations, Rab27 KDs could be a useful tool to induce secretion of WPBs without the use of a drug. Lastly, in this investigation only one protein was linked to pro-angiogenic signaling, yet WPBs house many other proteins that should be explored.

Investigating Rab35 was a very difficult endeavor, to say the least. Data was often inconsistent or conflicting which ultimately led to the comprehensiveness of the study. The conclusion that Rab35 down-regulated actin assembly at the plasma membrane was difficult to come to and should be scrutinized. The complex mechanism by which Rab35 changes cytoskeletal behaviors could best be unraveled by identifying effectors, GEFs and GAPs that are compartment or context dependent. Given the ubiquitous nature of Rab35, it is logical to assume a considerable network of proteins regulate it.

The Rab35 project was similar to the Arf6 investigation in several ways. The Arf6 literature was also vast and, at times, conflicting; and Arf6 was also reportedly an actin-regulating protein. The data presented here is in agreement that Arf6 modulates actin, and we further show that Arf6 is relatively specific to Clathin-coated pits. Nevertheless, the mechanism by which Arf6 accomplishes this remains an outstanding question. Continued examination of Arf6 should attempt to identify direct effectors of Arf6 that link it to its mechanism.

The last study presented in this dissertation was an attempt to identify a Rab GTPase linked to podxl trafficking. In the beginning, the initial objective of investigating Rab27 was with respect to podxl. As it turned out, podxl trafficking was not associated with the Rab27 pathway. Rab35 was the next candidate investigated. Again, no relationship was identified between Rab35 and podxl. Alas, Rab8 was the last candidate investigated with respect to podxl trafficking.

Rab8 is a relatively upstream Rab. To conclude that Rab8 traffics podxl is akin to concluding the Golgi traffics podxl. Which would not inform much. Therefore, the objective of this investigation became identification of membrane domains which were

impacted by Rab8. Also, the determination of whether WPB biogenesis was dependent on Rab8. Based on the data, Rab8 traffics primarily apical cargo, however junctions are disrupted. It is possible the hyper-sprouting observed in Rab8 deficient sprouts was due to junctional instability. This is a very interesting notion and follow-up experimentation on this would be very beneficial.

In conclusion, the scope of this work contributes to the field of cell biology by providing novel 3D in vitro trafficking data. Ideally, future studies will employ 3D assays to address the discrepancies between 2D and 3D trafficking patterns shown here. The in vivo data was invaluable to these studies and validated our findings at the organismal level. Finally, this data will, ideally, inspire novel therapeutics and treatment of disease.

References

1. Hunt SD, Stephens DJ. The role of motor proteins in endosomal sorting. Biochem Soc Trans. 2011;39(5):1179–1184. doi: 10.1042/BST0391179.

2. Simons M, Gordon E, Claesson-Welsh L. Mechanisms and regulation of endothelial VEGF receptor signalling. Nat Rev Mol Cell Biol. 2016;17(10):611–625. doi: 10.1038/nrm.2016.87.

3. Kempers L, et al. The endosomal RIN2/Rab5C machinery prevents VEGFR2 degradation to control gene expression and tip cell identity during angiogenesis. Angiogenesis. 2021;24(3):695–714. doi: 10.1007/s10456-021-09788-4.

4. Agola JO, et al. Rab GTPases as regulators of endocytosis, targets of disease and therapeutic opportunities. Clin Genet. 2011;80(4):305–318.

5. Mizuno-Yamasaki E, Rivera-Molina F, Novick P. GTPase networks in membrane traffic. Annu Rev Biochem. 2012;81:637–659.

6. Muller MP, Goody RS. Molecular control of Rab activity by GEFs, GAPs and GDI. Small GTPases. 2018;9(1–2):5–21.

7. Grosshans BL, Ortiz D, Novick P. Rabs and their effectors: achieving specificity in membrane traffic. Proc Natl Acad Sci USA. 2006;103(32):11821–11827.

8. Homma Y, Hiragi S, Fukuda M. Rab family of small GTPases: an updated view on their regulation and functions. FEBS J. 2021;288(1):36–55.

9. Stenmark H. Rab GTPases as coordinators of vesicle traffic. Nat Rev Mol Cell Biol. 2009;10(8):513–525.

10. Hutagalung AH, Novick PJ. Role of Rab GTPases in membrane traffic and cell physiology. Physiol Rev. 2011;91(1):119–149.

11. Pfeffer SR. Rab GTPases: master regulators that establish the secretory and endocytic pathways. Mol Biol Cell. 2017;28(6):712–715.

12. Chappell JC, Wiley DM, Bautch VL. How blood vessel networks are made and measured. Cells Tissues Organs. 2012;195(1–2):94–107.

13. Arima S, et al. Angiogenic morphogenesis driven by dynamic and heterogeneous collective endothelial cell movement. Development. 2011;138(21):4763–4776.

14. Arroyo AG, Iruela-Arispe ML. Extracellular matrix, inflammation, and the angiogenic response. Cardiovasc Res. 2010;86(2):226–235.

15. Ballermann BJ, Obeidat M. Tipping the balance from angiogenesis to fibrosis in CKD. Kidney Int Suppl (2011) 2014;4(1):45–52.

16. Bazzoni G, Dejana E. Endothelial cell-to-cell junctions: molecular organization and role in vascular homeostasis. Physiol Rev. 2004;84(3):869–901.

17. Carmeliet P, Jain RK. Molecular mechanisms and clinical applications of angiogenesis. Nature. 2011;473(7347):298–307.

18. Xie Y, et al. Regulation of VEGFR2 trafficking and signaling by Rab GTPase-activating proteins. Sci Rep. 2019;9(1):13342.

19. Smith GA, et al. VEGFR2 trafficking, signaling and proteolysis is regulated by the ubiquitin isopeptidase USP8. Traffic. 2016;17(1):53–65.

20. Simons M. An inside view: VEGF receptor trafficking and signaling. Physiology (Bethesda) 2012;27(4):213–222.

21. Basagiannis D, et al. Dynasore impairs VEGFR2 signalling in an endocytosis-independent manner. Sci Rep. 2017;7(1):45035.

22. Basagiannis D, et al. VEGF induces signalling and angiogenesis by directing VEGFR2 internalisation through macropinocytosis. J Cell Sci. 2016;129(21):4091–4104.

23. Jopling HM, et al. Endosome-to-plasma membrane recycling of VEGFR2 receptor tyrosine kinase regulates endothelial function and blood vessel formation. Cells. 2014;3(2):363–385.

24. Gampel A, et al. VEGF regulates the mobilization of VEGFR2/KDR from an intracellular endothelial storage compartment. Blood. 2006;108(8):2624–2631.

25. Labrecque L, et al. Regulation of vascular endothelial growth factor receptor-2 activity by caveolin-1 and plasma membrane cholesterol. Mol Biol Cell. 2003;14(1):334–347.

26. Singh V, Lamaze C. Membrane tension buffering by caveolae: a role in cancer? Cancer Metastasis Rev. 2020;39(2):505–517.

27. Sinha B, et al. Cells respond to mechanical stress by rapid disassembly of caveolae. Cell. 2011;144(3):402–413.

28. Lanzetti L, et al. Rab5 is a signaling GTPase involved in actin remodeling by receptor tyrosine kinases. Nature. 2004;429(6989):309–314.

29. Goh LK, Sorkin A. Endocytosis of receptor tyrosine kinases. Cold Spring Harb Perspect Biol. 2013;5(5):a017459.

30. Saxena S, et al. The small GTPase Rab7 controls the endosomal trafficking and neuritogenic signaling of the nerve growth factor receptor TrkA. J Neurosci. 2005;25(47):10930–10940.

31. Vanlandingham PA, Ceresa BP. Rab7 regulates late endocytic trafficking downstream of multivesicular body biogenesis and cargo sequestration. J Biol Chem. 2009;284(18):12110–12124.

32. Pinilla-Macua I, et al. EGF receptor signaling, phosphorylation, ubiquitylation and endocytosis in tumors in vivo. Elife. 2017;6:e31993.

33. Gao H, Shi W, Freund LB. Mechanics of receptor-mediated endocytosis. Proc Natl Acad Sci USA. 2005;102(27):9469–9474.

34. Kumari S, Mg S, Mayor S. Endocytosis unplugged: multiple ways to enter the cell. Cell Res. 2010;20(3):256–275.

35. Gourlaouen M, et al. Essential role for endocytosis in the growth factor-stimulated activation of ERK1/2 in endothelial cells. J Biol Chem. 2013;288(11):7467–7480.

36. Yoshioka K, et al. Endothelial PI3K-C2α, a class II PI3K, has an essential role in angiogenesis and vascular barrier function. Nat Med. 2012;18(10):1560–1569.

37. Bhattacharya R, et al. Regulatory role of dynamin-2 in VEGFR-2/KDR-mediated endothelial signaling. FASEB J. 2005;19(12):1692–1694.

38. Basagiannis D, Christoforidis S. Constitutive endocytosis of VEGFR2 protects the receptor against shedding. J Biol Chem. 2016;291(32):16892–16903.

39. Hsu C, et al. Regulation of exosome secretion by Rab35 and its GTPase-activating proteins TBC1D10A-C. J Cell Biol. 2010;189(2):223–232.

40. Itoh T, Fukuda M. Identification of EPI64 as a GTPase-activating protein specific for Rab27A. J Biol Chem. 2006;281(42):31823–31831.

41. Kofler N, et al. The Rab-effector protein RABEP2 regulates endosomal trafficking to mediate vascular endothelial growth factor receptor-2 (VEGFR2)-dependent signaling. J Biol Chem. 2018;293(13):4805–4817.

42. Bachir AI, et al. Actin-based adhesion modules mediate cell interactions with the extracellular matrix and neighboring cells. Cold Spring Harb Perspect Biol. 2017;9(7):a023234.

43. Jopling HM, et al. Rab GTPase regulation of VEGFR2 trafficking and signaling in endothelial cells. Arterioscler Thromb Vasc Biol. 2009;29(7):1119–1124.

44. Barbera S, et al. The small GTPase Rab5c is a key regulator of trafficking of the CD93/Multimerin-2/β1 integrin complex in endothelial cell adhesion and migration. Cell Commun Signal. 2019;17(1):55.

45. Norden PR, Sun Z, Davis GE. Control of endothelial tubulogenesis by Rab and Ral GTPases, and apical targeting of caveolin-1-labeled vacuoles. PLoS ONE. 2020;15(6):e0235116.

46. Lee JL, Streuli CH. Integrins and epithelial cell polarity. J Cell Sci. 2014;127(Pt 15):3217–3225.

47. Hu Y-L, et al. FAK and paxillin dynamics at focal adhesions in the protrusions of migrating cells. Sci Rep. 2014;4(1):6024.

48. Mana G, et al. PPFIA1 drives active α5β1 integrin recycling and controls fibronectin fibrillogenesis and vascular morphogenesis. Nat Commun. 2016;7(1):13546.

49. Sundararaman A, et al. RhoJ regulates α5β1 integrin trafficking to control fibronectin remodeling during angiogenesis. Curr Biol. 2020;30(11):2146–2155.e5.

50. Dunphy JL, et al. The Arf6 GEF GEP100/BRAG2 regulates cell adhesion by controlling endocytosis of beta1 integrins. Curr Biol. 2006;16(3):315–320.

51. Gamara J, et al. Assessment of Arf6 deletion in PLB-985 differentiated in neutrophil-like cells and in mouse neutrophils: impact on adhesion and migration. Mediat Inflamm. 2020;2020:2713074.

52. Hashimoto S, et al. ARF6 and AMAP1 are major targets of KRAS and TP53 mutations to promote invasion, PD-L1 dynamics, and immune evasion of pancreatic cancer. Proc Natl Acad Sci USA. 2019;116(35):17450–17459.

53. Van Acker T, Tavernier J, Peelman F. The small GTPase Arf6: an overview of its mechanisms of action and of its role in host–pathogen interactions and innate immunity. Int J Mol Sci. 2019;20(9):2209.

54. Jones CA, et al. Slit2-Robo4 signalling promotes vascular stability by blocking Arf6 activity. Nat Cell Biol. 2009;11(11):1325–1331.

55. Harris ES, Nelson WJ. VE-cadherin: at the front, center, and sides of endothelial cell organization and function. Curr Opin Cell Biol. 2010;22(5):651–658.

56. Duong CN, Vestweber D. Mechanisms ensuring endothelial junction integrity beyond VE-cadherin. Front Physiol. 2020

57. Szymborska A, Gerhardt H. Hold me, but not too tight-endothelial cell–cell junctions in angiogenesis. Cold Spring Harb Perspect Biol. 2018;10(8):a029223.

58. Chichger H, et al. p18, a novel adaptor protein, regulates pulmonary endothelial barrier function via enhanced endocytic recycling of VE-cadherin. FASEB J. 2015;29(3):868–881.

59. Yan Z, et al. Rab11a mediates vascular endothelial-cadherin recycling and controls endothelial barrier function. Arterioscler Thromb Vasc Biol. 2016;36(2):339–349.

60. Brüser L, Bogdan S. Adherens junctions on the move—membrane trafficking of E-cadherin. Cold Spring Harb Perspect Biol. 2017;9(3):a029140.

61. Malinova TS, et al. A junctional PACSIN2/EHD4/MICAL-L1 complex coordinates VE-cadherin trafficking for endothelial migration and angiogenesis. Nat Commun. 2021;12(1):2610.

62. Lucken-Ardjomande Häsler S, et al. GRAF2, WDR44, and MICAL1 mediate Rab8/10/11-dependent export of E-cadherin, MMP14, and CFTR ΔF508. J Cell Biol. 2020

63. Fölsch H, et al. The AP-1A and AP-1B clathrin adaptor complexes define biochemically and functionally distinct membrane domains. J Cell Biol. 2003;163(2):351–362.

64. Gravotta D, et al. The clathrin adaptor AP-1A mediates basolateral polarity. Dev Cell. 2012;22(4):811–823.

65. Lock JG, et al. E-cadherin transport from the trans-Golgi network in tubulovesicular carriers is selectively regulated by golgin-97. Traffic. 2005;6(12):1142–1156.

66. Han J, Pluhackova K, Böckmann RA. The multifaceted role of SNARE proteins in membrane fusion. Front Physiol. 2017;8:5.

67. Szule JA, Coorssen JR. Revisiting the role of SNAREs in exocytosis and membrane fusion. Biochim Biophys Acta. 2003;1641(2–3):121–135.

68. Li X, et al. SNARE expression and localization in renal epithelial cells suggest mechanism for variability of trafficking phenotypes. Am J Physiol Ren Physiol. 2002;283(5):F1111–F1122.

69. Garrett JP, et al. Regulation of endothelial barrier function by p120-catenin·VE-cadherin interaction. Mol Biol Cell. 2017;28(1):85–97.

70. Nanes BA, et al. p120-catenin regulates VE-cadherin endocytosis and degradation induced by the Kaposi sarcoma-associated ubiquitin ligase K5. Mol Biol Cell. 2017;28(1):30–40.

71. Grimsley-Myers CM, et al. VE-cadherin endocytosis controls vascular integrity and patterning during development. J Cell Biol. 2020

72. Su W, Kowalczyk AP. The VE-cadherin cytoplasmic domain undergoes proteolytic processing during endocytosis. Mol Biol Cell. 2017;28(1):76–84.

73. Nanes BA, et al. p120-catenin binding masks an endocytic signal conserved in classical cadherins. J Cell Biol. 2012;199(2):365–380.

74. van der Beek J, et al. CORVET, CHEVI and HOPS—multisubunit tethers of the endo-lysosomal system in health and disease. J Cell Sci. 2019

75. Xing R, et al. The Rab7 effector WDR91 promotes autophagy-lysosome degradation in neurons by regulating lysosome fusion. J Cell Biol. 2021

76. Peplowska K, et al. The CORVET tethering complex interacts with the yeast Rab5 homolog Vps21 and is involved in endo-lysosomal biogenesis. Dev Cell. 2007;12(5):739–750.

77. Davis GE, et al. Molecular basis for endothelial lumen formation and tubulogenesis during vasculogenesis and angiogenic sprouting. Int Rev Cell Mol Biol. 2011;288:101–165.

78. Xu K, Cleaver O. Tubulogenesis during blood vessel formation. Semin Cell Dev Biol. 2011;22(9):993–1004.

79. Barlow HR, Cleaver O. Building blood vessels-one rho GTPase at a time. Cells. 2019;8(6):545.

80. Phng L-K, Belting H-G. Endothelial cell mechanics and blood flow forces in vascular morphogenesis. Semin Cell Dev Biol. 2021;120:32–43.

81. Bryant DM, et al. A molecular network for de novo generation of the apical surface and lumen. Nat Cell Biol. 2010;12(11):1035–1045.

82. Wang Y, et al. Moesin1 and VE-cadherin are required in endothelial cells during in vivo tubulogenesis. Development. 2010;137(18):3119–3128.

83. Francis CR, Kushner EJ. Capturing membrane trafficking events during 3D angiogenic development in vitro. Microcirculation. 2021

84. Francis CR, Claflin S, Kushner EJ. Synaptotagmin-like protein 2a regulates angiogenic lumen formation via Weibel-Palade body apical secretion of angiopoietin-2. Arterioscler Thromb Vasc Biol. 2021

85. Lyakhova TA, Knight JD. The C2 domains of granuphilin are high-affinity sensors for plasma membrane lipids. Chem Phys Lipids. 2014;182:29–37.

86. Hayes MJ, et al. Annexin 2 binding to phosphatidylinositol 4,5-bisphosphate on endocytic vesicles is regulated by the stress response pathway. J Biol Chem. 2004;279(14):14157–14164.

87. Leslie NR, et al. Understanding PTEN regulation: PIP2, polarity and protein stability. Oncogene. 2008;27(41):5464–5476.

88. Davis GE, Cleaver OB (2014) Outside in: inversion of cell polarity controls epithelial lumen formation. Dev Cell, 31(2):140–142

89. Strilić B, et al. Electrostatic cell-surface repulsion initiates lumen formation in developing blood vessels. Curr Biol. 2010;20(22):2003–2009.

90. Strilic B, et al. The molecular basis of vascular lumen formation in the developing mouse aorta. Dev Cell. 2009;17(4):505–515.

91. Cait J, et al. Podocalyxin is required for maintaining blood–brain barrier function during acute inflammation. Proc Natl Acad Sci USA. 2019;116(10):4518–4527.

92. Horrillo A, et al. Loss of endothelial barrier integrity in mice with conditional ablation of podocalyxin (Podxl) in endothelial cells. Eur J Cell Biol. 2016;95(8):265–276.

93. Galvez-Santisteban M, et al. Synaptotagmin-like proteins control the formation of a single apical membrane domain in epithelial cells. Nat Cell Biol. 2012;14(8):838–849.

94. Bierings R, et al. The interplay between the Rab27A effectors Slp4-a and MyRIP controls hormone-evoked Weibel-Palade body exocytosis. Blood. 2012;120(13):2757–2767.

95. Richards M, Hetheridge C, Mellor H. The formin FMNL3 controls early apical specification in endothelial cells by regulating the polarized trafficking of podocalyxin. Curr Biol. 2015;25(17):2325–2331.

96. Youker RT, et al. Multiple motifs regulate apical sorting of p75 via a mechanism that involves dimerization and higher-order oligomerization. Mol Biol Cell. 2013;24(12):1996–2007.

97. Levic DS, Bagnat M. Self-organization of apical membrane protein sorting in epithelial cells. FEBS J. 2021;289(3):659–670.

98. Levic DS, et al. Distinct roles for luminal acidification in apical protein sorting and trafficking in zebrafish. J Cell Biol. 2020

99. Tao T, et al. Golgi-resident TRIO regulates membrane trafficking during neurite outgrowth. J Biol Chem. 2019;294(28):10954–10968.

100. Grigoriev I et al (2011) Rab6, Rab8, and MICAL3 cooperate in controlling docking and fusion of exocytotic carriers. Curr Biol 21(11):967–974

101. Lopes-da-Silva M et al (2019) A GBF1-dependent mechanism for environmentally responsive regulation of ER-Golgi transport. Dev Cell 49(5):786-801.e6

102. Quillard T, Charreau B (2013) Impact of Notch signaling on inflammatory responses in cardiovascular disorders. Int J Mol Sci 14(4):6863–6888

103. Chitnis A (2006) Why is delta endocytosis required for effective activation of notch? Dev Dyn 235(4):886–894

104. Lovendahl KN, Blacklow SC, Gordon WR (2018) The molecular mechanism of Notch activation. Adv Exp Med Biol 1066:47–58

105. Six E et al (2003) The Notch ligand Delta1 is sequentially cleaved by an ADAM protease and gamma secretase. Proc Natl Acad Sci USA 100(13):7638-7643

106. Gordon WR, Arnett KL, Blacklow SC (2008) The molecular logic of Notch signaling—a structural and biochemical perspective J Cell Science 121(Pt 19):3109-3119

107. Shergill B et al (2012) Optical tweezers studies on Notch: single molecule interaction strength is independent of ligand endocytosis. Dev Cell 22(6):1313-1320

108. Meloty-Kapella L et al (2012) Notch ligand endocytosis generates mechanical pulling force dependent on dynamin, epsins, and actin. Dev Cell 22(6):1299–1312

109. Webb AM et al (2021) EHD2 modulates Dll4 endocytosis during blood vessel development. Microcirculation. https://doi.org/10. 1111/micc.12740

110. Heuss SF et al (2008) The intracellular region of Notch ligands Dll1 and Dll3 regulates their trafficking and signaling activity. Proc Natl Acad Sci USA 105(32):11212–11217

111. Emery G et al (2005) Asymmetric Rab 11 endosomes regulate delta recycling and specify cell fate in the Drosophila nervous system. Cell 122(5):763–773

112. Adam MG et al (2013) Synaptojanin-2 binding protein stabilizes the Notch ligands DLL1 and DLL4 and inhibits sprouting angio- genesis. Circ Res 113(11):1206–1218

113. Antfolk D et al (2017) Selective regulation of Notch ligands dur- ing angiogenesis is mediated by vimentin. Proc Natl Acad Sci USA 114(23):E4574–E4581

114. Shao X et al (2017) Mammalian Numb protein antagonizes Notch by controlling postendocytic trafficking of the Notch ligand Delta-like 4. J Biol Chem 292(50):20628–20643

115. Benhra N et al (2011) AP-1 controls the trafficking of Notch and Sanpodo toward E-cadherin junctions in sensory organ precur- sors. Curr Biol 21(1):87–95

116. Weinmaster G, Fischer JA (2011) Notch ligand ubiquitylation: what is it good for? Dev Cell 21(1):134–144

117. Wu G et al (2001) SEL-10 is an inhibitor of notch signaling that targets notch for ubiquitin-mediated protein degradation. Mol Cell Biol 21(21):7403–7415

118. Lim R et al (2019) Deubiquitinase USP10 regulates Notch signal- ing in the endothelium. Science 364(6436):188–193

119. Bridges E et al (2020) RHOQ is induced by DLL4 and regulates angiogenesis by determining the intracellular route of the Notch intracellular domain. Angiogenesis 23(3):493–513

120. Wang M et al (2021) Intracellular trafficking of Notch orches- trates temporal dynamics of Notch activity in the fly brain. Nat Commun 12(1):2083

121. Shimizu S et al (2021) Class II phosphatidylinositol 3-kinase- C2α is essential for Notch signaling by regulating the endocytosis of γ-secretase in endothelial cells. Sci Rep 11(1):5199

122. Lenting PJ, Christophe OD, Denis CV (2015) von Willebrand factor biosynthesis, secretion, and clearance: connecting the far ends. Blood 125(13):2019–2028

123. Berriman JA et al (2009) Structural organization of Weibel-Pal- ade bodies revealed by cryo-EM of vitrified endothelial cells. Proc Natl Acad Sci USA 106(41):17407–17412

124. Randi AM, Smith KE, Castaman G (2018) Von Willebrand factor regulation of blood vessel formation. Blood 132(2):132–140

125. Schillemans M et al (2019) Exocytosis of Weibel-Palade bodies: how to unpack a vascular emergency kit. J Thromb Haemost 17(1):6–18 126.

126. Nightingale TD et al (2018) Tuning the endothelial response: differential release of exocytic cargos from Weibel-Palade bodies. J Thromb Haemot 16(9):1873-1886

127. Holthenrich A et al (2019) Proximity proteomics of endothelial Weibel-Palade bodies identifies novel regulator of von Willebrand factor secretion. Blood 134(12):979–982

128. Marks MS, Heijnen HF, Raposo G (2013) Lysosome-related organelles: unusual compartments become mainstream. Curr Opin Cell Biol 25(4):495-505

129. Streetley J et al (2019) Stimulated release of intraluminal vesicles from Weibel-Palade bodies. Blood 133(25):2707–2717

130. Harrison-Lavoie KJ et al (2006) P-selectin and CD63 use different mechanisms for delivery to Weibel-Palade bodies. Traffic 7(6):647-662

131. Kim I et al (2000) Angiopoietin-1 regulates endothelial cell survival through the phosphatidylinositol 3'-kinase/Akt signal transduction pathway. Circ Res 86(1):24–29

132. Felcht M et al (2012) Angiopoietin-2 differentially regulates angiogenesis through TIE2 and integrin signaling. J Clin Investig 122(6):1991–2005

133. Mazzieri R et al (2011) Targeting the ANG2/TIE2 axis inhibits tumor growth and metastasis by impairing angiogenesis and disabling rebounds of proangiogenic myeloid cells. Cancer Cell 19(4):512–526

134. Saint-Lu N et al (2012) Identification of galectin-1 and galectin-3 as novel partners for von Willebrand factor. Arterioscler Thromb Vasc Biol 32(4):894–901

135. Griffioen AW, Thijssen VL (2014) Galectins in tumor angiogenesis. Ann Transl Med 2(9):90

136. Lenzi C et al (2019) Synaptotagmin 5 regulates Ca -dependent Weibel-Palade body exocytosis in human endothelial cells. J Cell Sci.

137. van Breevoort D et al (2014) STXBP1 promotes Weibel-Palade body exocytosis through its interaction with the Rab27A effector Slp4-a. Blood 123(20):3185–3194

138. Karampini E et al (2019) Defective AP-3-dependent VAMP8 trafficking impairs Weibel-Palade body exocytosis in Herman- sky-Pudlak Syndrome type 2 blood outgrowth endothelial cells. Haematologica 104(10):2091–2099

139. Zografou S et al (2012) A complete Rab screening reveals novel insights in Weibel-Palade body exocytosis. J Cell Sci 125(Pt 20):4780–4790

140. Kushner EJ, Bautch VL. Building blood vessels in development and disease. Curr Opin Hematol. 2013;20:231–236.

141. Kushner EJ, Ferro LS, Liu JY, Durrant JR, Rogers SL, Dudley AC, Bautch VL. Excess centrosomes disrupt endothelial cell migration via centrosome scattering. J Cell Biol. 2014;206:257–272

142. Kushner EJ, Ferro LS, Yu Z, Bautch VL. Excess centrosomes perturb dynamic endothelial cell repolarization during blood vessel formation. Mol Biol Cell. 2016;27:1911–1920.

143. Iruela-Arispe ML. LUMENating blood vessels. Dev Cell. 2011;20:412–414.

144. Iruela-Arispe ML, Davis GE. Cellular and molecular mechanisms of vascular lumen formation. Dev Cell. 2009;16:222–231.

145. Davis GE, Cleaver OB. Outside in: inversion of cell polarity controls epithelial lumen formation. Dev Cell. 2014;31:140–142.

146. Barry DM, Koo Y, Norden PR, Wylie LA, Xu K, Wichaidit C, Azizoglu DB, Zheng Y, Cobb MH, Davis GE, et al. Rasip1-mediated Rho GTPase signaling regulates blood vessel tubulogenesis via nonmuscle myosin II. Circ Res. 2016;119:810–826.

147. Strilić B, Kucera T, Eglinger J, Hughes MR, McNagny KM, Tsukita S, Dejana E, Ferrara N, Lammert E. The molecular basis of vascular lumen formation in the developing mouse aorta. Dev Cell. 2009;17:505–515.

148. Strilić B, Eglinger J, Krieg M, Zeeb M, Axnick J, Babál P, Müller DJ, Lammert E. Electrostatic cell-surface repulsion initiates lumen formation in developing blood vessels. Curr Biol. 2010;20:2003–2009. doi: 10.1016/j.cub.2010.09.061 Crossref. PubMed.

149. Bryant DM, Datta A, Rodríguez-Fraticelli AE, Peränen J, Martín-Belmonte F, Mostov KE. A molecular network for de novo generation of the apical surface and lumen. Nat Cell Biol. 2010;12:1035–1045. doi: 10.1038/ncb2106 Crossref. PubMed.

150. Bryant DM, Roignot J, Datta A, Overeem AW, Kim M, Yu W, Peng X, Eastburn DJ, Ewald AJ, Werb Z, et al. A molecular switch for the orientation of epithelial cell polarization. Dev Cell. 2014;31:171–187. doi: 10.1016/j.devcel.2014.08.027 Crossref. PubMed.

151. Román-Fernández Á, Roignot J, Sandilands E, Nacke M, Mansour MA, McGarry L, Shanks E, Mostov KE, Bryant DM. The phospholipid PI(3,4)P2 is an apical identity determinant. Nat Commun. 2018;9:5041. doi: 10.1038/s41467-018-07464-8 Crossref. PubMed.

152. Yu M, Kasai K, Nagashima K, Torii S, Yokota-Hashimoto H, Okamoto K, Takeuchi T, Gomi H, Izumi T. Exophilin4/Slp2-a targets glucagon granules to the plasma membrane through unique Ca2+-inhibitory phospholipid-binding activity of the C2A domain. Mol Biol Cell. 2007;18:688–696. doi: 10.1091/mbc.e06-10-0914 Crossref. PubMed.

153. Fukuda M. Versatile role of Rab27 in membrane trafficking: focus on the Rab27 effector families. J Biochem. 2005;137:9–16. doi: 10.1093/jb/mvi002 Crossref. PubMed.

154. Gálvez-Santisteban M, Rodriguez-Fraticelli AE, Bryant DM, Vergarajauregui S, Yasuda T, Bañón-Rodríguez I, Bernascone I, Datta A, Spivak N, Young K, et al. Synaptotagmin-like proteins control the formation of a single apical membrane domain in epithelial cells. Nat Cell Biol. 2012;14:838–849. doi: 10.1038/ncb2541 Crossref. PubMed.

155. Kuroda TS, Fukuda M. Rab27A-binding protein Slp2-a is required for peripheral melanosome distribution and elongated cell shape in melanocytes. Nat Cell Biol. 2004;6:1195–1203. doi: 10.1038/ncb1197 Crossref. PubMed.

156. Yasuda T, Saegusa C, Kamakura S, Sumimoto H, Fukuda M. Rab27 effector Slp2-a transports the apical signaling molecule podocalyxin to the apical surface of MDCK II cells and regulates claudin-2 expression. Mol Biol Cell. 2012;23:3229–3239. doi: 10.1091/mbc.E12-02-0104 Crossref. PubMed.

157. Nightingale TD, McCormack JJ, Grimes W, Robinson C, Lopes da Silva M, White IJ, Vaughan A, Cramer LP, Cutler DF. Tuning the endothelial response:

differential release of exocytic cargos from Weibel-Palade bodies. J Thromb Haemost. 2018;16:1873–1886. doi: 10.1111/jth.14218 Crossref. PubMed.

158. Boucher JM, Clark RP, Chong DC, Citrin KM, Wylie LA, Bautch VL. Dynamic alterations in decoy VEGF receptor-1 stability regulate angiogenesis. Nat Commun. 2017;8:15699. doi: 10.1038/ncomms15699 Crossref. PubMed.

159. Nakatsu MN, Davis J, Hughes CC. Optimized fibrin gel bead assay for the study of angiogenesis. J Vis Exp. 2007:186. doi: 10.1016/S0076-6879(08)02004-1 PubMed.

160. Nakatsu MN, Hughes CC. An optimized three-dimensional in vitro model for the analysis of angiogenesis. Methods Enzymol. 2008;443:65–82. doi: 10.1016/S0076-6879(08)02004-1 Crossref. PubMed.

161. Honigmann A, van den Bogaart G, Iraheta E, Risselada HJ, Milovanovic D, Mueller V, Müllar S, Diederichsen U, Fasshauer D, Grubmüller H, et al. Phosphatidylinositol 4,5-bisphosphate clusters act as molecular beacons for vesicle recruitment. Nat Struct Mol Biol. 2013;20:679–686. doi: 10.1038/nsmb.2570 Crossref. PubMed.

162. Stauffer TP, Ahn S, Meyer T. Receptor-induced transient reduction in plasma membrane PtdIns(4,5)P2 concentration monitored in living cells. Curr Biol. 1998;8:343–346. doi: 10.1016/s0960-9822(98)70135-6 Crossref. PubMed.

163. Bierings R, Hellen N, Kiskin N, Knipe L, Fonseca AV, Patel B, Meli A, Rose M, Hannah MJ, Carter T. The interplay between the Rab27A effectors Slp4-a and MyRIP controls hormone-evoked Weibel-Palade body exocytosis. Blood. 2012;120:2757–2767. doi: 10.1182/blood-2012-05-429936 Crossref. PubMed.

164. Benedetti L, Barentine AES, Messa M, Wheeler H, Bewersdorf J, De Camilli P. Light-activated protein interaction with high spatial subcellular confinement. Proc Natl Acad Sci U S A. 2018;115:E2238–E2245. doi: 10.1073/pnas.1713845115 Crossref. PubMed.

165. Westbroek W, Tuchman M, Tinloy B, De Wever O, Vilboux T, Hertz JM, Hasle H, Heilmann C, Helip-Wooley A, Kleta R, et al. A novel missense mutation (G43S) in the switch I region of Rab27A causing Griscelli syndrome. Mol Genet Metab. 2008;94:248–254. doi: 10.1016/j.ymgme.2008.02.009 Crossref. PubMed.

166. Mrozowska PS, Fukuda M. Regulation of podocalyxin trafficking by Rab small GTPases in 2D and 3D epithelial cell cultures. J Cell Biol. 2016;213:355–369. doi: 10.1083/jcb.201512024 Crossref. PubMed.

167. Fiedler U, Scharpfenecker M, Koidl S, Hegen A, Grunow V, Schmidt JM, Kriz W, Thurston G, Augustin HG. The Tie-2 ligand angiopoietin-2 is stored in and rapidly released upon stimulation from endothelial cell Weibel-Palade bodies. Blood. 2004;103:4150–4156. doi: 10.1182/blood-2003-10-3685 Crossref. PubMed.

168. Scharpfenecker M, Fiedler U, Reiss Y, Augustin HG. The Tie-2 ligand angiopoietin-2 destabilizes quiescent endothelium through an internal autocrine loop mechanism. J Cell Sci. 2005;118(pt 4):771–780. doi: 10.1242/jcs.01653 Crossref. PubMed.

169. Yuan HT, Khankin EV, Karumanchi SA, Parikh SM. Angiopoietin 2 is a partial agonist/antagonist of Tie2 signaling in the endothelium. Mol Cell Biol. 2009;29:2011–2022. doi: 10.1128/MCB.01472-08 Crossref. PubMed.

170. Kim I, Kim JH, Moon SO, Kwak HJ, Kim NG, Koh GY. Angiopoietin-2 at high concentration can enhance endothelial cell survival through the phosphatidylinositol 3'-kinase/Akt signal transduction pathway. Oncogene. 2000;19:4549–4552. doi: 10.1038/sj.onc.1203800 Crossref. PubMed.

171. Mochizuki Y, Nakamura T, Kanetake H, Kanda S. Angiopoietin 2 stimulates migration and tube-like structure formation of murine brain capillary endothelial cells through c-Fes and c-Fyn. J Cell Sci. 2002;115(pt 1):175–183. Crossref. PubMed.

172. Fiedler U, Reiss Y, Scharpfenecker M, Grunow V, Koidl S, Thurston G, Gale NW, Witzenrath M, Rosseau S, Suttorp N, et al. Angiopoietin-2 sensitizes endothelial cells to TNF-alpha and has a crucial role in the induction of inflammation. Nat Med. 2006;12:235–239. doi: 10.1038/nm1351 Crossref. PubMed.

173. Gale NW, Thurston G, Davis S, Wiegand SJ, Holash J, Rudge JS, Yancopoulos GD. Complementary and coordinated roles of the VEGFs and angiopoietins during normal and pathologic vascular formation. Cold Spring Harb Symp Quant Biol. 2002;67:267–273. doi: 10.1101/sqb.2002.67.267 Crossref. PubMed.

174. Makinde T, Agrawal DK. Intra and extravascular transmembrane signalling of angiopoietin-1-Tie2 receptor in health and disease. J Cell Mol Med. 2008;12:810–828. doi: 10.1111/j.1582-4934.2008.00254.x Crossref. PubMed.

175. Thurston G. Role of Angiopoietins and Tie receptor tyrosine kinases in angiogenesis and lymphangiogenesis. Cell Tissue Res. 2003;314:61–68. doi: 10.1007/s00441-003-0749-6 Crossref. PubMed.

176. Davis S, Papadopoulos N, Aldrich TH, Maisonpierre PC, Huang T, Kovac L, Xu A, Leidich R, Radziejewska E, Rafique A, et al. Angiopoietins have distinct modular domains essential for receptor binding, dimerization and superclustering. Nat Struct Biol. 2003;10:38–44. doi: 10.1038/nsb880 Crossref. PubMed.

177. Gebala V, Collins R, Geudens I, Phng LK, Gerhardt H. Blood flow drives lumen formation by inverse membrane blebbing during angiogenesis in vivo. Nat Cell Biol. 2016;18:443–450. doi: 10.1038/ncb3320 Crossref. PubMed.

178. Hoshijima K, Jurynec MJ, Klatt Shaw D, Jacobi AM, Behlke MA, Grunwald DJ. Highly efficient CRISPR-Cas9-based methods for generating deletion mutations and F0 embryos that lack gene function in zebrafish. Dev Cell. 2019;51:645–657.e4. doi: 10.1016/j.devcel.2019.10.004 Crossref. PubMed.

179. Trubiroha A, Gillotay P, Giusti N, Gacquer D, Libert F, Lefort A, Haerlingen B, De Deken X, Opitz R, Costagliola S. A rapid CRISPR/Cas-based mutagenesis assay in zebrafish for identification of genes involved in thyroid morphogenesis and function. Sci Rep. 2018;8:5647. doi: 10.1038/s41598-018-24036-4 Crossref. PubMed

180. Varshney GK, Carrington B, Pei W, Bishop K, Chen Z, Fan C, Xu L, Jones M, LaFave MC, Ledin J, et al. A high-throughput functional genomics

workflow based on CRISPR/Cas9-mediated targeted mutagenesis in zebrafish. Nat Protoc. 2016;11:2357–2375. doi: 10.1038/nprot.2016.141 Crossref. PubMed.

181. Wu RS, Lam II, Clay H, Duong DN, Deo RC, Coughlin SR. A rapid method for directed gene knockout for screening in G0 zebrafish. Dev Cell. 2018;46:112–125.e4. doi: 10.1016/j.devcel.2018.06.003 Crossref. PubMed.

182. Sankaranarayanan S, De Angelis D, Rothman JE, Ryan TA. The use of pHluorins for optical measurements of presynaptic activity. Biophys J. 2000;79:2199–2208. doi: 10.1016/S0006-3495(00)76468-X Crossref. PubMed.

183. Thurston G, Daly C. The complex role of angiopoietin-2 in the angiopoietin-tie signaling pathway. Cold Spring Harb Perspect Med. 2012;2:a006550. doi: 10.1101/cshperspect.a006650 Crossref. PubMed.

184. Richmond JE, Davis WS, Jorgensen EM. UNC-13 is required for synaptic vesicle fusion in C. elegans. Nat Neurosci. 1999;2:959–964. doi: 10.1038/14755 Crossref. PubMed.

185. Bhattacharya S, Stewart BA, Niemeyer BA, Burgess RW, McCabe BD, Lin P, Boulianne G, O'Kane CJ, Schwarz TL. Members of the synaptobrevin/vesicle-associated membrane protein (VAMP) family in Drosophila are functionally interchangeable in vivo for neurotransmitter release and cell viability. Proc Natl Acad Sci U S A. 2002;99:13867–13872. doi: 10.1073/pnas.202335999 Crossref. PubMed.

186. Jenny Zhou H, Qin L, Zhang H, Tang W, Ji W, He Y, Liang X, Wang Z, Yuan Q, Vortmeyer A, et al. Endothelial exocytosis of angiopoietin-2 resulting

from CCM3 deficiency contributes to cerebral cavernous malformation. Nat Med. 2016;22:1033–1042. doi: 10.1038/nm.4169 Crossref. PubMed.

187. Lenzi C, Stevens J, Osborn D, Hannah MJ, Bierings R, Carter T. Synaptotagmin 5 regulates Ca2+-dependent Weibel-Palade body exocytosis in human endothelial cells. J Cell Sci. 2019;132:jcs221952. doi: 10.1242/jcs.221952 Crossref. PubMed.

188. van Breevoort D, van Agtmaal EL, Dragt BS, Gebbinck JK, Dienava-Verdoold I, Kragt A, Bierings R, Horrevoets AJ, Valentijn KM, Eikenboom JC, et al. Proteomic screen identifies IGFBP7 as a novel component of endothelial cell-specific Weibel-Palade bodies. J Proteome Res. 2012;11:2925–2936. doi: 10.1021/pr300010r Crossref. PubMed.

189. Kim I, Kim HG, So JN, Kim JH, Kwak HJ, Koh GY. Angiopoietin-1 regulates endothelial cell survival through the phosphatidylinositol 3’-Kinase/Akt signal transduction pathway. Circ Res. 2000;86:24–29. doi: 10.1161/01.res.86.1.24 Crossref. PubMed.

190. Fiedler U, Krissl T, Koidl S, Weiss C, Koblizek T, Deutsch U, Martiny-Baron G, Marmé D, Augustin HG. Angiopoietin-1 and angiopoietin-2 share the same binding domains in the Tie-2 receptor involving the first Ig-like loop and the epidermal growth factor-like repeats. J Biol Chem. 2003;278:1721–1727. doi: 10.1074/jbc.M208550200 Crossref. PubMed.

191. Felcht M, Luck R, Schering A, Seidel P, Srivastava K, Hu J, Bartol A, Kienast Y, Vettel C, Loos EK, et al. Angiopoietin-2 differentially regulates

angiogenesis through TIE2 and integrin signaling. J Clin Invest. 2012;122:1991–2005. doi: 10.1172/JCI58832 Crossref. PubMed.

192. Mazzieri R, Pucci F, Moi D, Zonari E, Ranghetti A, Berti A, Politi LS, Gentner B, Brown JL, Naldini L, et al. Targeting the ANG2/TIE2 axis inhibits tumor growth and metastasis by impairing angiogenesis and disabling rebounds of proangiogenic myeloid cells. Cancer Cell. 2011;19:512–526. doi: 10.1016/j.ccr.2011.02.005 Crossref. PubMed.

193. Sundberg C, Kowanetz M, Brown LF, Detmar M, Dvorak HF. Stable expression of angiopoietin-1 and other markers by cultured pericytes: phenotypic similarities to a subpopulation of cells in maturing vessels during later stages of angiogenesis in vivo. Lab Invest. 2002;82:387–401. doi: 10.1038/labinvest.3780433 Crossref. PubMed.

194. Wakui S, Yokoo K, Muto T, Suzuki Y, Takahashi H, Furusato M, Hano H, Endou H, Kanai Y. Localization of Ang-1, -2, Tie-2, and VEGF expression at endothelial-pericyte interdigitation in rat angiogenesis. Lab Invest. 2006;86:1172–1184. doi: 10.1038/labinvest.3700476 Crossref. PubMed.

195. Kushner, E. J. & Bautch, V. L. Building blood vessels in development and disease. Curr Opin Hematol 20, 231-236 (2013).

196. Chappell, J. C., Wiley, D. M. & Bautch, V. L. How blood vessel networks are made and measured. Cells Tissues Organs 195, 94–107 (2012).

197. Ehling, M., Adams, S., Benedito, R. & Adams, R. H. Notch controls retinal blood vessel maturation and quiescence. Development 140, 3051-3061, doi:10.1242/dev.093351 (2013).

198. Eilken, H. M. & Adams, R. H. Dynamics of endothelial cell behavior in sprouting angiogenesis. Curr Opin Cell Biol 22, 617-625, doi:10.1016/j.ceb.2010.08.010 (2010).

199. Kofler, N. et al. The Rab-effector protein RABEP2 regulates endosomal trafficking to mediate vascular endothelial growth factor receptor-2 (VEGFR2)-dependent signaling. J. Biol. Chem. 293, 4805–4817 (2018).

200. Kempers, L. et al. The endosomal RIN2/Rab5C machinery prevents VEGFR2 degradation to control gene expression and tip cell identity during angiogenesis. Angiogenesis https://doi.org/10.1007/s10456-021-09788-4 (2021).

201. Francis, C. R., Claflin, S. & Kushner, E. J. Synaptotagmin-Like Protein 2a Regulates Angiogenic Lumen Formation via Weibel-Palade Body Apical Secretion of Angiopoietin-2. Arterioscler Thromb Vasc Biol, Atvbaha121316113, doi:10.1161/atvbaha.121.316113 (2021).

202. Gross, S. J. et al. Notch regulates vascular collagen IV basement membrane through modulation of lysyl hydroxylase 3 trafficking. Angiogenesis, doi:10.1007/s10456-021-09791-9 (2021).

203. Agola, J. O., Jim, P. A., Ward, H. H., Basuray, S. & Wandinger-Ness, A. Rab GTPases as regulators of endocytosis, targets of disease and therapeutic opportunities. Clin. Genet. 80, 305–318 (2011).

204. Jovic, M., Sharma, M., Rahajeng, J. & Caplan, S. The early endosome: a busy sorting station for proteins at the crossroads. Histol Histopathol 25, 99-112, doi:10.14670/hh-25.99 (2010).

205. Kaksonen, M. & Roux, A. Mechanisms of clathrin-mediated endocytosis. Nat Rev Mol Cell Biol 19, 313-326, doi:10.1038/nrm.2017.132 (2018).

206. Hutagalung, A. H. & Novick, P. J. Role of Rab GTPases in membrane traffic and cell physiology. Physiol. Rev. 91, 119–149 (2011).

207. Pfeffer, S. A model for Rab GTPase localization. Biochem Soc Trans 33, 627-630, doi:10.1042/bst0330627 (2005).

208. Francis, C. R. & Kushner, E. J. Trafficking in blood vessel development. Angiogenesis, doi:10.1007/s10456-022-09838-5 (2022).

209. Klinkert, K. & Echard, A. Rab35 GTPase: A Central Regulator of Phosphoinositides and F-actin in Endocytic Recycling and Beyond. Traffic 17, 1063-1077, doi:10.1111/tra.12422 (2016).

210. Mrozowska, P. S. & Fukuda, M. Regulation of podocalyxin trafficking by Rab small GTPases in 2D and 3D epithelial cell cultures. J Cell Biol 213, 355-369, doi:10.1083/jcb.201512024 (2016).

211. Klinkert, K., Rocancourt, M., Houdusse, A. & Echard, A. Rab35 GTPase couples cell division with initiation of epithelial apico-basal polarity and lumen opening. Nature Communications 7, 11166, doi:10.1038/ncomms11166 (2016).

212. Kobayashi, H. & Fukuda, M. Rab35 regulates Arf6 activity through centaurin-β2 (ACAP2) during neurite outgrowth. J Cell Sci 125, 2235-2243, doi:10.1242/jcs.098657 (2012).

213. Miyamoto, Y., Yamamori, N., Torii, T., Tanoue, A. & Yamauchi, J. Rab35, acting through ACAP2 switching off Arf6, negatively regulates

oligodendrocyte differentiation and myelination. Mol Biol Cell 25, 1532-1542, doi:10.1091/mbc.E13-10-0600 (2014).

214. Bhat, S. et al. Rab35 and its effectors promote formation of tunneling nanotubes in neuronal cells. Scientific Reports 10, 16803, doi:10.1038/s41598-020-74013-z (2020).

215. Rahajeng, J., Giridharan, S. S., Cai, B., Naslavsky, N. & Caplan, S. MICAL-L1 is a tubular endosomal membrane hub that connects Rab35 and Arf6 with Rab8a. Traffic 13, 82-93, doi:10.1111/j.1600-0854.2011.01294.x (2012).

216. Frémont, S. et al. Oxidation of F-actin controls the terminal steps of cytokinesis. Nature Communications 8, 14528, doi:10.1038/ncomms14528 (2017).

217. Zhang, J., Fonovic, M., Suyama, K., Bogyo, M. & Scott, M. P. Rab35 controls actin bundling by recruiting fascin as an effector protein. Science 325, 1250-1254, doi:10.1126/science.1174921 (2009).

218. Remsburg, C., Testa, M. & Song, J. L. Rab35 regulates skeletogenesis and gastrulation by facilitating actin remodeling and vesicular trafficking. Cells Dev 165, doi:10.1016/j.cdev.2021.203660 (2021).

219. Campeau, E. et al. A versatile viral system for expression and depletion of proteins in mammalian cells. PLoS One 4, e6529, doi:10.1371/journal.pone.0006529 (2009).

220. Nakatsu, M. N., Davis, J. & Hughes, C. C. Optimized fibrin gel bead assay for the study of angiogenesis. J Vis Exp., 186. doi: 110.3791/3186. Epub 2007 Apr 3729. (2007).

221. Francis, C. R. & Kushner, E. J. Capturing membrane trafficking events during 3D angiogenic development in vitro. Microcirculation, e12726, doi:10.1111/micc.12726 (2021).

222. Chesneau, L. et al. An ARF6/Rab35 GTPase cascade for endocytic recycling and successful cytokinesis. Curr Biol 22, 147-153, doi:10.1016/j.cub.2011.11.058 (2012).

223. Dambournet, D. et al. Rab35 GTPase and OCRL phosphatase remodel lipids and F-actin for successful cytokinesis. Nature Cell Biology 13, 981-988, doi:10.1038/ncb2279 (2011).

224. Kouranti, I., Sachse, M., Arouche, N., Goud, B. & Echard, A. Rab35 regulates an endocytic recycling pathway essential for the terminal steps of cytokinesis. Curr Biol 16, 1719-1725, doi:10.1016/j.cub.2006.07.020 (2006).

225. Biesemann, A., Gorontzi, A., Barr, F. & Gerke, V. Rab35 protein regulates evoked exocytosis of endothelial Weibel-Palade bodies. J Biol Chem 292, 11631-11640, doi:10.1074/jbc.M116.773333 (2017).

226. Jackson, T. R. et al. ACAPs are arf6 GTPase-activating proteins that function in the cell periphery. J Cell Biol 151, 627-638, doi:10.1083/jcb.151.3.627 (2000).

227. Cauvin, C. et al. Rab35 GTPase Triggers Switch-like Recruitment of the Lowe Syndrome Lipid Phosphatase OCRL on Newborn Endosomes. Curr Biol 26, 120-128, doi:10.1016/j.cub.2015.11.040 (2016).

228. Lin, L. et al. Rab35/ACAP2 and Rab35/RUSC2 Complex Structures Reveal Molecular Basis for Effector Recognition by Rab35 GTPase. Structure 27, 729-740.e723, doi:10.1016/j.str.2019.02.008 (2019).

229. Parachoniak, C. A., Luo, Y., Abella, J. V., Keen, J. H. & Park, M. GGA3 functions as a switch to promote Met receptor recycling, essential for sustained ERK and cell migration. Dev Cell 20, 751-763, doi:10.1016/j.devcel.2011.05.007 (2011).

230. Marat, A. L. & McPherson, P. S. The connecdenn family, Rab35 guanine nucleotide exchange factors interfacing with the clathrin machinery. J Biol Chem 285, 10627-10637, doi:10.1074/jbc.M109.050930 (2010).

231. Marat, A. L., Ioannou, M. S. & McPherson, P. S. Connecdenn 3/DENND1C binds actin linking Rab35 activation to the actin cytoskeleton. Mol Biol Cell 23, 163-175, doi:10.1091/mbc.E11-05-0474 (2012).

232. Chaineau, M., Ioannou, M. S. & McPherson, P. S. Rab35: GEFs, GAPs and effectors. Traffic 14, 1109-1117, doi:10.1111/tra.12096 (2013).

233. Allaire, P. D. et al. The Connecdenn DENN domain: a GEF for Rab35 mediating cargo-specific exit from early endosomes. Mol Cell 37, 370-382, doi:10.1016/j.molcel.2009.12.037 (2010).

234. Mullins, R. D., Heuser, J. A. & Pollard, T. D. The interaction of Arp2/3 complex with actin: nucleation, high affinity pointed end capping, and formation of branching networks of filaments. Proc Natl Acad Sci U S A 95, 6181-6186, doi:10.1073/pnas.95.11.6181 (1998).

235. Hetrick, B., Han, M. S., Helgeson, L. A. & Nolen, B. J. Small molecules CK-666 and CK-869 inhibit actin-related protein 2/3 complex by blocking an activating conformational change. Chem Biol 20, 701-712, doi:10.1016/j.chembiol.2013.03.019 (2013).

236. Farrants, H. et al. Chemogenetic Control of Nanobodies. Nat Methods 17, 279-282, doi:10.1038/s41592-020-0746-7 (2020).

237. Morozova, K. S. et al. Far-red fluorescent protein excitable with red lasers for flow cytometry and superresolution STED nanoscopy. Biophys J 99, L13-15, doi:10.1016/j.bpj.2010.04.025 (2010).

238. Lauffenburger, D. A. & Horwitz, A. F. Cell migration: a physically integrated molecular process. Cell 84, 359-369, doi:10.1016/s0092-8674(00)81280-5 (1996).

239. Svitkina, T. M. & Borisy, G. G. Arp2/3 complex and actin depolymerizing factor/cofilin in dendritic organization and treadmilling of actin filament array in lamellipodia. J Cell Biol 145, 1009-1026, doi:10.1083/jcb.145.5.1009 (1999).

240. Barry, D. J., Durkin, C. H., Abella, J. V. & Way, M. Open source software for quantification of cell migration, protrusions, and fluorescence intensities. J Cell Biol 209, 163-180, doi:10.1083/jcb.201501081 (2015).

241. Maruthamuthu, V. & Gardel, M. L. Protrusive activity guides changes in cell-cell tension during epithelial cell scattering. Biophys J 107, 555-563, doi:10.1016/j.bpj.2014.06.028 (2014).

242. Milligan, R. A., Whittaker, M. & Safer, D. Molecular structure of F-actin and location of surface binding sites. Nature 348, 217-221, doi:10.1038/348217a0 (1990).

243. Lee, Chi W. et al. Dynamic Localization of G-Actin during Membrane Protrusion in Neuronal Motility. Current Biology 23, 1046-1056, doi:https://doi.org/10.1016/j.cub.2013.04.057 (2013).

244. Byrne, Kate M. et al. Bistability in the Rac1, PAK, and RhoA Signaling Network Drives Actin Cytoskeleton Dynamics and Cell Motility Switches. Cell Systems 2, 38-48, doi:https://doi.org/10.1016/j.cels.2016.01.003 (2016).

245. Piekny, A. J. & Glotzer, M. Anillin is a scaffold protein that links RhoA, actin, and myosin during cytokinesis. Curr Biol 18, 30-36, doi:10.1016/j.cub.2007.11.068 (2008).

246. Hoshijima, K. et al. Highly Efficient CRISPR-Cas9-Based Methods for Generating Deletion Mutations and F0 Embryos that Lack Gene Function in Zebrafish. Dev Cell 51, 645-657.e644, doi:10.1016/j.devcel.2019.10.004 (2019).

247. White, R. M. et al. Transparent adult zebrafish as a tool for in vivo transplantation analysis. Cell Stem Cell 2, 183-189, doi:10.1016/j.stem.2007.11.002 (2008).

248. Al-Awar, O., Radhakrishna, H., Powell, N. N. & Donaldson, J. G. Separation of membrane trafficking and actin remodeling functions of ARF6 with an effector domain mutant. Mol Cell Biol 20, 5998-6007, doi:10.1128/mcb.20.16.5998-6007.2000 (2000).

249. Boshans, R. L., Szanto, S., van Aelst, L. & D'Souza-Schorey, C. ADP-ribosylation factor 6 regulates actin cytoskeleton remodeling in coordination with Rac1 and RhoA. Mol Cell Biol 20, 3685-3694, doi:10.1128/mcb.20.10.3685-3694.2000 (2000).

250. Gebala, V., Collins, R., Geudens, I., Phng, L. K. & Gerhardt, H. Blood flow drives lumen formation by inverse membrane blebbing during angiogenesis in vivo. Nat Cell Biol 18, 443-450, doi:10.1038/ncb3320 (2016).

251. Phng, L. K. et al. Formin-mediated actin polymerization at endothelial junctions is required for vessel lumen formation and stabilization. Dev Cell 32, 123-132, doi:10.1016/j.devcel.2014.11.017 (2015).

252. Paatero, I. et al. Junction-based lamellipodia drive endothelial cell rearrangements in vivo via a VE-cadherin-F-actin based oscillatory cell-cell interaction. Nature Communications 9, 3545, doi:10.1038/s41467-018-05851-9 (2018).

253. van Geemen, D. et al. F-actin-anchored focal adhesions distinguish endothelial phenotypes of human arteries and veins. Arterioscler Thromb Vasc Biol 34, 2059-2067, doi:10.1161/atvbaha.114.304180 (2014).

254. Iruela-Arispe, M. L. & Davis, G. E. Cellular and molecular mechanisms of vascular lumen formation. Dev Cell 16, 222-231, doi:10.1016/j.devcel.2009.01.013 (2009).

255. Bayless, K. J. & Johnson, G. A. Role of the cytoskeleton in formation and maintenance of angiogenic sprouts. J Vasc Res 48, 369-385, doi:10.1159/000324751 (2011).

256. Barry, D. M. et al. Rasip1-Mediated Rho GTPase Signaling Regulates Blood Vessel Tubulogenesis via Nonmuscle Myosin II. Circ Res 119, 810-826, doi:10.1161/circresaha.116.309094 (2016).

257. Barry, D. M. et al. Cdc42 is required for cytoskeletal support of endothelial cell adhesion during blood vessel formation in mice. Development 142, 3058-3070, doi:10.1242/dev.125260 (2015).

258. Kondrychyn, I. et al. Marcksl1 modulates endothelial cell mechanoresponse to haemodynamic forces to control blood vessel shape and size. Nat Commun 11, 5476, doi:10.1038/s41467-020-19308-5 (2020).

259. Norden, P. R., Kim, D. J., Barry, D. M., Cleaver, O. B. & Davis, G. E. Cdc42 and k-Ras Control Endothelial Tubulogenesis through Apical Membrane and Cytoskeletal Polarization: Novel Stimulatory Roles for GTPase Effectors, the Small GTPases, Rac2 and Rap1b, and Inhibitory Influence of Arhgap31 and Rasa1. PLoS One 11, e0147758, doi:10.1371/journal.pone.0147758 (2016).

260. Kulasekaran, G. et al. An Arf/Rab cascade controls the growth and invasiveness of glioblastoma. J Cell Biol 220, doi:10.1083/jcb.202004229 (2021).

261. Villagomez, F. R., Medina-Contreras, O., Cerna-Cortes, J. F. & Patino-Lopez, G. The role of the oncogenic Rab35 in cancer invasion, metastasis, and immune evasion, especially in leukemia. Small GTPases, 1-12, doi:10.1080/21541248.2018.1463895 (2018).

262. Villagomez, F. R., Medina-Contreras, O., Cerna-Cortes, J. F. & Patino-Lopez, G. The role of the oncogenic Rab35 in cancer invasion, metastasis, and

immune evasion, especially in leukemia. Small GTPases 11, 334-345, doi:10.1080/21541248.2018.1463895 (2020).\

263. Gibson, D. G. et al. Enzymatic assembly of DNA molecules up to several hundred kilobases. Nat Methods 6, 343-345, doi:10.1038/nmeth.1318 (2009).

264. Luo, J. et al. A protocol for rapid generation of recombinant adenoviruses using the AdEasy system. Nat Protoc 2, 1236-1247, doi:10.1038/nprot.2007.135 (2007).

265. Webb, A. M. et al. EHD2 modulates Dll4 endocytosis during blood vessel development. Microcirculation 29, e12740, doi:10.1111/micc.12740 (2021).

266. Mizuno, T., Shinya, M. & Takeda, H. Cell and tissue transplantation in zebrafish embryos. Methods Mol Biol. 127, 15-28. (1999).

267. Watanabe, K. et al. Networks of polarized actin filaments in the axon initial segment provide a mechanism for sorting axonal and dendritic proteins. Cell Rep 2, 1546-1553, doi:10.1016/j.celrep.2012.11.015 (2012).

268. Singh, Vikash, et al. "Arf GTPase interplay with Rho GTPases in regulation of the actin cytoskeleton." Small GTPases 10.6 (2019): 411-418.

269. Moravec, Radim, et al. "BRAG2/GEP100/IQSec1 interacts with clathrin and regulates α5β1 integrin endocytosis through activation of ADP ribosylation factor 5 (Arf5)." Journal of Biological Chemistry 287.37 (2012): 31138-31147.

270. Mukhamedova, Nigora, et al. "Small GTPase ARF6 regulates endocytic pathway leading to degradation of ATP-binding cassette transporter A1." Arteriosclerosis, thrombosis, and vascular biology 36.12 (2016): 2292-2303.

271. Santy, Lorraine C., and James E. Casanova. "Activation of ARF6 by ARNO stimulates epithelial cell migration through downstream activation of both Rac1 and phospholipase D." The Journal of cell biology 154.3 (2001): 599-610.

272. Hernández-Deviez, Delia, Alan Mackay-Sim, and Jean M. Wilson. "A Role for ARF6 and ARNO in the regulation of endosomal dynamics in neurons." Traffic 8.12 (2007): 1750-1764.

273. Hurtado-Lorenzo, Andrés, et al. "V-ATPase interacts with ARNO and Arf6 in early endosomes and regulates the protein degradative pathway." Nature cell biology 8.2 (2006): 124-136.

274. Cohen, Lee Ann, et al. "Active Arf6 recruits ARNO/cytohesin GEFs to the PM by binding their PH domains." Molecular biology of the cell 18.6 (2007): 2244-2253.

275. Ikeda, Satoshi, et al. "Novel role of ARF6 in vascular endothelial growth factor–induced signaling and angiogenesis." Circulation research 96.4 (2005): 467-475.

276. Davis, Chadwick T., et al. "ARF6 inhibition stabilizes the vasculature and enhances survival during endotoxic shock." The Journal of Immunology 192.12 (2014): 6045-6052.

277. Abdul-Salam, Vahitha B., et al. "CLIC4/Arf6 pathway: a new lead in BMPRII inhibition in pulmonary hypertension." Circulation research 124.1 (2019): 52-65.

278. Li, Wenlu, et al. "Annexin A2 is a Robo4 ligand that modulates ARF6 activation-associated cerebral trans-endothelial permeability." Journal of Cerebral Blood Flow & Metabolism 39.10 (2019): 2048-2060.

279. Hongu, Tsunaki, et al. "Pathological functions of the small GTPase Arf6 in cancer progression: Tumor angiogenesis and metastasis." Small GTPases 7.2 (2016): 47-53.

280. Hongu, Tsunaki, et al. "Arf6 regulates tumor angiogenesis and growth through HGF-induced endothelial β1 integrin recycling." Nature communications 6.1 (2015): 1-12.

281. Randazzo, Paul A., and Dianne S. Hirsch. "Arf GAPs: multifunctional proteins that regulate membrane traffic and actin remodeling." Cellular signaling 16.4 (2004): 401-413.

282. Frank, Scott R., Jessica C. Hatfield, and James E. Casanova. "Remodeling of the actin cytoskeleton is coordinately regulated by protein kinase C and the ADP-ribosylation factor nucleotide exchange factor ARNO." Molecular biology of the cell 9.11 (1998): 3133-3146.

283. Humphreys, Daniel, et al. "Arf6 coordinates actin assembly through the WAVE complex, a mechanism usurped by Salmonella to invade host cells." Proceedings of the National Academy of Sciences 110.42 (2013): 16880-16885.

284. Santy, Lorraine C., and James E. Casanova. "Activation of ARF6 by ARNO stimulates epithelial cell migration through downstream activation of both Rac1 and phospholipase D." The Journal of cell biology 154.3 (2001): 599-610.

285. Takatsu, Hiroyuki, et al. "GGA proteins associate with Golgi membranes through interaction between their GGAH domains and ADP-ribosylation factors." Biochemical Journal 365.2 (2002): 369-378.

286. Premont, Richard T., et al. "β2-Adrenergic receptor regulation by GIT1, a G protein-coupled receptor kinase-associated ADP ribosylation factor GTPase-activating protein." Proceedings of the National Academy of Sciences 95.24 (1998): 14082-14087.

287. Randazzo, Paul A., et al. "The Arf GTPase-activating protein ASAP1 regulates the actin cytoskeleton." Proceedings of the National Academy of Sciences 97.8 (2000): 4011-4016.

288. Liu, Yunhao, et al. "The association of ASAP1, an ADP ribosylation factor-GTPase activating protein, with focal adhesion kinase contributes to the process of focal adhesion assembly." Molecular biology of the cell 13.6 (2002): 2147-2156.

289. Adarska, Petia, Luis Wong-Dilworth, and Francesca Bottanelli. "ARF GTPases and their ubiquitous role in intracellular trafficking beyond the Golgi." Frontiers in Cell and Developmental Biology 9 (2021).

290. Hongu, Tsunaki, and Yasunori Kanaho. "Activation machinery of the small GTPase Arf6." Advances in biological regulation 54 (2014): 59-66.

291. Yamauchi, Yohei, Yuki Miura, and Yasunori Kanaho. "Machineries regulating the activity of the small GTPase Arf6 in cancer cells are potential targets for developing innovative anti-cancer drugs." Advances in biological regulation 63 (2017): 115-121

292. Martin, T. F. J. "Phosphoinositide lipids as signaling molecules: common themes for signal transduction, cytoskeletal regulation, and membrane trafficking." Annual review of cell and developmental biology 14.1 (1998): 231-264.

293. Rogers, Stephen L., and Vladimir I. Gelfand. "Membrane trafficking, organelle transport, and the cytoskeleton." Current opinion in cell biology 12.1 (2000): 57-62.

294. Lundquist, Erik A. "Small GTPases." WormBook (2006): 1.

295. Krishna, Radha G., and Finn Wold. "Post-translational modifications of proteins." Methods in protein sequence analysis (1993): 167-172.

296. Neel, Benjamin G., and Nicholas K. Tonks. "Protein tyrosine phosphatases in signal transduction." Current opinion in cell biology 9.2 (1997): 193-204.

297. Shenoy, Sudha K. "Seven-transmembrane receptors and ubiquitination." Circulation research 100.8 (2007): 1142-1154.

298. Rogers, Stephen L., and Vladimir I. Gelfand. "Membrane trafficking, organelle transport, and the cytoskeleton." Current opinion in cell biology 12.1 (2000): 57-62.

299. Qualmann, Britta, and Michael M. Kessels. "Endocytosis and the cytoskeleton." International review of cytology 220 (2002): 93-144.

300. Cosen-Binker, Laura I., and András Kapus. "Cortactin: the gray eminence of the cytoskeleton." Physiology 21.5 (2006): 352-361.

301. Aunis, D. O. M. I. N. I. Q. U. E., and MARIE-FRANCE Bader. "The cytoskeleton as a barrier to exocytosis in secretory cells." Journal of Experimental Biology 139.1 (1988): 253-266.

302. Li, Fu, et al. "The role of the hypervariable C-terminal domain in Rab GTPases membrane targeting." Proceedings of the National Academy of Sciences 111.7 (2014): 2572-2577.

303. Pereira-Leal, José B., Alistair N. Hume, and Miguel C. Seabra. "Prenylation of Rab GTPases: molecular mechanisms and involvement in genetic disease." FEBS letters 498.2-3 (2001): 197-200.

304. Wu, Shih-Kwang, et al. "Structural insights into the function of the Rab GDI superfamily." Trends in biochemical sciences 21.12 (1996): 472-476.

305. Donaldson, Julie G. "Multiple roles for Arf6: sorting, structuring, and signaling at the plasma membrane." Journal of Biological Chemistry 278.43 (2003): 41573-41576.

306. Schweitzer, Jill Kuglin, Alanna E. Sedgwick, and Crislyn D'Souza-Schorey. "ARF6-mediated endocytic recycling impacts cell movement, cell division and lipid homeostasis." Seminars in cell & developmental biology. Vol. 22. No. 1. Academic Press, 2011.

307. Takakura, Nobuyuki, et al. "Critical role of the TIE2 endothelial cell receptor in the development of definitive hematopoiesis." Immunity 9.5 (1998): 677-686.

308. Goud, Bruno, Shijie Liu, and Brian Storrie. "Rab proteins as major determinants of the Golgi complex structure." Small GTPases 9.1-2 (2018): 66-75.

309. Pfeffer, Suzanne R. "Rab GTPase localization and Rab cascades in Golgi transport." Biochemical Society Transactions 40.6 (2012): 1373-1377.

310. Pfeffer, Suzanne R. "How the Golgi works: a cisternal progenitor model." Proceedings of the National Academy of Sciences 107.46 (2010): 19614-19618.

311. Goud, Bruno, and Paul A. Gleeson. "TGN golgins, Rabs and cytoskeleton: regulating the Golgi trafficking highways." Trends in cell biology 20.6 (2010): 329-336.

312. Sato, Takashi, et al. "The Rab8 GTPase regulates apical protein localization in intestinal cells." Nature 448.7151 (2007): 366-369.

313. Nakajo, Atsuhiro, et al. "EHBP1L1 coordinates Rab8 and Bin1 to regulate apical-directed transport in polarized epithelial cells." Journal of Cell Biology 212.3 (2016): 297-306.

314. Peränen, Johan. "Rab8 GTPase as a regulator of cell shape." Cytoskeleton 68.10 (2011): 527-539.

315. Mrozowska, Paulina S., and Mitsunori Fukuda. "Regulation of podocalyxin trafficking by Rab small GTPases in epithelial cells." Small GTPases 7.4 (2016): 231-238.

316. Lizama, Carlos O., and Ann C. Zovein. "Polarizing pathways: balancing endothelial polarity, permeability, and lumen formation." Experimental cell research 319.9 (2013): 1247.

317. Richards, Mark, Clare Hetheridge, and Harry Mellor. "The formin FMNL3 controls early apical specification in endothelial cells by regulating the polarized trafficking of podocalyxin." Current Biology 25.17 (2015): 2325-2331.

318. Abhinand, Chandran S., et al. "VEGF-A/VEGFR2 signaling network in endothelial cells relevant to angiogenesis." Journal of cell communication and signaling 10.4 (2016): 347-354.

319. Peters, Kevin G., et al. "Functional significance of Tie2 signaling in the adult vasculature." Recent progress in hormone research 59.1 (2004): 51-71.

320. Maisonpierre, Peter C., et al. "Angiopoietin-2, a natural antagonist for Tie2 that disrupts in vivo angiogenesis." Science 277.5322 (1997): 55-60.

321. Wang, Ying, et al. "Moesin1 and Ve-cadherin are required in endothelial cells during in vivo tubulogenesis." Development 137.18 (2010): 3119-3128.

322. Francis, Caitlin R., Hayle Kincross, and Erich J. Kushner. "Rab35 Governs Apicobasal Polarity Through Regulation of Actin Dynamics During Sprouting Angiogenesis." bioRxiv (2022).

323. Sciaky, Noah, et al. "Golgi tubule traffic and the effects of brefeldin A visualized in living cells." The Journal of cell biology 139.5 (1997): 1137-1155.

324. Van Breevoort, Dorothee, et al. "Proteomic screen identifies IGFBP7 as a novel component of endothelial cell-specific Weibel-Palade bodies." Journal of proteome research 11.5 (2012): 2925-2936.

325. Hare, James F. "Mechanisms of membrane protein turnover." Biochimica et Biophysica Acta (BBA)-Reviews on Biomembranes 1031.1 (1990): 71-90.

326. MacGurn, Jason A., Pi-Chiang Hsu, and Scott D. Emr. "Ubiquitin and membrane protein turnover: from cradle to grave." Annual review of biochemistry 81 (2012): 231-259.

327. Sambamurti, Kumar, et al. "A partial failure of membrane protein turnover may cause Alzheimer's disease: a new hypothesis." Current Alzheimer Research 3.1 (2006): 81-90.

328. Hattula, Katarina, et al. "Characterization of the Rab8-specific membrane traffic route linked to protrusion formation." Journal of cell science 119.23 (2006): 4866-4877.

329. Abhinand, Chandran S., et al. "VEGF-A/VEGFR2 signaling network in endothelial cells relevant to angiogenesis." Journal of cell communication and signaling 10.4 (2016): 347-354.

330. Soares, Carolina Pontes, et al. "2D and 3D-organized cardiac cells shows differences in cellular morphology, adhesion junctions, presence of myofibrils and protein expression." PloS one 7.5 (2012): e38147.

331. Myungjin Lee, Janet, et al. "A three-dimensional microenvironment alters protein expression and chemosensitivity of epithelial ovarian cancer cells in vitro." Laboratory investigation 93.5 (2013): 528-542.

332. Halpern, Marnie E., et al. "Gal4/UAS transgenic tools and their application to zebrafish." Zebrafish 5.2 (2008): 97-110.

333. Katzen, Federico. "Gateway® recombinational cloning: a biological operating system." Expert opinion on drug discovery 2.4 (2007): 571-589.

334. Eaton, Samantha L., et al. "Total protein analysis as a reliable loading control for quantitative fluorescent Western blotting." PloS one 8.8 (2013): e72457.

335. Linder, Matts D., et al. "Rab8 regulates ABCA1 cell surface expression and facilitates cholesterol efflux in primary human macrophages." Arteriosclerosis, thrombosis, and vascular biology 29.6 (2009): 883-888.

Appendix A: Methods and Materials

Cell Culture.

Pooled human umbilical vein ECs were purchased from PromoCell and cultured in proprietary media (PromoCell Growth Medium, ready-to-use) for 2 to 5 passages. For experiments, glass-bottomed imaging dishes were exposed to deep UV light for 6 minutes and coated with Poly-D-Lysine (ThermoFisher) for a minimum of 20 minutes. Small interfering RNA (ThermoFisher) was introduced into primary human umbilical vein ECs using the Neon transfection system (ThermoFisher). See Appendix Table 5 for sources of siRNA. All siRNA were resuspended to a 20 μmol/L stock concentration and used at 0.5 μmol/L. Normal human lung fibroblasts (Lonza) and HEK-A (ThermoFisher) were maintained in DMEM supplemented with 10% fetal bovine serum and pen/strep antibiotics. Both normal human lung fibroblasts and HEKs were used up to 15 passages. All cells were maintained in a humidified incubator at 37 °C and 5% CO_2.

Drug Treatments.

Phorbol myristate acetate or histamine (Sigma) was used to induce secretion of WPB components. To achieve this, cells were serum-starved for 6 hours and treated with a final concentration of 100 ng/mL phorbol myristate acetate or 100 μmol/L histamine for 15 minutes. Cells were then washed with PBS and fixed promptly in 4% paraformaldehyde. For Tie-2 inhibition, cells were treated with BAY-826 (TOCRIS) at a final concentration of 1.3 nmol/L for 1 to 3 days during sprouting.

Cells treated with CK-666 received a final concentration of 1uM; for PitStop2 the final concentration was 50uM. All live imaging of drug treatments included recording baseline cell behavior followed by immediately recording cell behavior following drug administration. For ligand-modulated antibody fragments tethered to the mitochondria (Mito-LAMA), TMP administration was carried out as previously described [236].

Cells treated with Brefeldin A received a final concentration of 0.55ug/mL. Cells were treated with Brefeldin A overnight and fixed the following morning. All drugs used in each investigation are listed in the Appendix Table 3.

Sprouting Angiogenesis Assay.

Fibrin-bead assay was performed as reported by Nakatsu et al [159]. Briefly, human umbilical vein ECs were coated onto microcarrier beads (Amersham) and plated overnight. SiRNA-treatment or viral transduction was performed the same day the beads were coated. The following day, the EC-covered microbeads were embedded in a fibrin matrix. Once the clot was formed, media was overlaid along with approximately 100,000 normal human lung fibroblasts. Media was changed daily along with monitoring of sprout development. Sprout characteristics were quantified in the following manner. Sprout numbers were determined by counting the number of multicellular sprouts (sprouts that did not contain at least 3 cells were not counted) emanating from an individual microcarrier beads across multiple beads in a given experiment. Sprout lengths were determined by measuring the length of a multicellular sprout beginning from the tip of the sprout to the microcarrier bead surface across multiple beads. Percent of non-lumenized sprouts were determined by quantifying the proportion of multicellular sprouts whose length (microcarrier bead surface to sprout tip) was <80% lumenized across

multiple beads. Sprout widths were determined by measuring the sprout width at the midpoint between the tip and the microcarrier bead across multiple beads. Experimental repeats are defined as an independent experiment in which multiple cultures, containing numerous sprouting beads were quantified; this process of quantifying multiple parameters across many beads and several cultures was replicated on different days for each experimental repeat.

Lentivirus Generation and Transduction.

Lentivirus was generated by using the LR Gateway Cloning method [333]. Genes of interest and fluorescent proteins were isolated and incorporated into a pME backbone via Gibson reaction (8). Following confirmation of the plasmid by sequencing the pME entry plasmid was mixed with the destination vector and LR Clonase. The destination vector used in this study was pLenti CMV Neo DEST (705-1) (gift from Eric Campeau & Paul Kaufman; Addgene plasmid #17392). Once validated, the destination plasmids were transfected with the three required viral protein plasmids: pMDLg/pRRE (gift from Didier Trono; Addgene plasmid # 12251), pVSVG (gift from Bob Weinberg; Addgene plasmid #8454) and psPAX2 (gift from Didier Trono; Addgene plasmid #12260) into HEK 293 cells. The transfected HEKs had media changed 4 hours post transfection. Transfected cells incubated for 3-4 days and virus was harvested.

Immunoblotting and Protein Pull-Down.

HUVEC cultures were trypsinized and lysed using Ripa buffer (20 mM Tris-HCl [pH 7.5], 150 mM NaCl, 1 mM Na2EDTA, 1 mM EGTA, 1% NP-40, 1% sodium deoxycholate, 2.5 mM sodium pyrophosphate, 1 mM β-glycerophosphate, 1 mM Na3VO4, 1 μg/mL leupeptin) containing 1× ProBlock™ Protease Inhibitor Cocktail-50

(GoldBio) and processed as previously described [334]. GGA3, Rac1 and RhoA activity blots were performed using commercially available kits (Cytoskeleton; Appendix Table 2).

Total concentration of protein in lysate was quantified using the PierceTM BCA Protein Assay Kit measured at 562 nm and compared to a standard curve. 20-50 μg protein was prepared in 0.52 M SDS, 1.2 mM bromothymol blue, 58.6% glycerol, 75 mM Tris pH 6.8, and 0.17 M DTT. Samples were boiled for 10 minutes, then loaded in a 7-12% SDS gel and run at 150 V. Protein was then transferred to Immun-Blot PVDF Membrane (BioRad) at 4°C, 100 V for 1 hour 10 minutes. Blots were blocked in 2% milk proteins for 1 hour, then put in primary antibody at specified concentrations overnight. After 3 10-minute washes with PBS, secondary antibodies at specified concentrations were applied for 4 hours. After 3 additional PBS washes, blots were developed with ProSignal® Pico ECL Spray.

For Rab27a pull-down experiments, GST-Slp2a was grown overnight in 50 mL of Laria- Bertani broth in NiCo21 E Coli (NEB). The following day the overnight culture was transferred to 1L of terrific buffer. The culture was monitored for growth and induced at OD600 with IPTG (GoldBio, 12481) at a final concentration of 100uM. Following induction, bacteria were incubated for an additional 3 hours. Induced cells were collected and pelleted, with the pellet resuspended in cold PBS containing 1mg/ml lysozyme and 1x ProBlockTM Protease Inhibitor Cocktail -50 and then sonicated to lyse bacteria. Cell lysate was clarified by centrifugation and glutathione agarose resin (GoldBio) was added to affinity purify the GST-Slp2a. After incubation, agarose resin was washed 2-3 times with PBS and stored at -20oC.

Immunofluorescence and Microscopy.

For immunofluorescence imaging of 2-dimensional cells, prior to seeding cells, coverslips were treated with poly-D Lysine for ≈20 minutes and washed 2× with PBS. HUVECs were fixed with 4% paraformaldehyde (PFA) for 7 min. ECs were then washed three times with PBS and permeabilized with 0.5% Triton-X (Sigma) for 10 min. After permeabilization, cells were washed three times with PBS. ECs were then blocked with 2% bovine serum albumin (BSA) for 30 min. Once blocked, primary antibodies were incubated for approximately 4–24 h. Thereafter, primary antibodies were removed, and the cells were washed 3 times with PBS. Secondary antibody with 2% BSA were added and incubated for approximately 1–2 h, washed 3 times with PBS, and mounted on a slide for imaging. All primary and secondary antibodies are listed in the Supplemental Data 3. All images were taken on a Nikon Eclipse Ti inverted microscope equipped with a CSU-X1 Yokogawa spinning disk field scanning confocal system and a Hamamatusu EM-CCD digital camera. Images were captured using a Nikon Plan Apo 60x NA 1.40 oil objective using Olympus type F immersion oil NA 1.518, Nikon Apo LWD 20× NA 0.95 or Nikon Apo LWD 40× NA 1.15 water objective. All images were processed using ImageJ (FIJI).

For imaging the fibrin-bead assay, first fibroblasts were removed from the clot with a 1-minute trypsin incubation. Following incubation, the trypsin was neutralized with DMEM contain 10% BSA, washed 3× with PBS, and fixed using 4% paraformaldehyde for 40 minutes. After fixation, the clot was washed 3× with PBS, permeabilized with 0.5% Triton-X for 2 hours and then blocked with 2% BSA for 1 hour before overnight incubation with primary antibodies. The following day, primary antibodies were removed

and the clot was washed 5× with PBS and secondary antibody was added with 2% BSA and incubated overnight. Before imaging, the clot was washed 5× with PBS. All primary and secondary antibodies are listed in the Data Supplement. Images were taken on a Nikon Eclipse Ti inverted microscope equipped with a CSU-X1 Yokogawa spinning disk field scanning confocal system and a Hamamatusu EM-CCD digital camera. Cell culture images were captured using a Nikon Plan Apo 60x NA 1.40 oil objective using Olympus type F immersion oil NA 1.518. All images were processed using ImageJ (FIJI).

Zebrafish Microangiography.

48 hpf embryos were (anesthetized) with 1X tricaine for approximately 20 min prior to perfusion. Embryos were then loaded ventral side up onto an injection agarose facing the injection needle. Qdots (ThermoFisher) were sonicated prior to injection. Qdots were loaded into a pulled capillary needle connected to an Eppendorf CellTram and 1–3 µl of perfusion solution was injected into the pericardial cavity. Once successfully perfused, embryos were embedded in 0.7% low melt agarose and imaged promptly. Images were taken on a Nikon Eclipse Ti inverted microscope equipped with a CSU-X1 Yokogawa spinning disk field scanning confocal system and a Hamamatusu EM-CCD digital camera using either Nikon Apo LWD 20× NA 0.95 or Nikon Apo LWD 40× NA 1.15 water objective.

Zebrafish Live Imaging and Quantification.

All zebrafish presented were imaged at 36 and 48hpf. Prior to imaging, embryos were treated with 1% Tricaine for 20 minutes and afterwards embedded in 0.7% low melt agarose. Live imaging of Zebrafish intersomic vessels (ISVs) was performed using a spinning-disk confocal microscopy system mentioned above. Zebrafish embryos were

quantified at 36hpf and 48hpf. ISVs that were analyzed were between the end of the yolk extension and tail. Parameters measured included ISV number, number non-lumenized vessels (no visible separation between opposing endothelial cells in vessels), number of ectopic vessels (extra vessels), and number of incomplete vessels (vessels that do not contact the dorsal longitudinal anastomotic vessel at 48 hpf). For the Rab35 investigation, number of actin accumulations (actin accumulations with a diameter greater than 4 μm).

Table 2 Major Resources

Reagent	Vendor	Catalog #
OPTI-MEM 1 Reduced Serum Medium, no phenol red	ThermoFisher	31985070
Polyethyleneamine Branched (PEI)	Sigma-Aldrich	408727
Chloroquine Diphosphate Crystalline (CQ)	Sigma-Aldrich	C6628-25G
Endothelial Cell Growth Medium 2	PromoCell	C-22011
DMEM, High Glucose, with L-Glutamine	Genesee Scientific	25-500
GenClone Fetal Bovine Serum (FBS)	Genesee Scientific	25-514
Penicillin-Streptomycin 100X Solution	Genesee Scientific	P4333-100ML
DPBS, no Calcium, no Magnesium	ThermoFisher	14190250
Trypsin-EDTA, o.25% 1X, phenol red	Genesee Scientific	25-510

Paraformaldahyde 20% Aqueous Sol. EM Grade	Electron Microscopy Sciences	15713
BSA Lyophilized Powder, Fraction V	Genesee Scientific	25-529
Cytoskeleton G actin/ F actin In Vivo Assay Kit	Cytoskeleton, Inc.	BK037-BK037
Culture-Insert 2 Well in μ-Dish 35	Ibidi	81176
Dimethyl Sulfoxide (DMSO)	Sigma-Aldrich	D2650-5X10ML
Cytodex Microcarrier Beads	Sigma-Aldrich	C3275-10G
Trimethoprim (TMP)	Sigma-Aldrich	T7883-5G
High Capacity Reverse Transcription Kit	ThermoFisher	4368814
Fibrinogen Type 1-S from Bovine Plasma	Sigma-Aldrich	F8630-1G
Thrombin from Bovine Plasma	Sigma-Aldrich	T7513-500UN
Aprotinin Protease Inhibitor	ThermoFisher	78432
Phenol-Red (Zebrafish Injection Mixture)	Avantor/ VWR	34487-61-1

CRIPSR gRNA	Integrated DNA Technologies (IDT)	
Alt-R® S.p. Cas9 Nuclease V3, 100 µg	Integrated DNA Technologies (IDT)	1081058
CellTracker Deep Red	ThermoFisher	M22426
3-Aminobenzoic Acid Ethyl Ester (Tricaine)	Sigma-Aldrich	A5040-25G
Latex Beads, Polystyrene Carboxylate Mod	Sigma-Aldrich	L3280-1ML
Dynabeads™ Protein G for Immunoprecipitation	ThermoFisher	10003D
MitoTracker DeepRed	ThermoFisher	M22426
Trizol Reagent	ThermoFisher	15596026
Chloroform	Sigma-Aldrich	288306
MEGAscript™ T3 Transcription Kit	ThermoFisher	AM1338
BCA Protein Assay Kit	ThermoFisher	23225
NHLF	Lonza	CC-2512
HEK 293-A	ThermoFisher	R70507
Microcarrier beads	Amersham	17-0485-01

Protease inhibitor cocktail	GoldBio	GB-334-20
Agarose Resin	GoldBio	G-250-G
Fura Red™, AM, cell permeant	ThermoFisher	F3020
Arf6 Pull-Down Activation Assay Biochem Kit	Cytoskeleton, Inc.	BK033
RhoA Pull-Down Activation Assay Biochem Kit	Cytoskeleton, Inc.	BK036
Rac1 Pull-Down Activation Assay Biochem Kit	Cytoskeleton, Inc.	BK035
Mem-PER™ Plus Membrane Protein Extraction Kit	ThermoFisher	89842

Table 3 Drugs

Name	Vendor or Source	Catalog No./ Clone	Working Concentration
Brefeldin-A	Sigma-Aldrich	B7651-5MG	1 ug/mL
Phorbol12-myristate13-acetate (PMA)	Sigma-Aldrich	P1585	100 ng/mL
BAY-826	R&D	6579/5	1.3 nmol/L
Histamine Free Base Crystalline	Sigma-Aldrich	H7125-1G	100 µmol/L
NP-G2-044	Selleck Chem	S2962	1 uM
CN02	Cytoskeleton, Inc.	CN02-A	100ng/mL
CN03	Cytoskeleton, Inc.	CN03-A	1ug/mL
NSC	Sigma-Aldrich	SML0952-5MG	50 uM
Y-27632	Sigma-Aldrich	688001-500UG	10 uM
CK-666	Sigma-Aldrich	SML0006-5MG	1uM

Table 4 Antibodies

Target Antigen	Vendor or Source	Catalog No./ Clone	Working Concentration
Rab8	Proteintech	55296-1-AP	1:500 (WB)
GM130	Abcam	Ab52649	1:1000 (IHC)
VEGFR2	R&D	AF357	1:500 (WB)
h-TIE-2	R&D	AF313	1:500 (WB)
Slp2a	ThermoFisher	PA524730	1:500 (WB)
Slp4a	ThermoFisher	PA5-51605	1:500 (WB)
Rab27a	ThermoFisher	PA5-51561	1:500 (WB)
Ang2	R&D	AF623	1:200 (WB)
Rab35	ThermoFisher	PA531674	1:500 (WB)
ACAP2	ThermoFisher	PA557069	1:500 (WB)
OCRL	ThermoFisher	PA527844	1:200 (WB)
MICAL-L1	ThermoFisher	PA5107177	1:200 (WB)
RUSC2	ThermoFisher	PA572752	1:200 (WB)
Arf6	Santa Cruz	sc-7971	1:200 (WB)
Myc-tag	ThermoFisher	132500	1:1000 (IHC)
HA-tag	ThermoFisher	26183	1:1000 (IHC)

cyan	Bio-Rad	AHP2986	1:1000 (IHC)
Alpha-tubulin	Abcam	ab52866	0.0648ug/mL (1:10,000) (WB)
GAPDH	ThermoFisher	PA1988	1:1000 (WB)
Moesin	Abcam	ab52490	0.05ug/mL (1:1000) (IHC)
VE-Cadherin	ThermoFisher	14-1441-82	0.5ug/mL (1:1000) (IHC)
Podocalyxin	R&D	AF1658	15ug/mL (1:200) (WB & IHC)
Von Willebrand Factor	Abcam	ab6994	10ug/mL (1:1000) (IHC)
β-Integrin	Abcam	ab30394	1:500 (IHC)
MICAL-1	ThermoFisher	14818-1-AP	1:500 (WB)
Phosphorylated TIE-2/TEK (Tyr992)	Sigma Aldrich	ABF131	0.25 ug/mL (1:500) (IHC)
Anti-HA-Tag, Rabbit Monoclonal	Sigma-Aldrich	SAB5600116-100UG	5ug/mL
Alexa Fluor™ 488 Phalloidin	ThermoFisher	A12379	1 uM (1:200)

Alexa Fluor™ 647 Phalloidin	ThermoFisher	A22287	1 uM (1:200)
Alexa Fluor™ 555 Phalloidin	ThermoFisher	A34055	1 uM (1:200)
Goat anti-Rabbit IgG (H+L) Secondary Antibody, Alexa Fluor 488	ThermoFisher	A11008	1ug/mL (1:500)
Donkey anti-Rabbit IgG (H+L) Secondary Antibody, Alexa Fluor 555	ThermoFisher	A31572	1ug/mL (1:500)
Donkey anti-goat IgG (H+L) Secondary Antibody, Alexa Flour 488	ThermoFisher	A11055	1ug/mL (1:500)
Donkey anti-Goat IgG (H+L) Cross-Adsorbed	ThermoFisher	A21432	1ug/mL (1:500)

Secondary Antibody, Alexa Fluor 555			
Chicken anti-Rabbit IgG (H+L) Cross-Adsorbed Secondary Antibody, Alexa Fluor 647	ThermoFisher	A21443	1ug/mL (1:500)
Goat Anti-Rabbit HRP	Genesee Scientific	20-303	1ug/mL (1:500)

Table 5 siRNA

siRNA Target	Vendor	ID #
Silencer™ Negative Control No. 1 siRNA	ThermoFisher	AM4611
Rab8	ThermoFisher	siRNA ID: s8681
Slp2a	ThermoFisher	siRNA ID: s224321
Slp4a	ThermoFisher	siRNA ID: s230068
Ang2	ThermoFisher	siRNA ID: s1361
Rab27a	ThermoFisher	siRNA ID: s11695
Rab35	ThermoFisher	siRNA ID: s21709
ACAP2	ThermoFisher	siRNA ID: s24011
OCRL	ThermoFisher	siRNA ID: s9819
MICAL-L1	ThermoFisher	siRNA ID: s39940
RUSC2	ThermoFisher	siRNA ID: s19070
Podxl	ThermoFisher	siRNA ID: s10771
DENNd1a	ThermoFisher	siRNA ID: s33637
DENNd1b	ThermoFisher	siRNA ID: s29140
DENNd1c	ThermoFisher	siRNA ID: s36719
MICAL-1	ThermoFisher	siRNA ID: s230028

Arf6	ThermoFisher	siRNA ID: s1565

Table 6 Plasmids

Name	Vendor or Source	Catalog No.
EGFP-Rab8a-TN	Addgene	86077
EGFP-Rab8a-QL	Addgene	86076
EGFP-Rab8a-WT	Addgene	86075
EGFP-Rab6A		49469
RAB3D (NM_004283) Human Tagged ORF Clone	Origene	RC202236
pmCherry-C1 hSlp2-a	Addgene	40056
pEGFP-C1 hSlp4-a	Addgene	40032
GFP-C1-PLCdelta-PH	Addgene	21179
pEGFP-C1 hSlp2-a C2AB	Addgene	40051
GFP-Rab27A	Addgene	89237
Angpt2 (NM_007426) Human Tagged ORF Clone	Origene	MR207970
GFP-Rab35 WT	Addgene	47426
GFP_Rab35 Q67L active	Addgene	47425

GFP-Rab35 S22N inactive	Addgene	47426
pARF6-CFP	Addgene	11382
pARF6(T27N)-CFP	Addgene	11386
pARF6(Q67L)-CFP	Addgene	11387
pcDNA3-HA-human OCRL	Addgene	22207
mEmerald-Fascin-C-10	Addgene	54094
mEmerald-ARP2-C-14	Addgene	53992
mCherry-ARP2-N-14	Addgene	54980
pCDNA3.0_mitoLAMA-G97	Addgene	130705
pEGFP-RhoA Biosensor	Addgene	68026
MICALL1 (GFP-tagged) - Human MICAL-like 1 (MICALL1)	Origene	RG214051
DENND1C (NM_024898) Human Tagged ORF Clone	Origene	RC206410
mTagRFP-T-Clathrin-15	Addgene	58005

Table 7 Oligo's and sgRNA

Name	Sequence	Function
Slp2a crRNA	TCCTGGAAGTGTTGAAAAGA	sgRNA Target
Slp2b crRNA	AGACACAACCCGTTCAACAG	sgRNA Target
Slp2a_seqF	CAGCCTTCAAATTGCCCACAGTGA	Sequencing Primer
Slp2a_seqR	TCGTCTGACTTCTTCAGCTCTGC	Sequencing Primer
Slp2b_seqF	GTTCGGGATCACCTTGTTGATGTGAG	Sequencing Primer
Slp2b_seqR	CAGAGCCCCTGTCTAAAGATTTCCTG	Sequencing Primer
Rab35a crRNA	CCATCGGTGTGGACTTCAAG	sgRNA Target
Rab35b crRNA	CTATAGGAGTCGACTTCAAG	sgRNA Target
Rab35a_seqF	GCCAATCAGATTCGAGATCCAGAC	Sequencing Primer
Rab35a_seqR	CACTCACGTGGAGGTGATTGTCCTG	Sequencing Primer
Rab35b_seqF	CACGCATAGTTCAATGGTGTGTG	Sequencing Primer
Rab35b_seqR	GCACACCCCTATCATGACACTACTC	Sequencing Primer
Rab8a crRNA	ACAACATCAAGAACTGGATC	sgRNA Target
Rab8b crRNA	ATGAGAAGTCATTTGACAAC	sgRNA Target

Appendix B: Chapter 2 Supplemental Figures

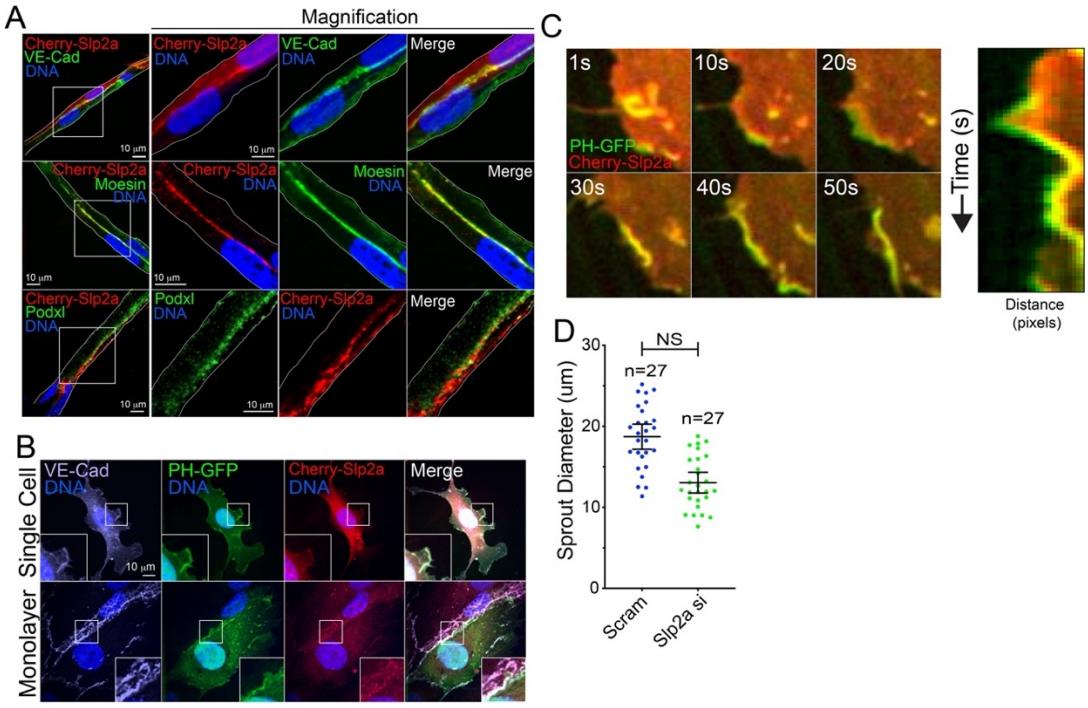

Supplemental Figure 1: Slp2a localizes with PI(4,5)P2 at junctions. A, Sprouts expressing mCherry(Cherry)-tagged Slp2a fixed prior to lumen development and stained for VE-Cadherin (VE-cad), moesin, and podocalyxin (Podxl). B, Cells transduced with PH-GFP (PIP2 biosensor) and Cherry-Slp2a and stained as indicated. C, Live imaging of Cherry-Slp2a co-transduced with PH-GFP. Time points are shown in 10 second intervals with kymograph on right. D, Sprout diameter (um) of scramble (scram) and Slp2a siRNA(si) treated HUVECs. N-value represents individual sprouts over three experimental repeats. All experiments use human umbilical vein endothelial cells. In all panels L denotes lumen; white box denotes magnification; white lines denote exterior of sprout. NS= not significant, values are means +/- SEM; N= individual sprouts; significance: Statistical significance was assessed with unpaired t-test. All experiments were performed in triplicate.

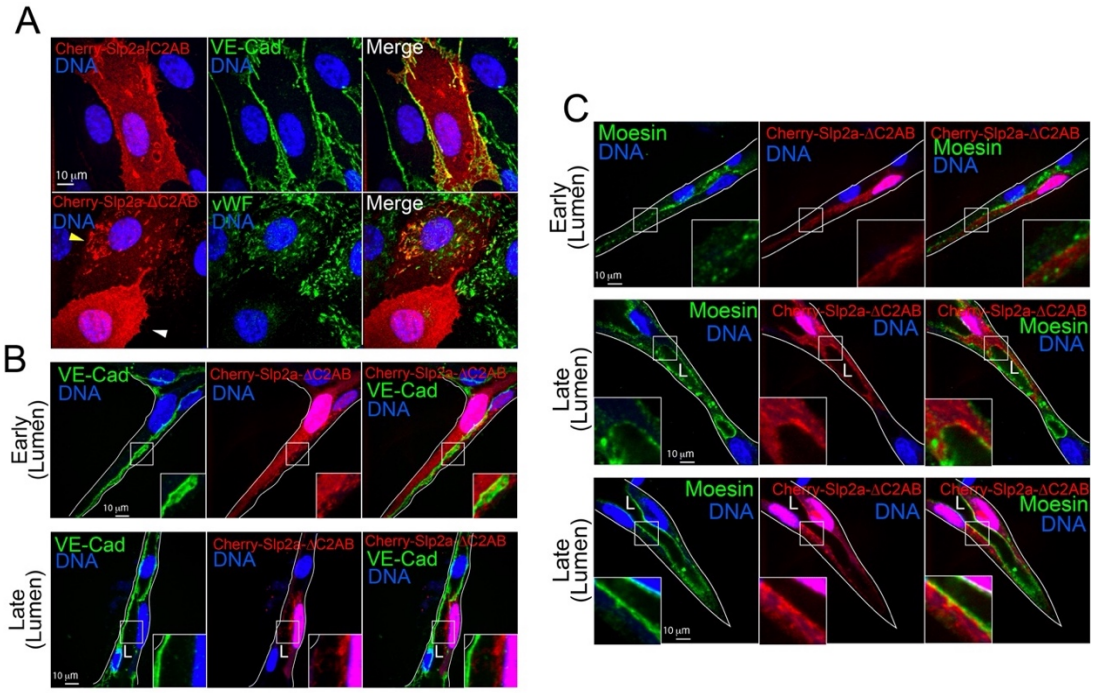

Supplemental Figure 2: Slp2a-ΔC2AB Localization throughout lumen formation. A, Cells expressing mCherry(Cherry)-Slp2a-C2AB (top row) and stained for VE-Cadherin (VE-Cad). Bottom row, cells expressing Cherry-Slp2a-ΔC2AB and stained for von-Willebrand factor (vWF). Yellow arrow indicates cherry-Slp2a-ΔC2AB localization in cell expressing vWF and white arrow indicates cherry-Slp2a-ΔC2AB localization in cell lacking vWF expression. B, Cherry-Slp2a- ΔC2AB transduced sprouts fixed at early and late stages of lumen formation and stained for VE- Cad. C, Cherry-Slp2a-ΔC2AB expressing sprouts fixed at early and late stages of lumen formation. Sprouts were probed for moesin to highlight lumen cavity. White box denotes magnification. All experiments were performed in triplicate.

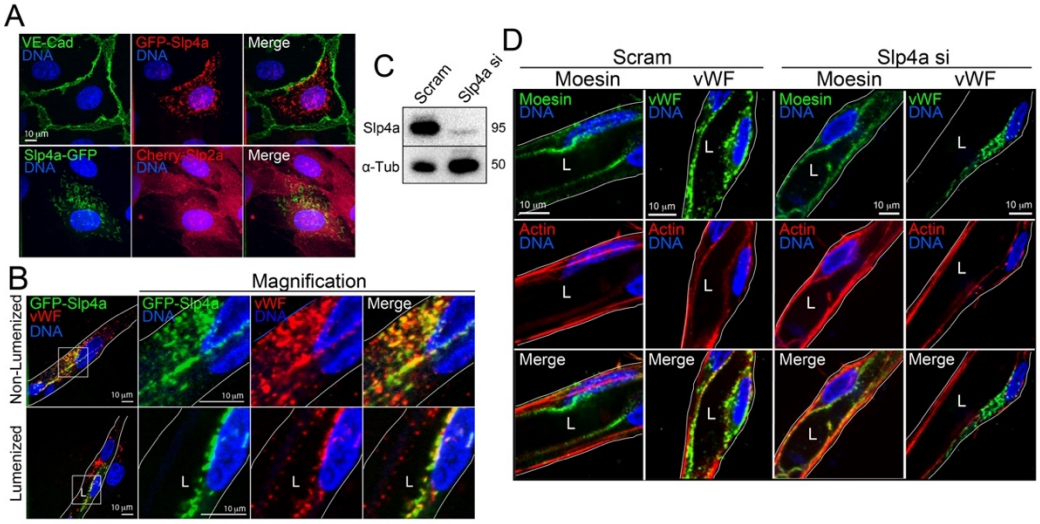

Supplemental Figure 3: Slp2a, but not Slp4a, influences lumen development. A, Cells expressing GFP-Slp4a, mCherry(Cherr)-Slp2a, and stained for VE-Cadherin (VE-Cad). B, Sprouts expressing GFP-Slp4a and stained as indicated fixed before (non-lumenized) and after (lumenized) lumen formation. C, Representative western blot confirmation of Slp4a siRNA(si) knockdown. D, Images of Slp4a knockdown sprouts stained as indicated. All experiments use human umbilical vein endothelial cells. In all panels L denotes lumen; white box denotes magnification; white lines denote exterior of sprout. All experiments were performed in triplicate.

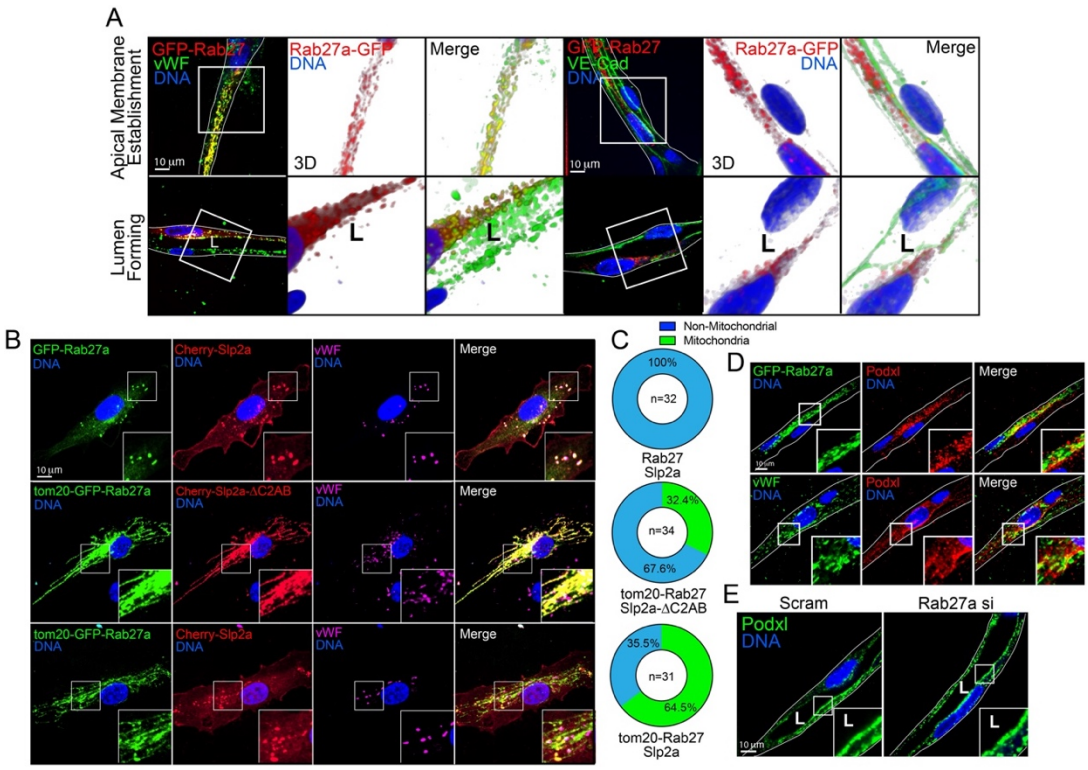

Supplemental Figure 4: Rab27a localizes to WPBs and does not influence lumen formation. A, Sprouts expressing GFP-Rab27a and stained for VE-cadherin (VE-cad) and von Willebrand factor (vWF). Images were reconstructed in 3D. B, Three different scenarios for vWF localization endogenously and at the mitochondria. Top row, GFP-Rab27a co-expressed with Cherry-slp2a in cells stained for vWF. Middle row, tom20-GFP-Rab27a coexpressed with Cherry- Slp2a-ΔC2AB stained for vWF. Bottom row, tom20-GFP-Rab27a coexpressed with Cherry-Slp2a showing vWF colocalization at the mitochondria. C, Quantification of vWF localization at the mitochondria. n= individual cells across three experimental repeats. D, Localization of podocalyxin (Podxl) in sprouts relative to GFP-Rab27a and vWF. E, Scramble (scram) vs Rab27a siRNA (si)-treated sprouts stained for Podxl. All experiments use human umbilical vein endothelial cells. In all panels L denotes lumen; white box denotes magnification; white lines denote exterior of sprout. All experiments were performed in triplicate.

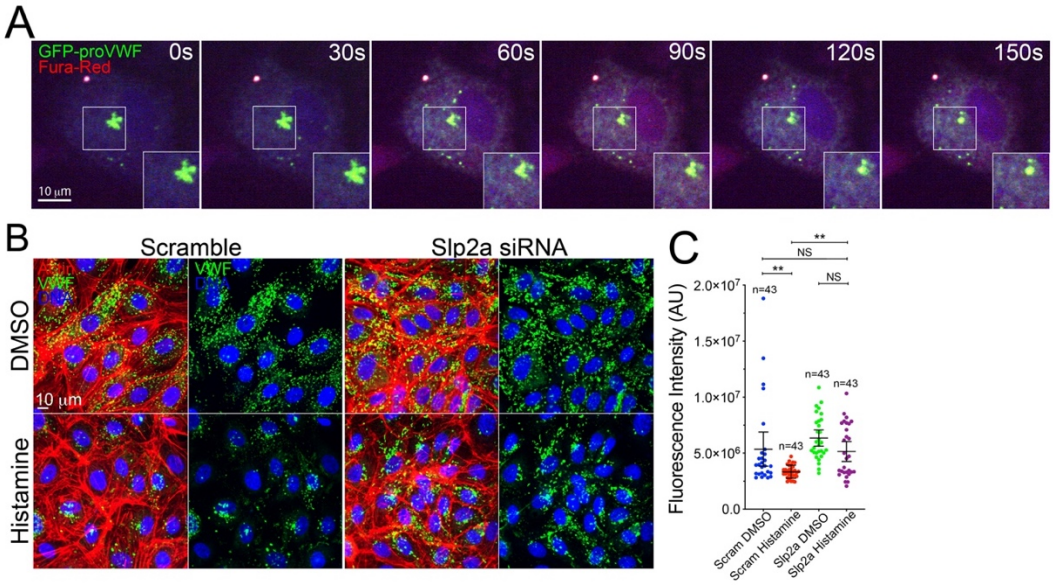

Supplemental Figure 5: Slp2a is required for vWF secretion. A, Optimization experiment for histamine induced secretion. Fura-red indicator for calcium influx beginning at 0 seconds (histamine addition) to 150 seconds. Cell expressing GFP-pro-vWF to visualize secretion over time. B, Images of histamine and vehicle (DMSO)-treated cells between indicated groups. C, Quantification of vWF fluorescent intensity between indicated conditions. n= individual cells across three experimental repeats. White box denotes magnification; NS= not significant, values are means +/- SEM; n= individual sprouts; significance: **P<0.01, NS=Not Significant. Statistical significance was assessed with 1-way ANOVA followed by a Dunnett multiple comparisons test. All experiments were performed in triplicate.

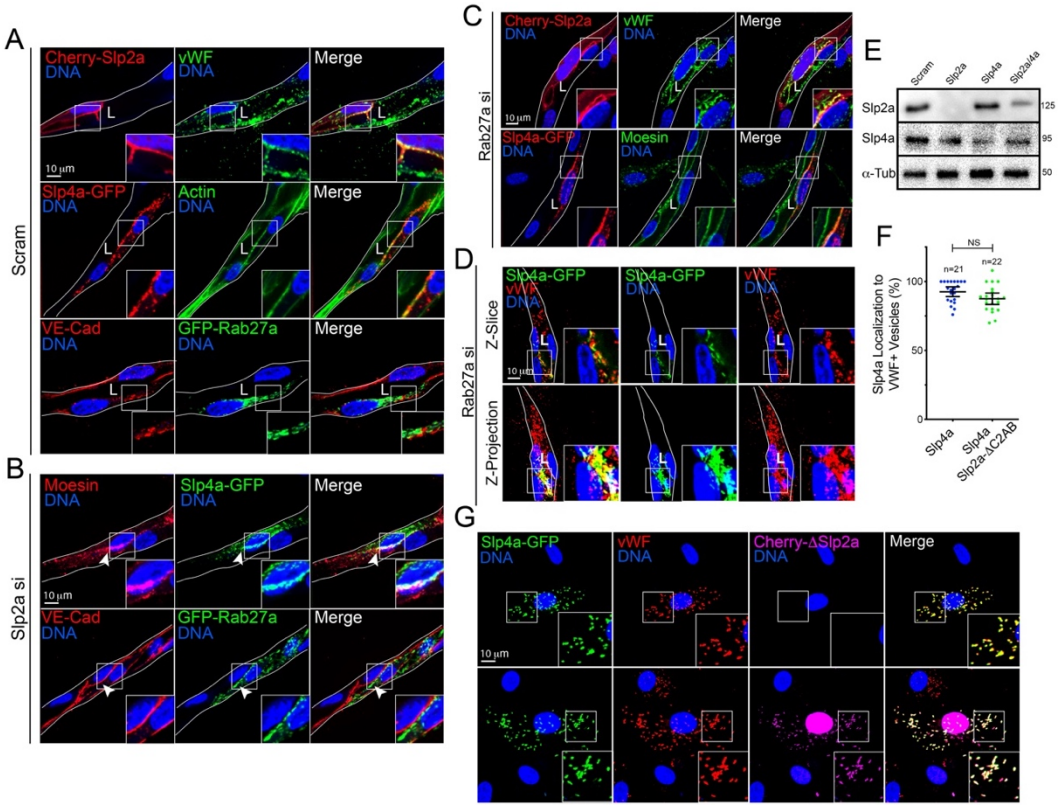

Supplemental Figure 6: Slp2a and Rab27a do not affect each other's localization during lumen formation. A, Scramble (scram) siRNA(si) knockdown sprouts showing localization of mCherry(Cherry)-Slp2a, GFP-Slp4a, and GFP-Rab27a. Sprouts were stained for von-Willebrand factor (vWF), actin and VE-cadherin (VE-cad). B, Slp2a siRNA knockdown sprouts expressing GFP-Slp4a and GFP-Rab27a probed for moesin and VE-cadherin. Arrowheads indicate a lack of lumen. C, Rab27a siRNA knockdown sprouts expressing mCherry-Slp2a and Slp4a-GFP stained for vWF and moesin. D, Rab27a siRNA knockdown sprouts expressing GFP-Slp4a and stained for vWF. The top row shows a single z-slice of the sprout and the bottom row shows a z-projection. E, Western blot confirmation of effects of Slp2a siRNA treatment on Slp4a expression as well as the reciprocal, Slp4a siRNA effects on Slp2a expression. n=3. F, Quantification of Slp4a localization intensity to vWF-positive vesicles with and without Cherry-Slp2a-ΔC2AB coexpression in sprouts. n= number of individual cells located in sprouts over three experimental repeats. G, Localization of Slp4a to vWF-positive vesicles with and without expression of cherry- Slp2a-ΔC2AB. In all panels L denotes lumen; white box denotes magnification; white lines denote exterior of sprout, NS denotes Not-Significant. NS= not significant, values are means +/- SEM; significance: Statistical significance was assessed with unpaired t-test.

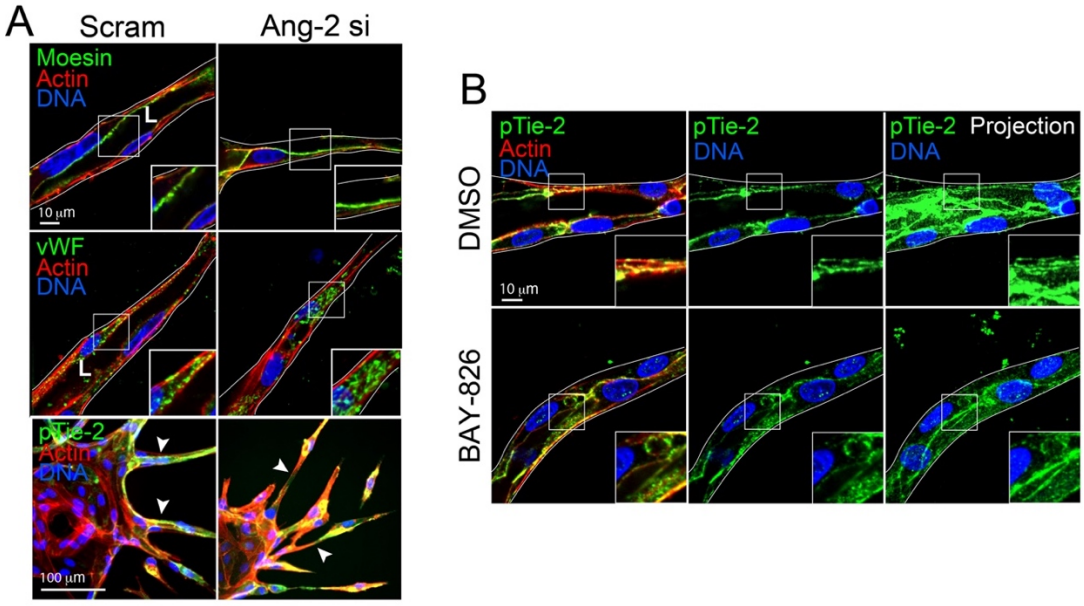

Supplemental Figure 7: Ang-2 and Tie-2 inhibition promotes lumen defects. A, Scramble (scram) control and angiopoietin-2 (Ang-2) siRNA (si) knockdown sprouts stained for moesin, von Willebrand factor (vWF) and phosphorylated Tie-2 (pTie2). B, DMSO and BAY-826 (Tie-2 small molecule inhibitor) treated sprouts. Projections show level of pTie-2 staining compared with DMSO control. All experiments use human umbilical vein endothelial cells. In all panels L denotes lumen; white box denotes magnification; white lines denote exterior of sprout. All experiments were performed in triplicate.

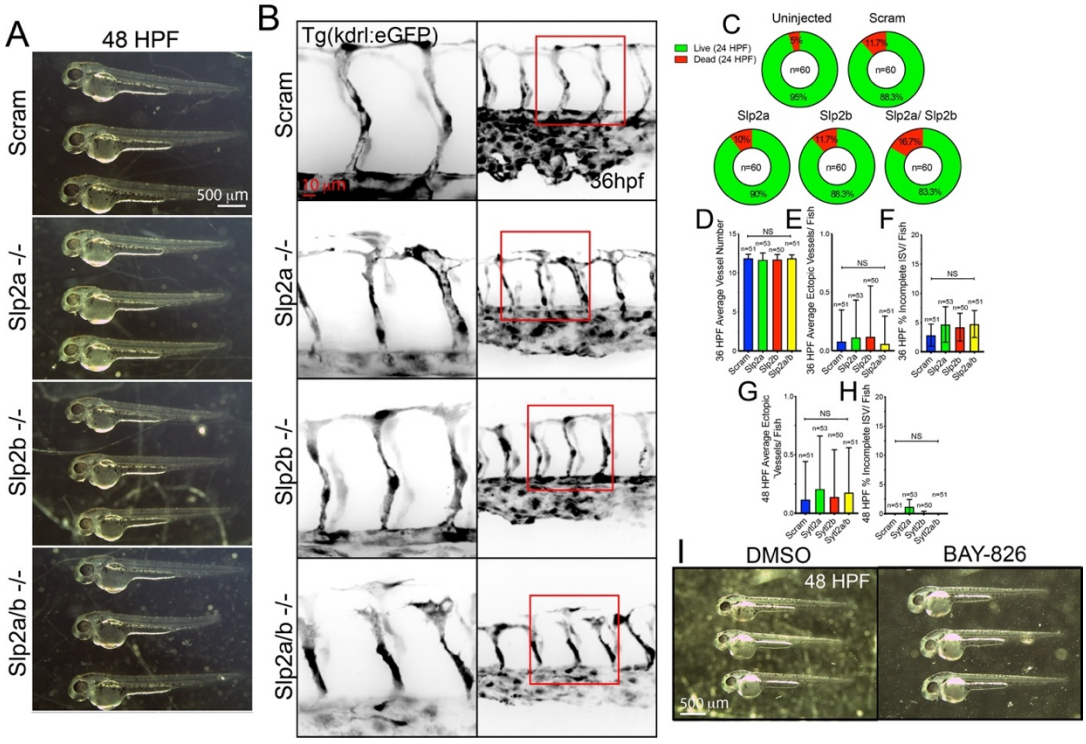

Supplemental Figure 8: Slp2a/b KO zebrafish defects at 36 hpf and whole embryo morphology. A, Whole embryo morphology at 48 hours post fertilization (hpf) for indicated conditions. B, 36 hpf zebrafish intersomitic vessels (ISVs) for indicated conditions. Red boxes are area of higher magnification. C, Injection death rate at 24 hpf. n= number of fish D, Quantification of intersomitic vessel (ISVs) number at 36 hpf. n= number of ISVs. E, Quantification of number ectopic vessels per fish at 36 hpf. n= number of ISVs. F, Quantification of percent incomplete ISVs per fish at 36 hpf. n= number of ISVs. G, Quantification of ectopic vessels per fish at 48 hpf. H, Quantification of percent incomplete ISVs per fish at 48 hpf. n= number of ISVs. I, Representative image of 48 hpf larvae treated with DMSO (vehicle) or Tie-2 inhibitor Bay-826. NS= not significant, values are means +/- SEM; significance: NS=Not Significant. Statistical significance was assessed with 1-way ANOVA followed by a Dunnett multiple comparisons test. All experiments were performed in triplicate.

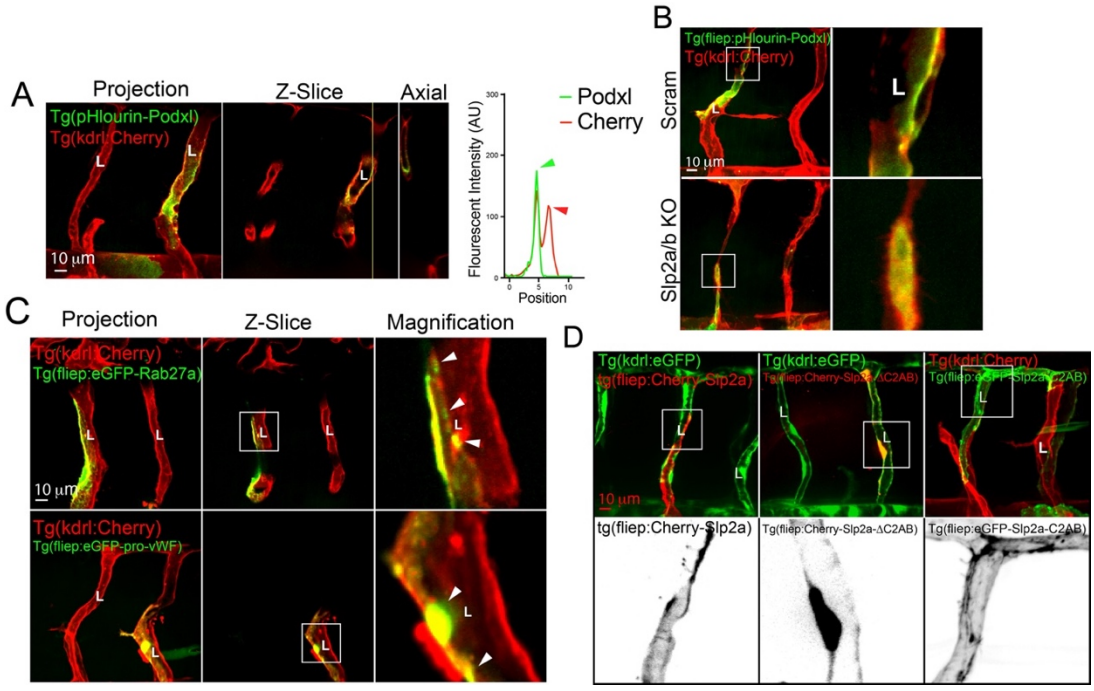

Supplemental Figure 9: Visualization of lumen defects caused by Slp2a/b KO and localization of vWF, Rab27a and Slp2a. A, PHluorin-podocalyxin (Podxl) expression marking apical membrane in zebrafish intersomitc vessels (ISVs) on indicated background. Line scan depicts peaks in fluorescent intensity at the apical membrane. Green is apically localized pHluorin and red is endothelial mCherry (Cherry). B, PHlourin-Podxl localization between indicated scrambled (scram) and Slp2a/b CRISPR knockouts (KO). C, Mosaic expression of Human eGFP- Rab27a and pro-von Willebrand factor (vWF) in zebrafish ISVs. Arrowhead denote puncta. D, Zebrafish ISVs expressing Human mCherry(Cherry)-Slp2a, Cherry-Slp2a-ΔC2AB and Cherry- Slp2a-C2AB on a tg(kdrl:GFP) background. All zebrafish are at 48 hours post fertilization. In all panels L denotes lumen; white box denotes magnification.

Appendix C: Chapter 3 Supplemental Figures

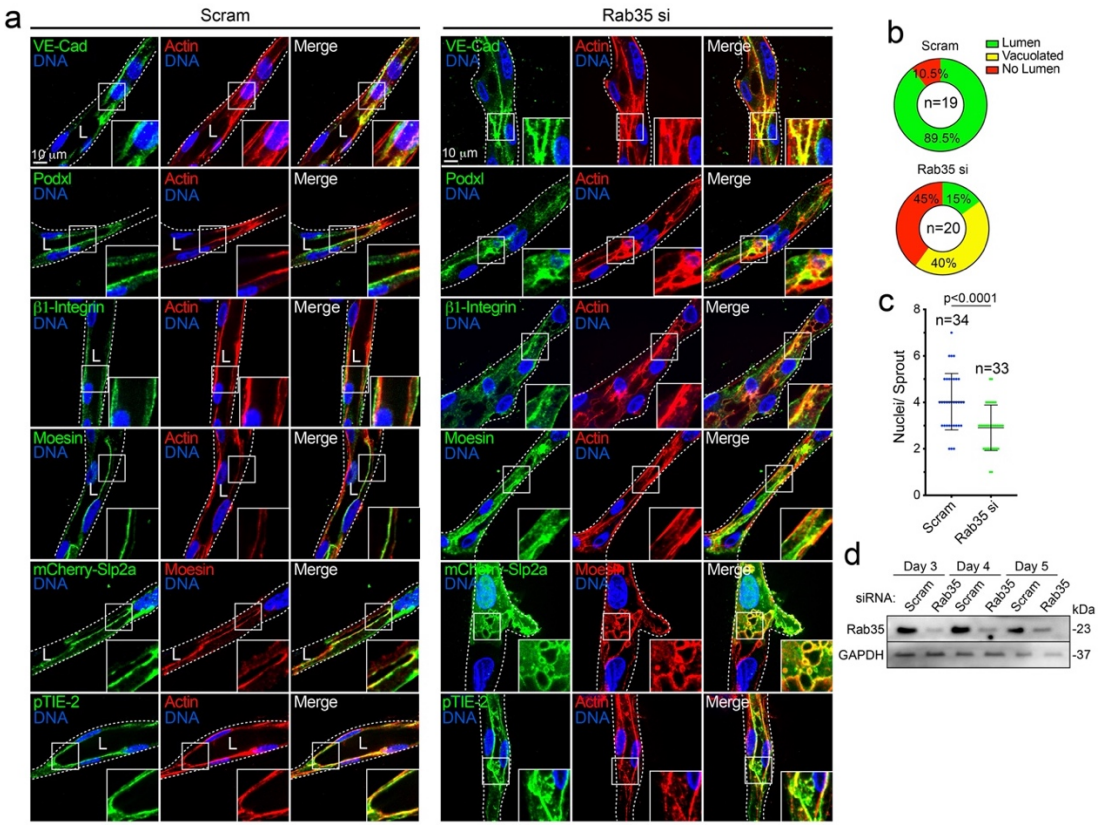

Supplemental Figure 10: Knockdown of Rab35 distorts cell apicobasal polarity. (A) Scramble (Scram) and Rab35 siRNA(si)-treated sprouts stained for VE-cadherin (VE-cad), podocalyxin (Podxl), β1-integrin, moesin or phosphorylated Tie2 (pTie2) apical and basal protein markers. Apical marker synaptotagmin-like protein 2a (mCherry-Slp2a) was transduced into sprouts. L denotes lumen and white dotted lines outline sprout exterior. (B) Quantification of lumen formation in Scram and Rab35 siRNA-treated sprouts. Lumens were defined as an open continuous cavity. Vacuolated sprouts were defined as sprouts lacking a contiguous lumen, while exhibiting an excess of large vacuoles. The no lumen group was defined as sprouts that had no visible cavity or vacuoles. n=number of sprouts. (C) Quantification of nuclei per sprout in Scram and Rab35 siRNA treated sprouts. n=number of sprouts. Error bars represent standard deviation, middle bars are the mean. (D) Western blot of Rab35 knockdown (KD) cells lysed 3 days, 4 days, and 5 days post siRNA treatment. Statistical significance was assessed with an unpaired t-test or a 1-

way ANOVA followed by a Dunnett multiple comparisons test. Insets are areas of higher magnification. All experiments were done using human umbilical vein endothelial cells in triplicate.

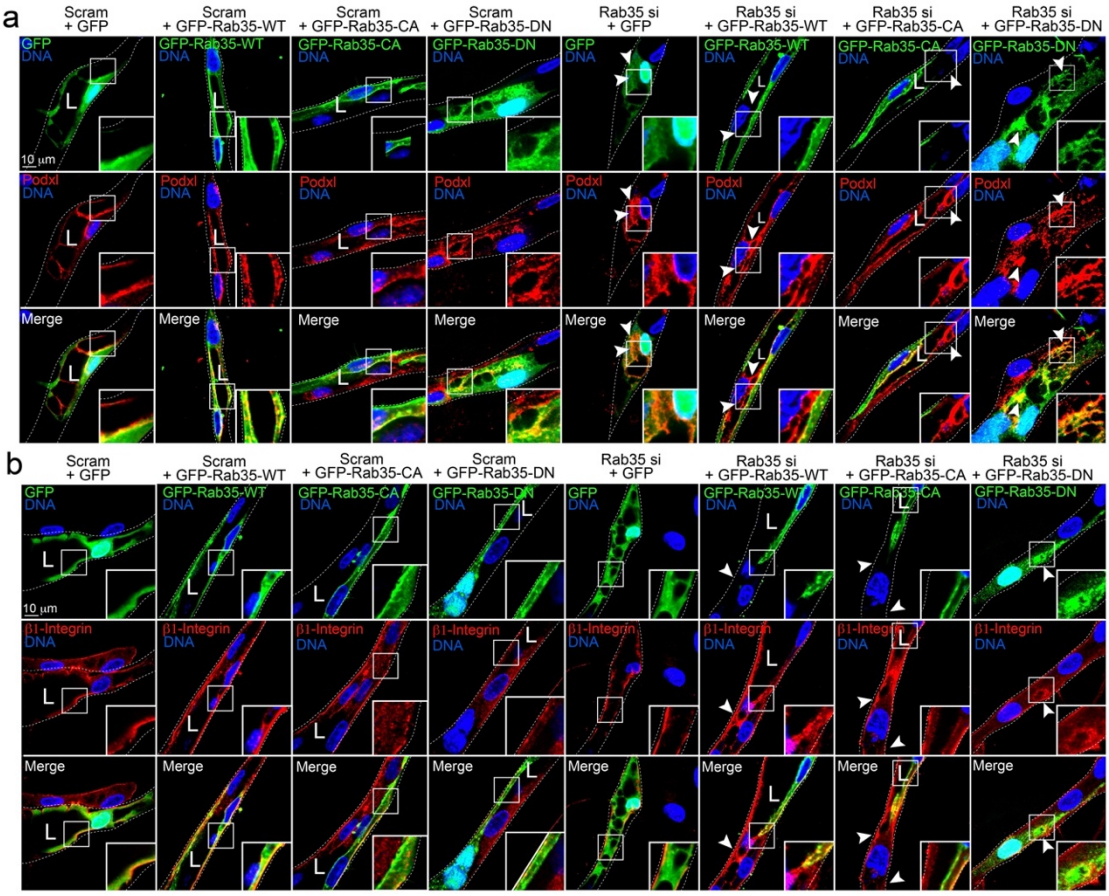

Supplemental Figure 11: Rab35 knockdown disrupts sprout polarity programs. (A,B) Representative images of Scram and Rab35 siRNA (si) knockdown (KD) sprouts transfected with GFP or GFP-Rab35 wild-type (WT), constitutively-active (CA) or dominant-negative (DN) for rescues. Sprouts were also stained for apical marker podocalyxin (Podxl) or basal marker β1- integrin. Arrowheads denote abnormal localization of podocalyxin or β1-integrin. L denotes lumen in all images. White dotted lines mark sprout exterior. Insets are areas of higher magnification. All experiments were done using human umbilical vein endothelial cells in triplicate.

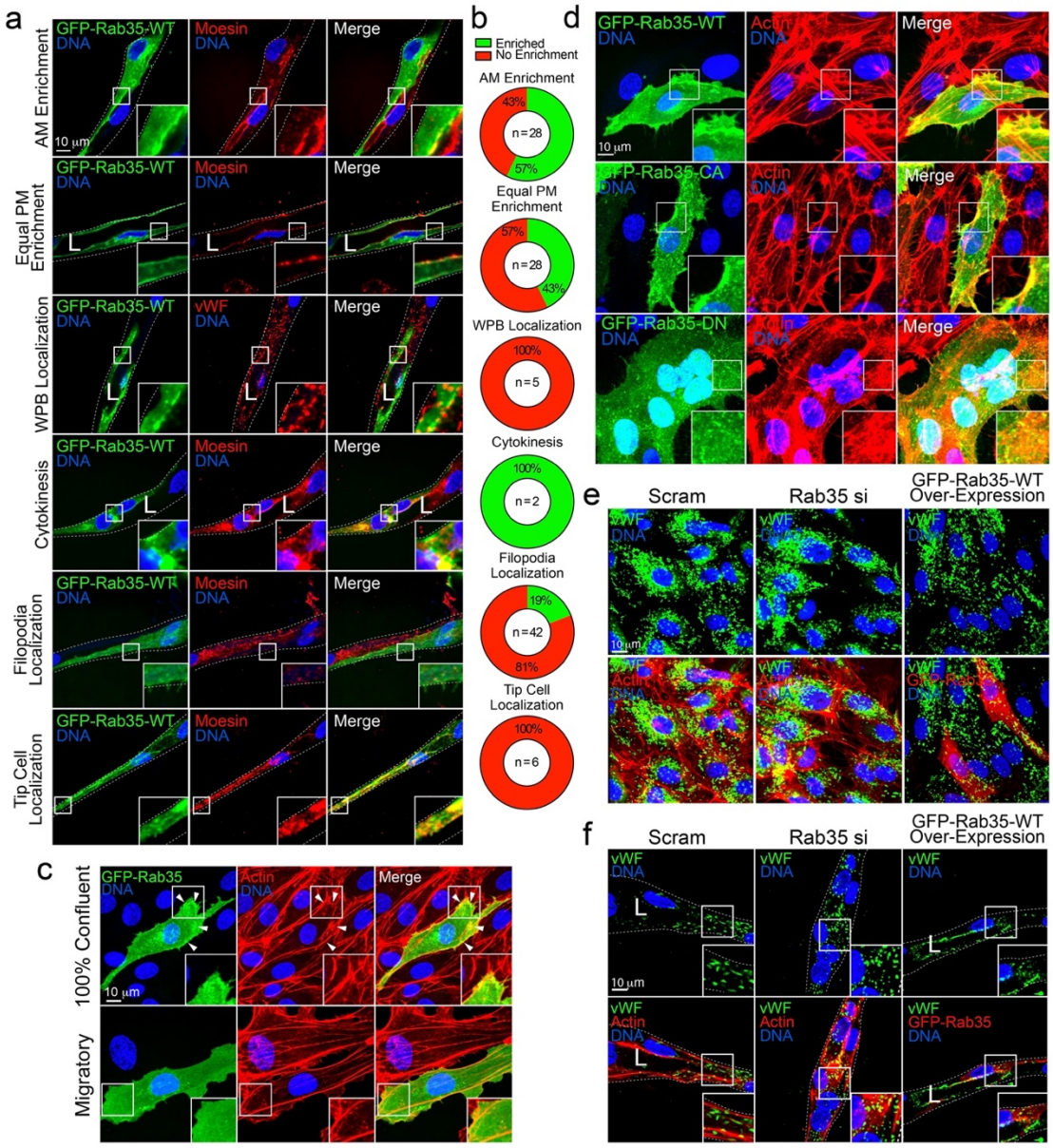

Supplemental Figure 12: Rab35 localizes to the plasma membrane and not to Weibel-Palade Bodies. (A) Representative images of GFP-Rab35-wild-type (WT) localization binned by its proximity to the apical plasma membrane (AM), equal enrichment at the basal and apical plasma membrane (equal plasma membrane (PM) enrichment), Weibel-Palade bodies (WPBs), at sites of cytokinesis, filopodia, and most distal cell in the sprout (tip cell). Sprouts were stained for moesin to mark the apical membrane. (B) Quantification of GFP-Rab35-WT enrichment with respect to the described conditions in panel A. (C) Representative images of GFP-Rab35 localization in 2-dimensional culture stain for actin. The top panels are of a confluent monolayer and the bottom panels are of migratory sub-confluent cells. Arrowheads indicate colocalization of actin and GFP-Rab35. (D) Representative images of 2-dimensional localization of GFP-Rab35- WT (top

panels), constitutively-active (CA, middle panels), and dominant-negative (DN, bottom panels) stained for actin. (E) Representative images of cells treated with scramble (Scram) or Rab35 siRNA (si) and stained for WPB marker von Willebrand Factor (vWF) and actin or overexpressing GFP-Rab35-WT. (F) Representative images of sprouts treated with Scram or Rab35 siRNA stained for vWF and actin or expressing GFP-Rab35-WT in sprouts. Insets are areas of higher magnification. White dotted lines mark sprout exterior. All experiments were done using human umbilical vein endothelial cells in triplicate.

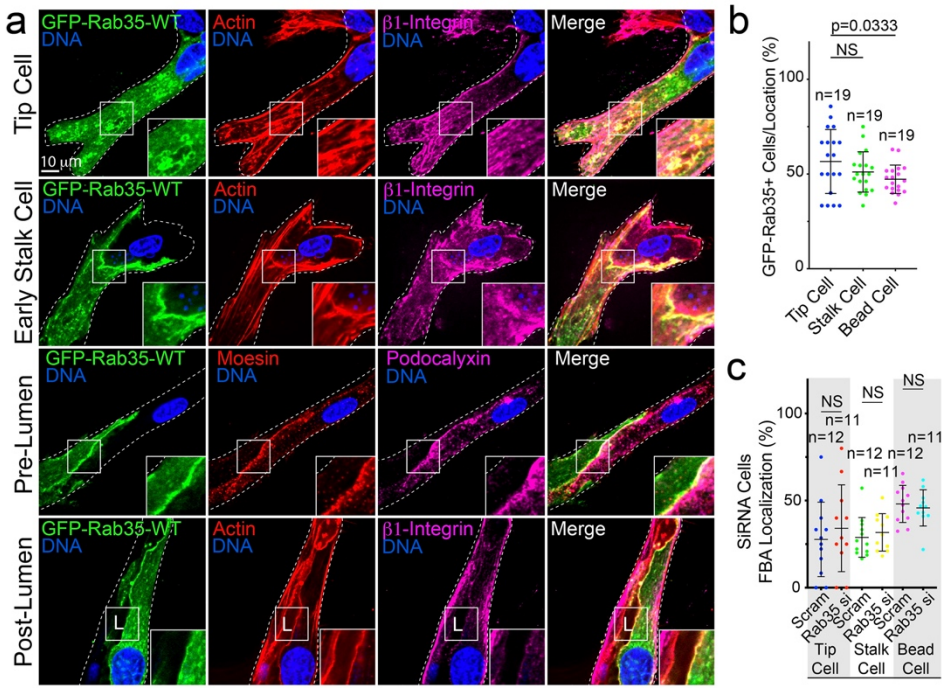

Supplemental Figure 13: Rab35 knockdown does not distort cell positioning in sprouts. (A) Representative image of GFP-Rab35-wild-type (WT) expression in the described sprout locations. (B) Quantification of GFP-Rab35-WT mosaic expression in the described sprout locations. n=number of cells. Error bars represent standard deviation, middle bars are the mean. (C) Quantification of siRNA (si)-treated cells marked with cell tracker binned by sprout location. n=number of cells. Error bars represent standard deviation, middle bars are the mean. NS=non- significant. Statistical significance was assessed with an unpaired t-test or a 1-way ANOVA followed by a Dunnett multiple comparisons test. Insets are areas of higher magnification. All experiments were done using human umbilical vein endothelial cells in triplicate.

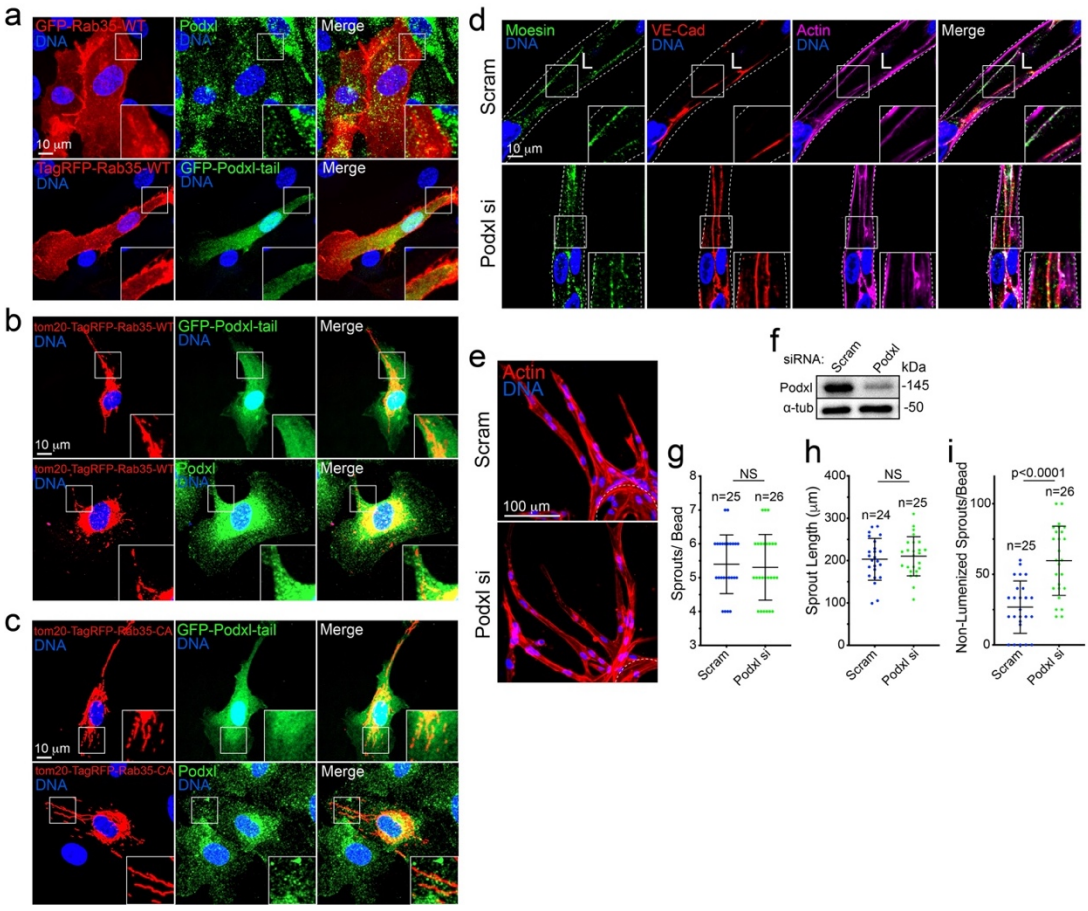

Supplemental Figure 14: Rab35 does not affect podocalyxin trafficking. (A) Two-dimensional localization of GFP-Rab35-wild-type (WT) stained for podocalyxin (Podxl) (top panels) or expressing of GFP-Podxl-tail (bottom panels). (B). Top panels- cell co-expressing tom20- TagRFP-Rab35-WT with GFP-Podxl-tail. Bottom panels- cell expressing tom20-TagRFP-Rab35- WT stained for endogenous podocalyxin. (C) Representative image of a cell co-expressing tom20-TagRFP-Rab35-constitutively active (CA) mutant with GFP-Podxl-tail. Bottom panels show a cell expressing tom20-tagRFP-Rab35-CA mutant stained for endogenous podocalyxin. (D) Representative image of sprouts treated with scramble (Scram) or podocalyxin siRNA (si) and stained for moesin, VE-cadherin (VE-cad) and actin. L denotes lumen. White dotted lines mark sprout exterior. (E) Sprout morphology for the same conditions as D. (F) Confirmation of siRNA- mediated knockdown by western blot. (G-I) Quantification of indicated sprouting parameters across groups. n=number of sprouts. Error bars represent standard deviation, middle bars are the mean. NS=non-significant. Statistical significance was assessed with an unpaired t-test or a 1- way ANOVA followed by a Dunnett multiple comparisons test. Insets are areas of higher magnification. All experiments were done using human umbilical vein endothelial cells in triplicate.

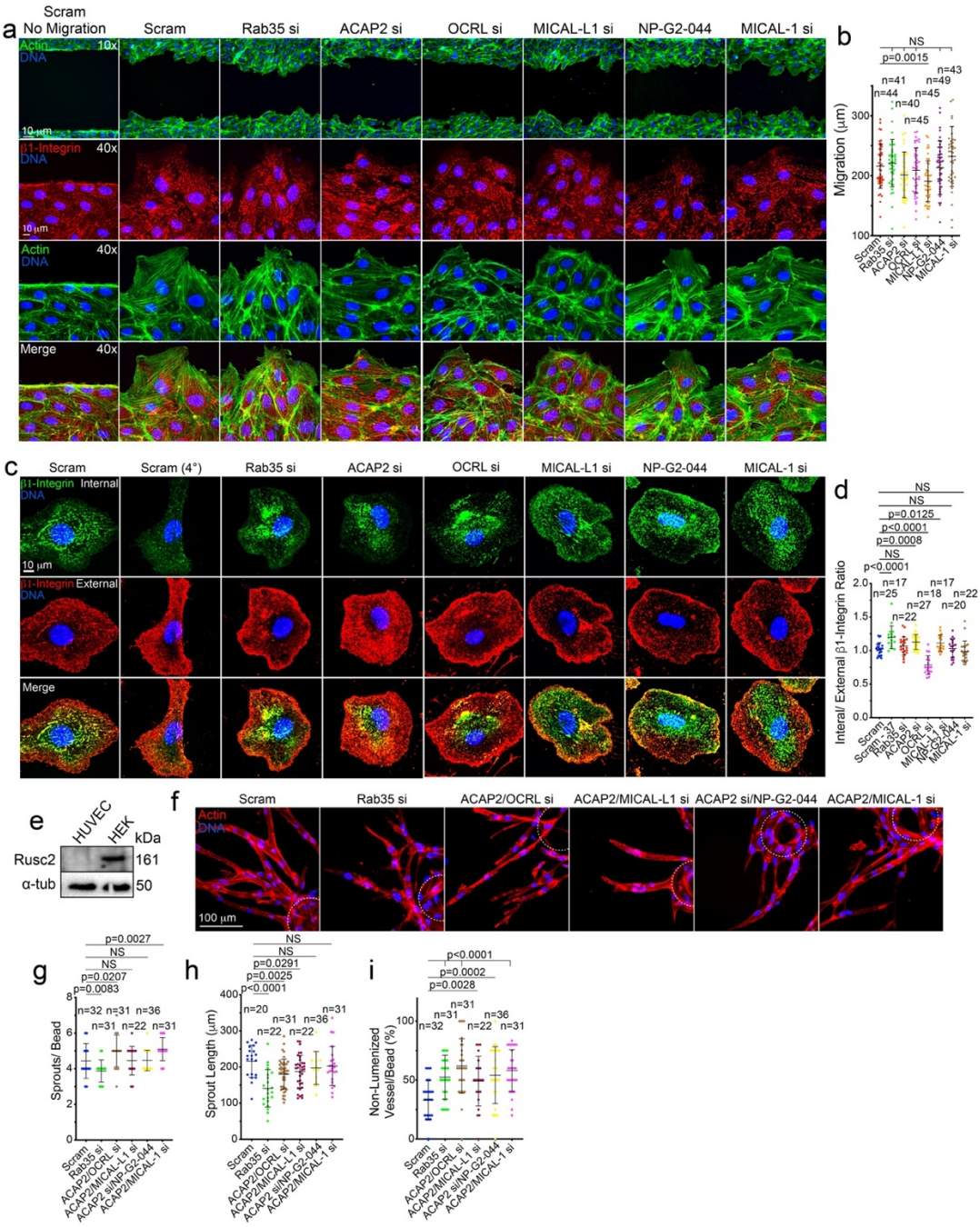

Supplemental Figure 15: Knockdown of Rab35 impacts integrin internalization, but not cell migration. A. Migration assay in cells treated with scramble (Scram), Rab35, ACAP2, OCRL, MICAL-L1, or MICAL-1 siRNA (si) or Fascin inhibitor NP-G2-044. Cells were stained for β1- integrin and actin. B. Quantification for the migration assay in A. n=number of measurements. Error bars represent standard deviation, middle bars are the mean. C. Antibody feeding assay to test for β1-integrin turnover between conditions. Cells were treated with indicated siRNA. Green channel represents internalized integrins,

while the red channel marks only external integrins. As a control to inhibit endocytosis a group was held at 4oC. D. Fluorescence intensity ratio of internalized to external β1-integrin in panel C. n=number of cells. Error bars represent standard deviation, middle bars are the mean. E. Western blot image probing for Rusc2 in both HEK293 cells and human umbilical vein endothelial cells (HUVECs). F. Representative images of sprout morphology between indicated groups. Dashed lines outline microbeads. G-I. Graphs of indicated sprout parameters between groups. n= number of sprouts. Error bars represent standard deviation, middle bars are the mean. NS=non-significant. Statistical significance was assessed with an unpaired t-test or a 1-way ANOVA followed by a Dunnett multiple comparisons test. All experiments were done using Human umbilical vein endothelial cells in triplicate.

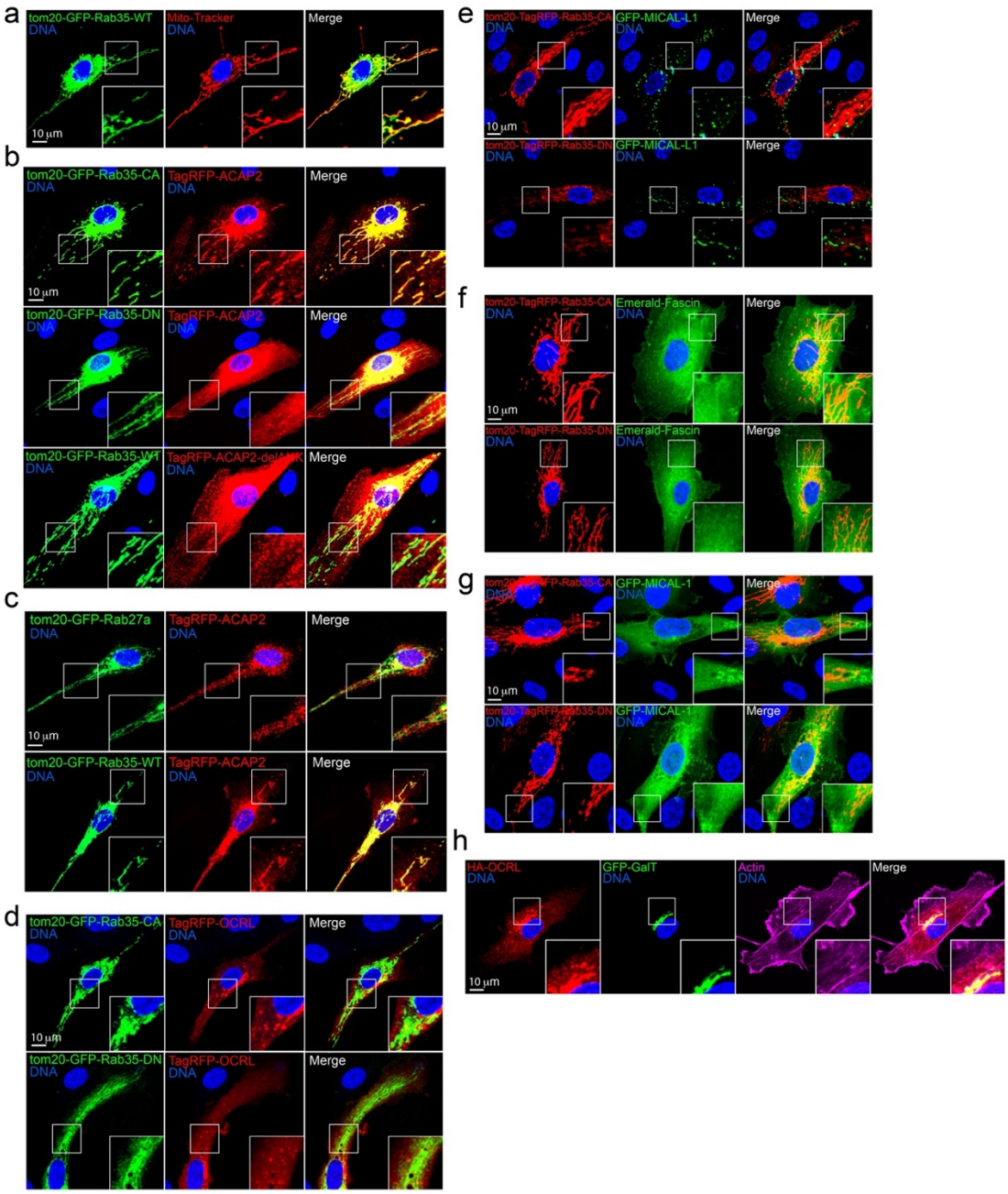

Supplemental Figure 16: Rab35 binds only ACAP2. (A) Cells stained for mitochondria (Mito- tracker) and transfected with tom20-tagRFP-Rab35-wild-type (WT). (B) Representative images of a cell co-expressing tom20-tagRFP-Rab35-WT, constitutively-active (CA), or dominant- negative (DN) variants with TagRFP-ACAP2 or ACAP2 with deleted ankyrin repeat domain (delANK). (C) Representative image of a cell expressing tagRFP-ACAP2 and tom20-GFP- Rab27a-WT (top panels). Bottom panel is a representative image of a cell expressing of tom20- GFP-Rab35-WT with tagRFP-ACAP2. (D) Top panels- representative image of a cell expressing tom20-GFP-Rab35-CA and OCRL. Bottom panels- cell expressing tom20-GFP-Rab35-DN and TagRFP-

OCRL. (E) Top panels- representative image of a cell expressing tom20-TagRFP- Rab35-CA and GFP-MICAL-L1. Bottom panels- cell expressing tom20-TagRFP-Rab35-DN and GFP-MICAL-L1. (F) Top panels- representative image of a cell expressing tom20-TagRFP- Rab35-CA and Emerald-Fascin. Bottom panels- cell expressing tom20-TagRFP-Rab35-DN and Emerald-Fascin. (G) Top panels- representative image of a cell expressing tom20-TagRFP- Rab35-CA and GFP-MICAL-1. Bottom panels- cell expressing tom20-TagRFP-Rab35-DN and GFP-MICAL-1. (H) Representative image of HA-OCRL and GFP-GalT (Golgi marker) localization. Insets are areas of higher magnification. All experiments were done using human umbilical vein endothelial cells in triplicate.

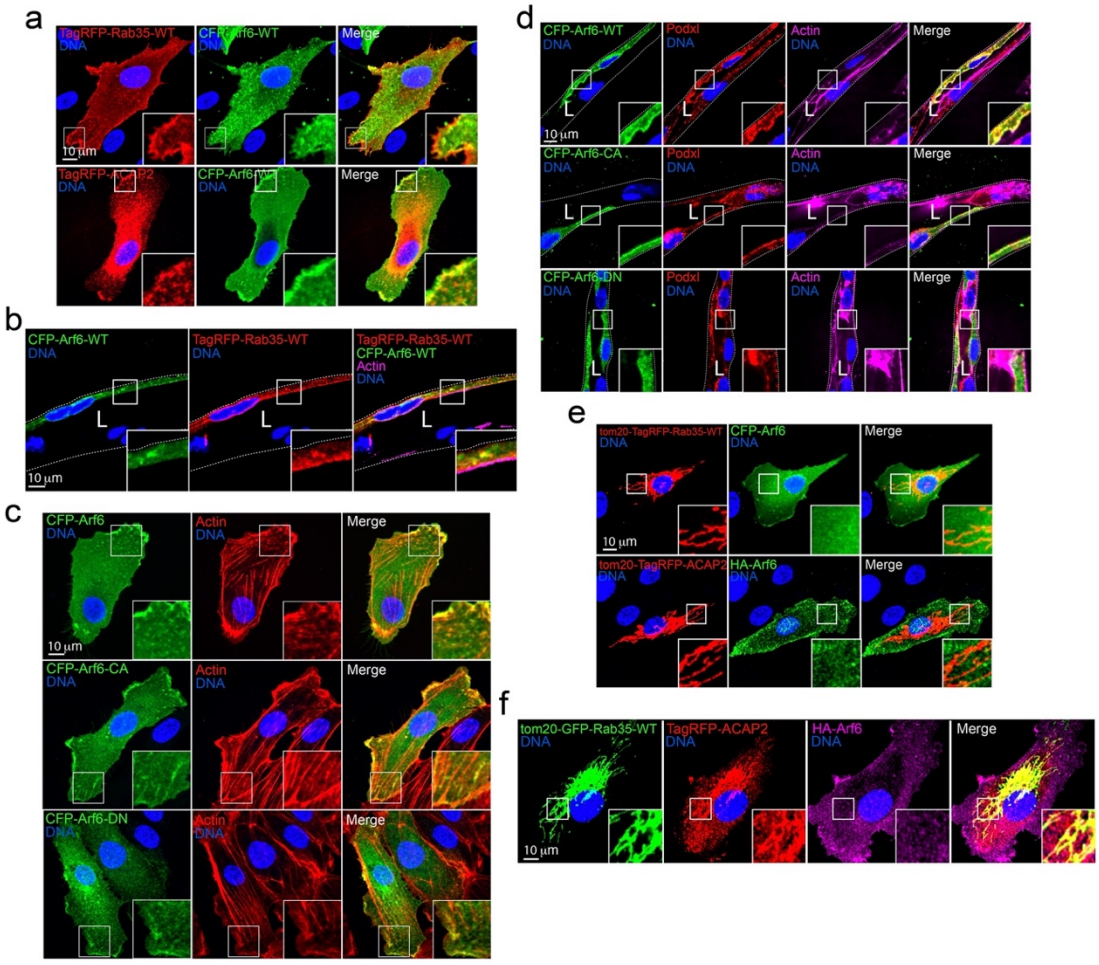

Supplemental Figure 17: Arf6 localization and interactions with Rab35 and ACAP2. (A) Two- dimensional localization of CFP-Arf6 with tagRFP-Rab35-wild-type (WT) (top panels) or tagRFP- ACAP2 (bottom panels). (B) Localization of tag-RFP-Rab35-WT and CFP-Arf6 in a sprout. (C) Two-dimensional localization of CFP-Arf6-WT (top panels), constitutively-active (CA, middle panels), or dominant-negative (DN, bottom panels) stained for actin. (D) Representative images of sprouts transduced with WT, CA, or DN CFP-Arf6 stained for podocalyxin (Podxl) and actin. (E) Top panel- representative image of a cell expressing tom20-tagRFP-Rab35-WT and CFP-Arf6. Bottom panel- representative image of a cell expressing tom20-tagRFP-ACAP2 and HA-Arf6-WT. (F) Representative image of a cell expressing tom20-GFP-Rab35-WT, tagRFP-ACAP2 and HA- Arf6-WT. L denotes lumen in all images. White dotted lines mark sprout exterior. Insets are areas of higher magnification. All experiments were done using human umbilical vein endothelial cells in triplicate.

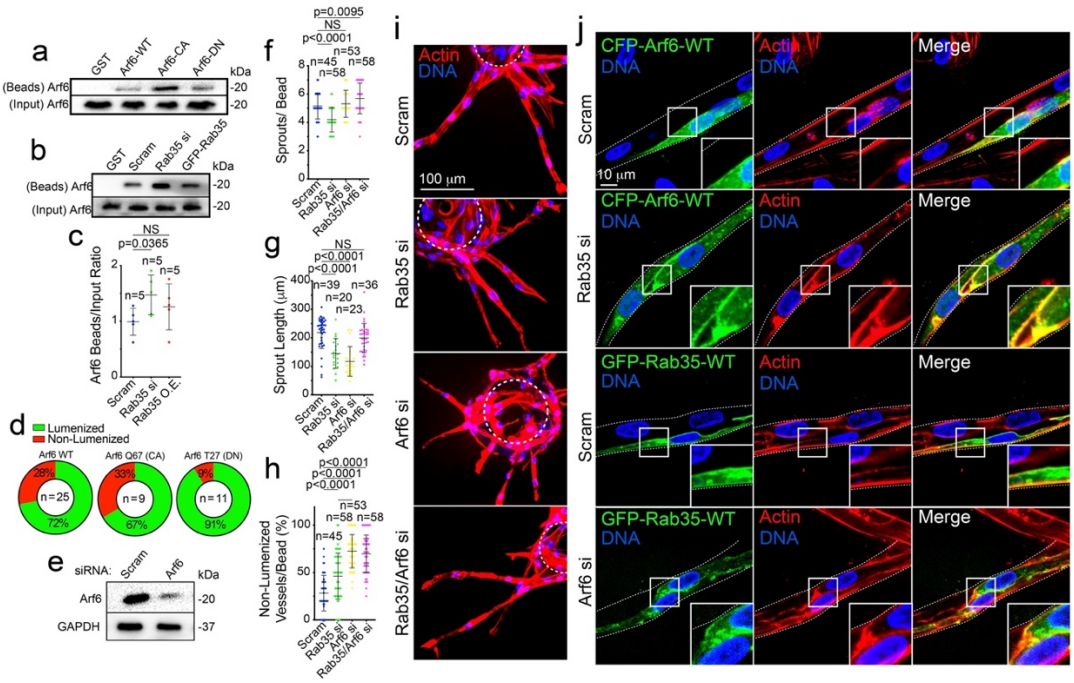

Supplemental Figure 18: Loss of Rab35 affects Arf6 activity. (A) Pulldown assay using GGA3 to probe for activated Arf6. Cells were transfected with wild-type (WT), constitutively-active (CA), or dominant-negative (DN) Arf6. (B) Pulldown assay using GGA3 to probe for activated Arf6. Cells were treated with scramble (Scram) or Rab35 siRNA (si) or transduced with GFP-Rab35-WT. (C) Quantification of Arf6 activity. n=number of pull-downs. Error bars represent standard deviation, middle bars are the mean. (D) Quantification of open or collapsed lumens after transduction with WT, CA, or DN CFP-Arf6. n= number of sprouts. (E) Western blot confirmation of siRNA knockdown (KD) of Arf6 (average 60.8% KD relative to control, n=3). (F-H) Graphs of indicated sprout parameters between groups. n=number of sprouts. Error bars represent standard deviation, middle bars are the mean. (I) Representative images of sprout morphology between indicated groups. Dashed lines outline microbeads. (J) Epistasis experiment showing CFP-Arf6- WT localization in Scram or Rab35 siRNA sprouts (top 2 panels) as well as GFP-Rab35-WT localization in Scram and Arf6 siRNA sprouts (bottom two panels). L denotes lumen in all images. White dotted lines mark sprout exterior. Insets are areas of higher magnification. NS=non-significant. Statistical significance was assessed with an unpaired t-test or a 1-way ANOVA followed by a Dunnett multiple comparisons test. All experiments were done using human umbilical vein endothelial cells in triplicate.

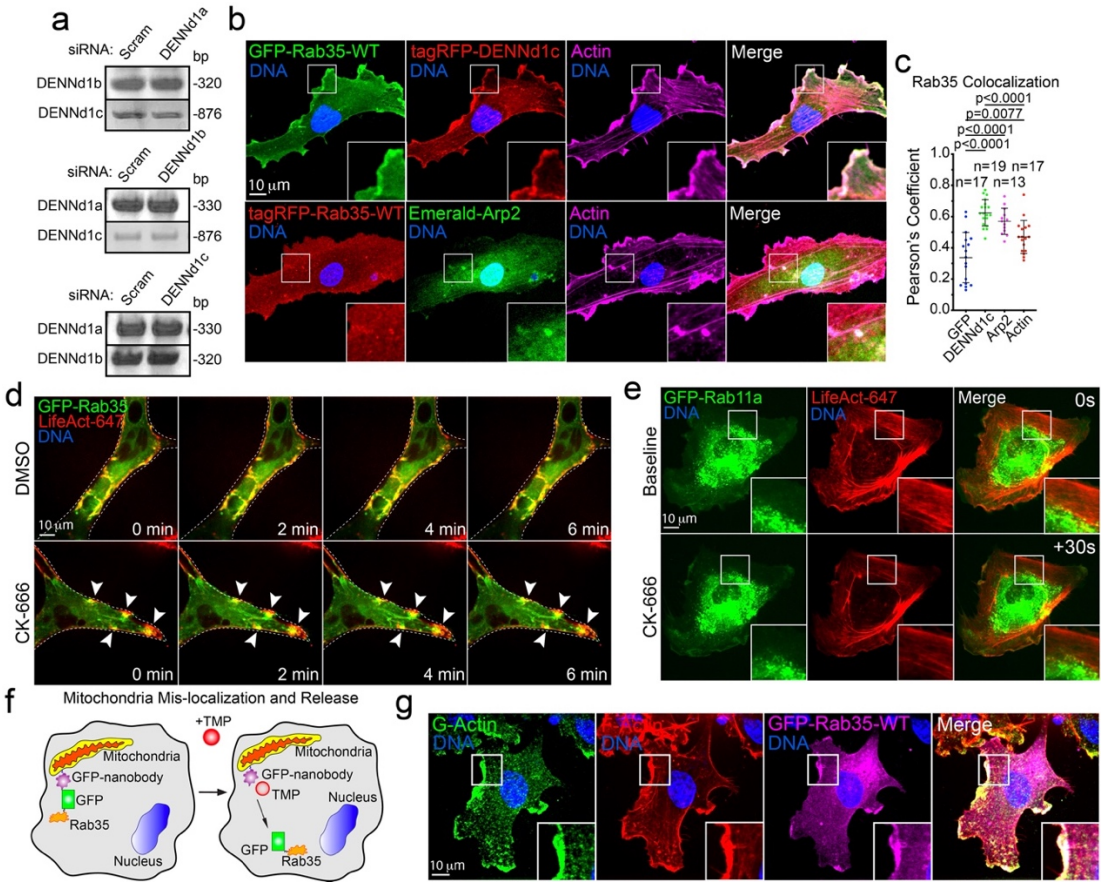

Supplemental Figure 19: Rab35 is recruited to sites of actin polymerization. (A) RT-PCR of DENNd1a-c knockdown. DENNd1's were individually knocked down using siRNA (si) and expression of the remaining two DENND1s were probed to test for compensation effects. Base- pair (BP). (B) Top panel- representative image of a cell expressing GFP-Rab35-wild-type (WT) and tagRFP-DENNd1c. Bottom panel- representative image of a cell expressing GFP-Rab35-WT and Emerald-Arp2. (C) Pearson's coefficient of Rab35 co-localization with described proteins. n=number of cells. Error bars represent standard deviation, middle bars are the mean. (D) GFP- Rab35-WT and LifeAct-tagRFP647 (647) co-expression in sprouts live-imaged with vehicle or following treatment with CK-666. Arrowheads indicate accumulations of GFP-Rab35-WT and LifeAct-647. Dotted line indicates sprout exterior. (E) Representative live-image of a cell expressing GFP-Rab11a and LifeAct-647 before and after CK-666 treatment. (F) Cartoon of a mitochondria-localized GFP-nanobody and controlled release of GFP-Rab35 upon treatment with Trimethoprim (TMP). In the absence of TMP the nanobody sequesters GFP or GFP-tagged proteins. In the presence of TMP the GFP cargo is released. (G) Representative image of a cell expressing GFP-Rab35-WT and stained for filamentous (F) and globular (G) actin. Insets are areas of higher magnification. Statistical significance was assessed with an unpaired t-test or a 1-way ANOVA followed by a Dunnett multiple comparisons test. All experiments were done using human umbilical vein endothelial cells in triplicate.

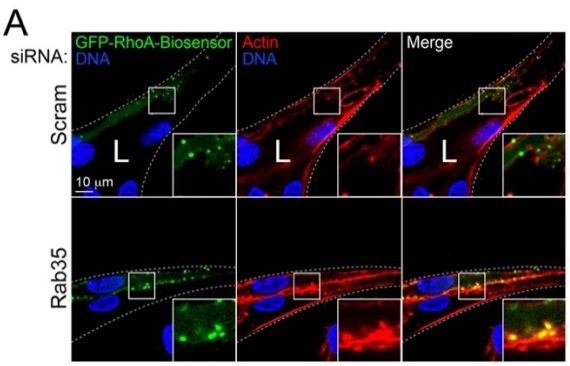

B

CRISPR Off-Target Gene Identification

Target	*Target Sequence*	*Mismatch*	*Number of Found Targets*	*Exonic Targets*	*Intronic Targets*
Rab35-A	CTTGAAGTCCACACCGAT	1	1	0	1
Rab35-B	CTTGAAGTCGACTCCTATA	1	1	0	1
Rab35-A	CTTGAAGTCCACACCGAT	2	4	1	3
Rab35-B	CTTGAAGTCGACTCCTATA	2	1	0	1

Mismatches identified by Cas OFFFinder.

Supplemental Figure 20: Rab35 alters RhoA activity in sprouts and CRISPR off-target sites in zebrafish. (A) Representative image of GFP-RhoA-Biosensor in scramble (Scram) and Rab35 siRNA (si) treated sprouts. L denotes lumen, white dashed line outlines sprouts and insets are higher magnification. (B) Table showing Rab35A/B single-guide RNA potential off- target genes with one or two nucleotide mismatches.

Appendix D: Chapter 4 Supplemental Figures

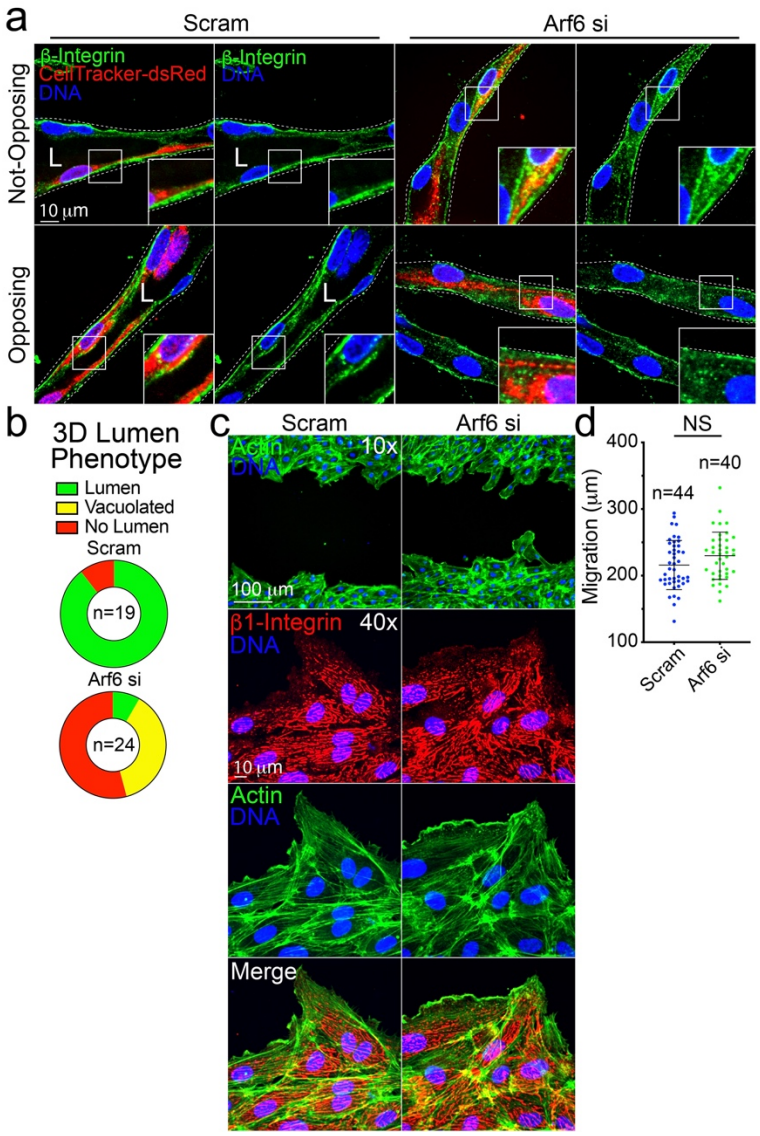

Supplemental Figure 21: Arf6 is Not Required for 2D Migration. A. Representative images of non-opposing (top panels, an isolated siRNA treated cell) and opposing (bottom panels, two adjacent siRNA treated cells) cells stained as indicated. L denotes lumen. Dashed line marks sprout exterior. B. Quantification for lumen phenotypes in scramble (Scram) control and Arf6 siRNA knockdown (KD) sprouts. Vacuolated

indicates large round vacuoles with no contiguous lumen. C. Migration assay in cells treated with Scram or Arf6 siRNA (si). Cells were stained for β1- integrin and actin. D. Quantification for the migration assay in A. n=number of measurements. Error bars represent standard deviation, middle bars are the mean. Statistical significance was assessed with an unpaired t-test or a 1-way ANOVA followed by a Dunnett multiple comparisons test. All experiments were done using human umbilical vein endothelial cells in triplicate.

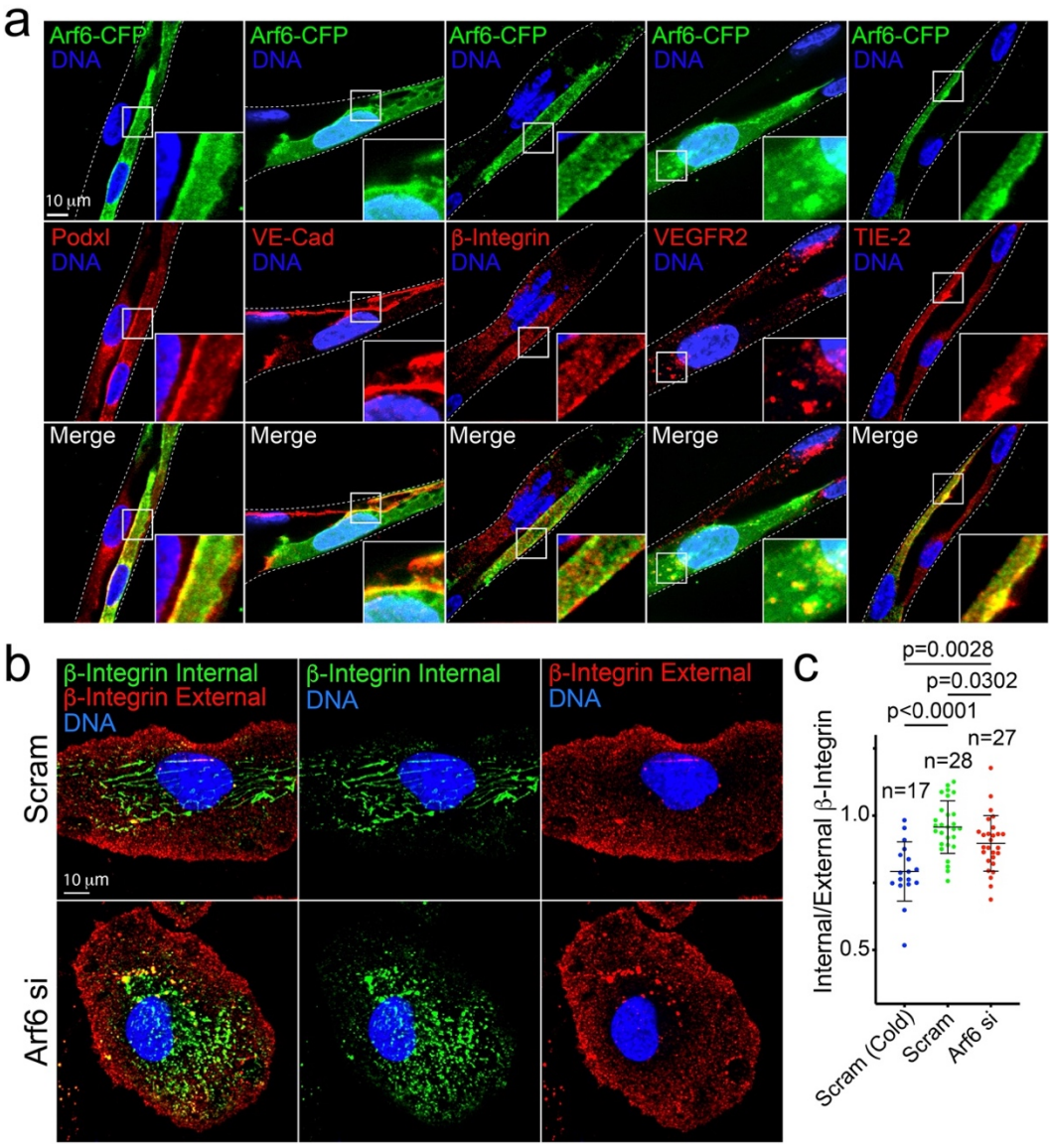

Supplemental Figure 22: Arf6 Co-Localization and Seeding Assay. A. Arf6-CFP (top panels) co-localization with podocalyxin (podxl), VE-Cadherin (VE-Cad), β-Integrin, VEGFR2, and TIE-2 (mid panels). B. Image representatives of Scram (top panels) and Arf6 (bottom panels) siRNA knockdown cells. Green channel is internalized β-integrin and red channel is external β-integrin. C. Ratio of detectable internal β-integrin by

external β-integrin. n = number of cells. Statistical significance was assessed with an unpaired t-test or a 1-way ANOVA followed by a Dunnett multiple comparisons test. All experiments were done using human umbilical vein endothelial cells in triplicate.

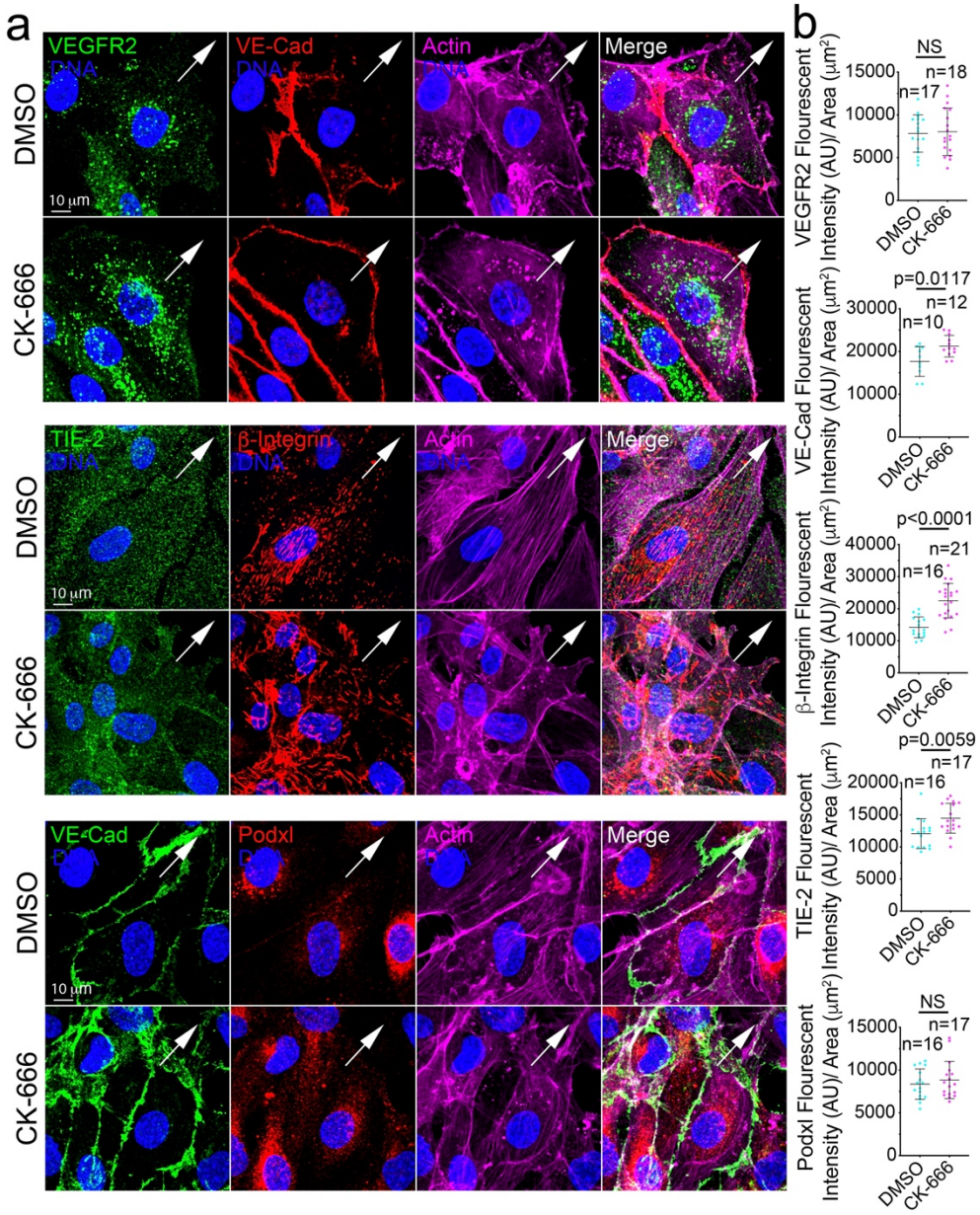

Supplemental Figure 23: Actin Polymerization is Required for Endocytosis. A. Image representatives of indicated staining for cells treated with DMSO and Arp-inhibitor (CK-666). White arrows are indicative of direction of cell migration. B. Quantification of fluorescent intensity of indicated proteins by cell area. n = number of cells. NS=non-significant. Statistical significance was assessed with an unpaired t-test or a 1-way ANOVA followed by a Dunnett multiple comparisons test. All experiments were done using human umbilical vein endothelial cells in triplicate.

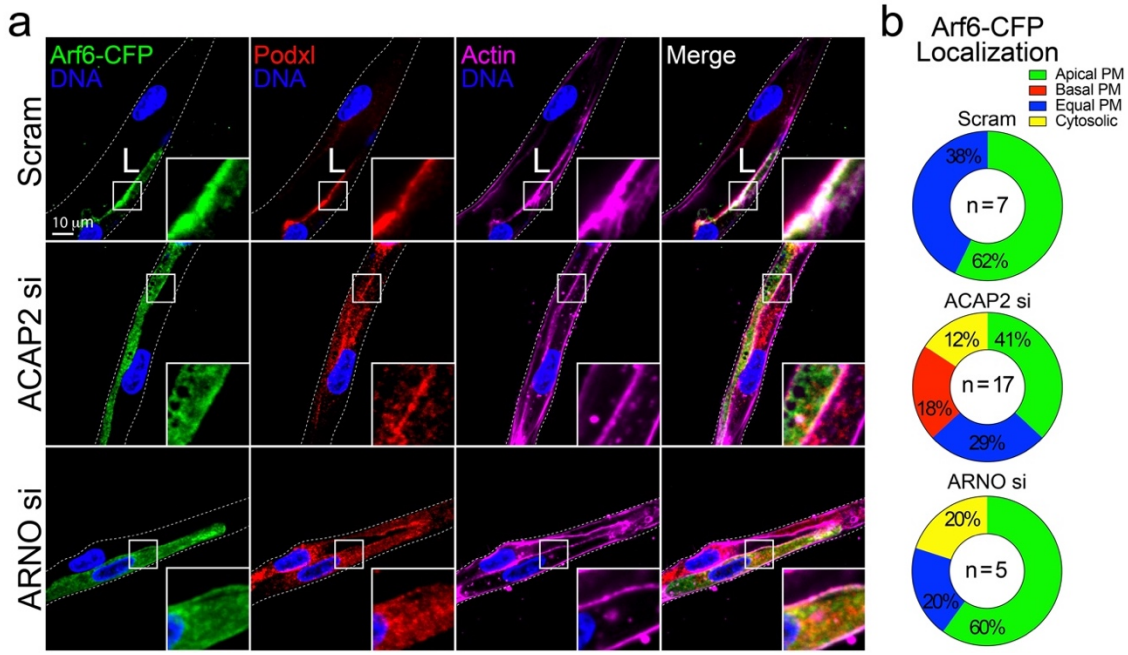

Supplemental Figure 24: ARNO and ACAP2 Knockdowns with Arf6-CFP Localization. A. Image representatives of Arf6-CFP localization in sprouts treated with scramble (Scram), ACAP2 and ARNO siRNA (si) knockdown (KD)in the fibrin-bead assay (FBA). Cells were stained for podocalyxin (podxl) and actin. B. Quantification of Arf6-CFP localization in scram, ACAP2 and ARNO KD sprouts.

Appendix E: Chapter 5 Supplemental Figures

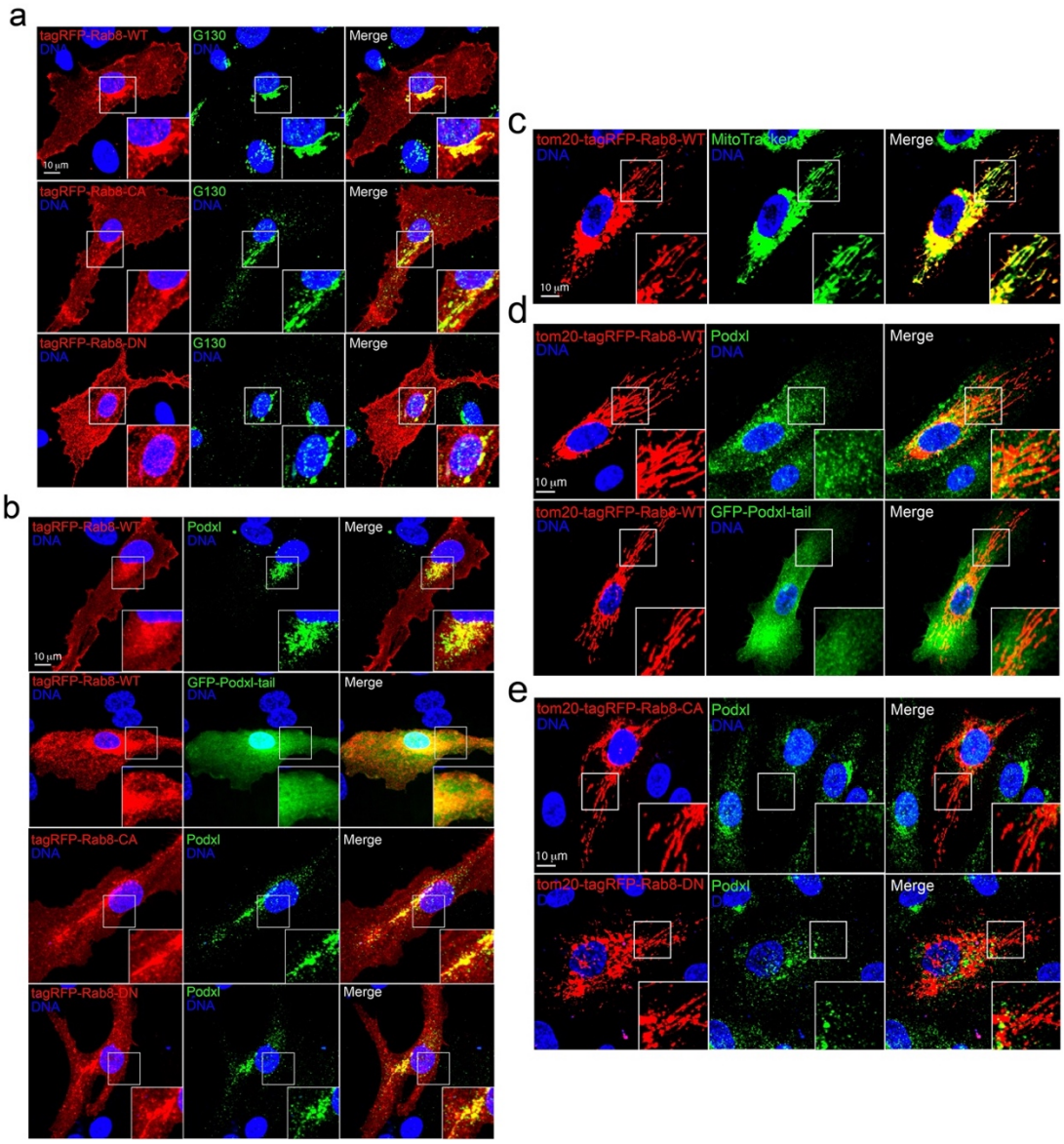

Supplemental Figure 25: Rab8 Does Not Bind Podocalyxin Directly. A. Image representatives of tagRFP-Rab8-wildtype (WT), -constitutively active (CA), and -dominant negative (DN) with GM130 (green). B. Image representatives of tagRFP-Rab8-WT, -CA, and -DN with podocalyxin (green, top, third, and bottom rows) and the

cytosolic domain of podxl mutant (GFP-podxl-tail, second row). C. Image representative of mitochondria mis-localized Rab8 (red, tom20-tagRFP-Rab8) with mito-tracker (green). D. Image representatives of tom20-tagRFP-Rab8 with podxl (green, top panels) and GFP-podxl-tail (bottom panels). E. Image representatives of tom20-tagRFP-Rab8-CA and -DN with podxl. In all panels, white box denotes area of inset.

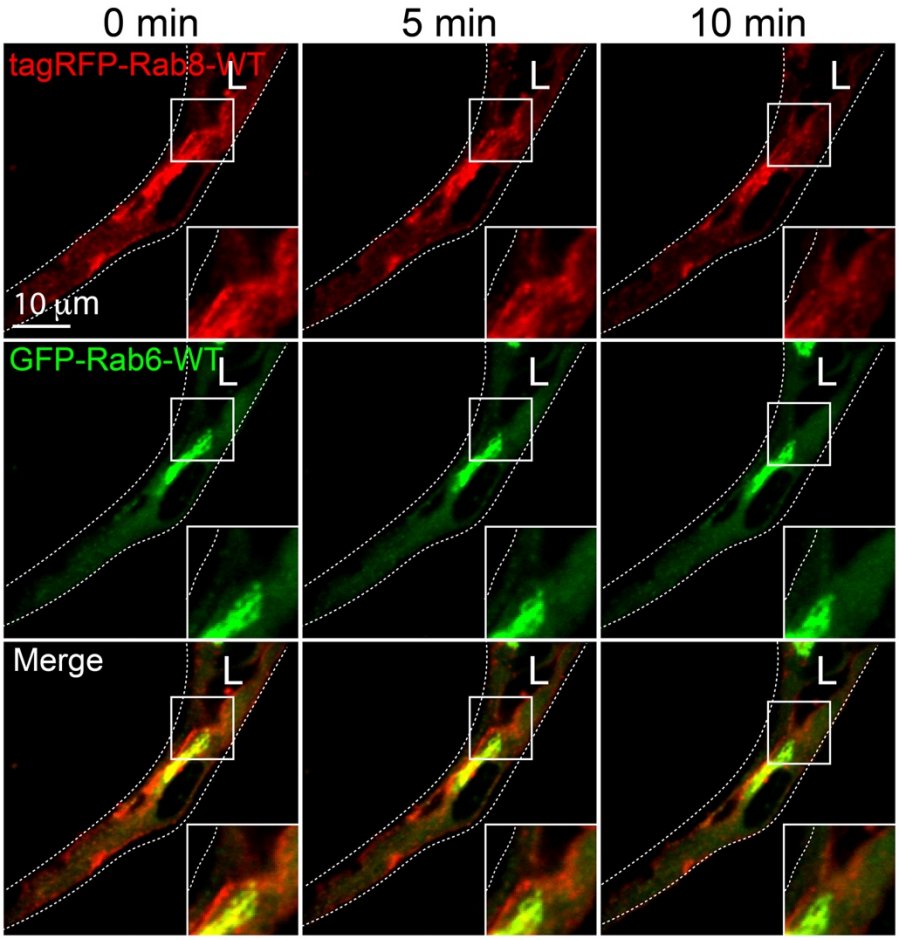

Supplemental Figure 26: Live imaging of tagRFP-Rab8-WT and GFP-Rab6-WT in endothelial cell sprouts over 10 minutes (min). White dashed line marks sprout exterior. L denotes lumen. White box represents area of inset.